School of Doctoral Studies in Biological Sciences

University of South Bohemia in České Budějovice

Faculty of Science

Modulation of *C. elegans* vulva organogenesis by nuclear hormone receptor NHR-25

Ph.D. Thesis

Nagagireesh Bojanala

Supervisor: M.Sc. Masako Asahina-Jindrová, Ph.D.
Institute of Parasitology
Biology Centre of the Academy of Sciences, the Czech Republic

České Budějovice 2015

This thesis should be cited as:

Bojanala, N., 2015: Modulation of *C. elegans* vulva organogenesis by nuclear hormone receptor NHR-25. Ph.D. Thesis. University of South Bohemia, Faculty of Science, School of Doctoral Studies in Biological Sciences, České Budějovice, Czech Republic, 161, xiv pp. In English.

Annotation

The present work analyzes the role of conserved nuclear hormone receptor NHR-25 during vulva formation in *C. elegans* through genetic, cellular, and biochemical techniques. NHR-25 is expressed in graded manner during vulva cell fate specifications and migrations. *In vitro* and *in vivo* sumoylation assays identified that a proper ratio of sumoylated to un-sumoylated NHR-25 specifies 3^0 cell fates. In addition, *nhr-25(RNAi)* and *nhr-25(ku217)* studies identified a pivotal role for NHR-25 during vulva cell migrations, fusions and morphogenesis. Altered gene expression pattern of EGF/LIN-3, HOX/LIN-39, and Semaphorin SMP-1 were seen in *nhr-25(lf)* within vulva. Thus NHR-25 orchestrates proper vulva organogenesis.

Declaration:

I hereby declare that I did all the work presented in this thesis by myself or in collaboration with co-authors of the published article. Further, I declare that in accordance with the Czech legal code § 47b law No. 111/1998 in its valid version, I consent to the publication of my Ph.D. thesis (in an edition made by removing marked parts archived by the Faculty of Science) in an electronic way to the public access on the STAG database run by the University of South Bohemia, České Budejovice.

……..

České Budejovice May 16, 2015 Nagagireesh Bojanala

Declaration [in Czech]

Prohlašuji, že svoji disertační práci jsem vypracoval samostatně pouze s použitím pramenů a literatury uvedených v seznamu citované literatury.

Prohlašuji, že v souladu s § 47b zákona č. 111/1998 Sb. v platném znění souhlasím se zveřejněním své disertační práce, a to v úpravě vzniklé vypuštěním vyznačených částí archivovaných Přírodovědeckou fakultou elektronickou cestou ve veřejně přístupné části databáze STAG provozované Jihočeskou univerzitou v Českých Budějovicích na jejích internetových stránkách, a to se zachováním mého autorského práva k odevzdanému textu této kvalifikační práce. Souhlasím dále s tím, aby toutéž elektronickou cestou byly v souladu s uvedeným ustanovením zákona č. 111/1998 Sb. zveřejněny posudky školitele a oponentů práce i záznam o průběhu a výsledku obhajoby kvalifikační práce. Rovněž souhlasím s porovnáním textu mé kvalifikační práce s databází kvalifikačních prací Theses.cz provozovanou Národním registrem vysokoškolských kvalifikačních prací a systémem na odhalování plagiátů.

….....

České Budějovice, May 16, 2015 Nagagireesh Bojanala

This thesis originated from partnership of Faculty of Science, University of South Bohemia, and Institute of Parasitology, Biology Centre of the ASCR, support from Doctoral studies in the Molecular, Cellular Biology, and Genetics graduate program.

Financial support

This work was supported by grants from the Czech Science Foundation (204/09/H058), the Czech Academy of Sciences (Z60220518 and 500960906), the Czech Ministry of Education (MSM6007665801), and MODBIOLIN (7FP-REGPOT-2012-2013-1, GA316304). This work is supported by stipend from the University, Paru: Z60220518

Acknowledgements

I would like to thank Masako for her guidance and friendship during my studies. Her belief in NHR-25 was my strong motivational asset. Special thanks goes to Marek for teaching me molecular biology techniques and tricks in scientific writing. Sincere thanks to Keith and Jordan (UCSF) for initiating a productive collaboration regards to 'SUMO-NHR-25' story, Teiji and Rik Korswagen (Utrecht) for a two week assistance with smFISH studies, and Wendy (Pennstate) for the unexpected postdoctoral opportunity. I wish my heartfelt wishes to all members of Marek and Wendy labs for their collegial environment. Personal thanks to Sasa, Martina, and Linda for the initial help in & out of Masako Lab in Ceske Budejovice. Will never forget memorable experiences shared with Anir, Som, Sameer, Sneha, Vasanth, Sahu, Ray and Suresh. Our 'Tennis court-Cricket matches' were the best pastime activities. I would like to thank my parents and family members for their never ending support. Finally, my very special thanks goes to my wife Sangeetha for her support both in good and bad times and to my angel 'Anora'.

List of papers and author's contribution

1) Ward JD*, **Bojanala N***, Bernal T, Ashrafi K, Asahina M, Yamamoto KR (2013). Sumoylated NHR-25/NR5A regulates cell fate during *C. elegans* vulval development. *PLoS Genetics* 9(12): e1003992. (IF= 8.167).

* Equal contribution

This paper constitutes Chapter 3 in the thesis.

Nagagireesh Bojanala participated in conception, data analysis and interpretation of following results:

- Performed RNAi experiments and phenotypic analysis to support genetic interaction between *smo-1* and *nhr-25* during vulva development (Figure 1B, C).
- Provided the cartoon diagram (Figure 2)
- Performed all cell lineage experiments in *smo-1(lf)* and *nhr-25(lf)* (Table 1).
- Performed Pn.p induction analysis in wild type and transgenic animals (Figure 8).
- Analyzed NHR-25::GFP expression patterns in wild type and *smo-1(RNAi)* animals (Figure 9).
- Supplementary data, Figure S1 and Table S1.
- Responded to & dealt with reviewer comments.

Masako Asahina Ph.D, the co-corresponding author of the above paper approves the contributions of Nagagireesh Bojanala as mentioned above.

…….

Masako Asahina Jindrova Ph.D

2) **S**eetharaman A, Cumbo P, **Bojanala N*,** Gupta B.P. (2010). Conserved mechanism of Wnt signaling function in the specification of vulval precursor fates in *C. elegans* and *C. briggsae*. *Developmental Biology* 346: 128–139. (IF= 3.637)

*Second author

- Performed complementation tests, vulva cell lineage, fate specification, and ablation experiments for Cbr-pry-1 alleles, sy5353, sy5270 and sy5411.

3) Devika Sharanya, Bavithra Thillainathan, Sujatha Marri, **Nagagireesh Bojanala***, Stephane Flibotte, Donald G. Moerman, Robert H. Waterston, and Bhagwati P Gupta. Genetic Control of Vulval Development in *Caenorhabditis briggsae*. G3 (Bethesda) 2012. doi: 10.1534/g3.112.004598. (IF= 2.511)

*Co-author.

- Performed cell lineage analysis in Cbr-lin-11 mutants.

Table of Contents

Acknowledgments……...iv

Author contributions……v

List of Abbreviations……...x

List of Figures…….....xii

List of Tables…….....xiii

Rationale and Research Objectives…… xiv

Chapter 1: Introduction..... 1

1.1 C. elegans as a model to study development..... 1

1.2 *C. elegans* vulva organogenesis 1

1.2.1 Cellular aspects 2

1.2.2 Genetic aspects..... 3

1.2.3 Molecular aspects..... 3

1.3 Regulation of EGF/LIN-3 during vulva formation 6

1.4 Multiple developmental processes orchestrate vulva morphogenesis 8

1.4.1 Short range migrations and invariant cell divisions 8

1.4.2 Orientation of asymmetric cell divisions and polarities..... 9

1.4.3 Vulva terminal differentiations 10

1.5 Signaling pathways regulating vulva morphogenesis 11

1.5.1 Wnt signaling and vulva cell polarities 11

1.5.2 GRNs governing vulva terminal differentiations..... 12

1.5.3 SMP-1/PLX-1 system 13

1.5.4 RAC/RHO system 14
1.5.5 LET-60/Ras signal 14
1.5.6 LIN-39/Hox and its effectors 15
1.5.7 LET-502/ROCK and actomyosin contractions 16
1.6 Nuclear hormone receptors 17
1.6.1 General Overview 17
1.6.2 Orphan nuclear receptor NHR-25 17
1.6.3 Developmental roles and interactions of NHR-25 in *C. elegans* 18
Chapter 2: Materials and Methods 41
2.1 Strains and Genetics 43
2.2 Scoring vulva induction patterns of VPCs 43
2.3 Scoring vulva lineage patterns 44
2.4 Temporal *nhr-25(RNAi)* 44
2.5 Confocal Microscopy 45
2.6 Transformations and Microinjections 45
2.7 qRT-PCR 45
2.8 smFISH technique 46
Chapter 3: Research article: Sumoylated NHR-25/NR5A regulates cell fate during *C. elegans* vulval development. 47
Chapter 4: Unpublished results 78
4.1 *nhr-25(L2-RNAi)* results in normal vulva cell competences and cell fates. 79

4.2 NHR-25 activity is necessary for vulva cell migration. 79

4.3 NHR-25 is expressed in graded manner during vulva cell migration.80

4.4 *nhr-25(lf)* causes abnormal expression of terminal markers, *egl-17* and *egl-26.* 81

4.5 *lin-3* is ectopically upregulated in the primary vulva cells in *nhr-25 (lf).* 81

4.6 LIN-39 expression is altered in *nhr-25 (lf).* 83

4.7 NHR-25 enhances cell migration defects caused by mutations in Semaphorin pathway. 84

4.8 SMP-1 expression is altered in *nhr-25(lf).* 84

4.9 EGF/Ras/MAPK pathways regulate NHR-25 expression in vulva...

.....85

4.10 Abnormal actin organization was seen in *nhr-25 (lf)* during vulva morphogenesis. 85

Figures……87 -104

Remarks 111

Chapter 5: Finals conclusions 115

Chapter 6: References 117

Supplementary articles……...126

Curriculum Vitae 157

LIST OF ABBREVIATIONS

AC	Anchor cell
ACEL	Anchor cell enhancer element
DIC	Diffraction interference contrast
DNA	Deoxyribonucleic acid
DSL	Delta-serrate ligands
ECM	Extra cellular matrix
EGF	Epidermal growth factor
EGFR	Epidermal growth factor receptor
Egl	Egg-laying defective
FGF	Fibroblast growth factor
Ftz-F1	Fushi tarazu factor-1
Gf	gain-of-function
GRNs	Gene regulatory networks
GTPases	Guanine triphosphatases
HDACs	Histone deacetylases
HGF	Hepatocyte growth factor
Hox	Homeobox
Lf	loss-of-function
Lin	Lineage defective
LIP-1	Lateral inhibitor phosphatase-1
LRH-1	Liver receptor homolog-1
MAPK	Mitogen activated protein kinase-1
Muv	Multivulva
NGM	Nematode growth media
NHR-25	Nuclear hormone receptor-25

NR5A	Nuclear receptor subfamily 5, group A
NURD	Nucleosome remodeling complexes
PLX-1	Plexin-1
PRY-1	Polyray-1
Pvl	Protruding vulva
RNA	Ribonucleic acid
RNAi	RNA interference
ROCK	Rho associated protein kinase
ROM-1	Rhomboid-1
SF-1	Steroidogenic factor-1
SGPs	Somatic gonad precursors
smFISH	single molecule fluorescent in situ hybridization
SMP-1	Semaphorin-1
SUMO	Small ubiquitin modifier
SynMuv	Synthetic multivulva
TF	Transcription factor
VPCs	Vulva precursor cells
Vul	Vulvaless
Wnt	Wingless
ZMP-1	Zinc metalloprotease-1

LIST OF FIGURES

Figure 1.1 *C. elegans* life cycle and larval stages. 21

Figure 1.2 Vulva cell fates and lineages. 22

Figure 1.3 Ras signaling pathway is involved in vulva formation. 24

Figure 1.4 Temporal expression pattern of *egl-17* in vulva. 25

Figure 1.5 Cross talk between Ras and Notch regulates vulva cell fate patterning. 26

Figure 1.6 Synmuv genes redundantly regulate LIN-3 expression and vulva inductions. 27

Figure 1.7 Alternate splicing generates three LIN-3 isoforms 28

Figure 1.8 Model representing regulation of *lin-3* expression in AC. 29

Figure 1.9 Vulva cell migrations, homotypic fusions and toroid formation. 30

Figure 1.10 Wnt signaling regulates vulva cell polarities. 32

Figure 1.11 Expression profile of vulva terminal differentiation markers *egl-17* and *zmp-1*. 33

Figure 1.12 Nhr-67 controls Gene Regulatory Networks (GRNs) that govern terminal differentiations. 34

Figure 1.13 Signaling pathways regulating vulva cell migrations. 35

Figure 1.14 Vulva toroid contractions and expansions mediated by actomyosin myofibrils. 36

Figure 1.15 Structure and functions of NHRs. 37

Figure 1.16 NHR-25 interacts with β-catenins to regulate gonad axis formation. 39

Figure 1.17 Sumoylation machinery and target activation. 40

LIST OF TABLES

Table 4.1 Generation of ACs and Pn.p inductions in *nhr-25(RNAi)* treated animals. 105

Table 4.2 Pn.p competence properties in temporal *nhr-25(RNAi)* treated animals. 106

Table 4.3 VPC lineage analysis in wild type and *nhr-25 (lf)* animals 107

Table 4.4 L4 stage *lin-3::gfp* expression pattern in *nhr-25(lf)* situation..... 108

Table 4.5 Summary of vulva cell migration defects in various genetic backgrounds 109

Table 4.6 Primer list for *lin-3* qRT-PCR studies. 110

Rationale and Research objectives

Genetic analysis identified multiple roles for NHR-25 during *C. elegans* development such as molting, male tail morphogenesis, and gonad axis formation. During these processes, NHR-25 works in a cell type and tissue specific manner. It is not clear how NHR-25 elicits distinct gene regulatory networks in different cell types. Studies from mammalina SF-1, NHR-25 ortholog showed that SUMO modification is an important regulatory mechanism of nuclear receptor function. NHR-25 has four potential sumo consensus motifs and so far no information is available to account for the effect of sumoylation on NHR-25 activity.

Six epidermal cells have equal potential to receive signal from gonad and develop into mature vulva in *C. elegans*. Strong *nhr-25(lf)* through RNAi severely effects generation of both goand and epidermal cells and hypomorphic allele, *nhr-25(ku217)* show weaker phenotypes. Abnormal vuvla morphology was also reported in *nhr-25(ku217)* animals. But, how NHR-25 regulates vulva morphogenesis and what genes interact with it is unknown. Sumo deletion mutant, *smo-1(ok359)* is known to regulate vulva and gonad morphogenesis.

The following specific aims were postulated to study the role of NHR-25 during vulva formation:

1. To analyze the effect of SUMO modification on NHR-25 transcriptional activity and its localization properties (Chapter 3).
2. To study genetic interactions between *smo-1* and *nhr-25* during vulva formation (Chapter 3).
3. To analyze the spatio-temporal expression of NHR-25 during vulva formation and to comprehend the repertoire of vulva phenotypes observed in *nhr-25(lf)* (Chapter 4).
4. To identify signaling networks that interact with NHR-25 during vulva morphogenesis (Chapter 4).

Towards the goals, available *C. elegans* genetic, cellular, molecular and biochemical techniques were applied. A minor portion of the obtained results were duplicated in chapter 3 & 4 to suit the context.

Chapter 1: Introduction

1.1 *C. elegans* as a model to study development

Caenorhabditis elegans (or *C. elegans* or the worm) measures ~1mm in length and is found in natural soils that are rich in organic matter. The worm possess a long, cylindrical, transparent and un-segmented body and is non-parasitic. They exists as males (XO) and hermaphrodites (XX). An adult male consists of 1031 cells and hermaphrodite 959 that constitute reproductive, muscle, intestine and nervous tissue systems. The transparent body of the worm allows direct observations of cells and cell divisions through simple diffraction contrast microscopy (DIC). Through this advantage, John Sulston developed complete cell lineage history starting from an egg to adult animal (Horvitz & Sulston, 1980). In addition, complete neuronal circuitry was also mapped with a total of 302 neurons. These features can help to study cell fates during development with single cell resolution. The pioneering efforts by Nobel laureate Sydney Brenner made *C. elegans* as a model organism to study developmental biology and neurobiology.

In the laboratory, the worms were grown on NGM agar plates with E. coli OP50 as a food source. Its life cycle involves four larval stages and is very short ~ 3.5 days at 20^0 (Figure 1.1). Under unfavorable conditions such as starving, the worms survive through dauer larvae. *C. elegans* is approachable to both forward and reverse genetics. The genome is organized into five autosomes and one sex chromosome and is composed of 100 Mbps. The complete genome sequence is available and thus facilitates RNAi and gene knock out technologies (Fraser et al., 2000; Kamath et al., 2003)

1.2 *C. elegans* vulva organogenesis

During animal development, individual cells acquire specific fates and develop into unique tissues and organs. Execution of cell fates require precise spatial and temporal control of gene expression which regulates pattern of cell divisions, polarities,

fusions and migrations. These features modulate cellular differentiation and organogenesis.

C. elegans reproductive system, the vulva is an excellent model system to study cell fate specifications and morphogenesis (Sternberg, 2005). The vulva is a non-essential organ for survival which serves as a passage way between uterus and external environment and helps in egg-laying and copulation (Figure 1.2A). The mature vulva is composed of seven multi-nucleate concentric rings called toroids that provide structural integrity and stability during egg-laying behavior. The cellular, genetic, and molecular events that regulate vulva organogenesis and its orchestration by cross talk among multiple conserved signaling pathways such as Egf, Ras, Wnt and Hox networks are well known and are summarized as below (Schindler & Sherwood, 2013; Sharma-Kishore et al., 1999; Sternberg, 2005)

1.2.1 Cellular aspects

The somatic gonad cell known as anchor cell (AC) is the source for vulva induction process (Sulston & White, 1980). The ventral hypodermal cells, P(3-8).p cells receive the inductive signal and develop into mature vulva. They are referred as Vulval Precursor Cells (VPCs) or Pn.p cells. The AC signal acts as morphogen. The VPC that receives the maximum signal adopts 1^0 fate, while moderate levels produces 2^0 fate, and further low levels 3^0 fates. Accordingly, the AC ensures 1^0 fate in P6.p, 2^0 fate in P5.p and P7.p and 3^0 fate in the remaining VPCs (Figure 1.2B). The 1^0 and 2^0 cells undergo three rounds of cell divisions (Pn.x to Pn.pxxx) and the 3^0 cells one round of division (1.2C-E). In both 1^0 and 2^0 cell fates, the first two rounds of cell divisions are identical and occur longitudinally (L) which results in 12 daughter cells that are arranged in bilateral symmetry along the anterior-posterior axis (AB-CD-EF/FE-DC-BA). But they differ in their third and final round of division during which the daughters of the 1^0 cells divide transversely in a TTTT fashion and the 2^0 cells divide in LLTN fashion (Figure 1.2E). The 3^0 cells divide once and their daughters fuse with the syncytial hypodermis (SS fate),

except P3.p which fuses with hypodermis without dividing in roughly 50% of the animals (F or fused fate). The final invariant cell lineages of P(3-8).p are represented as (F/SS-SS-LLTN-TTTT-NTLL-SS) or ($F/3^0$-3^0-2^0-1^0-2^0-3^0). Thus the mature vulva is formed from the descendants of 1^0 and 2^0 cell lineages and is composed of 22 cells, 8 from 1^0 and 7 from each 2^0 cell (I. Greenwald, 2005; Sternberg, 2005). The 1^0 and 2^0 cell fates are called as vulval fates and 3^0 as non-vulval or syncytial fates.

1.2.2 Genetic aspects

Genetic screens aimed towards defective vulva formation resulted in many viable mutants that are generally described as egg-laying defective (*Egl*). In addition, two other classes of vulval mutants: vulvaless (*Vul*) and multivulva (*Muv*) are isolated based on induction properties of the VPCs (Horvitz & Sulston, 1980). In *Vul* P(5-7).p adopt 3^0 fates resulting in non-functional vulva. In *Muv* the VPCs, P3.p, P4.p and P8.p which usually adopt 3^0 non-vulval fates acquire either 2^0 or 1^0 fates. Everted or protruding vulva (Pvl) mutants are also isolated based on the abnormal protruding vulva structures in adult animals (D. M. Eisenmann & Kim, 2000). In normal animals, P(5-7).p cells generate vulva (index 3), in Vul index is <3 and in Muv index >3. Many genes that regulate vulva invariant cell lineages were also identified through direct observation of cell divisions and orientation of division axes (Sulston & Horvitz, 1981). These mutants are typically referred as *lin*, defective for lineage.

1.2.3 Molecular aspects

Several conserved signaling pathways work in concert to regulate vulva cell fate pattering (Sternberg, 2005). Biochemical studies identified LIN-3, an EGF family protein expressed in AC as the source of inductive signal (Hill & Sternberg, 1992). The LIN-3/EGF signal works as a morphogen and ensures 2^0-1^0-2^0 fates within P(5-7).p cells. The P6.p receives maximum amount of LIN-3 from the extra cellular matrix (ECM) through its cognate receptor LET-23, an EGFR family protein. This interaction elicits the

conserved LET-60(Ras)-LIN-45(RAF)-MPK-1(MAPK) cascade within the cytoplasm (Aroian et al., 1991; Han et al., 1990). Activation of Ras/MAPK pathway phosphorylates LIN-1 which in a complex with LIN-31/Fork Head and LIN-39/HOX regulates 1^0 fates positively (Beitel et al, 1995; Wagmaister et al., 2006) (Figure 1.3). Intriguingly, in the absence of Ras pathway, LIN-1 is sumoylated and inhibits 1^0 fates (Leight et al., 2005). Thus LIN-1 regulates 1^0 fates both positively and negatively and acts downstream of LET-23-LET-60-MPK-1 pathway.

The FGF (Fibroblast Growth Factor) protein EGL-17 is temporally expressed in vulval cell lineages from Pn.p to Pn.pxxx stages (Burdine et. al, 1998) (Figure 1.4). After inductive signaling highest *egl-17* expression was observed in P6.p and intermediate levels in P(5,7).p and still low levels in the remaining cells (Inoue et al., 2002; Yoo & Greenwald, 2005). Interestingly, the early P6.p expression was completely abolished in AC ablated animals and strong *loss-of-function* of LET-23/EGFR where inductive signaling is absent (Cui & Han, 2003). Thus providing evidence that early *egl-17* expression in the P6.p lineages corresponds to 1^0 fate and is a good read out for LIN-3/LET-23/MAPK signaling in the VPCs. At Pn.pxxx stage *egl-17* expression disappears in primary lineages and was seen in VulC and D of 2^0 lineages. This activity is regulated by LIN-12/Notch signaling. *Egl-17* mutants show normal vulva development.

The precise patterning of 2^0-1^0-2^0 fates within P(5-7).p cells results from the orchestration of 'love and hate' relationship between Ras and Notch pathways through 'lateral inhibition process' ((I. S. Greenwald et al., 1983; Sternberg, 2005; Greenwald, 2005) (Figure 1.5). EGF/Ras/MAPK cascade promotes 1^0 fate within P6.p and LIN-12/Notch pathway promotes 2^0 fates in P(5,7).p. Notch receptors are activated by Delta-Serrate-LAG-2 (DSL) family ligands. Activated EGF/Ras/MAPK promotes LAG-2 expression and also degrades LIN-12/NOTCH pathway to prevent P6.p from adopting 2^0 fates. Once activated, LAG-2 from P6.p up-regulates LIN-12 within P5.p and P7.p cells. In turn, LIN-12 pathway activates LIP-1(Lateral Signal induced Phosphotase-1) to reduce Ras activity through endocytosis and degradation of LET-23/EGFR within P(5,7).p cells,

thus inhibiting 1^0 fates (Berset et al., 2001). Ablation of AC before inductions or *loss-of-function* of LIN-3/LET-23/LET-60/LIN-12 results in *Vul* and hyper-activation of LIN-3/LET-23/LET-60/LIN-12 results *Muv*.

Canonical WNT signaling also plays significant role in the regulation of LIN-39 expression and vulva inductions. Multiple Wnt ligands and receptors, BAR-1/ β-catenin and POP-1/TCF are the key players (D M Eisenmann, 2005). Five WNT ligands; LIN-44, CWN-1, CWN-2, EGL-20 and MOM-2 and four receptors; LIN-17/Fz, MIG-5/dsh, MOM-5 and MIG-1 and LIN-18/ryk act redundantly to control vulva induction process (D M Eisenmann, 2005; Gleason et al, 2006). MOM-2 and LIN-44 are expressed in the AC and other ligands are known to act in multiple tissues surrounding the VPCs, such as, neurons and muscles and also within VPCs (Inoue et al., 2004; Myers & Greenwald, 2007). The β-catenin BAR-1 acts in concert with LET-60/RAS in the positive regulation of vulval fates and PRY-1/AXIN and APC/APR homolog inhibit BAR-1 activity within the VPCs (D M Eisenmann et al., 1998; Gleason et al., 2002). *Loss-of-function* of PRY-1 produces phosphorylated BAR-1 that translocate to nucleus and forms an activating complex with POP-1 to up-regulate genes involved in vulva inductions. Thus *pry-1(lf)* results in *Muv* situation which can be suppressed by *lin-39(lf)* or *pop-1(lf)* (Gleason et al., 2002, Seetharaman et al., 2010).

Another level of regulation of vulva inductions are maintained by components of Nucleosome Remodeling (NuRD) complexes or chromatin regulators (Fay & Yochem, 2007). Based on the level of genetic redundancy, these components are classified into class A, B and C groups. Mutations within a single class appear wild type but in combination with any of the two classes (A-B, B-C or A-C) are *Muv*. This particular mutants are described as *synmuv* – synthetic multivulva mutants. The conserved family of proteins LIN-35RB, HDAC-1, HPL-1, HP1 and components of sumoylation pathway (*smo-1*, *ubc-2* and *ubc-9*) are encoded by *synmuv* genes (Cui et al., 2004; Cui & Han, 2007; Davison et al., 2011; Poulin et al., 2005; Saffer et al., 2011). *SynMuv* A and *synMuv* B genes redundantly repress *lin-3*/EGF in the hypodermis and as such in *lin-15AB* mutant animals,

lin-3 is ectopically expressed in hyp 7, resulting in highly penetrant Muv animals (Cui et al., 2006; Myers & Greenwald, 2005; Saffer et al., 2011) (Figure 1.6). In accordance, *lin-15AB* multivulva phenotype is suppressed by loss-of-activity of *lin-3* or *let-23* genes, suggesting that the synMuv components work either upstream or in parallel to *lin-3/let-23* pathway during vulva induction. Some classes of synMuv genes are known to act outside of hyp7, such as *lin-36B* and *lin-15A* (Sternberg 2005). *synmuv* genes regulate LIN-39 activity through transcriptional repression autonomously in VPCs (Zhe Chen & Han, 2001).

1.3 Regulation of EGF/LIN-3 during vulva formation

C. elegans genome encodes for only one EGF family protein, the LIN-3 which is located on chromosome IV. LIN-3 protein contains an extra cellular domain with one EGF motif (50-60 AA), a trans-membrane domain and a cytoplasmic domain (Hill and Sternberg 1992). The N terminal cytoplasmic portion of LIN-3 is required for its general functionality and the C terminal portion regulates its tissue –specific activities (Liu et al., 1999). Alternative splicing within the *lin-3* locus spanning the EGF repeat and trans-membrane domains, in the region of exons 5 to 7, resulted in three splice variants, LIN-3S, LIN-3L and LIN-3XL (Dutt et al., 2004; Hill & Sternberg, 1992) (Figure 1.7). The two mutually exclusive splice variants, LIN-3XL and LIN-3L were resulted from the insertion of 41 and 15 amino acid residues, respectively, when compared to the LIN-3S. The LIN-3L variant results from the donor splicing region located at the 3' end of exon 6a and LIN-3XL results from the insertion of additional exon 6b between 6a and 7. Thus both LIN-3L and XL variants include the common region, 6a that encodes for LIN-3S variant. All the three LIN-3 isoforms were detected by RT-PCR during the time of AC induction at L2/L3 transition. But their tissue specific distribution during *C. elegans* development is unknown. The Rhomboid/ROM-1 regulates the activity of LIN-3L autonomously during vulva development. LIN-3 is cleaved in a ROM-1 dependent and later LIN-3 signal is propagated in a relay manner from proximal to distal VPCs (Dutt et al., 2004).

The molecular lesion within *lin-3* allele *e1417* is located in the regulatory region of *lin-3* and not in the coding sequences (Liu et al 1999). Accordingly, deletion analysis of *lin-3* locus, spanning the *e1417* lesion resulted in the loss of *lin-3* expression specifically in the AC (Hwang & Sternberg, 2004). Further biochemical and molecular studies identified 59 bp enhancer element within the *lin-3* regulatory region that is necessary for AC specific *lin-3* transcription. This anchor cell specific enhancer element (ACEL) is known to contain one nuclear hormone receptor (NHR) binding site and two E boxes (Figure 1.8). The *e1417* is mutated within the NHR binding site of ACEL. Mutations in E-boxes and NHR binding sites in the ACEL eliminated AC specific *lin-3* expression.

The Drosophila E-protein/daughterless homolog HLH-2 is expressed in the AC during *C. elegans* vulva formation. HLH-2 binds to the two E-boxes (CACCTG motif) in ACEL and post-embryonic RNAi treatment of *hlh-2* abolishes *lin-3::gfp* in the AC (Hwang and Sternberg 2004). The *C. elegans* FTZ-F1 family protein, NHR-25 binds specifically to the 'TCAAGGTCA' FTZ-F1 motif (Lavorgna et al 1991). The wild type ACEL sequence possesses homology to eight bases (TCA**G**GGTCA) within the FTZ-F1 motif and the *e1417* mutation has a substitution (G-A) at the 5^{th} base position within this motif (TCAG**A**GTCA). NHR-25 exists in two isoforms, α -FTZ-F1 and β-FTZ-F1 (Asahina et al., 2000; C R Gissendanner & Sluder, 2000). The β- form contains partially deleted DBD sequences and results in impairment of DNA binding ability of FTZ-F1. In EMSA based binding assays, α – form bound to wild type ACEL but not to the mutated *e1417* motif and β- form to neither of the probes (Hwang and Sternberg 2004). These results suggested that NHR-25 indeed binds to wild type ACEL and not to the mutated version. Surprisingly, post-embryonic RNAi of *nhr-25* does not abolish *lin-3::gfp* in the AC, suggesting that other NHR related genes in *C. elegans* (270*nhrs*) may be involved in this process.

1.4 Multiple developmental processes orchestrate vulva morphogenesis

The entire process of vulva morphogenesis occurs over a period of 20 hrs starting from late L3 (Pn.pxx) to L4 stage (Pn.pxxx) and involves similar mechanisms to common epithelial invaginations, such as; short range migrations, acquisition of polarities, cell shape changes accompanied by re-organization of adherens junctions and cell-cell fusion events (Estes & Hanna-Rose, 2009; A J Schindler & Sherwood, 2013; Sharma-Kishore et al., 1999; Shemer et al., 2000) (Figure 1.9).

1.4.1 Short range migrations and invariant cell divisions

At Pn.pxx stage, 12 daughter cells of P(5-7).p cells align themselves along the ventral hypodermis in anterior-posterior position (ABCD-EF/FE-DCBA) (Figure 1.9A). Later short range migrations of outer P5.pxx and P7.pxx cells towards the vulva midline results in upward movement of inner P6.pxx cells allowing them to detach from the ventral cuticle to leave a small lumen space (Estes and Hanna Rose 2009). This event is the hall mark of advent of vulva morphogenesis. Afterwards, P5.pxx and P7.pxx cells divide invariably, acquire crescent shapes and extend their adherens junctions laterally towards the midline to reach their contra-lateral homologs (Sharma kishore et al., 1999, Shemmer and Podbilewicz 2000, Figure 1.9C,D).

The stereotypical cell migrations of vulva cells are well coordinated through time and space. Each half of the vulva primordia develop independently of the other (Shrama kishore 1999 and Shemmer and Podbilewicz 2000). The vulval cells of the most dorsal toroid VulF play a key role in the regulation of midline oriented vulva cell migration and is referred as dorsal organizer. In absence of VulF and E cells, the next vulva cell type in the hierarchy VulD will become the dorsal organizer (Shemmer et al 2000). VulE cells divide first and extend their lateral projections towards the vulva midline along the ventral surface of VulF cells. Similar pattern is followed up by VulD, C, B1, B2 and A cell types

in a hierarchical manner. These cellular behaviors of the vulva primordia during migration are described as “collective vulva cell migrations” (Dalpe et al., 2005) (Figure 1.9C-E).

The final and terminal events of morphogenesis are revealed by the midline fusions of contra-lateral homologs of VulA to F in a temporal fashion to form syncytial toroidal rings, VulA to F, except VulB1 and B2 which never fuse with their homologs (Sharma kishore et al., 1999, Shemmer and Podbilewicz 2000, Figure 1.9F,G). These seven vulva toroids are arranged in a pyramidal manner along the proximal/ventral – distal/dorsal axis.

Thus the integration of stereotypic vulva cell divisions and migrations move the vulva cells from initial ventral positions to dorsally inwards to generate distinct dorsal (by VulE and F) and ventral lumens (by VulABCD). Finally, the uterine, sex muscles and seam cells make appropriate contacts with the toroids and ensure proper functioning of the egg-laying system (Schindler and Sherwood 2012).

1.4.2 Orientation of asymmetric cell divisions and polarities

During development, asymmetric cell division generates two different daughter cell types from a single mother cell. Vulva formation also involves asymmetric cell divisions. The daughters of P(5-7).p generate different vulva cell types by dividing asymmetrically at Pn.px. P(5,7).px cells will generate 4 cell types each which arrange themselves in mirror symmetric fashion (ABCD-DCBA). P6.px generates 4 cell types (EF-FE). The final pattern is represented as (AB-CD-EF/FE-DC-BA) where ‘/ ’ depicts the axis of symmetry (Figure 1.10).

For the establishment of EFFE pattern within 1^0 lineages a direct physical contact between VulF (F-F) cells and AC is required (Wang & Sternberg, 2000). For ABCD-DCBA pattern within 2^0 lineages two types of polarities establishments are required; default and refined (Green et al., 2008)The default polarity maintains ABCD-ABCD

orientation for both P5.p and P7.p daughters along the anterior-posterior axis. But refined polarity reverses the orientation of P7.p from ABCD to DCBA. So that the mirror asymmetry ABCD-DCBA is established. Wnt signaling plays crucial roles in both 1^0 and 2^0 lineages pattern and polarity formation and will be discussed later.

1.4.3 Vulva terminal differentiations

During the final and third round of vulva cell division the daughters of P(5-7).p undergo terminal differentiation process to develop into seven cell types VulA to F that constitute 22 cells arranged in AAB1B2CCDEEFFFFEEDCCB2B1AA fashion (Schindler and Sherwood 2012). Direct observations through nomarski optics helps in identifying terminal vulva cell positions. But in a mutant situation it is extremely difficult to specify the vulva cell lineages by position owing to perturbations in division axes, timing of cell divisions and altered migratory behaviors. To compensate for these inequalities GFP based reporter gene fusions were used as an alternative to lineage analysis. Spatio-temporal expression of various GFP fusion reporter genes was observed in certain vulva lineages and cell types during terminal differentiation process (Takao inoue et al., 2002). The expression analyses of these reporters in wild type and mutant animals facilitates cell type identity purely based on positive GFP expression in the corresponding cell types without any prior knowledge of their cell lineages and positional information.

Precise gene expression pattern associates with vulva cell fate pattering (Takao inoue et al., 2002). The FGF (Fibroblast Growth Factor) protein EGL-17 is temporally expressed in vulval cell lineages from Pn.p to Pn.pxxx stages (Burdine et al 1998). Late *egl-17* expression appears in VulC and D lineages of 2^0 cells beginning from early to mid L4 stages (Figure 1.11). The Zinc Metalloprotease protein, *zmp-1::gfp* expression was seen in VulD and E at late L4 stage and in Vul A in adults (Figure 1.11). The VulE expression is used as a read out for proper 1^0 cell fate specifications. The Nlpc family proten EGL-26 is also expressed in VulE and VulB from mid to late L4 stages (Estes et al., 2007; Hanna-

Rose & Han, 2002). The cadherin related protein CDH-3 is expressed in VulC, D, E and F beginning form L3 to adults (Pettitt et al., 1996). The EGF/LIN-3 is expressed in AC at the time of vulva induction process and later re-appears in VulF cells from early L4 stage onwards (Chang et al., 1999). The expression of *lin-3::gfp* in VulF is also used as a read out for proper 1^0 cell fate specifications. The Pax 2/5/8 family protein EGL-38 is also expressed in VulF (Fernandes & Sternberg, 2007; Ririe et al., 2008). The homeodomain protein belonging to Drosophila *empty spiracles, ceh-2* is expressed in VulB1 and B2 at L4 and in VulC during L4 lethargus (Jolene Fernandes 2007, T. inoue et al 2002).

Thus the mature vulval cell types VulA to F have distinct and precise pattern of gene expression code that attributes for proper vulva terminal differentiations.

1.5 Signaling pathways regulating vulva morphogenesis

1.5.1 Wnt signaling and vulva cell polarities

Wnt signaling plays crucial roles during the orientation of secondary vulva lineages (Gleason et al., 2006; Green et al., 2008; Inoue et al., 2004) (Figure 1.10). The default orientation of secondary vulva lineages P5.p and P7.p is to face posteriorly through ground polarity. But Wnt signaling re-orients the posterior P7.p lineages to face anteriorly through refined polarity. Wnt ligands EGL-20 expressed from the tail and MOM-2 expressed within AC and surrounding cells regulate these polarity events. At the receptor level both LIN-17/Fz and ROR family CAM-1 and LIN-18/Ryk and components of PCP pathway VANG-1 are involved (Green et al., 2008). At the signal transduction level, β-catenins BAR-1, LIT-1, SYS-1, WRM-1 and TCF homolog POP-1 are involved. These components work in concert both canonically through WNT/FZ/BAR-1/POP-1 and non-canonically through WNT/Ryk or ROR or Van Gough/SYS-1 or WRM-1 or LIT-1.

At Pn.px stage, POP-1 is localized in a high-low manner between VulA and B; VulC and D lineages stage and specifies proper mirror image cell fates (ABCD-DCBA) (Deshpande et al., 2005). Alteration in POP-1 localization results in mis-specification of cell fates, for example a high level of POP-1 in VulB changes its fate to VulA (ref). In *lin-17* and *lin-18* mutants, POP-1 localization is revered in P7.p lineages so that the cells acquire default ground polarities and the mirror symmetry is broken (ABCD – ABCD).

Cell ablation and mutant analysis aimed to understand the patterning of primary vulva lineages suggested that the preferential invasion of AC towards the inner P6.pxx cells makes them future VulF cells and the neighboring outer P6.pxx cells as future VulE cells, thus regulating E-F-F-E pattern formation (Wang & Sternberg, 2000). They also showed that the two halves of the primary lineages, [EF] and [FE] develop autonomously during development. The outer and inner cells possess intrinsic polarities and also can communicate with each other during the invariant E-F-F-E pattern formation. Ablation of AC specifically after AC induction i.e., at P6.px and P6.pxx stage resulted in abnormal expression pattern of *zmp-1::gfp* in VulE and F cells at P6.pxxx stage, suggesting alterations in E-F-F-E pattern formation. Similar results were seen in a situation where Ras signaling activity is reduced within vulva cells specifically after AC induction. Mutation in the Wnt receptor, *lin-17/fz* results in wild type patterning of primary vulva lineages. In the double mutant, *lin-17/fz* and *lin-18/ryk*, abnormal primary cell fate patterning was seen. Thus both Wnt and Ras signaling regulates EFFE pattern formation after AC induction.

1.5.2 GRNs governing vulva terminal differentiations

What factors regulate the differential gene expression within VulA to F cell types within vulva? RNAi based screens aimed to identify the gene regulatory networks governing vulva organogenesis resulted in two nuclear hormone receptors *nhr-67* and *nhr-113* as potential transcription factors regulating vulval cell fate patterning (Jolene Fernandes 2007, Ririe et al 2008,). *nhr-67* regulates cell fate pattering in multiple cell

types by forming a combinatorial regulatory code with *lin-11(LIM), cog-1* and *egl-38* (Jolene Fernandes 2007, Figure 1.12). *nhr-113* is known to regulate pattering of Vul A specific gene, *zmp-1::gfp* expression but does not regulate other expression markers, such as, *cdh-3, ceh-2* and *lin-3* (Ririe et al 2008). The heterochronic gene LIN-29 that functions in developmental regulation of L4-adult transition is also known to regulate gene expression pattern in vulva cell types (Jolene Fernandes 2007, Ririe et al 2008, T. inoue et al 2002). LIN-29 regulates the expression of *egl-17* in VulC and D, *ceh-2* in VulC, and *zmp-1* in VulD and E during mid L4 stage but does not regulate *lin-3* expression in VulF (Ririe et al 2008). *nhr-67* regulates VulF *lin-3* expression positively. *vab-23* also positively regulates VulF/*lin-3* and VulE/*egl-26* expressions (Pellegrino et al., 2011).

1.5.3 SMP-1/PLX-1 system

Specific ligand-receptor interactions at the cell membrane triggers cell migration process. The conserved family of type I transmembrane proteins, the semaphorins interacts with their receptors, plexins (Plexin 1A family) to regulate diverse morphogenetic events, such as, axon guidance, cardiac development and growth of endothelial cells (Kruger et al., 2005). Translational control of cytoskeletal proteins was identified as the key mechanism by which semaphorin-plexin interactions target mRNA molecules of RhoA (Wu et al., 2005), β-actin (Leung et al., 2006)and ADF/cofilin (Piper et al., 2006). During *C. elegans* male tail development, the semaphorin-plexin system targets phosphorylation of elF-α and regulates translation of UNC-60/Cofilin to mediate ray morphogenesis (Nukazuka et al., 2008).

The SMP-1/PLX-1 system in *C. elegans* also regulates seam cell and vulva morphogenesis (Dalpé et al, 2005; Fujii et al., 2002; Z. Liu et al., 2005). The spatio-temporal expression pattern of SMP-1/PLX-1 GFP reporters corresponds with the cellular migration behavior of vulva primordia (Dalpe et al., 2005, Figure 1.13). The dorsal organizer VulF initiates SMP-1 expression on the lumen facing side of vulva cells to

attract PLX-1 expressing VulE cells. Once VulE reaches the midline, it switches on SMP-1 expression and attracts the neighboring VulD through PLX-1. This cycle of SMP-1/PLX-1 attraction repeats until the remaining secondary vulva cells (Vul C, B and A) migrate to the midline and align themselves in a pyramidal manner. In accordance with this model mis-expression of SMP-1 through *plx-1* promoter in the secondary vulva cells results in two SMP-1 organizers, peripheral artificial SMP-1 levels away from the midline and inner endogenous SMP-1 levels at the midline. In this scenario, the vulva cells that are aligned between two SMP-1 signals show confused state of migration (Dalpe et al., 2005).

Smp-1(ev715) and *plx-1(ev724)* presumptive null mutants show partial penetrance levels for vulva defects where the outer secondary cells failed to migrate towards the vulva midline. Genetic epistasis studies suggested that *ced-10* acts in the same pathway as *smp-1/plx-1* and *mig-2* and *unc-73* work in other parallel pathways (Dalpe et al., 2005).

1.5.4 RAC/RHO system

Collective cell movements during cell migration and morphogenesis involve re-arrangements of actin cytoskeleton within the cytoplasm and initiation of transcription of genes responsible for cell migration with in the nucleus. Studies from mammalian cell migration systems identified RAC family GTPase molecules as key players in regulating cell migration processes (Tapon & Hall, 1997). The *C. elegans* Rac proteins, CED-10 and MIG-2 were identified to redundantly control orientation of division axes and secondary vulva cell migration during vulva fate execution and migration processes, respectively (Kishore & Sundaram, 2002) (Figure 1.13). The guanine nucleotide exchange factor, UNC-73*/Trio* regulates CED-10 and MIG-2 activities during this process.

1.5.5 LET-60/Ras signal

In addition to regulating cellular fates *let-60* also helps in the extension of filopodia during vulva cell migration and in intra-toroidal fusions during vulva morphogenesis (Shemmer and Podbilewicz 2000). In *let-60(gf)* animals, a subset of vulva cells showed abnormal cell fusions and migrations (Shemmer and Podbilewicz 2000). Especially the outer secondary cells, VulA and B failed to direct their midline oriented cell migrations. Thus the ectopic activation of *let-60* perturbs vulva morphogenesis and provides a first indication that continuous activity of EGF/Ras/MAPK is necessary for vulva organogenesis.

1.5.6 LIN-39/Hox and its effectors

The *C. elegans* LIN-39/HOX activity is regulated by multiple signaling inputs, such as Egf, Wnt and synmuv pathways to ensure proper vulva cell fusions, competence, induction and morphogenesis events (Clark et al., 1993; Maloof & Kenyon, 1998; Pellegrino et al., 2011; Gidi Shemer & Podbilewicz, 2002). LIN-39 binds to its cofactors and effectors through the conserved HOX/PBX domains 'TGATNNAT' to regulate development (Jiang et al., 2009). It interacts with CEH-20/PBX and UNC-62/MEIS and the Zinc Finger Transcription factor VAB-23 during vulva cell migrations and morphogenesis (Jiang et al., 2009, Pellegrino et al., 2011).

Before vulva inductions, *lin-39* activity within P(3-8).p cells renders them competent to respond to vulva signals. In *lin-39(lf)* situation, P(3-8).p cells fuse with hypodermis and lose their vulva competence. This fusion event is regulated by fusogen EFF-1 (Gidi Shemer & Podbilewicz, 2002). LIN-39 inhibits EFF-1 activity to inhibit Pn.p cell fusion. After vulva inductions, LIN-39 is upregulated by EGF/Ras/MAPK pathway and regulates competence of P(5-7).p cells to adopt 2^0-1^0-2^0 fates. This event is also maintained by preventing fusion of vulva cells to hypodermis. In *lin-39(lf); eff-1(lf)* situation, P(5-7).p cells escaped fusions but failed to proliferate and prematurely stopped their cell divisions. Surprisingly these non-proliferative cells were able to differentiate terminally and

develop into toroids. Thus LIN-39 regulates multiple events during vulva formation at multiple times.

VAB-23 is the direct target of LIN-39 and its cofactor CEH-20. LIN-39 regulates VAB-23 expression positively during early and later vulva morphogenesis events. This interaction is mediated by EGF/Ras/MAPK pathway that acts upstream of LIN-39. In turn, VAB-23 regulates SMP-1 expression during vulva cell guidance (Figure 1.13). *Vab-23* mutants show abnormal vulva cell contacts, toroidal fusions and defective vulva cell migrations towards the midline (Pellegrino et al., 2011). VAB-23 down-regulates *smp-1::gfp* expression during vulva morphogenesis. Smp-1 is a direct transcriptional target for VAB-23 and its promoter contains VAB-23 binding sites. Both VAB-23 and SMP-1 have similar expression pattern during vulva formation and their loss-of-function mutations show similar phenotypes for vulva migration defects.

1.5.7 LET-502/ROCK and actomyosin contractions

What changes in cytoskeleton constitute vulva cell migrations and how are they regulated? Rho-associated protein kinase (ROCK) family member LET-502 generates the actomyosin contractions that initiate vulva dorsal migrations (Farooqui et al., 2012) (Figure 1.14). EGF/Ras/MAPK and NOTCH pathways regulate LET-502 activity. The LIN-12/NOTCH signaling upregulates LET-502 (ROCK) within secondary vulva cells through non-phosphorylated LIN-1 (Farooqui et al., 2012). This results in midline oriented secondary cell migrations. In primary lineages, EGF/Ras/MAPK pathway down-regulates LET-502 to allow their expansion to facilitate their fusion with AC during L4 stage. Thus both the primary and secondary vulva pathways antagonize each other to regulate LET-502 expression to ensure proper vulva morphogenesis. This study provides concrete evidence that same signaling pathways involved in initial vulva cell fate specifications have additional roles in fate execution process at a later time during vulva organogenesis.

1.6 Nuclear hormone receptors

1.6.1 General Overview

Nuclear Hormone Receptors (NHRs) are special kind of transcription factors (TFs) that regulate gene expression either positively or negatively (Antebi 2006) (Figure 1.15). The molecular structure of NHRs is conserved across metazoans and contains N-terminal DNA binding domain (DBD) and C-terminal Ligand Binding Domain (LBD). The DBD consists of two Cys4 Zinc Finger domains and LBD contains multiple domains that can bind several co-activators and co-repressor molecules.

NHRs are activated by ligands of lipophilic properties such as, steroids, retinoids, thyroid hormones, and farsenoids, etc. Binding of these ligands to receptor LBDs results in homo or heterodimerization followed by confirmation changes within C- terminal transactivation helix (AF-2) that results in functional consequences. NHRs mediate diverse biological processes during physiology, development, metabolism and xenobiotics (Antebi 2006).

NHR family is sub-divided into six classes NR1-NR6 based on sequence comparisons and phylogenetic analyses across metazoan (Laudet, 1997). Humans consists of 48 NHRs and Drosophila 21. Surprisingly, NHR family in *C. elegans* is largely expanded and consists of 284 receptors with 15 orthologs to humans and flies (Antebi, 2006; Chris R. Gissendanner et al., 2004). *C. elegans* NHRs regulate molting, sex determination, dauer formation, and many developmental and metabolic processes.

1.6.2 Orphan nuclear receptor NHR-25

Sub-family of NHRs called orphan nuclear hormone receptors are regulated by ligands of unknown origin or no ligands at all. One of the orphan family member NHR-25 is genetically well studied in *C. elegans*. NHR-25 possesses unique DBD domain

called Ftz-F1 and belongs to Nuclear Receptor sub-family 5 group A (NR5A). NHR-25 exists in two isoforms α and β. α-Ftz-F1 regulates embryogenesis and β-Ftz-F1 molting and larval metamorphosis (Ueda et al.,1990; Yu et al., 1997).

Drosophila *fushi tarazu* (Ftz-F1), mammalian steroidogenic factor-1 (SF-1) and liver receptor homolog-1 (LRH-1) are orthologs to NHR-25. SF-1 regulates steroidogenesis, development of gonad and adrenal gland (Parker et al., 2002). LRH-1 controls bile metabolism and cholesterol homeostasis (Fayard et al., 2004)).

1.6.3 Developmental roles and interactions of NHR-25 in *C. elegans*

NHR-25 regulates multiple developmental processes in *C. elegans*. Null mutations of *nhr-25* results in severe embryonic lethality (*emb*) (Asahina et al., 2000; C R Gissendanner & Sluder, 2000). To further analyze roles of NHR-25 in post-embryonic development, genetic studies were carried through *nhr-25(RNAi)* and hypomorphic allele *nhr-25(ku217)* which cause less severe *emb* defects.

NHR-25 maintains cell-shape dynamics during the differentiation of seam cells (Silhánková et al., 2005). Seam cells undergo asymmetric cell divisions. After each division, the daughter cells renew their adherens junctions to elongate and reach their neighbors. This process of cell-cell contacts is necessary to maintain proper seam cell fate specifications. NHR-25 activity is necessary to maintain seam cell-cell contacts and thus cell fates. *Nhr-25(RNAi)* results in defective seam cell fates through disrupting cell contacts. *Nhr-25* also interacts with heterochronic gene *lin-29* to regulate proper seam cell proliferations during larval to adult transition (Hada et al., 2010).

NHR-25 regulates cell fate decisions during gonad development (Asahina et al., 2006) (Figure 1.16). *C. elegans* gonad is formed from the asymmetric cell divisions of the somatic gonad precursor cells (SGPs). Daughters of SGPs, Z1 and Z4 differentiate to

distal tip cells (DTCs) to establish a distal axis. Daughters of SGPs, Z2 and Z3 differentiate to anchor cell (AC) to establish a proximal axis. NHR-25 interacts with Wnt signaling components during gonad differentiation. WRM-1/β-catenin, SYS-1/β-catenin and POP-1/TCF regulate proximal fates of SGPs. Reciprocal asymmetric localization of SYS-1 and POP-1 in SGPs maintains proper gonad differentiations. *nhr-25(RNAi)* results in proximal to distal fate transformation and thus produces extra DTCs. Loss-of-function of single mutants of *pop-1, sys-1 and wrm-1* results in the opposite, a distal to proximal fate transformation and thus loss of DTCs. *nhr-25(RNAi)* rescues *pop-1(q645)* defects and thus DTCs formation. Thus NHR-25 antagonizes Wnt pathway during gonad differentiation. Wnt/β-catenin pathway also regulates asymmetric cell divisions during T cell differentiation in male tail development. Surprisingly, *nhr-25(lf)* enhances the T cell defects of *pop-1* and *sys-1* and thus cooperates with Wnt signaling (Hajduskova et al., 2009). This genetic interaction is opposite of the situation during gonad development. Thus depending on the tissue context NHR-25 can either synergize or antagonize Wnt/β-catenin pathway.

NHR-25 regulates cell fusion and morphogenesis events during vulva formation. P(3-8).p cells are competent to respond to AC signal. But their sister cells, P(1,2).p and P(9-11).p show no competence and fuse with hypodermis. These fusion events happen before AC induction at L1 stage and are regulated by three hox genes *lin-39*, *mab-5* and *nob-1*. Both *nhr-25(RNAi)* and *nhr-2(ku217)* results in abrupt fusion of P(3-8).p cells to hypodermis at L1 stage. At later stage and after AC induction, *nhr-25(lf)* animals show abnormal vulva cell proliferations, changes in axis of division and toroidal fusions (Z Chen et al., 2004). NHR-25 binds to HOX proteins LIN-39 and NOB-1 *in vitro* (Z Chen et al., 2004). NHR-25 acts independent of LIN-39 during L1 fusions but possibly cooperates with it to regulate vulva cell proliferations.

Gene regulation studies at the level of post-translational modifications from mammalian SF-1 showed that SUMO modification or sumoylation is an important regulatory mechanism of nuclear receptor function (W. Y. Chen et al., 2004). Sumo

attaches to lysine **(**Ψ-K-X-E) in target protein molecules by which their transcriptional activity and localization properties are affected (Figure 1.17). NHR-25 has four potential sumo consensus motifs **(**Ψ-K-X-E) (See Chapter 3). Only one sumo mutant was isolated in *C. elegans, smo-1(ok359)* and is known to regulate vulval development and gonad morphogenesis (Broday et al., 2004; Leight et al., 2005).

Figure 1.1 *C. elegans* life cycle and larval stages.

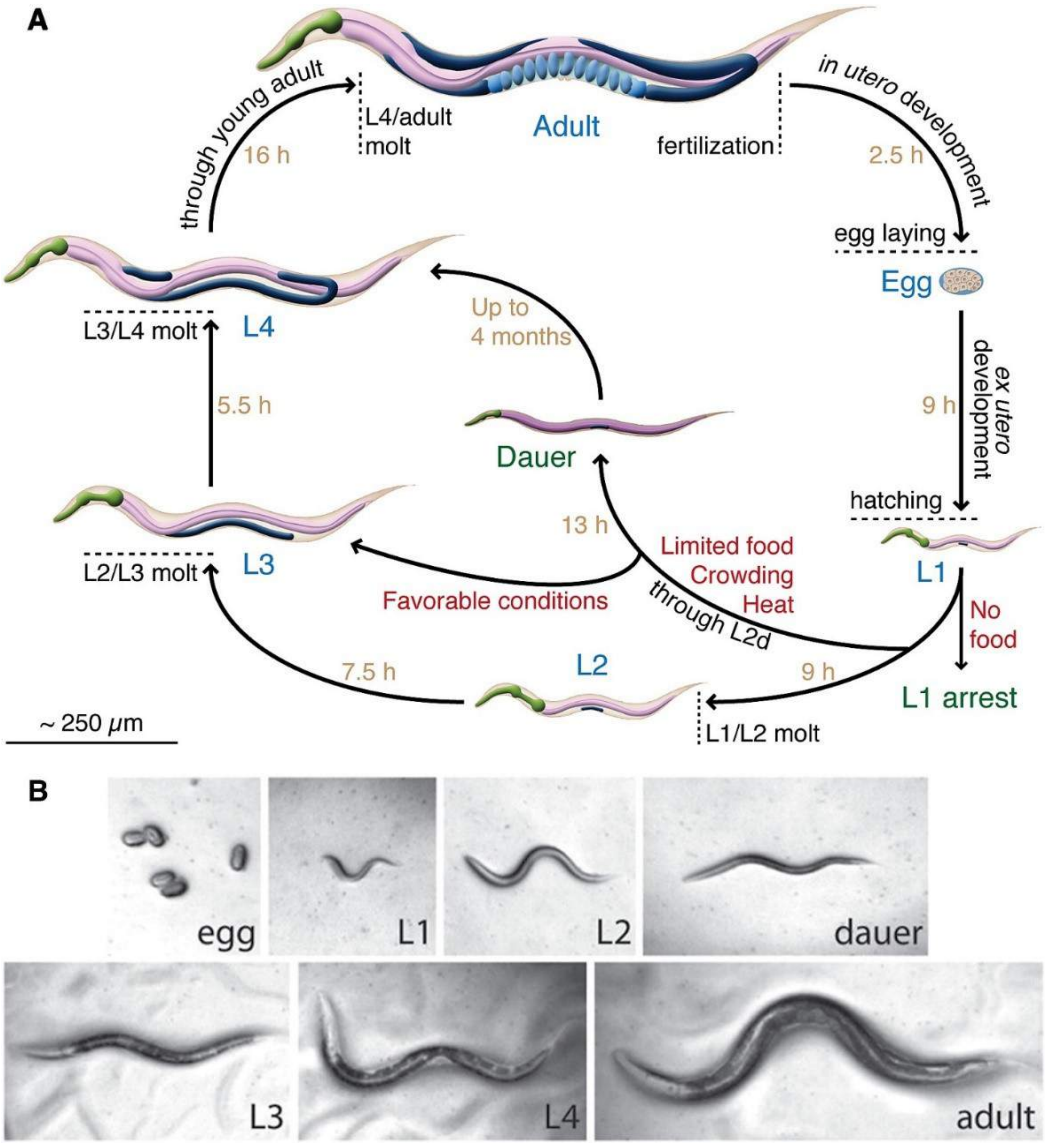

***C. elegans* life cycle and larval stages.** *C. elegans* transits from egg to adult through four larval stages, L1 to L4 in 3.5 days at 25^0 C. The larval transition involves molting followed by growth and development. L1-L4 larvae are distinguished by their body size. In unfavorable conditions, L1 larvae exits from normal life cycle to become dauer larvae which can survive up-to 4 months without food. (Adapted from Erkut, 2014).

Figure 1.2 Vulva cell fates and lineages.

(A) DIC images of adult *C. elegans* and close-up view of vulval structure which positions at the mid-body. Ut, uterus and Sp, spermathecae. (B,C,D,E and F) Depicts cartoon illustrations and the corresponding DIC images of Pn.p cell positions and their lineages during larval development. AC, anchor cell. P(5-7).p cells adopt 2-1-2 fates and develop into VulA to F cell types through 3 rounds of cell division. In (B) the cells are at Pn.p stage, (C) Pn.px stage, (D) Pn.pxx stage and in (E) Pn.pxxx stage where 'x' denotes the stage of cell cycle. (Adapted from Schindler and Sherwood 2013)

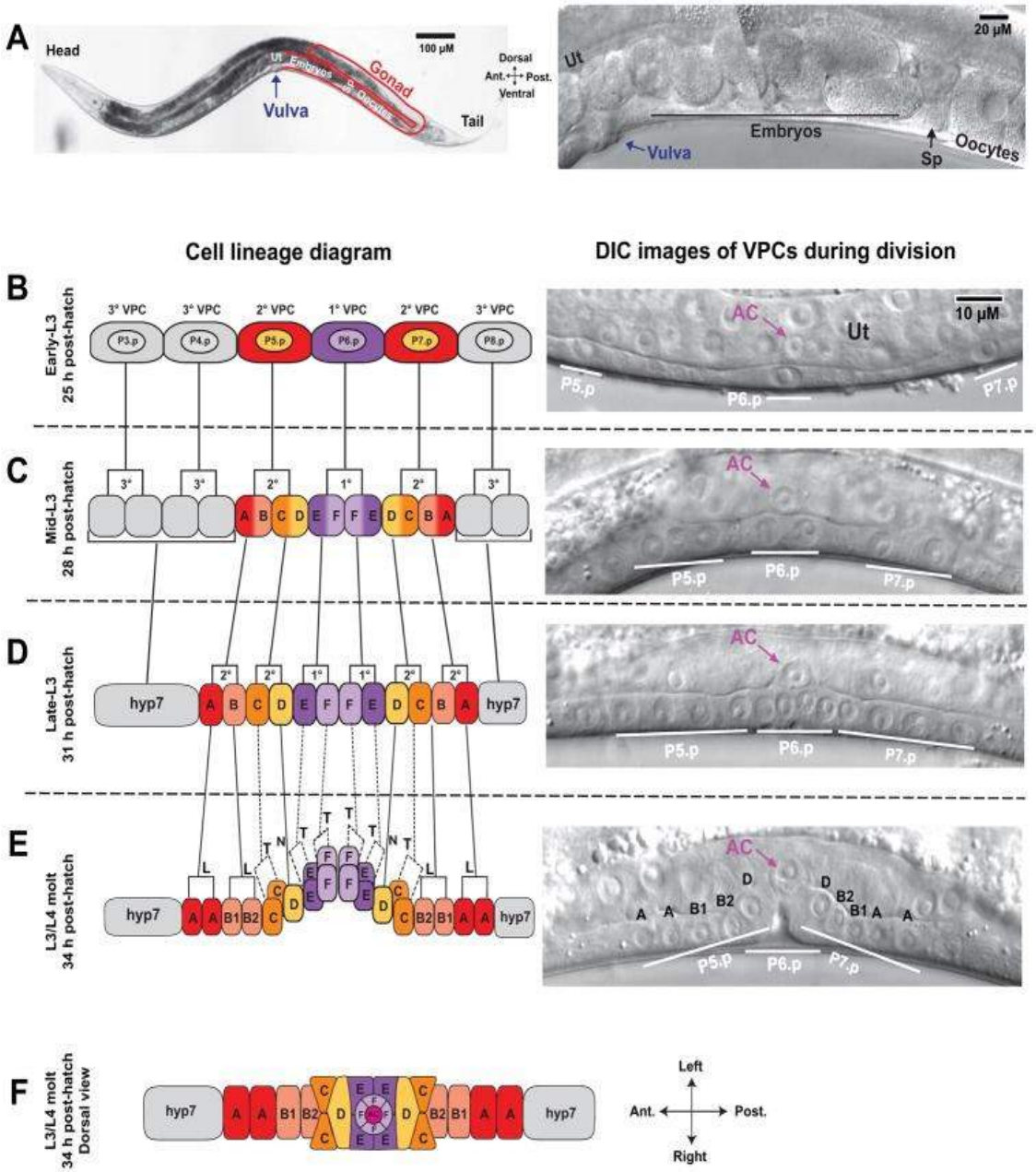
A
Head
Tail
Vulva
Gonad
Ut
Embryos
Sp
Oocytes
100 µM
Dorsal
Ant. Post.
Ventral
20 µM
Embryos
Vulva
Cell lineage diagram
DIC images of VPCs during division
B
Early-L3
25 h post-hatch
3° VPC
3° VPC
2° VPC
1° VPC
2° VPC
3° VPC
P3.p
P4.p
P5.p
P6.p
P7.p
P8.p
AC
Ut
10 µM
P5.p
P6.p
P7.p
C
Mid-L3
28 h post-hatch
3°
3°
2°
1°
2°
3°
A B C D E F F E D C B A
D
Late-L3
31 h post-hatch
hyp7
2° 2° 2° 1° 1° 2° 2°
A B C D E F F E D C B A
hyp7
E
L3/L4 molt
34 h post-hatch
hyp7
A A B1 B2 C D E F F E F F E D C B2 B1 A A hyp7
D
B2
B1
F
L3/L4 molt
34 h post-hatch
Dorsal view
hyp7
A A B1 B2 C D E F F E D C B2 B1 A A hyp7
Left
Ant.
Post.
Right

Figure 1.3 Ras signaling pathway is involved in vulva formation.

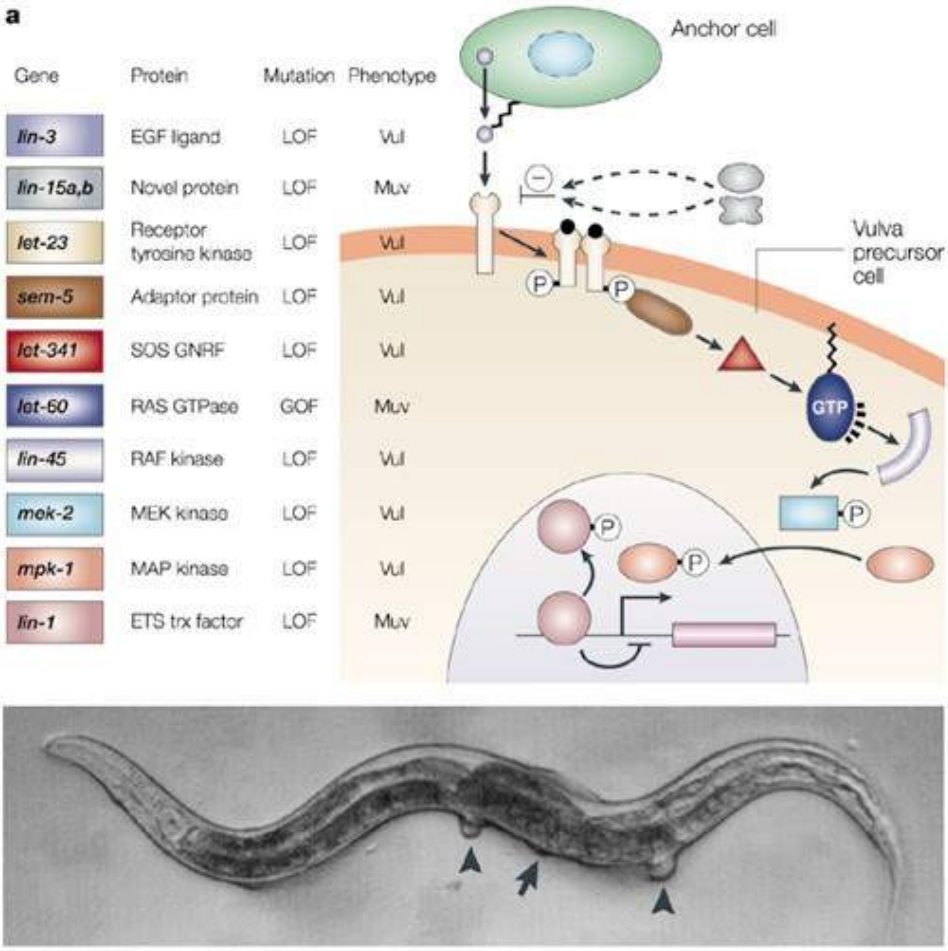

Ras signaling pathway is involved in vulva formation.

The Anchor cell (AC) secretes LIN-3. The VPCs receive LIN-3 signal through LET-23. Components of Ras signals further transduce the signals to regulate the activity of LIN-1 transcription factor. LOF – Loss Of Function situation of the pathway produces vulvaless, *Vul* animals and constitutive activation or GOF – Gain Of Function in multivulva, *Muv*. The DIC adult animal is a classic example of muv, where extra bumps (arrow heads) called as pseuovulvae represent ectopic inductions along with central vulva (arrow). (Adapted from Jorgensen & Mango, 2002).

Figure 1.4 Temporal expression pattern of *egl-17* in vulva.

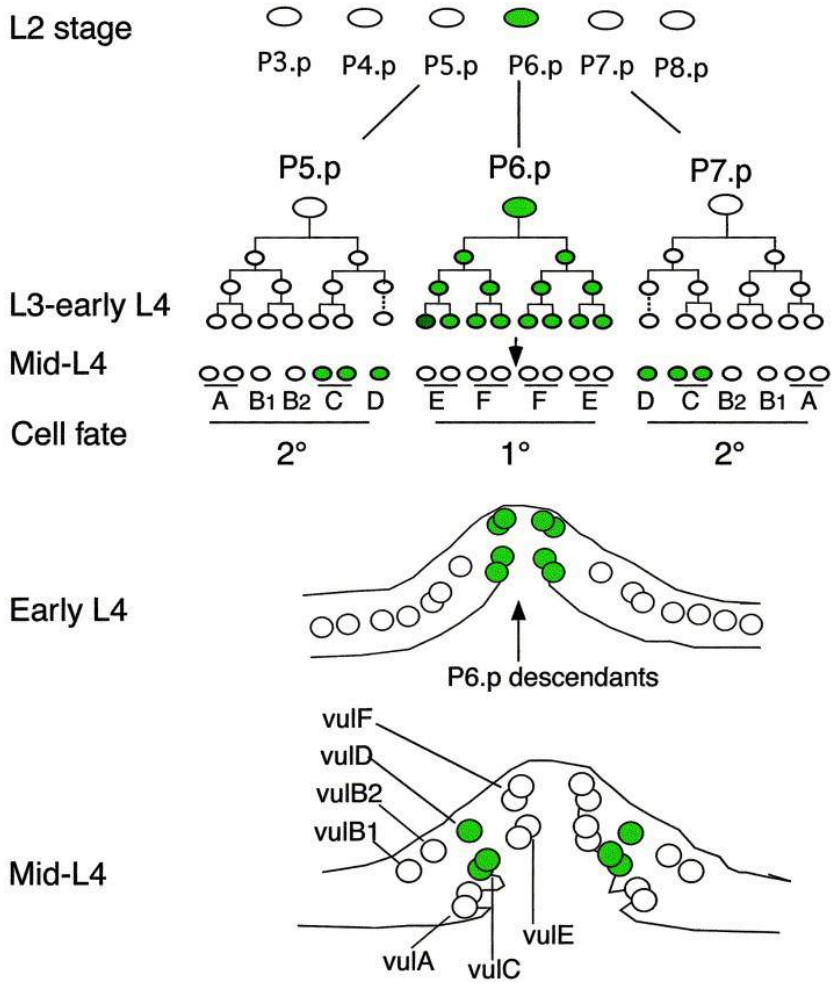

Temporal expression pattern of *egl-17* in vulva.

Inductive signaling upregulates *egl-17* in P6.p lineages from L3 to early L4 stages. Later this expression disappears at midL4 stage and is restricted to VulC and D lineages.(Adapted from Cui and Han 2003).

Figure 1.5 Cross talk between Ras and Notch regulates vulva cell fate patterning.

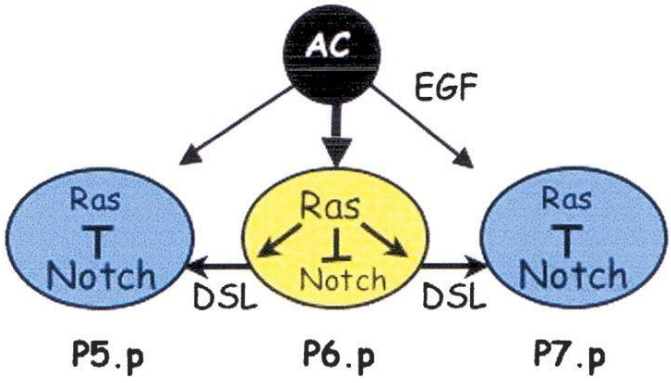

Cross talk between Ras and Notch regulates vulva cell fate patterning.

Activation of EGF pathway upregulates Ras in P6.p (yellow). Later the differentiated P6.p activates DSL/LAG-2 ligands that activate Notch in P(5,7).p cells (blue). Thus P6.p adopts the first fate (1^0) and P(5,7).p adopt the next secondary (2^0) fates.

(Adapted from Sundaram, 2005).

Figure 1.6 Synmuv genes redundantly regulate LIN-3 expression and vulva inductions.

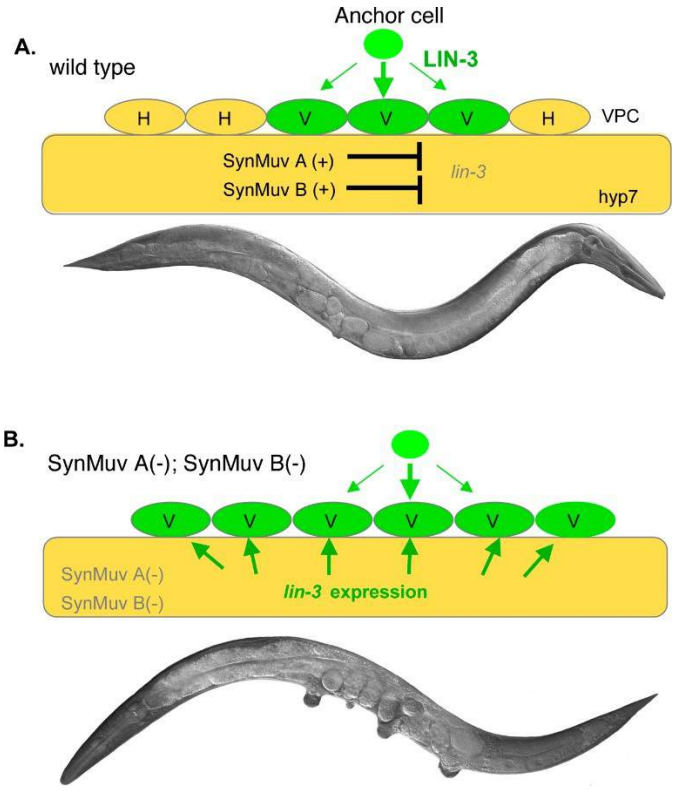

Synmuv genes redundantly regulate LIN-3 expression and vulva inductions. AC signal acts as a morphogen and induces vulva fates in P(5-7).p cells (V). The remaining three VPCs (H) divide once and fuse with hypodermis. In lf of both SynMuv A and B, *lin-3* is de-repressed from hypodermis (hyp7) resulting in all the six VPCs to adopt vulval fates. (Adapted from Mingxue Cui and Min Han 2006).

Figure 1.7 Alternate splicing generates three LIN-3 isoforms

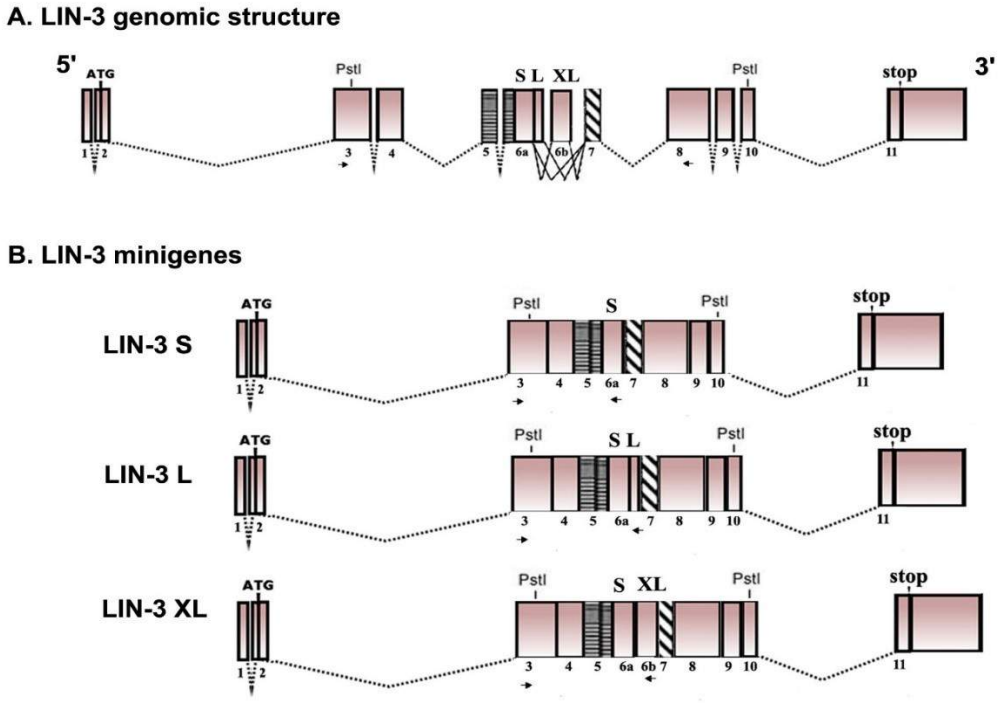

Alternate splicing generates three LIN-3 isoforms.

(A) The architecture of *lin-3* genomic region with intron-exon boundaries was adopted from Dutt et.al., 2004 and re-drawn using fancygene (*Rambaldi D. and Ciccarelli F.D.* 2009). The EGF repeat that occupies exon 5 and part of exon 6a. The trans-membrane domain in the exon 7. (B) Alternative splicing within the *lin-3* locus spanning the EGF repeat and trans-membrane domains, resulted in three splice variants or minigenes, LIN-3S, LIN-3L and LIN-3XL.

Figure 1.8 Model representing regulation of *lin-3* expression in AC.

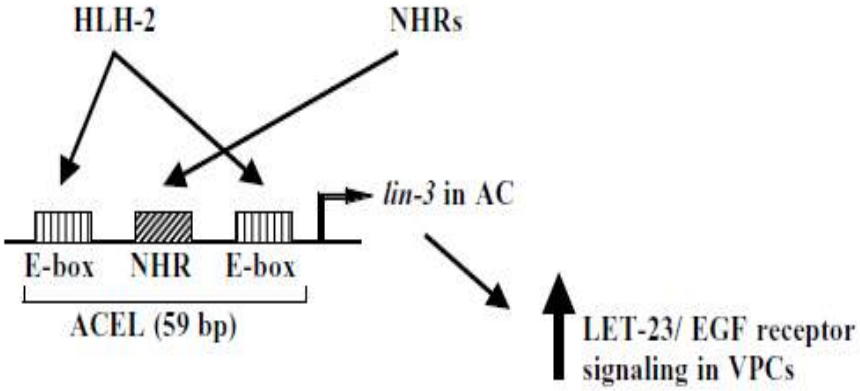

Model representing regulation of *lin-3* expression in AC.
The 59 bp enhancer element contains one FTZ-F1 NHR binding site and two E-boxes. HLH-2 binds to E-boxes and unknown NHRs bind to NHR box to regulate AC specific *lin-3* expression that activates LET-23 signaling in VPCs. (Adapted from Wang and Sternberg 2000).

Figure 1.9 Vulva cell migrations, homotypic fusions and toroid formation.

(A) During the first two rounds of cell divisions, P(5-7).p cells and their daughters divide longitudinally (L) resulting in 12 daughter cells that arrange themselves in bilateral symmetry along the anterior-posterior axis (ABCD-EFFE-DCBA). **(B)** Short range migrations of outer P5.pxx cells (A,B,C and D) towards the midline pushes inner P6.pxx cells (E and F) to move them dorsally. **(C,D and E)** Further stereotypic cell shape changes and migrations towards the midline moves initiates further dorsal movements. **(F)** Lateral view of mid-L4 stage vulva with typical Christmas tree morphology. The DIC image shows the position of 22 vulva cells and the fluorescence images shows the morphology of vulva toroids. VulF position at the top dorsal and VulA at the bottom ventral. **(G)** Terminally, the vulva cell types on either side of the midline recognize their counter-homologs and fuse temporally to form complete vulva toroids or rings. Except VulB1 and B2 which do not fuse. All the vuvla cell types are syncytial with VulF,E,C and A have 4 nuclei and VulB1,B2 and D have 2 nuclei (shaded circles with toroids). Ut, uterus. (Adapted from Schindler and Sherwood 2013).

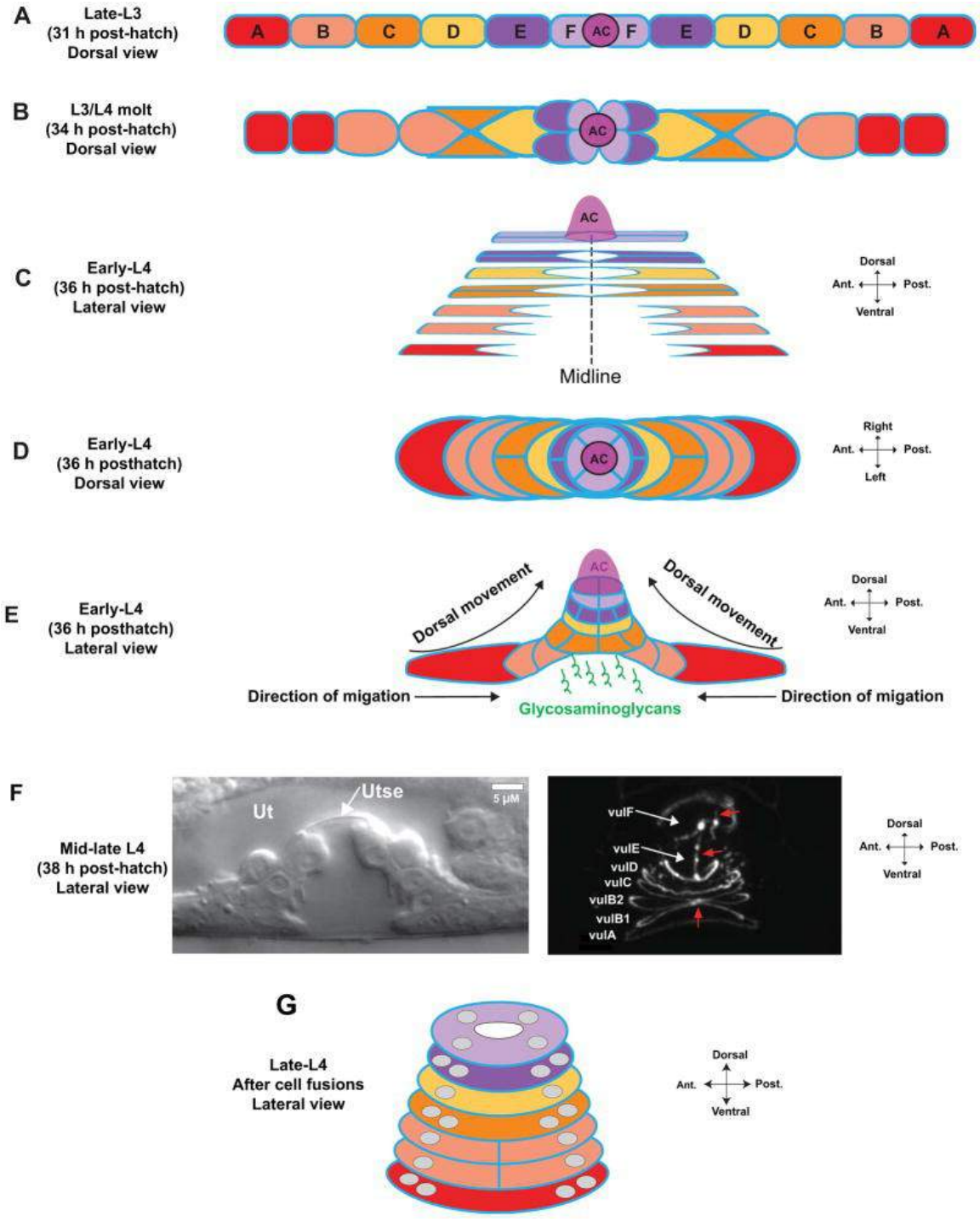
A
Late-L3
(31 h post-hatch)
Dorsal view
A B C D E F AC F E D C B A
B
L3/L4 molt
(34 h post-hatch)
Dorsal view
AC
C
Early-L4
(36 h post-hatch)
Lateral view
AC
Midline
Dorsal
Ant. Post.
Ventral
D
Early-L4
(36 h posthatch)
Dorsal view
AC
Right
Ant. Post.
Left
E
Early-L4
(36 h posthatch)
Lateral view
AC
Dorsal movement
Dorsal movement
Direction of migation
Direction of migation
Glycosaminoglycans
Dorsal
Ant. Post.
Ventral
F
Mid-late L4
(38 h post-hatch)
Lateral view
Ut
Utse
5 µM
vulF
vulE
vulD
vulC
vulB2
vulB1
vulA
Dorsal
Ant. Post.
Ventral
G
Late-L4
After cell fusions
Lateral view
Dorsal
Ant. Post.
Ventral

Figure 1.10 Wnt signaling regulates vulva cell polarities.

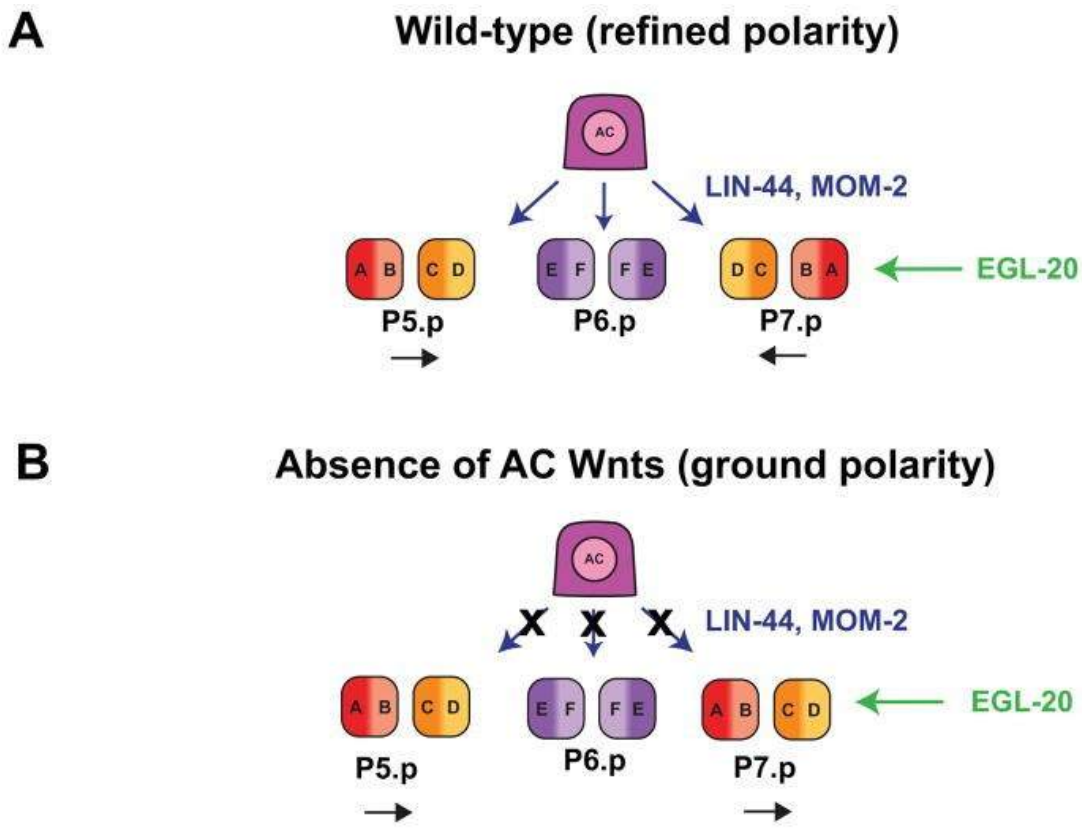

Wnt signaling regulates vulva cell polarities.
Wnts work in concert to regulate refined polarity and their absence defines ground polarity. AC produces Wnt ligands LIN-44 and MOM-2 and EGL-20 is secreted from tail region (Adapted from Schindler and Sherwood 2013).

.

Figure 1.11 Expression profile of vulva terminal differentiation markers *egl-17* and *zmp-1*.

Egl-17 is expressed from midL4 state onwards and *zmp-1* from late L4 to young adults (adapted from Inoue et al., 2002).

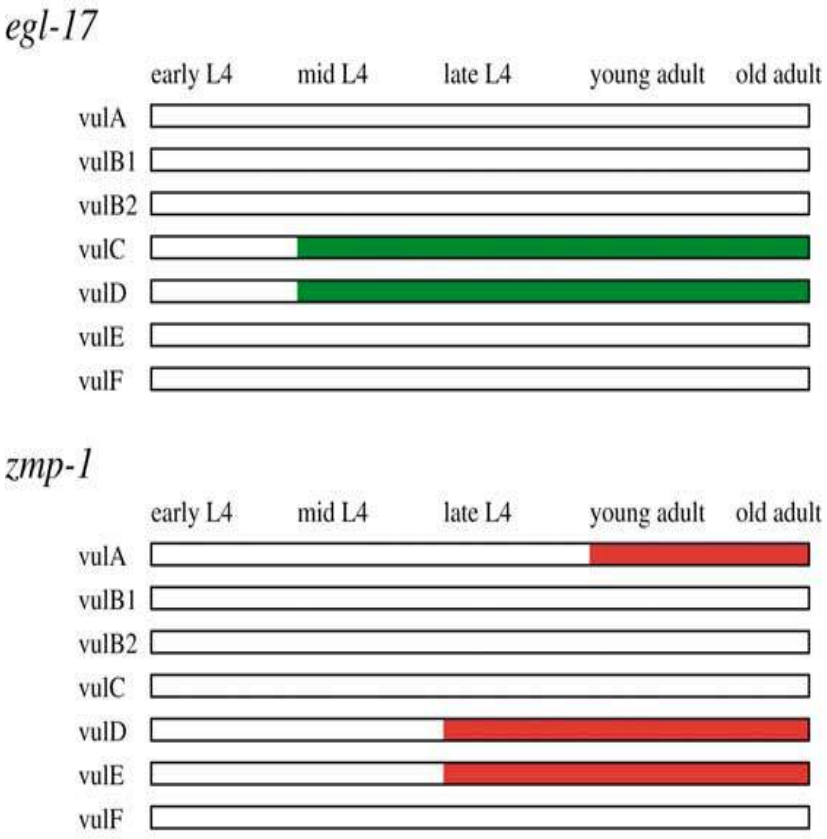

Figure 1.12 Nhr-67 controls Gene Regulatory Networks (GRNs) that govern terminal differentiations.

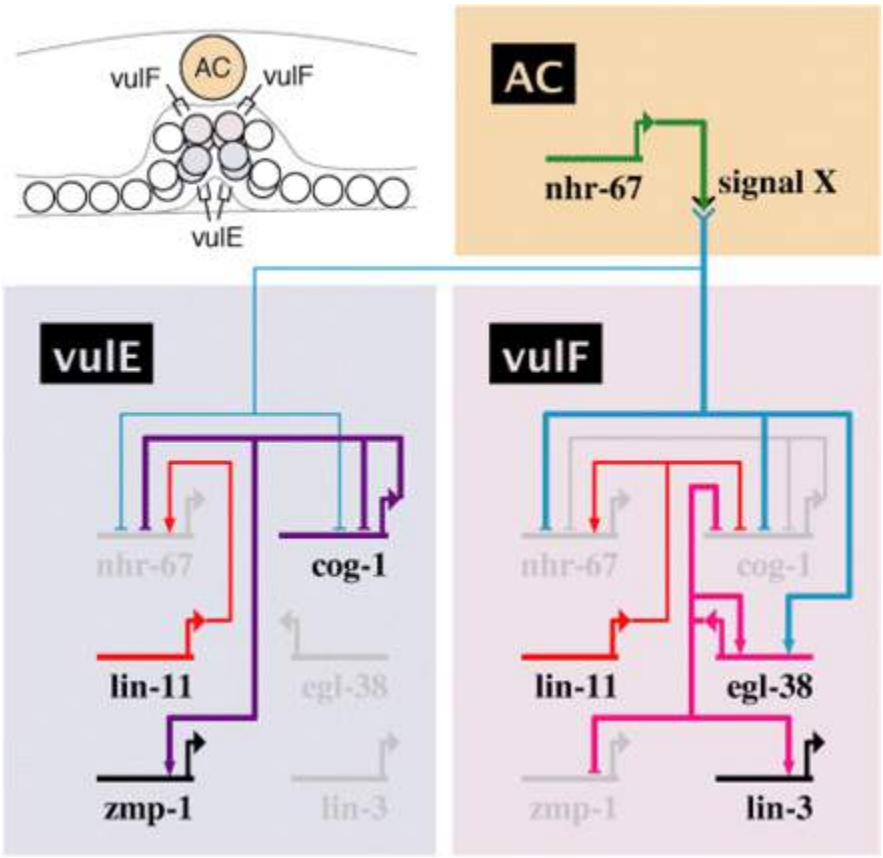

Nhr-67 controls Gene Regulatory Networks (GRNs) that govern terminal differentiations.

Nhr-67 expression from AC regulates distinct networks in VulE and F and helps in proper differentiation of each cell type. Network modules are generated by BioTapestry Editor, Version 2.1.0 (www.biotapestry.org). Bars indicate negative regulations and arrows indicate positive regulations (adapted from Fernandes and Sternberg 2007).

Figure 1.13 Signaling pathways regulating vulva cell migrations.

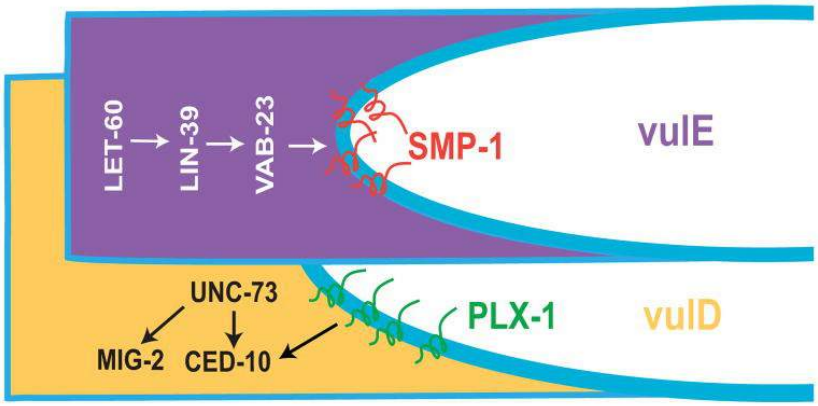

Signaling pathways regulating vulva cell migrations.
VulE expresses SMP-1 at its lumen facing side. The neighboring cell VulD follows similar expression pattern for PLX-1. SMP-1/PLX-1 interactions allow the cells to migrate towards the midline by activating Rac GTPase CED-10 and GEG UNC-73. SMP-1 expression at the midline is regulated by Ras LET-60 through HOX LIN-39 and VAB-23. Another parallel pathway regulated by MIG-2 is also involved in cell migration (Adapted from Schindler and Sherwood 2013).

Figure 1.14 Vulva toroid contractions and expansions mediated by actomyosin myofibrils.

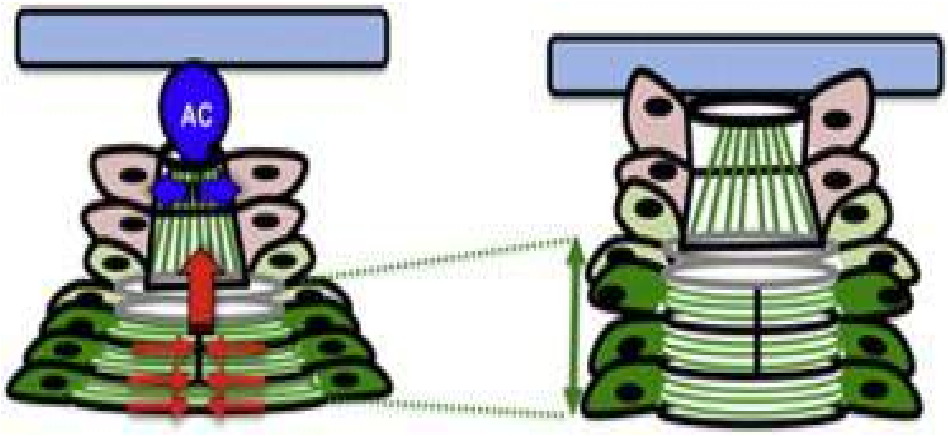

Vulva toroid contractions and expansions mediated by actomyosin myofibrils. Cell bodies in light red represent 1° VulF and VulE toroids, light green 2° VulD and VulC, and in dark green of VulB2, VulB1, and VulA. Actomyosin myofibrils (MFs) are shown in green lines and black and gray lines represent apical cell junctions. Rho kinase LET-502 regulates apical contractions of VulA, VulB, and VulB2 toroids which results in a dorsal pushing force (red arrows). Meanwhile invasion of the AC (dark blue) into the 1° toroids allow expansion of the dorsal toroid lumen (blue arrows). At the end, the AC fuses with the utse (light blue) to allow the attachments of toroids to the utse. Utse, uterine seam cell (adapted from Farooqui et al., 2012).

Figure 1.15 Structure and functions of NHRs.

(A) DNA binding domain of NHRs is composed of two Cys4 Zn fingers. DNA binding specificity is confirmed by typical P-box, (CEGCKG). Multiple coactivators and corepressors dock at the ligand binding domain. During hormonal activation the AF-2 transactivation helix allows closure of the ligand binding pocket. (B) Green triangle represent hormones. Hormonal activation results in binding of NRs to their hormone response elements (HREs). This results in assembly of coactivator complexes that regulates acetylation (ac, p300,etc) or methylation (me, CARM1, etc) of nucleosomes (NUC). Additional Mediator proteins associates with NRs to facilitate the recruitment of the basal transcription machinery, which turns on gene expression. In the absence of hormone, NRs associate with corepressor complexes, such as SMRT and NCoR to recruit histone deacetylases (HDACs) and represses gene transcription (adapted from Antebi 2006).

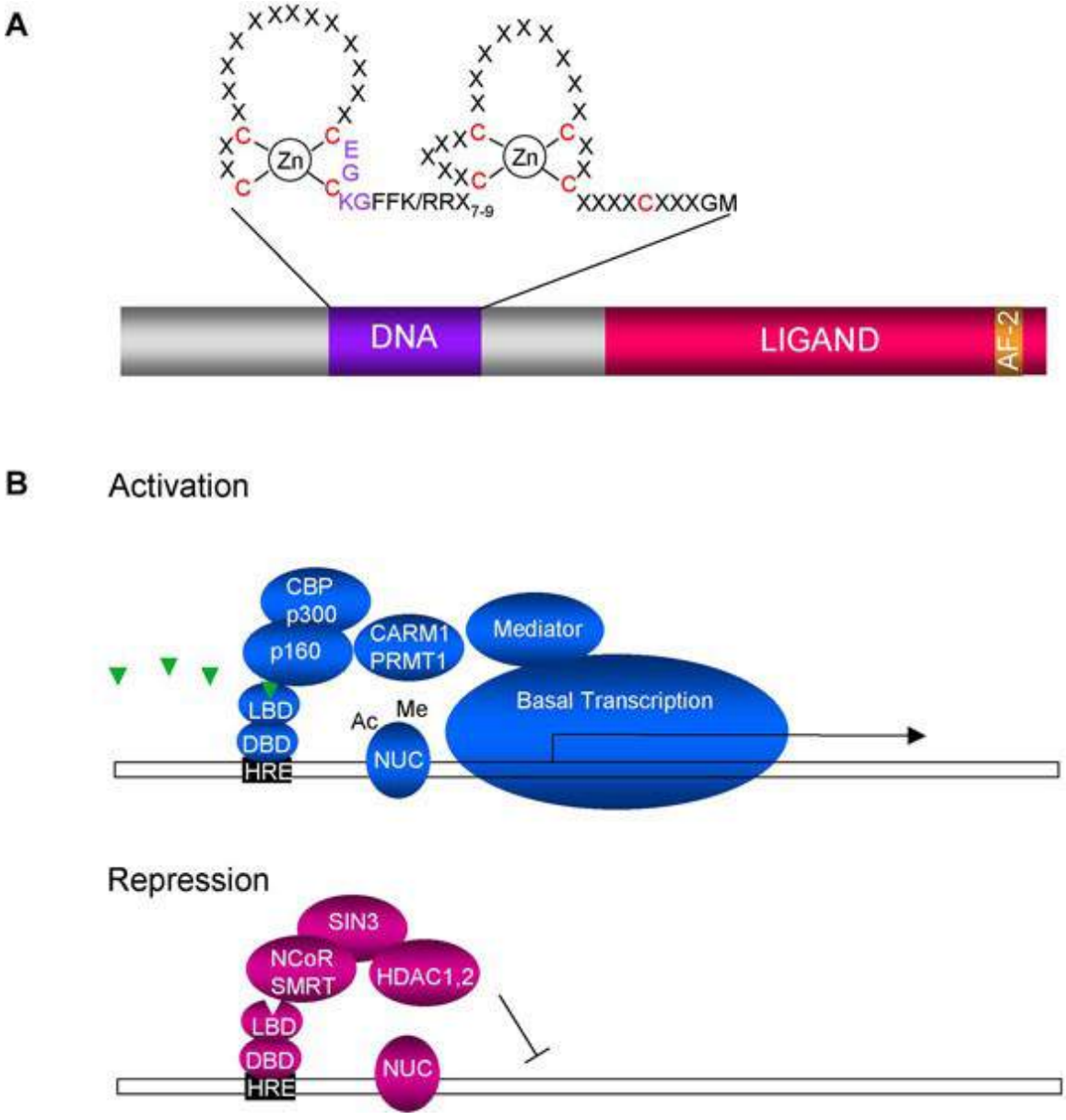
A
Zn
Zn
KGFFK/RRX7-9
XXXXCXXXGM
DNA
LIGAND
AF-2
B
Activation
CBP
p300
p160
CARM1
PRMT1
Mediator
LBD
DBD
HRE
Ac
Me
NUC
Basal Transcription
Repression
SIN3
NCoR
SMRT
HDAC1,2
LBD
DBD
HRE
NUC

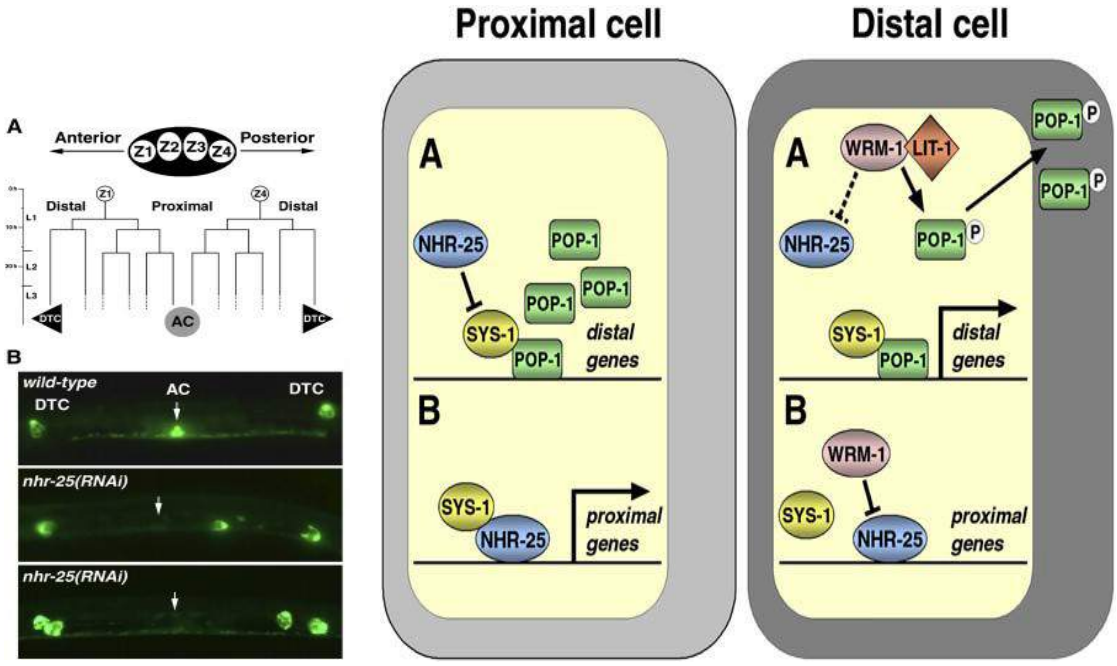

Figure 1.16 NHR-25 interacts with β-catenins to regulate gonad axis formation.

(A) Asymmetric cell divisions in Somatic Gonad Precursors (SGPs), Z1-Z4 results in adoption of distal and proximal cell fates. (B) *Nhr-25(lf)* results in proximal to distal cell fate changes, which results in extra Distal Tip Cells (DTCs). In the proximal cell, NHR-25 acts as a negative regulator by inhibiting SYS-1/POP-1 activity. In the distal cell, WRM-1 and LIT-1 allow SYS-1/POP-1 activity by mediating nuclear export of POP-1. SYS-1 association increases NHR-25 activity on gene expression and WRM-1 inhibits it (adapted from Asahina et al., 2006).

Figure 1.17 Sumoylation machinery and target activation.

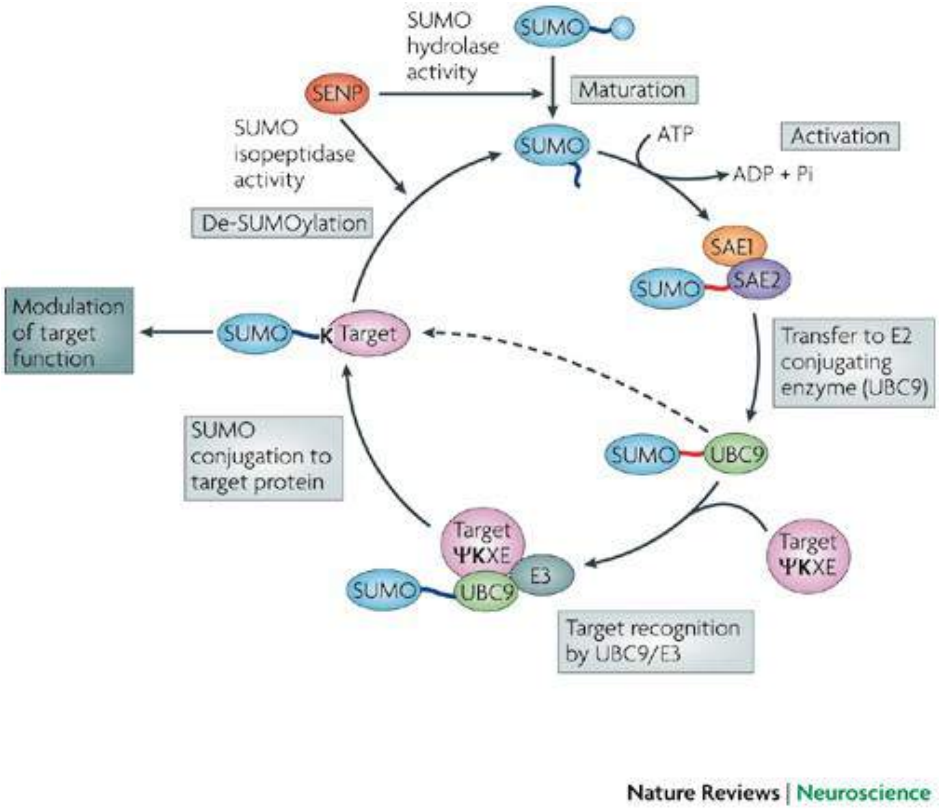

Sumoylation machinery and target activation.

SUMO pathway components are synthesized as precursor molecules, which later matured by the hydrolase activity of SUMO proteases (SENPs). After maturation, SUMO is activated in an energy/ATP-dependent process. Later by the association of SUMO activating enzyme 2 (SAE2), ubiquitin conjugating enzyme 9 (UBC9), and an E3 enzyme helps SUMO to bind target lysine. Usually the target lysine resides in The target lysine residue often lies in a Ψ-K-X-[D/E] consensus motif, where Ψ denotes large hydrophobic residue (I, V or L) and X denotes any residue. SUMO attachment to target proteins is dynamic and the dissociation is mediated by the isopeptidase activity of the SENP proteases (adapted from Martin et al., 2007).

Chapter 2: Materials and Methods

2.1 Strains and Genetics:

Wild type Bristol (N2) strain and additional transgenic lines were maintained at 20^0 C through standard protocols (Brenner 1974).

AH142: *lip-1::gfp- zhIs4[pTB10] III* (Berset et al., 2001)

PS3972 : *syIs90 [egl-17::yfp + unc-119(+)] III* (Sherwood 2003)

PS3239 : *syIs49[pMH86(dpy-20(+) + pJB100(zmp-1::GFP)] IV*. (Wang and Sternberg 2000).

PS4308 : *syIs107[unc-119(+) + lin-3(delta-pes-10)::GFP]* (Hwang and Sternberg 2004).

MH1564: *kuIs36[unc-119(+) egl-26::GFP] II*, (Wendy Hanna Rose and Han, 2004)

NW1644: *evEx170[smp-1::GFP(pVGS1a::GFP) + rol-6(su1006)]*. (Dalpe et al., 2005).

OP18: *wgIs18 [lin-39::TY1::EGFP::3xFLAG + unc-119(+)]*.TY1::EGFP::3xFLAG tag inserted in frame at C-terminus of *lin-39* coding sequence of fosmid ID#WRM0616aE11 by recombineering. Expression of transgene confirmed by GFP. (www.modencode.org).

OP33: *wgIs33 [nhr-25::TY1::EGFP::3xFLAG(92C12) + unc-119(+)]*.This construct contains over 30 Mb upstream sequence of *nhr-25* and full *nhr-25* gene including *nhr-25* 3'-utr. (A gift from Sarov) (www.modencode.org).

NW1702: *smp-1(ev715) I; jcIs1 IV; him-5(e1490) V* (Dalpe and Culotti J, 2005)

ST54: *plx-1(nc37) IV; him-5(e1490) V* (Fujii and Takagi 2002)

plx-1(nc37) IV; jcIs1 IV; him-5(e1490) V (Martina Hajduskova, present study)

MT688: *lin-12(n137)/unc-32(e189)III; him-5(e1467)V* (Horvitz B, 1980)

MT4007: *lin-39(n1760)III*. (Clark and Horvitz B, 1996)

SU93: *JcIs1* [(*ajm-1::gfp;unc-29(+); rol-6(su1006)*] *IV* (Mohler et al., 1998)

MH1955: *nhr-25(ku217) (X)* (Z Chen 2004)

CB1417: *lin-3(e1417)IV* (Horvitz B, 1980)

MT378: *lin-3(n378) IV* (Horvitz B, 1980)

MT309: *lin-15AB(n309) X* (Horvitz B, 1980)

MT1806: *lin-15A(n767) X*. (Ferguson and Horvitz 1995)

MT2495: *lin-15B(n765) X* (Ferguson and Horvitz 1995)

CB1026: *lin-1(e1026)IV* (Brenner S and Hodgkin J, 1969)

MT2124: *let-60(n1046) IV* (Feguson/Desai and Horvitz B,1985)

MT4866: *let-60(n2021)IV*. (Scott Clark and Horvitz B,1993)

PS21: *let-23(sy1) II; him-5(e1490) V.* (Paul Sternberg 1997)

pdlg::lifeact::gfp (II) and *pdlg::dlg-1::rfp*(III) (Farooqui et al., 2012). Obtained from Alex Hajnal group, Zurich.

VC186: s*mo-1(ok359)/szT1[lon-2(e678)] I; +/szT1 X*. (Broday et al., 2004)

syIs90;nhr-25(ku217)

syIs49; nhr-25(ku217)

syIs107; nhr-25(ku217)

jcIs1; nhr-25(ku217)

wgIs18; nhr-25(ku217)

lin-3(e1417); wgIs33,

lin-15AB(n309);wgIs33,

lin-1(e1026);wgIs33,

let-60(n1046gf);wgIs33

smo-1(ok359);syIs90

smo-1(ok359). syIs107

2.2 Scoring vulva induction patterns of VPCs:

All observed animals were anesthetized using 10mM levamisole dissolved in S. basal solution and mounted on 5% noble agar pads. In wild type, P(5-7).p adopt invariant cell lineages to produce a mature vulva of 22 cells. Vulva induction index of '1' is given to the Pn.p that adopts 1^0 or 2^0 fates, '0' for syncytial fates and '0.5' for mixed or hybrid

fates. Alternately, expression pattern of cell fate markers, *egl-17::yfp* (1^0) and *lip-1::gfp* (2^0) were used to decode induction patterns. Positive and wild type GFP expressions within Pn.p and their daughters confirms proper fates and thus inductions. In addition, AJM-1::GFP expression at the apical surfaces of Pn.ps and their daughters was also used to distinguish vulval, syncytial, and hybrid fates. The Pn.p cell that adopts syncytial fates fuses with hypodermis and loses its AJM-1 expression.

2.3 Scoring vulva lineage patterns:

Vulva lineage analyses wad done as previously described by (Sulston and Horvitz, 1977) and at 20^0 C. Complete vulva cell lineage analyses for P(3-8).p cells were observed through continuous DIC observations. Larvae were picked at 2 to 4 cell stage (Pn.px to Pn.pxx) and mounted on 5% noble agar pads without the anesthetic. Scrap of OP50 or HT115 was applied to the agar pads which serves as food for the worms. Periodical addition of S-basal with intervals of 15-30' were added to avoid desiccation. The final and third round of Pn.pxx cell divisions were analyzed based on their axes of nuclear divisions, L for longitudinal, O-oblique, S-syncytial, N-undivided and D-ambiguous.

2.4 Temporal *nhr-25(RNAi)*:

Feeding RNAi was performed as previously described and at 20^0 C (Timmons et al., 2001) Liquid culture of control (pPD129.36 vector), *nhr-25* and other *dsRNA* were initially induced as described in Silhankova et al., 2005, and later centrifuged bacteria was seeded onto NGM agarose plates mixed with 50 ug/ml carbenicillin, 12.5 ug/ml of tetracycline and 0.4 mM isopropyl-β-D-thiogalactosidase (IPTG). 30 ul of centrifuged bacteria was seeded on 3 cm NGM plates and 60 ul for 6 cm plates.

Synchronized populations of worms were obtained as described in Asahina et al., 2006. The freshly obtained L1 larvae were placed immediately (0 hrs after fertilization) onto control and *nhr-25(L1-RNAi)* plates and later observed for vulva phenotypes. For *nhr-25(L2-RNAi),* fresh larvae were placed on control treatment for 20 hrs and later placed on *nhr-25 RNAi* plates. Vulva lineages were analyzed after 32- 34 hrs developmental time in all RNAi treatments. By this time all larvae reached Pn.pxx stage. Terminal vuvla cell migrations and toroid morphogenesis were analyzed at L4 Stage. Double-target RNAi was performed similar to Asahina et al., 2006.

2.5 Confocal Microscopy:

Worms were anesthetized using 10mM levamisole and mounted on 5% agarose pads. Olympus Fluoview confocal microscope was used to observe fluorescent reporter gene expression patterns and toroid morphologies. Series of serial optical sections for z-axis were obtained with 0.5 -1 µm thickness for cell fate expressions and 0.2-0.5 µm for toroid morphology. Later, imaris v6.3.1 (Bitplane) was used to analyze vulva toroids in 3D (as per Dalpe et al., 2005). Finally all the images were manipulated using Adobe Photoshop.

2.6 Transformations and Microinjections:

Transgenesis and microinjections were performed as described by Mello et al., 1991. More details discussed in Chapter 3.

2.7 qRT-PCR:

Total RNA was isolated from synchronized worm populations from 14 to 38 hrs through TRIzol reagent (Invitrogen, Carlsbad, CA). A total of 2 mg of RNA was used for cDNA synthesis with Superscript II reverse transcriptase (Invitrogen). DNase treatment was done through TURBO (Ambion, Austin, TX). Quantitative RT-PCR was

performed through iQ SYBR Green Supermix kit and the C1000 Thermal Cycler (both from Bio-Rad Laboratories, Hercules, CA) and later relative transcript levels for *lin-3* isoforms were measured. Data was normalized to relative levels of ribosomal proteins *rpl-26* as per (Dolezel et al., 2008). Isoform specific *lin-3* primers used for qRT-PCR are listed in Table 4.6.

2.8 smFISH technique:

Lin-3 probes for detection were provided as a gift from Hendrik Korswagen and Teije Middlekoop (Utrecht, Netherlands). Preparation and hybridization steps of smFISH detection for *lin-3* were performed as described (Raj et al., 2008). Only *nhr-25(ku217)* animals carrying the syIs107 (*lin-3::gfp* transgene) were analyzed for detection. Several plates of worms carrying *nhr-25(ku217);lin-3::gfp* were grown until gravid stage and later bleached. After bleaching eggs were collected and allowed to grow synchronously at 20°C. Once the larvae reach Pn.pxx stage (~ 32 hrs after hatching) they were washed from the plates with ddH20 and later fixed in 4% formaldehyde and 70% ethanol. Hybridization with chemically coupled Cy5 *lin-3* probes was performed for >12 h at 30°C in dark conditions. The hybridized animals were washed with DAPI for nuclear staining and later mounted for microscopy. 0.5 um thickness z-stacks were collected using a Leica DM6000 microscope equipped with a Leica DFC360FX camera, 100 × objective, and an Y5 filter cube (Cy5). Images are analyzed with ImageJ through 1024 × 1024 resolution and 2 × 2 binning specifications. Quantification was performed by manually counting *lin-3* mRNA spots in AC and vulva cells of animals. The GFP expression of *syIs107* transgene helped to mark the boundaries of the corresponding cells. Fluorescent spots visible in at least two neighboring Z-slices were only counted to eliminate false positive signals.

Chapter 3: Research article

Sumoylated NHR-25/NR5A regulates cell fate during *C. elegans* vulval development

OPEN ACCESS Freely available online

PLOS | GENETICS

Sumoylated NHR-25/NR5A Regulates Cell Fate during *C. elegans* Vulval Development

Jordan D. Ward[1☯], Nagagireesh Bojanala[2,3☯], Teresita Bernal[1], Kaveh Ashrafi[4], Masako Asahina[1,2,3]*, Keith R. Yamamoto[1]*

1 Department of Cellular and Molecular Pharmacology, University of California San Francisco, San Francisco, California, United States of America, **2** Institute of Parasitology, Biology Centre ASCR, Ceske Budejovice, Czech Republic, **3** University of South Bohemia, Ceske Budejovice, Czech Republic, **4** Department of Physiology, University of California San Francisco, San Francisco, California, United States of America

Abstract

Individual metazoan transcription factors (TFs) regulate distinct sets of genes depending on cell type and developmental or physiological context. The precise mechanisms by which regulatory information from ligands, genomic sequence elements, co-factors, and post-translational modifications are integrated by TFs remain challenging questions. Here, we examine how a single regulatory input, sumoylation, differentially modulates the activity of a conserved *C. elegans* nuclear hormone receptor, NHR-25, in different cell types. Through a combination of yeast two-hybrid analysis and *in vitro* biochemistry we identified the single *C. elegans* SUMO (SMO-1) as an NHR-25 interacting protein, and showed that NHR-25 is sumoylated on at least four lysines. Some of the sumoylation acceptor sites are in common with those of the NHR-25 mammalian orthologs SF-1 and LRH-1, demonstrating that sumoylation has been strongly conserved within the NR5A family. We showed that NHR-25 bound canonical SF-1 binding sequences to regulate transcription, and that NHR-25 activity was enhanced *in vivo* upon loss of sumoylation. Knockdown of *smo-1* mimicked NHR-25 overexpression with respect to maintenance of the 3° cell fate in vulval precursor cells (VPCs) during development. Importantly, however, overexpression of unsumoylatable alleles of NHR-25 revealed that NHR-25 sumoylation is critical for maintaining 3° cell fate. Moreover, SUMO also conferred formation of a developmental time-dependent NHR-25 concentration gradient across the VPCs. That is, accumulation of GFP-tagged NHR-25 was uniform across VPCs at the beginning of development, but as cells began dividing, a *smo-1*-dependent NHR-25 gradient formed with highest levels in 1° fated VPCs, intermediate levels in 2° fated VPCs, and low levels in 3° fated VPCs. We conclude that sumoylation operates at multiple levels to affect NHR-25 activity in a highly coordinated spatial and temporal manner.

Citation: Ward JD, Bojanala N, Bernal T, Ashrafi K, Asahina M, et al. (2013) Sumoylated NHR-25/NR5A Regulates Cell Fate during *C. elegans* Vulval Development. PLoS Genet 9(12): e1003992. doi:10.1371/journal.pgen.1003992

Editor: David J. Mangelsdorf, University of Texas Southwestern Medical Center, United States of America

Received March 5, 2013; **Accepted** October 16, 2013; **Published** December 12, 2013

Copyright: © 2013 Ward et al. This is an open-access article distributed under the terms of the Creative Commons Attribution License, which permits unrestricted use, distribution, and reproduction in any medium, provided the original author and source are credited.

Funding: MA and NB were supported by grants from the Czech Science Foundation (204/09/H058), the Czech Academy of Sciences (Z60220518 and 500960906), the Czech Ministry of Education (MSM6007665801), and MODBIOLIN (7FP-REGPOT-2012-2013-1, GA316304). JDW was supported by postdoctoral fellowships from the Terry Fox Foundation (award #700046) and the Canadian Institutes of Health Research (award #234765). Research support was from the NIH (CA20535) and NSF (MCB-1157767) to KRY, and the National Institute of Environmental Health Sciences (ES021412-01) and the Program in Breakthrough Biomedical Research to KA. The funders had no role in study design, data collection and analysis, decision to publish, or preparation of the manuscript.

Competing Interests: I have read the journal's policy and have the following conflicts: spouse of JDW is a PLOS employee.

* E-mail: masako.asahina@ucsf.edu (MA); yamamoto@cmp.ucsf.edu (KRY)

☯ These authors contributed equally to this work.

Introduction

Tissue-specific and cell type-specific transcriptional networks underlie virtually every aspect of metazoan development and homeostasis. Single TFs, operating within gene-specific regulatory complexes, govern distinct gene regulatory networks in different cells and tissues; thus, combinatorial regulation underpins tissue- and cell type-specific transcription. Determining the precise mechanisms whereby such specificity arises and how networks nevertheless remain flexible in responding to environmental and physiological fluctuations is an interesting challenge. TFs integrate signaling information from co-factors, chromatin, post-translational modifications, and, in the case of nuclear hormone receptors, small molecule ligands, to establish transcription networks of remarkable complexity.

Here, we approach this problem by studying a covalent modification of a nuclear hormone receptor (NHR) in *C. elegans*, a simple metazoan with powerful genetic tools, a compact genome, and an invariant cell lineage leading to well-defined tissues. NHRs are DNA-binding TFs characterized by a zinc-finger DNA binding domain (DBD) and a structurally conserved ligand binding domain (LBD) [1]. The genome of *C. elegans* encodes 284 NHRs while humans only have 48 NHRs [1]. Of the 284 NHRs, 269 evolved from an HNF4α-like gene [2], and 15 have clear orthologs in other species. NHR-25 is the single *C. elegans* ortholog of vertebrate SF-1/NR5A1and LRH-1/NR5A2, and arthropod Ftz-F1 and fulfills many criteria for the study of tissue-specific transcriptional networks [1]. NHR-25 is broadly expressed in embryos and in epithelial cells throughout development [3,4]. It is involved in a range of biological functions such as molting [3–5], heterochrony [6], and organogenesis [7]. Furthermore, both NHR-25 and its vertebrate orthologs regulate similar processes. SF-1 and NHR-25 promote gonadal development and fertility [8,9], while NHR-25 and LRH-1 both play roles in embryonic

Author Summary

Animals precisely control when and where genes are expressed; failure to do so can cause severe developmental defects and pathology. Transcription factors must display extraordinary functional flexibility, controlling very different sets of genes in different cell and tissue types. To do so, they integrate information from signaling pathways, chromatin, and cofactors to ensure that the correct ensemble of genes is orchestrated in any given context. The number of regulatory inputs, and the complex physiology and large numbers of cell and tissue types in most experimentally tractable metazoans have rendered combinatorial regulation of transcription nearly impenetrable. We used the powerful genetics and simple biology of the model nematode, *C. elegans*, to examine how a single post-translational modification (sumoylation) affected the activity of a conserved TF (NHR-25) in different cell types during animal development. Our work suggests that sumoylation constrains NHR-25 activity in order to maintain proper cell fate during development of the reproductive organ.

development and fat metabolism [4,10–12]. The pleiotropic phenotypes seen following RNAi or mutation of *nhr-25* highlight the broad roles of the receptor, and its genetic interaction with numerous signaling pathways (β-catenin, Hox, heterochronic network) [6–8] make it an excellent model to study combinatorial gene regulation by NHRs.

SUMO (small ubiquitin-like modifier) proteins serve as post-translational modifiers and are related to but distinct from ubiquitin [13]; we show here that NHR-25 is sumoylated. Sumoylation uses similar enzymology as ubiquitination to conjugate the SUMO protein onto substrate lysines [13]. Briefly, SUMO is produced as an inactive precursor. A SUMO protease activates SUMO by cleaving residues off the C-terminus to expose a di-glycine [13]. A heterodimeric E1 protein consisting of UBA2 and AOS1 forms a thioester bond with the exposed diglycine and then transfers SUMO to an E2 enzyme (UBC9), also through a thioester bond [14]. The E2 enzyme then either directly conjugates SUMO onto a target lysine, or an E3 ligase can enhance the rate of sumoylation; that is, unlike in ubiquitination, E3 ligases are not always required. Like many post-translational modifications, sumoylation is reversible and highly dynamic. The same SUMO protease that initially activated SUMO cleaves the isopeptide linkage that covalently attaches SUMO to the target protein [14]. Indeed, global failure to remove SUMO from substrates compromises viability in mice and *S. pombe* [15,16].

The extent of sumoylation of a given target can be regulated by varying the expression, localization, stability or activity of components of the sumoylation machinery in response to external and internal cellular cues [14]. SUMO-regulated processes include nuclear-cytosolic transport, DNA repair, transcriptional regulation, chromosome segregation and many others [14]. For example, sumoylation of the glucocorticoid receptor prevents synergy between two GR dimers bound at a single response element [17]. In this sense, SUMO is analogous to the small hydrophobic hormones and metabolites that serve as noncovalent ligands for nuclear receptors, except it associates both covalently and non-covalently with its targets. Sumoylation modulates the activities of multiple classes of cellular proteins, such as transcriptional regulators, DNA replication factors and chromatin modifiers.

Elucidating how a single nematode NHR integrates cellular signals to regulate specific genes in distinct tissues will advance our understanding of metazoan transcription networks. To this end, we examined how sumoylation regulates the *C. elegans* nuclear hormone receptor NHR-25, and the physiological relevance of this nuclear hormone receptor-SUMO interaction. Using a combination of genetics, cell biology, and *in vitro* biochemistry we sought to understand how signaling through sumoylation impacts NHR-25's role in animal development, and how sumoylation affects the NHR-25 transcriptional network.

Results

NHR-25 physically interacts with SMO-1

We identified an interaction between NHR-25 and the single *C. elegans* SUMO homolog (SMO-1) in a genome-wide Y2H screen using the normalized AD-Orfeome library, which contains 11,984 of the predicted 20,800 *C. elegans* open reading frames [18]. SMO-1 was the strongest interactor in the screen on the basis of two selection criteria, staining for β-galactosidase activity and growth on media containing 3-aminotriazole (Figure 1A). To assess the selectivity of the SMO-1–NHR-25 interaction, we tested pairwise combinations of SMO-1 with full-length NHR-25, an NHR-25 isoform β that lacks the DNA-binding domain, and each of seven additional NHRs: NHR-2, NHR-10, NHR-31, NHR-91, NHR-105, FAX-1, and ODR-1 (Figure S1A). The NHR-25-SMO-1 interaction proved to be selective, as SMO-1 failed to bind the other NHRs tested. NHR-25 also interacted with the GCNF homolog, NHR-91 (Figure S1A).

nhr-25 and *smo-1* genetically interact during vulval development

SMO-1 was an enticing NHR-25 interacting partner to pursue. SUMO in *C. elegans* and other eukaryotes regulates TFs and chromatin, thus is well positioned to impact NHR-25 gene regulatory networks. Furthermore, spatial and temporal expression patterns of *smo-1* and *nhr-25* during development largely overlap [3,4,19]. SUMO interacts with the mammalian homologs of NHR-25, suggesting that the interaction is likely evolutionarily conserved [20,21]. Among its many phenotypes, *smo-1* loss-of-function (*lf*) mutants display a fully penetrant protruding vulva (Pvl) phenotype, reflecting disconnection of the vulva from the uterus [19] (Figure 1B, C). *smo-1* RNAi or mutation also cause low penetrance of ectopic induction of vulval cells, which can generate non-functional vulval-like structures known as multivulva (Muv) [22] (Figure 1B, C). Similar to *smo-1* mutants, *nhr-25* reduction-of-function leads to a Pvl phenotype, but does not cause Muv [7]. This *nhr-25* Pvl phenotype results from defects in cell cycle progression, aberrant division axes of 1° and 2° cell lineages, and altered vulval cell migration (Table 1, Figure 2, Bojanala *et al.*, manuscript in preparation). Because at an earlier stage NHR-25 is also necessary for establishing the anchor cell (AC) [8], which secretes the EGF signal that initiates vulval precursor cell (VPC) patterning, our RNAi treatments were timed to allow AC formation and examination of the effect of *nhr-25* depletion on later developmental events.

When *smo-1* and *nhr-25* were simultaneously inactivated, animals exhibited a fully penetrant vulvaless (Vul) phenotype and an exacerbated Muv phenotype (Figure 1B, C). The ectopically induced vulval cells expressed an *egl-17::YFP* reporter, indicating that 3°-fated cells aberrantly adopted 1° and 2° fates in these animals (Figure S2B). This *egl-17::YFP* reporter allowed us to monitor 1°/2° fate induction despite the cell division arrest phenotypes of *nhr-25(RNAi)* and *smo-1(lf);nhr-25(RNAi)* animals. Lineage analyses showed that following simultaneous inactivation of both *smo-1* and *nhr-25*, daughters of all VPCs normally

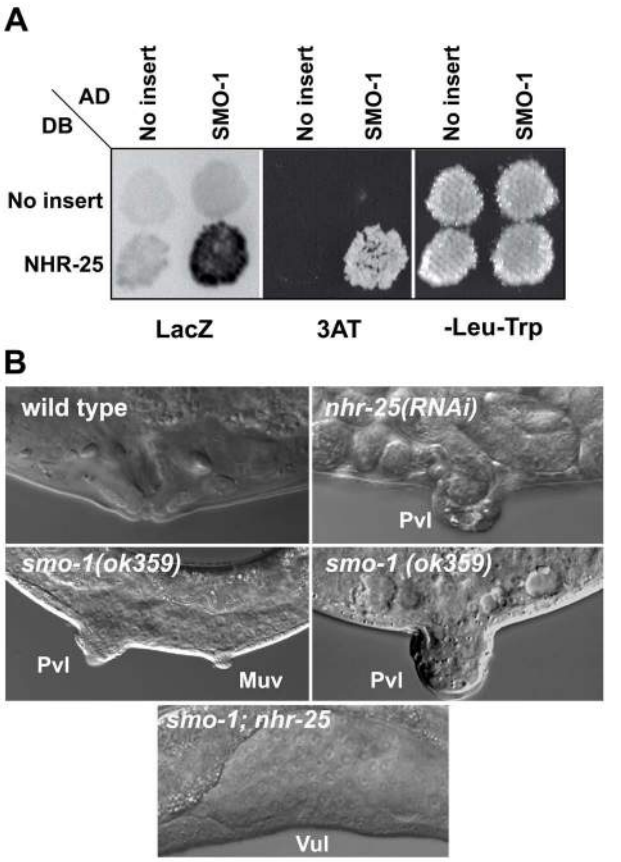

C

Genotype	Feeding RNAi	Vulva phenoypes				Sterility (%)	n
		WT	Pvl	Vul	Muv		
smo-1 +/-	*vector*	100	0	0	0	0	103
	nhr-25	21	34	45	0	0	85
smo-1 -/-	*vector*	0	100	0	15	100	147
	nhr-25	0	0	100	65	100	82

Figure 1. SMO-1 and NHR-25 physically and genetically interact. (A) NHR-25 fused to the Gal4 DNA binding domain (DB) interacted with wild type (WT) SMO-1 fused to the Gal4 activation domain (AD). No interaction was seen with empty vector (No insert). β-galactosidase (LacZ) and HIS3 (3AT; 3-aminotriazole) reporters were assayed, and yeast viability was confirmed by growth on a plate lacking leucine and tryptophan (-Leu-Trp). (B) DIC microscopy examining vulval morphology in animals of the indicated genotype. Characteristic protruding vulvae (Pvl) seen in *nhr-25(RNAi)* and *smo-1(ok359)* animals are indicated, as is the low penetrance multivulva phenotype (Muv) of *smo-1(lf)* animals. RNAi inactivation of *nhr-25* in a *smo-1(ok359)* mutant resulted in vulvaless (Vul) animals. (C) Table providing scoring of the Pvl, Vul, Muv, and sterility phenotypes of the indicated genotypes. n = number of animals scored.
doi:10.1371/journal.pgen.1003992.g001

responsible for vulva formation, (P5.p, P6.p and P7.p) failed to undergo the third round of vulval cell division (Table 1) resulting in premature cell division arrest and the Vul phenotype. Although P5.p, P6.p and P7.p VPCs were induced, the execution of 2° fate was abnormal: in both *smo-1(ok359)* and *smo-1(ok359);nhr-25(RNAi)* backgrounds, the expression of the 1° marker, *egl-17::YFP* exhibited ectopically high expression in P5.p and/or P7.p (Figure S2A) at the 4-cell stage. Moreover, in *smo-1;nhr-25(RNAi)* animals, the P(3,4,8).p cell, which normally divides only once and fuses into the hypodermal syncytium, kept dividing (Table 1). This continued division enhanced the Muv induction phenotype seen in *smo-1* mutants. Thus, reduction of SMO-1 activity enhanced cell division defects in 1° and 2° *nhr-25* mutant VPCs, while reduction of NHR-25 activity enhanced the *smo-1* mutant Muv phenotype in 3° fated cells.

SMO-1 binds NHR-25 covalently and non-covalently

NHR-25 and SMO-1 interact physically in Y2H assays and genetically *in vivo*, consistent with their overlapping expression patterns [4,19]. Furthermore, the mammalian NHR-25 homologs are sumoylated, suggesting that SMO-1-NHR-25 interactions are conserved and physiologically important. Y2H interactions with SUMO can reflect non-covalent binding, or covalent sumoylation where the SUMO protein is coupled onto the substrate through an isopeptide bond. These two possibilities can be distinguished genetically. Mutations in the β-sheet of SUMO interfere with non-covalent binding, whereas deletion of the terminal di-glycine in SUMO selectively compromises covalent sumoylation [23]. As can be seen in Figure 3A, deletion of the terminal di-glycine residues of SMO-1 (ΔGG) completely abrogated the interaction with NHR-25. The SMO-1 V31K mutation predicted to disrupt the conserved β-sheet of SMO-1 hampered the Y2H interaction between NHR-25 and SMO-1, although not as severely as the SMO-1 ΔGG mutation (Figure 3A). These findings are similar to those with DNA thymine glycosylase and the Daxx transcriptional corepressor, both of which bind SUMO non-covalently and are also sumoylated [24,25]. The V31K β-sheet mutant was competent to bind the *C. elegans* SUMO E2 enzyme, UBC-9, confirming its correct folding (Figure S3A). Together, these results suggested that NHR-25 is both sumoylated and binds SMO-1 non-covalently; conceivably, the two modes of interaction confer distinct regulatory outcomes.

Three lysines in the hinge region of NHR-25 are required for sumoylation

As our Y2H data suggested that NHR-25 was sumoylated, we identified candidate sumoylation sites within NHR-25 using the SUMOsp2.0 prediction program [26]. The sumoylation consensus motif is ψ-K-X-D/E, where ψ is any hydrophobic amino acid, K is the lysine conjugated to SUMO, X is any amino acid, and D or E is an acidic residue [14]. Three high scoring sites reside in the hinge region of the protein: two are proximal to the DBD (K165 and K170) and one (K236) is near the LBD (Figure 3C). We mutated these sites, conservatively converting the putative SUMO acceptor lysine residues to arginine to block sumoylation. Single mutation of any of the three candidate lysines had no apparent effect on the NHR-25 interaction with SMO-1 in Y2H assays, whereas the three double mutants had modest effects, and the NHR-25 3KR triple mutant (K165R K170R K236R) abrogated binding (Figure 3D). A fourth candidate sumoylation site (K84) located in the DBD was completely dispensable for the Y2H interaction (data not shown). To verify that the 3KR mutations blocked the interaction with SMO-1 specifically, rather than causing NHR-25 misfolding or degradation, we confirmed that NHR-25 3KR retained the capacity to bind NHR-91 (Figures S1, Figure 3B). These data suggested that either non-covalent binding is dispensable for the SMO-1-NHR-25 interaction and that this was a rare case in which the SUMO β-sheet mutation impaired sumoylation, or that the three lysines in NHR-25 were important for both the covalent and non-covalent interaction with SMO-1.

To ensure that our Y2H results indeed reflected NHR-25 sumoylation, we turned to *in vitro* sumoylation assays. As both

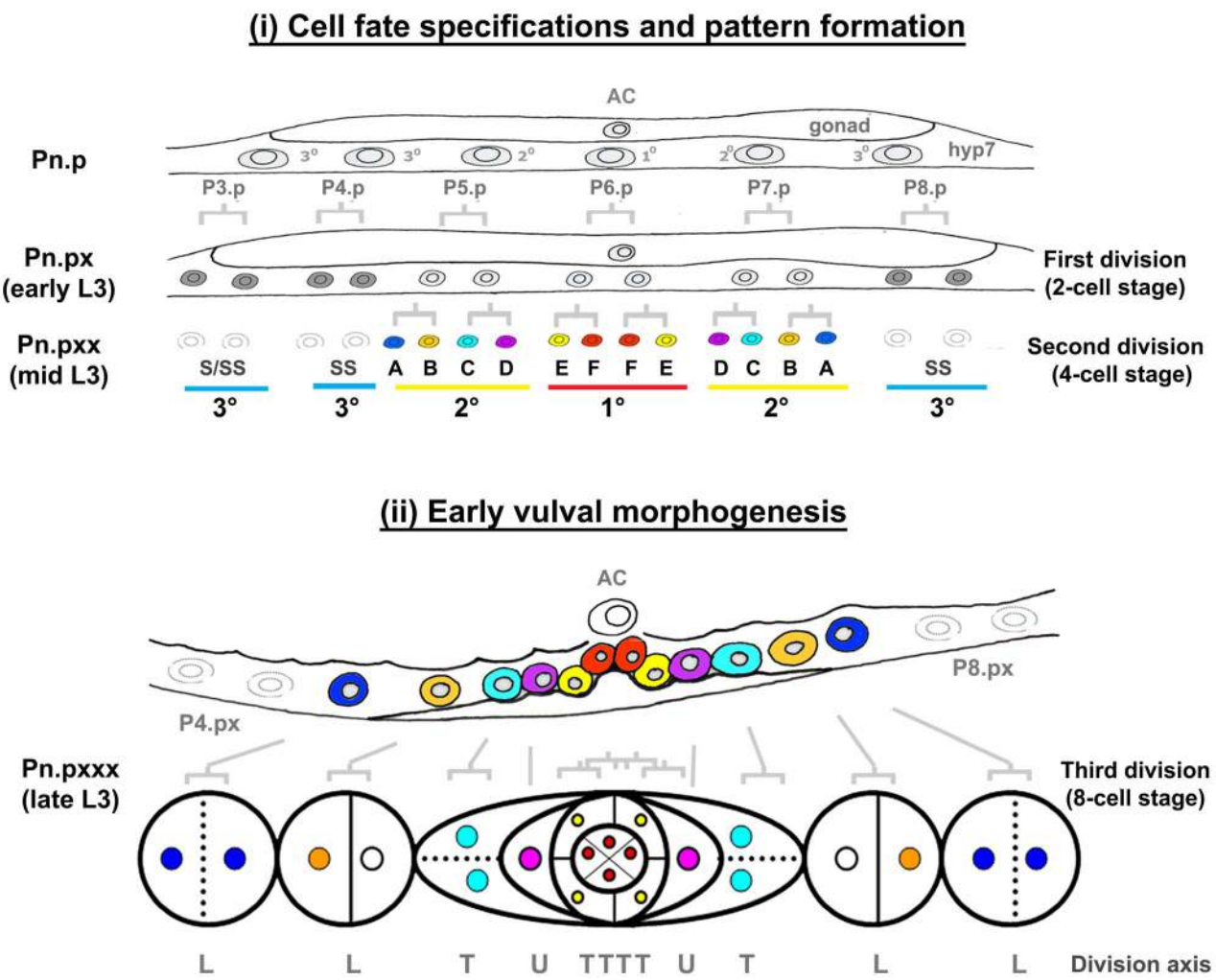

Figure 2. Vulval morphogenesis. The fully formed vulva of *C. elegans* is generated post-embryonically from cell divisions of three vulval precursor cells (VPCs). These three VPCs are denoted as P5.p, P6.p and P7.p and undergo a series of stereotyped divisions producing 22 cells. Cells arising from the P6.p precursor are designated as having the primary (1°) fate, while those arising from P5.p and P7.p precursors are designated as having the secondary (2°) fate. 2° cells generate vulA-D cells and 1° cells generate vulE and vulF. In early to mid L3 larvae, the proximity to a gonadal cell known as the anchor cell (AC) initiates vulval patterning by secretion of LIN-3/EGF [64]. The closest VPC to the AC (P6.p) receives the highest LIN-3/EGF dose, which activates LET-60/Ras signaling in P6.p [65–68], prompting it to adopt a 1° fate. This EGF-Ras signaling also induces P6.p to express the Notch ligand. The moderate level of LIN-3 received by neighboring P5.p and P7.p cells combined with lateral inhibition through the Notch pathway, induces P5.p and P7.p cells to adopt a 2° fate. In the L3 larval stage, the 1° and 2° cell lineages divide three times, and undergo a coordinated series of migrations and fusions during morphogenesis to complete vulval development [38]. Three VPCs (P3.p, P4.p and P8.p) normally adopt a 3° fate, which means that they divide once and fuse into an epidermal syncytial cell called hyp7, with the exception of P3.p of which about 50% of the lineage fuses without division (designated as S). Syncytial fate is designated S or SS in the figure. The pattern of cell division axes are depicted as L (longitudinal), T (transverse) and U (undivided).
doi:10.1371/journal.pgen.1003992.g002

human and *C. elegans* sumoylation enzymes were used in these experiments, we distinguish them with prefixes "h" and "Ce". As a positive control, we expressed and purified recombinant hE1, hUBC9, hSUMO1, and hSENP1 from *E. coli*. We also purified a recombinant partial hinge-LBD fragment of mouse SF-1 from *E. coli*; this fragment contains a single sumoylation site in the hinge region. SF-1 is a vertebrate ortholog of NHR-25 and the fragment that we used is a robust sumoylation substrate (Figure S4A) [27]. We then purified an N-terminally hexahistidine-Maltose Binding Protein (6×His-MBP) tagged fragment of NHR-25 (amino acids 161–541) containing most of the hinge region and ligand-binding domain, including all three candidate SUMO acceptor lysines. Coomassie staining and immunoblotting revealed three slower-migrating species, which were collapsed by the addition of the SUMO protease, hSENP1 (Figure 4A, S5A). We detected sumoylation of the same 6×HisMBP-NHR-25 fragment when it was expressed in rabbit reticulocyte lysates, followed by incubation with hE1, hE2 and hSUMO1 (Figure 4B).

We further tested NHR-25 substrates containing two (2KR; K170R K236R) or three arginine substitutions (NHR-25 3KR). When only one predicted acceptor lysine was available (2KR), we detected a single dominant sumoylated species, whereas for NHR-25 3KR, sumoylation was abrogated (Figure S5B). We performed sumoylation reactions on *in vitro* transcribed and translated wild type NHR-25, NHR-25 3KR, and NHR-25 3EA. In NHR-25 3EA (E167A E172A E238A) the acidic glutamic acid residues within the three consensus sumoylation sites were mutated to alanine. NHR-25 3EA leaves the acceptor lysines available, but is

Table 1. Vulva cell lineage analyses in *nhr-25(RNAi)* and *smo-1(lf)* animals.

Genotype	Pn.p lineages						
	P3.p	P4.p	P5.p	P6.p	P7.p	P8.p	n
wild type	S	SS	LLTU	TTTT	UTLL	SS	4
	SS	SS	LLTU	TTTT	UTLL	SS	3
smo-1(ok359)	S	SS	LLTU	TTTT	UTLL	SS	3
	SS	SS	LLTU	TTTT	UTLL	SS	2
nhr-25(RNAi)	S	SS	LLTU	TTTT	UTLL	SS	2
	SS	SS	LLUU	LUUL	UULL	SS	2
	SS	SS	LLUU	LUUL	ULLL	SS	1
smo-1(ok359);	S	SS	UUUU	UUUU	UUUU	SS	3
nhr-25(RNAi)	SS	SS	UUUU	UUUU	UUUU	SS	4
	S	S LU	UUUU	LUUL	UUUU	SS	1
	SS	SS	LLUU	UUUU	UUUU	SS	1
	SS	UU D	LLUU	UUUU	UU S	LU S	1
	S	UULL	UUUU	UUUU	UUUU	SS	1
	UULU	UUUU	UUUU	UUUU	UUUU	LUUU	1
	SS	UUUU	UUUU	UUUU	UUUU	SS	1
	SS	S LU	UUUU	UUUU	UUUU	SS	1
	SS	UUUL	UUUU	UUUU	UUUU	UUUU	1

S- syncytial fate; L- longitudinal; T – transverse; D-undetermined and U-undivided cell.

doi:10.1371/journal.pgen.1003992.t001

predicted to inhibit sumoylation by impairing interaction with UBC9. While wild type NHR-25 was clearly sumoylated, the 3EA mutation severely impaired sumoylation (Figure 4B).

When sumoylation reaction times were extended 5–20 fold, additional species of sumoylated NHR-25 were generated (Figure S6A). These species could reflect sumoylation of NHR-25 on other sites or formation of hSUMO1 chains. To distinguish between these possibilities, we used methyl-hSUMO1, which can be conjugated onto a substrate lysine, but chain formation is blocked by methylation. Long incubations with methyl-hSUMO1 resulted in only three sumoylated NHR-25 bands, as determined by NHR-25 immunoblotting, indicating that there are indeed only the three major acceptor lysines (Figure S6A). hSUMO2, which readily forms polySUMO chains, was included as a control in this experiment. Even with extended incubation times, we observed only three dominant sumoylated forms of NHR-25, suggesting that additional bands in reactions using hSUMO1 or CeSMO-1 reflect inefficient chaining. We conclude that NHR-25 is sumoylated *in vitro* on three lysines and that *C. elegans* SMO-1 does not readily form polySUMO chains, unlike yeast SMT3 and mammalian SUMO2.

Biochemical characterization of *C. elegans* UBC-9 and SMO-1

All studies of *C. elegans* sumoylation to date have used hE1, hUBC9, and hSUMO proteins [19,28,29]. We purified recombinant CeE1, CeUBC-9 and CeSMO-1 from *E. coli* and tested their activity in *in vitro* sumoylation assays. Our CeE1 preparation was inactive, but was effectively substituted by hE1. Under those conditions, our CeUBC-9 and CeSMO-1 catalyzed sumoylation of the SF-1 hinge-LBD fragment (Figure S4B). Similar to hUBC9 and hSUMO1, recombinant CeUBC-9 and CeSMO-1 yielded three sumoylated species using the 6×His-MBP-NHR-25 substrate (Figure 4C, S4C).

To determine the kinetics of the three SUMO modifications of NHR-25, we performed a time course of standard sumoylation reactions with hUBC9/CeUBC-9 and hSUMO1/CeSMO-1 proteins. In both cases, we detected a single band by 15 minutes, followed by two and then three sumoylated species as the reaction progressed (Figure S6B–E). These data imply that the three sumoylation sites are modified sequentially, in a particular order.

All of our reactions were performed without addition of an E3 ligase. The high efficiency of SF-1 sumoylation in the absence of E3 ligase is in part due to a direct interaction with UBC9 [30]. Surprisingly, we failed to detect an interaction between NHR-25 and CeUBC-9 either by Y2H assays or through immunoprecipitation of purified proteins (Figure S3B; data not shown). However, when we performed a yeast three-hybrid assay, where untagged CeSMO-1 was added to the system, we observed a weak interaction between NHR-25 and CeUBC-9, suggesting either that CeSMO-1 bridges NHR-25 and CeUBC-9 or that NHR-25 recognizes a CeSMO-1-bound CeUBC-9 species (Figure S3B).

NHR-25 binds consensus sequences derived from NR5 family binding sites

To begin to investigate how sumoylation affects NHR-25-dependent transcriptional activity, we employed a HEK293T cell-based assay. We used a luciferase reporter driven by four tandem Ftz-F1 (*Drosophila* homolog of NHR-25) consensus sites, previously shown to be responsive to NHR-25 [8]. When Myc-tagged wild type NHR-25 was transfected, reporter expression was enhanced (Figure 5A), and the sumoylation-defective mutant NHR-25 (3KR) activated the reporter more strongly (Figure 5A). Anti-Myc immunostaining indicated no detectable increase in protein level or nuclear localization (Figure 5B).

To better characterize NHR-25-dependent transcriptional activity and generate reporters that could subsequently be used for *in vivo* assays, we generated a construct based on the canonical, high affinity SF-1 regulatory elements derived from the Mullerian inhibiting substance (MIS) and CYP11A1 (CYP) genes. We assessed NHR-25 binding to these elements using yeast one-hybrid (Y1H) and electrophoretic mobility shift assays (EMSAs). The Y1H assays indicated that NHR-25 bound the MIS and CYP11A1 elements (Figure S7A, B). Mutations in the MIS binding site that block SF-1 binding (MIS MUT) [27] prevented NHR-25 binding (Figure S7B). Moreover, the NHR-25 L32F (*ku217*) mutant, which has impaired DNA binding *in vitro* [7], displayed reduced activity in the Y1H experiment (Figure S7B). Consistent with the Y1H data, we found that a 6×His-MBP tagged fragment of NHR-25 (amino acids 1–173) purified from *E. coli* clearly bound MIS and CYP11A1 sites singly (Figure S7C) or in combination (2×NR5RE WT, for nuclear receptor NR5 family Response Element; Figure S7D) but only weakly to the mutant sites (Figure S7C–D, 7A).

Sumoylation of SF-1 regulates binding to specific DNA sequences [27]. Therefore, we asked whether sumoylation could similarly affect DNA binding capacity of the 6×His-MBP tagged fragment of NHR-25. We found that this fragment, which encompasses the DBD and part of the hinge region of NHR-25 (amino acids 1–173), was an even more potent sumoylation substrate than the hinge-LBD fragment, as almost all of the DBD substrate could be sumoylated (Figure 6A). Unlike SF-1 [27], NHR-25 DNA binding did not inhibit sumoylation (data not shown). Use of methyl-hSUMO1 in our *in vitro* sumoylation assays indicated that there were three sumoylation sites within the 6×His-MBP tagged fragment of NHR-25 DBD substrate (Figure 6B). These corresponded to the hinge region K165 and

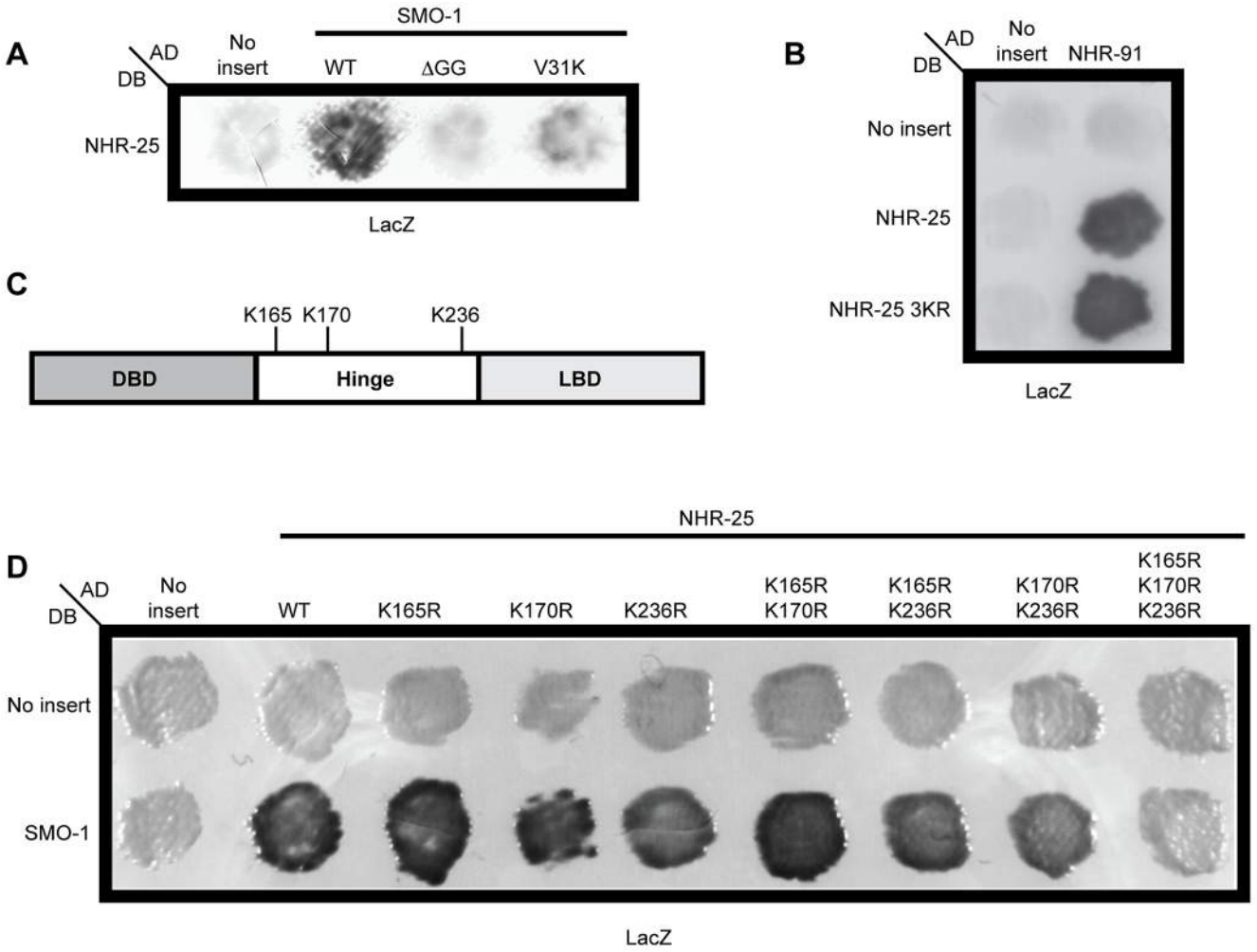

Figure 3. Three lysines in NHR-25 are necessary for the interaction with SMO-1. (A) NHR-25 fused to the Gal4 DNA binding domain (DB) interacted with wild type (WT) SMO-1 fused to the Gal4 activation domain (AD). No interaction was seen with empty vector (No insert), SMO-1 with the terminal di-glycine residues deleted (ΔGG), or SMO-1 with a β-sheet mutation (V31K). (B) The NHR-25 3KR (K165R K170R K236R) allele specifically blocked interaction with SMO-1, as both NHR-25 and NHR-25 3KR interacted with NHR-91. (C) Schematic of NHR-25 domain structure illustrating the DNA binding domain (DBD), hinge region, and ligand binding domain (LBD). The candidate SUMO acceptor lysines (K165, K170, K236) are indicated. (D) Mutating the indicated SUMO acceptor lysines to arginine in NHR-25 only abolished the interaction when all three were mutated (K165R K170R K236R). We note the non-reciprocality of our Y2H interactions: DB-NHR-25 interacted with AD-SMO-1 and AD-NHR-25 interacted with DB-NHR-91. Switching the Gal4 domains did not result in an interaction, as sometimes occurs in Y2H interactions [69]. β-galactosidase (LacZ) reporters were assayed in A, B, and D.
doi:10.1371/journal.pgen.1003992.g003

K170 acceptor lysines, which are analogous to the SF-1 fragment used by Campbell *et al.* (2008), and a third SUMO acceptor lysine (K84) within the DBD region between the second zinc finger and the conserved Ftz-F1 box (Figure 6C). This acceptor lysine is conserved in *D. melanogaster* Ftz-F1 as well as the mammalian LRH-1 (Figure 6C) [31]. EMSAs indicated that sumoylation diminished binding of the NHR-25 DBD fragment to the MIS and CYP derived binding sites (Figure S7D). Modifying the EMSAs such that the sumoylation reaction preceded incubation with the 2×NR5RE oligos severely impaired binding (Figure S7E). These *in vitro* findings are consistent with the notion that, as in mammals, sumoylation could diminish NHR-25 DNA binding.

Sumoylation inhibits NHR-25 dependent transcription *in vivo*

We next wanted to assess the effects of sumoylation on NHR-25-dependent transcription *in vivo*. To enhance the sensitivity of our assays, we constructed a reporter carrying four tandem repeats derived from each of MIS and CYP genes (Figure 7A, eight SF-1/NHR-25 binding sites designated as 8×NR5RE). The binding sites were spaced ten base-pairs apart to facilitate potential cooperative binding [32]. We generated transgenic *C. elegans* carrying the 8×NR5RE positioned upstream of a *pes-10* minimal promoter and driving a 3×Venus fluorophore bearing an N-terminal nuclear localization signal. In wild type animals, reporter expression was not detected (Figure 7B), whereas after *smo-1* RNAi, strong expression was detected in developing vulval cells, the hypodermis, seam cells, the anchor cell (Figure 7B) and embryos (not shown), tissues in which NHR-25 is known to be expressed (Figures 7F) and functional [4,7,33]. Reporter expression was especially prominent during the L3 and L4 stages. Mutation of the binding consensus, 8×NR5RE(MUT) abolished reporter expression in a *smo-1* (RNAi) background (Figure 7E), as expected for NHR-25-dependent reporter expression. Moreover,

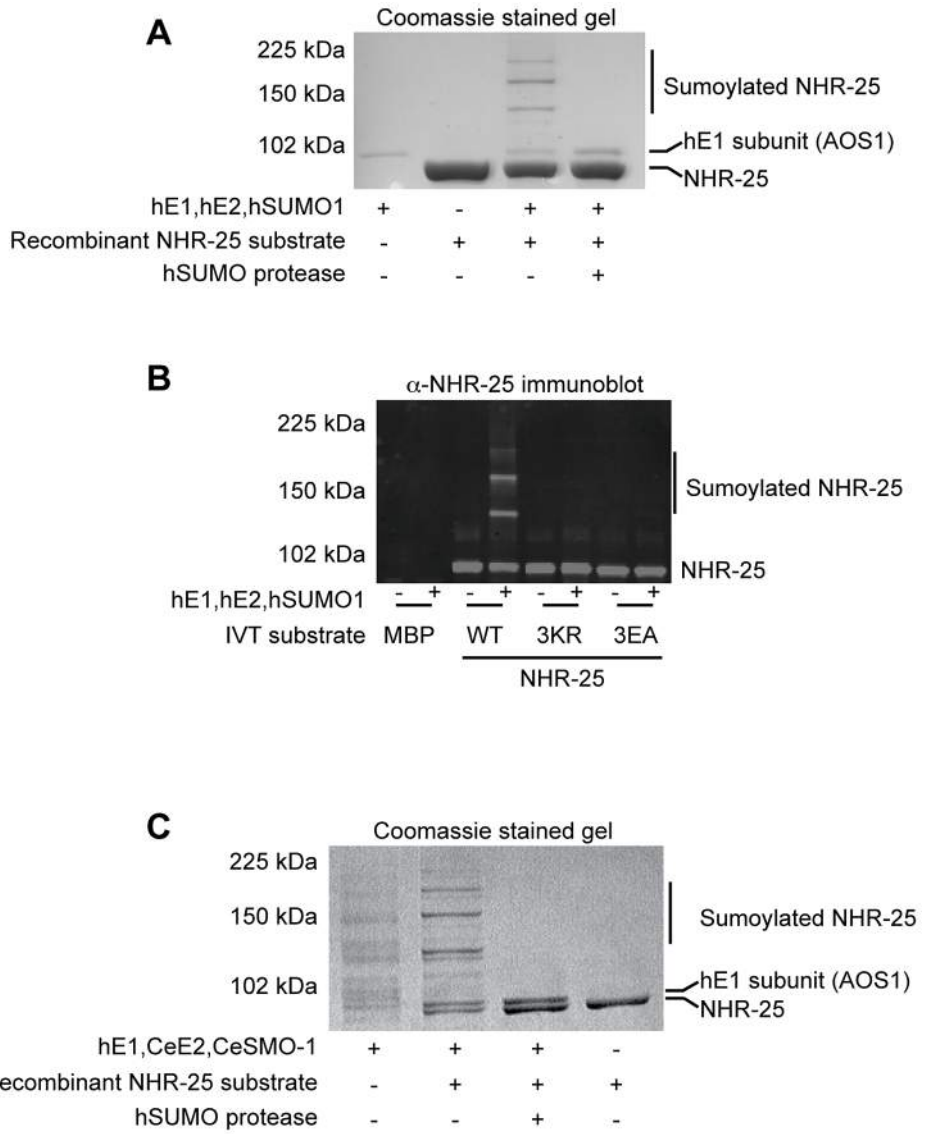

Figure 4. *In vitro* sumoylation of NHR-25. *In vitro* sumoylation reactions were resolved by SDS-PAGE and analyzed by either Coomassie staining (A,C) or immunoblotting with anti-NHR-25 antibody (B). (A and B) used recombinant human sumoylation enzymes (hE1, hE2, hSUMO1, hSENP1 SUMO protease), (C) used recombinant *C. elegans* CeUBC-9 and CeSMO-1 with hE1 and hSENP1. Substrates were recombinant 6×His-MBP-NHR-25 (amino acids 161–541; A,C), and the same construct *in vitro* transcribed and translated (B). In (B) an MBP control was *in vitro* transcribed and translated, as were the NHR-25 alleles 3KR (K165 K170R K236R) and 3EA(E167A E172A E238A). The positions of NHR-25, sumoylated NHR-25 and AOS1 (part of E1 heterodimer) are indicated. Size markers in kilodaltons (kDa) are provided.
doi:10.1371/journal.pgen.1003992.g004

genetic inactivation of *nhr-25* either by RNAi (*smo-1*, *nhr-25* double RNAi) or by use of *nhr-25(ku217)*, a reduction-of-function allele of *nhr-25*, abrogated reporter expression even in *smo-1* knockdown animals (Figure 7C, D). We conclude that sumoylation of NHR-25 strongly reduces its transcriptional activity *in vivo*.

Sumoylation of NHR-25 prevents ectopic vulval development

To examine functionally the consequences of NHR-25 sumoylation, we returned to the roles of *nhr-25* and *smo-1* in vulval organogenesis. Noting that *smo-1* mutants but not *nhr-25* reduction-of-function mutants display a Muv phenotype, we investigated whether this might reflect enhanced NHR-25 activity due to its reduced sumoylation. We therefore generated transgenic animals expressing tissue-specific NHR-25 and/or SMO-1 driven by three different promoters; *egl-17* for the VPCs, *grl-21* for the hypodermal hyp7 syncytium, and *wrt-2* for the seam cells. These transgenes included (i) wild type NHR-25; (ii) NHR-25 3KR; or (iii) SMO-1 alone. Although *egl-17* is typically used as a 1° and 2° cell fate marker during vulva development, it is expressed in all VPCs in earlier stages [34](Figure S2C). We used the *egl-17* promoter rather than commonly used VPC driver, *lin-31*, because the heterodimeric partner of LIN-31 is sumoylated and directly involved in vulva development [28].

Muv induction was scored by observing cell divisions of the six VPCs with the potential to respond to the LIN-3/EGF signal, which promotes differentiation. Normally, only P5.p, P6.p, and P7.p are induced while P3.p, P4.p and P8.p each produce no more than two cells as they are destined to fuse with the surrounding hyp7 syncytium (Figure 2). In wild type animals, overexpression of

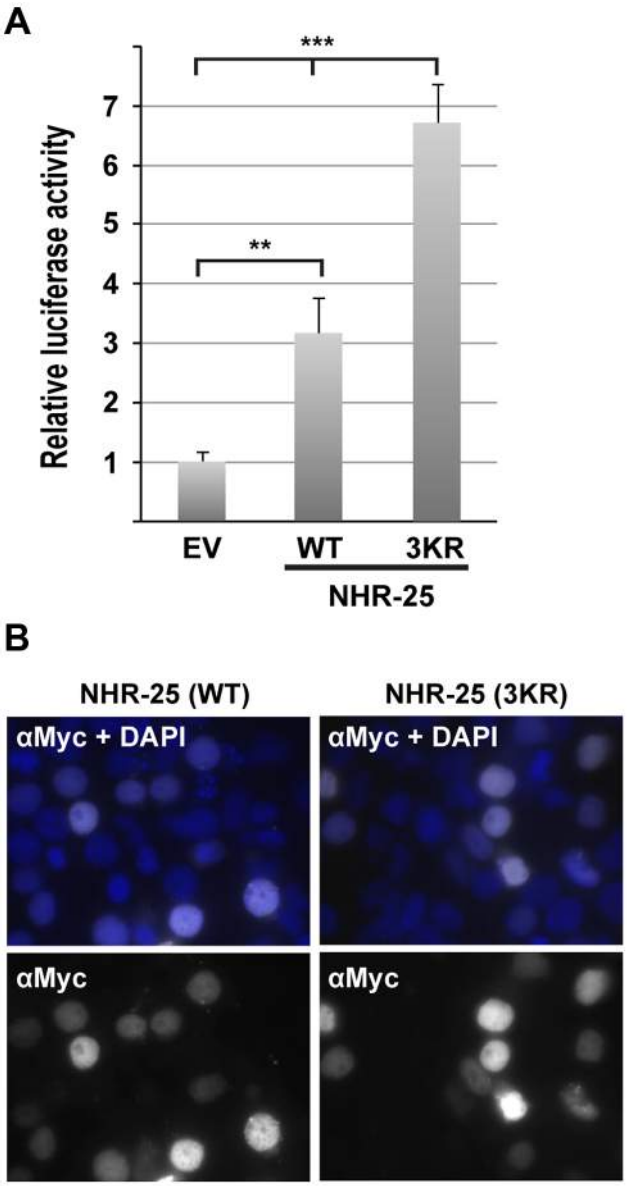

Figure 5. NHR-25(3KR) displays elevated activity in heterologous reporter assays. (A) A luciferase reporter vector containing four Ftz-F1/NHR-25 binding sites was transfected into HEK293T cells along with a Renilla internal control and either Myc-NHR-25 (WT) or Myc-NHR-25(3KR) expression constructs. Relative luciferase activity was normalized to the internal Renilla control and empty expression vector (EV). Eight biological replicates from three independent experiments were analyzed and error bars indicate standard deviation. (**T-test $p<0.01$; *** $p<0.0001$) (B) Transfected cells were stained with anti-Myc antibody. NHR-25(3KR) does not affect NHR-25 levels or localization. Nuclei were visualized with DAPI staining and an overlay of Myc and DAPI staining is shown.
doi:10.1371/journal.pgen.1003992.g005

NHR-25 in the VPCs (*egl-17* promoter) but not in hyp7 or seam cells (*grl-21* and *wrt-2* promoters, respectively) drove Muv induction at the P8.p position, mimicking *smo-1* RNAi (Figure 8, Table S1). Thus, high level NHR-25 acted cell-autonomously to produce a Muv phenotype. Overexpression of the NHR-25 3KR mutant in the VPCs resulted in an even more penetrant Muv phenotype and greater induction of P3.p, P4.p, and P8.p (Figure 8A). In contrast, overexpression of SMO-1 alone did not produce the Muv phenotype.

These overexpression experiments implied that excess unsumoylated NHR-25 altered 3° VPC fate, permitting extra divisions that produce the Muv phenotype. If sumoylation of NHR-25 normally constrains its activity, animals with decreased sumoylation activity would be expected to enhance the Muv phenotype. To test this hypothesis, we assessed the effect of *smo-1* RNAi in animals expressing a low-copy, integrated transgene expressing C-terminally GFP-tagged NHR-25 [35]. This transgene likely recapitulates the expression pattern of endogenous *nhr*-25, since the construct includes the complete 20 kb intergenic region upstream of *nhr-25*, and the entire *nhr-25* gene and 3′-UTR; the animals display normal vulvas. However, exposure to *smo-1* RNAi caused the Muv phenotype in about 30% of animals carrying the *nhr-25::gfp* transgene, which exceeded the 12% Muv frequency in *smo-1* RNAi controls (Figure 8). This extra vulva induction was seen in the P4.p. lineage in addition to P8.p. Together, our findings strongly suggest that in wild type animals, NHR-25 sumoylation prevents ectopic vulva induction in 3° fated cells.

Effects of *smo-1* deficiency on NHR-25 expression

One interpretation of our genetic and biochemical data is that the *in vivo* ratio of sumoylated to non-sumoylated NHR-25 specifies or maintains the 3° VPC fate. We were therefore interested in how NHR-25 sumoylation was regulated. SMO-1 is expressed at constant levels throughout vulval development [19], so we examined whether NHR-25 levels were regulated in VPCs during development. The low-copy, integrated NHR-25::GFP translational fusion allowed us to examine the developmental pattern of NHR-25 expression. NHR-25::GFP was evenly distributed prior to the first division in all VPCs, whereas after the first division the pattern became graded: highest in 1° P6.p daughters, lower in 2° P5.p and P7.p daughters, and lowest in 3° P(3,4,8).px (Figure 9A, B). After the third round of cell divisions NHR-25::GFP expression continued in all 22 P(5–7).pxxx cells and remained high during early vulva morphogenesis (Figure 9D) until it temporarily disappeared by the "Christmas tree stage" (data not shown).

smo-1 RNAi caused ectopic NHR-25::GFP expression in P(4,8).pxx cells (Figure 9E), which displayed the strongest Muv induction in *NHR-25::GFP;smo-1(RNAi)*, and *Pegl-17::NHR-25(3KR)* backgrounds (Figure 8). In wild type animals, NHR-25::GFP was normally expressed in the anchor cell at the time of the first VPC divisions, and subsequently decreased (Figure 9D). Interestingly, we noted that in nine of ten *smo-1(RNAi)* animals NHR-25::GFP was re-expressed in the AC at the "bell stage" (Figure 9F). Subsequently, no AC invasion occurred and the AC remained unfused. Therefore, in addition to restricting NHR-25 activity in 3° cells (previous section), sumoylation also limits NHR-25 accumulation in cells that are destined to assume the 3° fate. The resultant NHR-25 gradient combined with constant levels of SMO-1 may account for the observed pattern of NHR-25 sumoylation.

Discussion

The capacity of TFs to specify expression of precise networks of genes in a given context, yet remain flexible to govern dramatically different sets of genes in different cell or physiologic contexts, likely involves combinatorial regulation of transcription. In this study, we show that sumoylation represses bulk NHR-25 activity in multiple *C. elegans* tissues. In addition, our findings suggest that particular fractional sumoylation states of NHR-25 govern the appropriate course of cell divisions and the 3° fate decision of

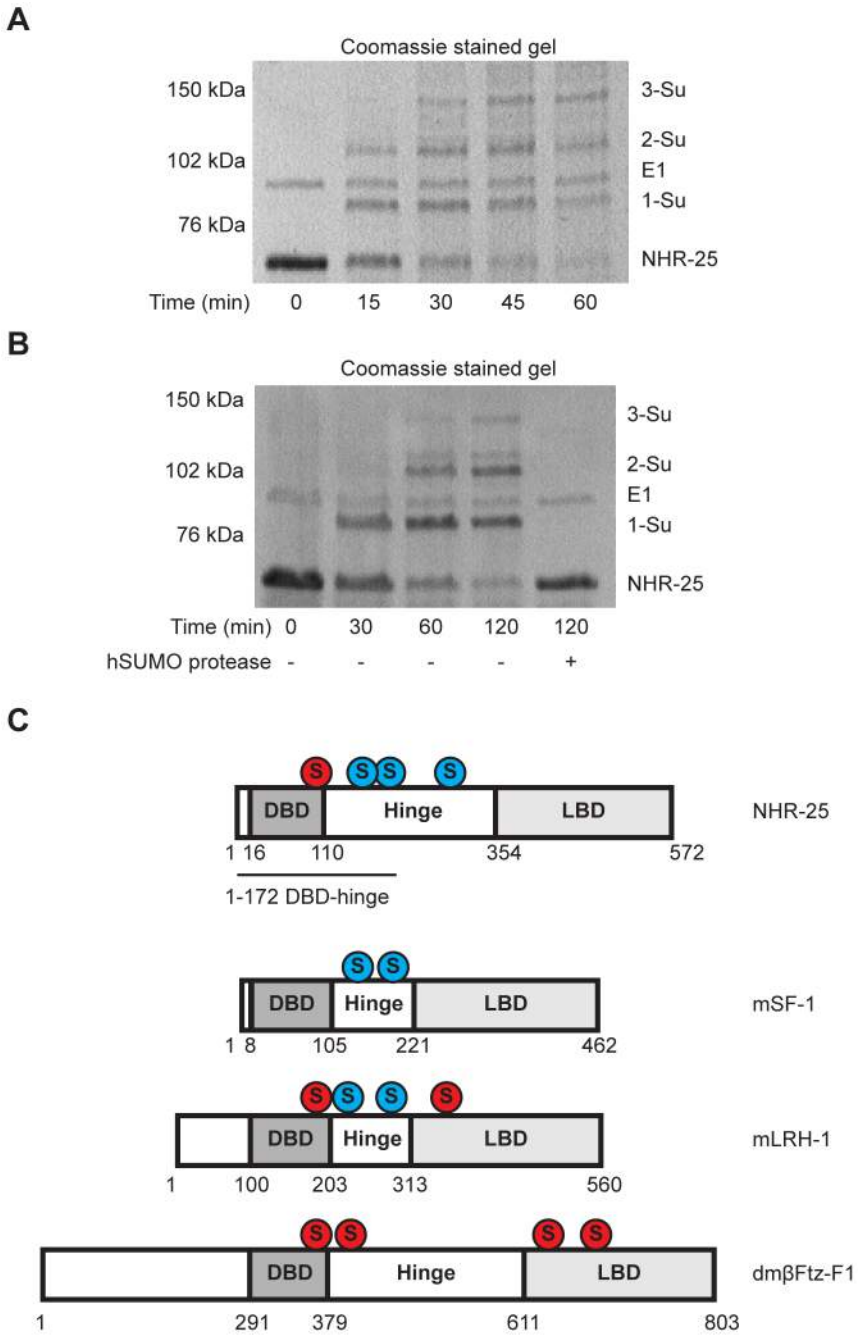

Figure 6. The NHR-25 DBD is robustly sumoylated. (A and B) *In vitro* sumoylation reactions were resolved by SDS-PAGE and Coomassie stained. A 6×His-MBP-NHR-25 (amino acids 1–173) substrate was used and incubated with hE1, hE2, and either CeSMO-1 (A) or methyl-hSUMO1 (B) for the indicated time in minutes. Methyl-hSUMO1 is a modified protein that blocks SUMO chain formation. Recombinant hSENP1 SUMO protease was included in (B) to demonstrate that bands reflected sumoylated species. A size standard in kilodaltons (kDa) is provided. (C) Schematic of sumoylation sites within NR5 family proteins. DNA-binding domains (DBD), hinge, and ligand-binding domains (LBD) are indicated. Sumoylation sites based on SUMOplot prediction and conservation in multi-species alignments are shaded red. SUMO acceptor lysines confirmed by *in vitro* biochemistry or cell-based sumoylation assays are shaded blue. The DBD-hinge fragment used in (A and B) is underlined.
doi:10.1371/journal.pgen.1003992.g006

vulval precursor cells, thereby determining morphogenesis of the entire organ.

Balance of NHR-25 sumoylation in vulval morphogenesis

Supporting the notion that sumoylation can constrain NHR-25 activity, we found that a reporter fusion responsive to NHR-25 was strongly upregulated upon depletion of *smo-1* by RNAi (Figure 7B). Our *in vitro* findings suggested that sumoylation of NHR-25 diminished DNA binding (Figure S7), while our *in vivo* studies suggested that reduction of *smo-1* caused ectopic accumulation of NHR-25 (either synthesis or impaired degradation) in VPCs P4.p and P8.p (Figure 9). These data suggest two modes, not mutually exclusive, through which sumoylation can regulate NHR-25. Moreover, overexpression of either NHR-25 or its

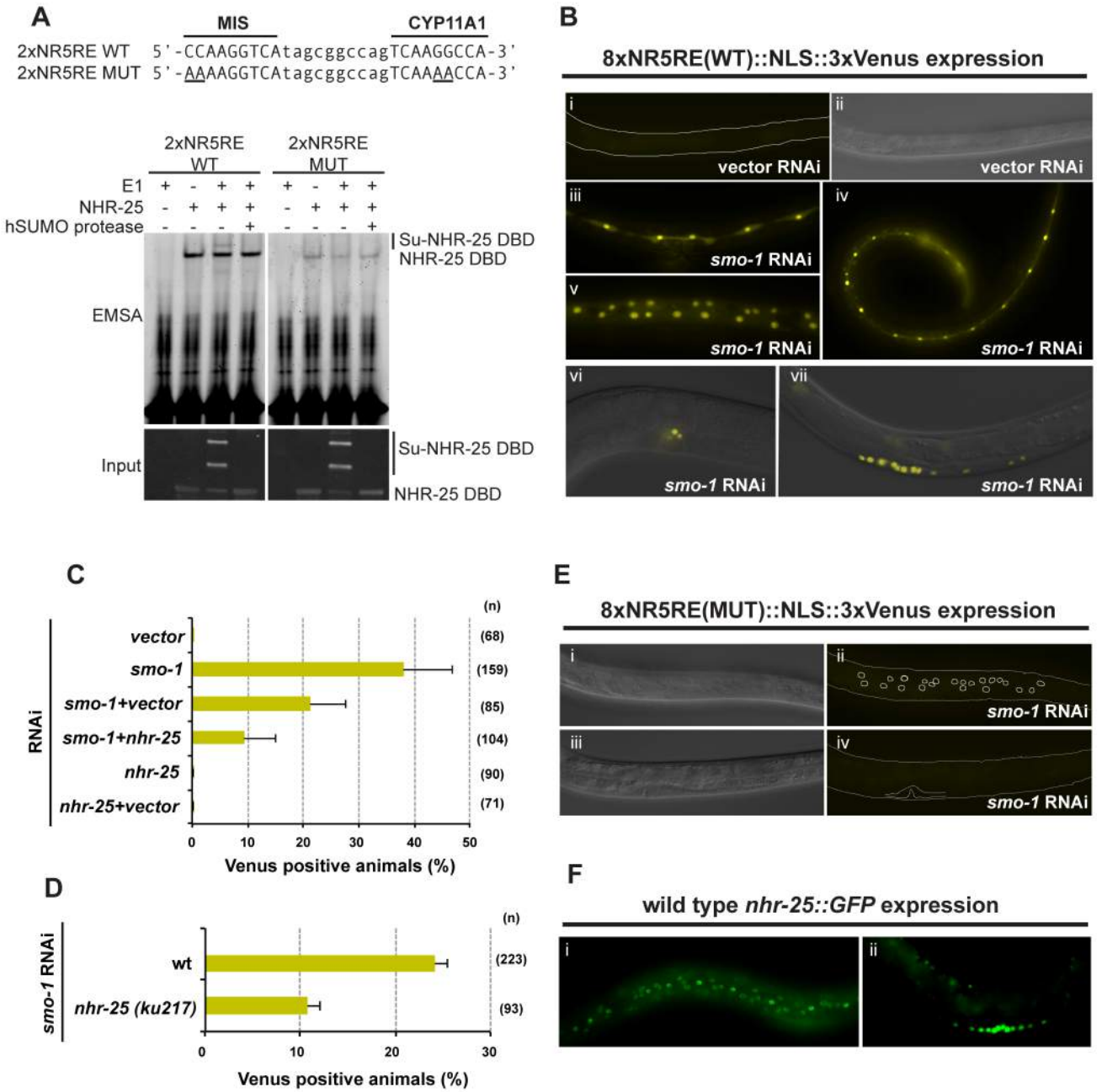

Figure 7. Sumoylation inhibits NHR-25-dependent transcription *in vivo*. (A) NHR-25 binds to canonical SF-1 target sequences. Sequence of the wild-type (WT) and mutant (MUT) MIS and CYP11A1 binding sites used are shown on top. Bases altered in the MUT sequences are underlined. The annealed 2×NR5RE oligonucleotides were incubated with combinations of the following: sumoylation enzymes (hUbc9+CeSMO-1) with or without hE1 enzyme, and NHR-25 DBD substrate. Recombinant hSENP1 SUMO protease was included to demonstrate that bands reflected sumoylated species. The corresponding proteins in the EMSA were detected by anti-MBP immunoblotting (input). The positions of unsumoylated and sumoylated NHR-25 DBD are indicated. (B) Animals carrying an *8×NR5RE (WT)::NLS::3×Venus* transgene as an extrachromosomal array were generated. No Venus expression was detected in transgenic animals on vector RNAi (i and ii). The nematode body is outlined in (i), and the corresponding differential interference contrast (DIC) image of the same animal is provided (ii). Representative Venus expression in transgenic animals treated with *smo-1* RNAi (iii–vii). Expression was observed in seam cells at L4 (iii), in seam cells and hyp7 at L3 (iv), in hyp7 at L4 (v), in the AC and vulF at early L4 (vi), and in developing vulval cells at L3 (vii). Fluorescent and DIC images were merged in vi and vii. (C and D) Transgenic animals expressing the Venus reporter in at least one of the following tissues: seam cells, hyp7, or vulval cells; were scored. Reduction of *nhr-25* function either by RNAi (C) or by *ku217* mutation (D) reduced the *8×NR5RE (WT)* reporter activity following *smo-1* RNAi. (n) number of animals scored. (E) Mutations (MUT) in NR5RE completely eliminated Venus expression following *smo-1* RNAi. DIC (i and iii) images corresponding to Venus fluorescence images (ii and iv, respectively) are provided. Positions of hypodermal nuclei (ii) and the developing vulva (iv) are outlined. (F) NHR-25::GFP is expressed in nuclei of seam cells and hyp7 (i) and the developing vulva (ii), similar to 8×NR5RE (WT)::NLS::3×Venus reporter expression. All animals are positioned with the anterior to the left.

doi:10.1371/journal.pgen.1003992.g007

A

Genotype/Strain	Muv (%)	Pn.p induction (%)						n
		P3.p	P4.p	P5.p	P6.p	P7.p	P8.p	
wild type	0	0	0	100	100	100	0	60
nhr-25(RNAi)	0	0	0	98	100	100	0	79
smo-1 (RNAi)	12.5	0	0	100	100	100	12.5	16
OP33 *[Pnhr-25::NHR-25::GFP]*								
OP33	0	0	0	100	100	100	0	45
OP33; *smo-1 (RNAi)*	30	0	10	100	100	100	20	10
[Pegl-17::NHR-25]								
HL102	8.5	0	0	100	100	100	8.5	23
[Pegl-17::NHR-25(3KR)]								
HL107	18	4.5	4.5	82	100	86	9	22
HL108	18.5	0	7.4	78	96	85	11	27
HL110	22	5.5	5	89	100	89	11	18
[Pegl-17::SMO-1]								
HL117	0	0	0	100	100	100	0	99

B

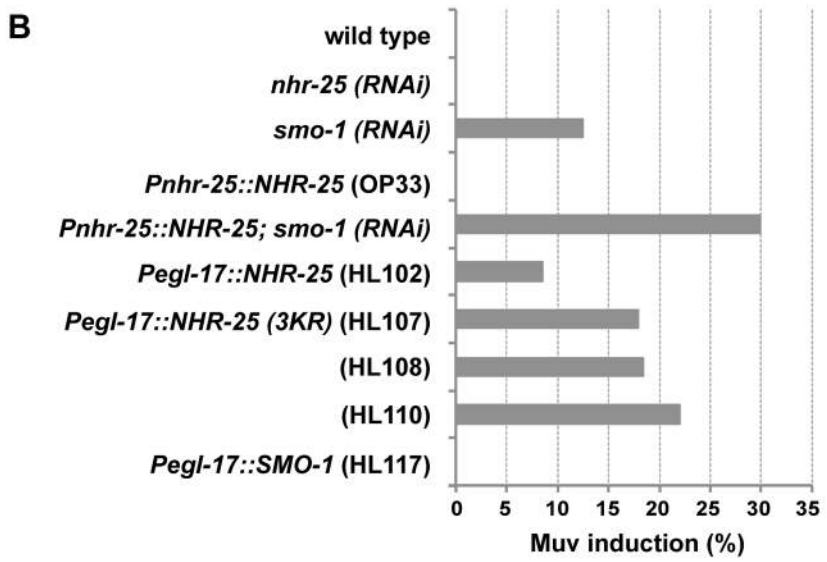

Figure 8. Overexpression of unsumoylated NHR-25 causes multivulva induction. (A) Table providing scoring of overall multivulva (Muv) induction in the indicated strains/genotypes, as well as induction in individual VPCs. Number of animals (n) scored for each strain genotype is provided. Use of brackets denotes transgenic genotypes. (B) Graphical representation of the overall percentage of animals for each strain that display Muv induction of any VPC.
doi:10.1371/journal.pgen.1003992.g008

sumoylation-defective form (NHR-25 3KR) led to multivulva induction in cells that normally adopt the 3° fate (Figure 8).

Together, our data support a model in which proper differentiation of VPCs depends on the appropriate balance of sumoylated and unsumoylated NHR-25 (Figure 10). Importantly, NHR-25 affects VPC specification cell-autonomously, as overexpression of NHR-25 in other epidermal cells, such as the seam cells or hyp7, did not cause a Muv phenotype (Table S1). Furthermore, NHR-25 appears to form a gradient across the VPC array, accumulating to high levels in 1° fated cells, intermediate levels in 2° fated cells and low levels in 3° fated cells (Figure 9). Our findings indicate that sumoylation promotes a specific pattern of NHR-25 activity in differentially fated VPCs and the relative level of NHR-25 sumoylation is

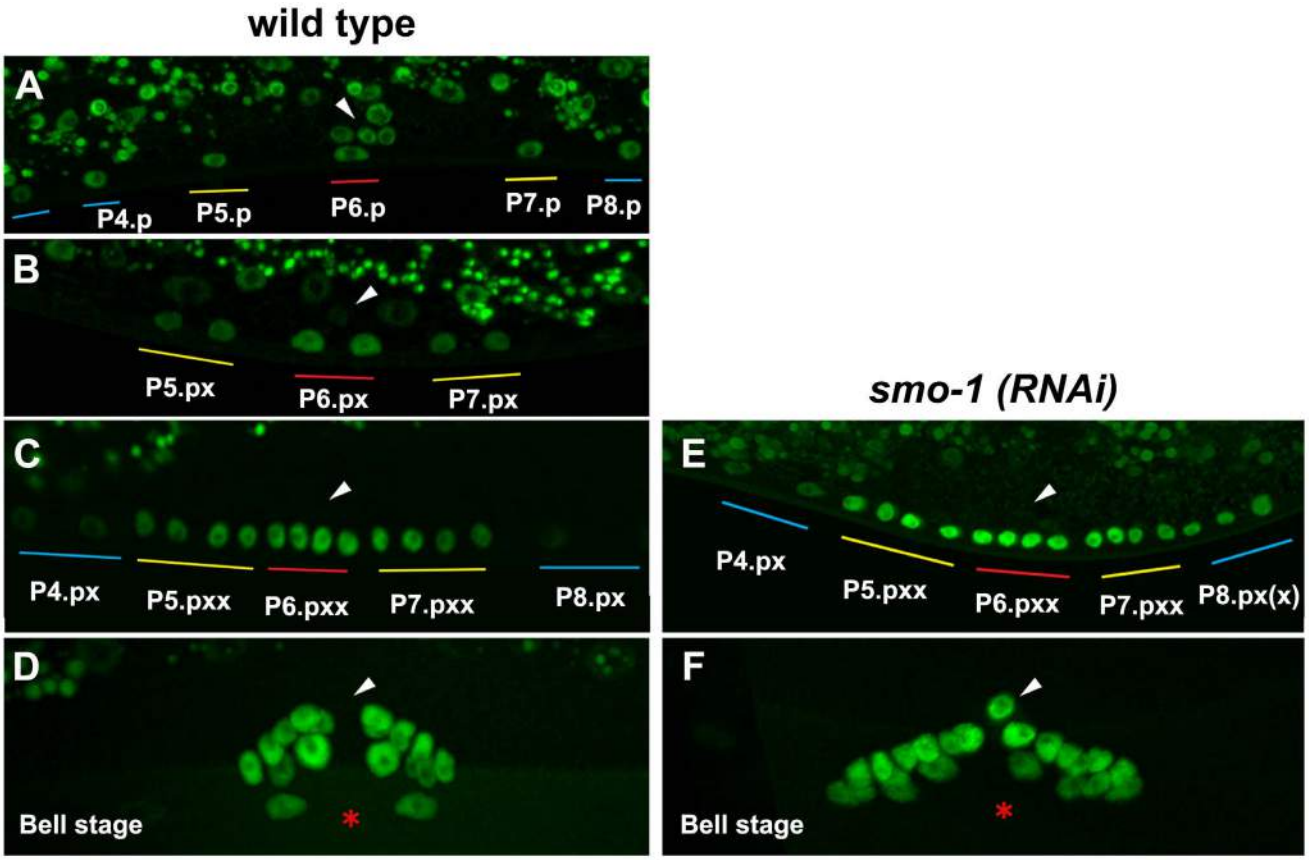

Figure 9. NHR-25::GFP (OP33) expression during vulval development. Expression in 1-cell stage Pn.p cells (A), in 2-cell stage Pn.px cells (B) and 4-cell stage Pn.pxx cells (C) in wild type and in *smo-1(RNAi)* animals (E). Higher levels and ectopic expression of NHR-25 were seen in P4.px and P8.px(x) in a *smo-1(RNAi)* background (E). Expression at the bell stage in wild type and *smo-1(RNAi)* animals (D,F). Ectopic expression in the AC observed in *smo-1(RNAi)* animals. Arrowheads indicate the position of the AC, red asterisk indicates the position of the invaginated vulva. Colored bars indicate 1° (red), 2° (yellow), and 3° (blue) lineages, as described in Figure 2.
doi:10.1371/journal.pgen.1003992.g009

critical for promotion and/or maintenance of the 3° cell fate (Figure 10).

The role(s) of NHR-25 and SMO-1 in vulval induction are likely pleiotropic. Multiple vulval development factors are sumoylated [22,28,29,36], including LIN-11, which is responsible in part for promoting vulval-uterine fusion [19]. Based on expression pattern and phenotypes, NHR-25 likely acts in other cell-types (hyp7, 1°/2° VPCs, or AC) and at different developmental time points to regulate vulval induction. The Muv phenotype of *smo-1*-deficient animals was enhanced by *nhr-25* RNAi (Figure 1). Synthetic multivulva (synMuv) genes inhibit *lin-3* activity in the syncytial hyp7 cell to prevent aberrant vulva induction in the neighboring 3° cells [37]. Yet, overexpression of NHR-25 in the hyp7 syncytium did not cause Muv induction (Table S1), thus it is unlikely that NHR-25 acts through this pathway. Our overexpression data indicates that NHR-25 acts cell-autonomously in the VPCs (Figure 8), and likely interacts with canonical signaling pathways that promote VPC fate. The NHR-25 expression gradient is reminiscent of the LIN-3/EGF gradient which promotes vulval induction through Ras activation and subsequent Notch signaling [38]. *nhr-25* appears to act downstream of LET-60/Ras signaling, as gain-of-function LET-60/Ras causes elevated NHR-25 expression (data not shown). However, regulation of *lin-3* by NHR-25 in the anchor cell has also been suggested [39]. Ectopic expression of NHR-25 in the AC following *smo-1* RNAi is unlikely to cause Muv induction since, developmentally, this expression occurs much later than VPC fate determination. In wild type animals, NHR-25 levels are therefore downregulated in the AC, which may be required for proper completion of AC invasion and/or fusion. Additionally, the cell division arrest seen in *nhr-25* RNAi leading to the Pvl phenotype was enhanced by inactivation of *smo-1* (Figure 1). For instance, the Pvl phenotype can arise from *nhr-25* reduction of function, which causes defective 1° and 2° cell divisions (Figure 1, Table 1), or from *smo-1(lf)*, which impairs uterine-vulval connections [19]. Thus, an exquisite interplay between various sumoylated targets as well as the balance between sumoylated and unsumoylated NHR-25 collaborate to ensure proper vulval formation.

How could unsumo:sumo NHR-25 balance regulate 3° cell fate? Sumoylation might alter NHR-25 levels or activity in a manner that shifts the unsumo:sumo NHR-25 ratio, which in turn acts as a switch to determine NHR-25 output. The activities of a mammalian nuclear hormone receptor have been shown to shift dramatically with signal-driven changes in levels of receptor activity [40]. Another possibility is that the sumoylated and unsumoylated versions of NHR-25 regulate distinct targets, and the unsumo:sumo ratio in different cells thereby determines the network of NHR-25-regulated genes. Indeed, sumoylation appears to affect the genomic occupancy of the NHR-25 ortholog SF-1 [27]. We note that NHR-25 sumoylation could be context-dependent. Sumoylation could increase NHR-25 activity at

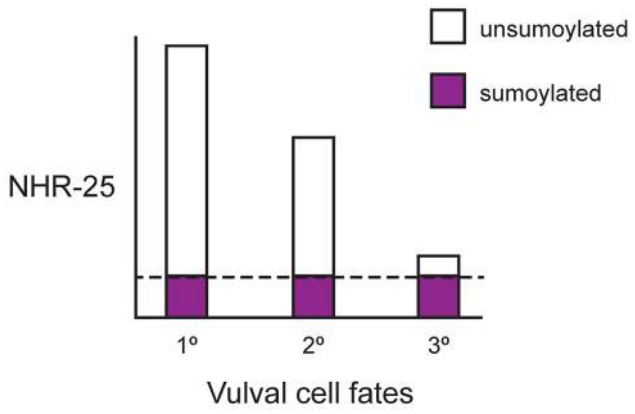

Figure 10. Ratio of sumoylated to unsumoylated NHR-25 and 3° cell fate. After the first round of cell division, VPCs adopt 1°, 2°, and 3° fates and NHR-25 accumulates in a gradient. The highest NHR-25 levels are in 1° fated cells, lower NHR-25 levels are in 2° fated cells, and the lowest levels are in 3° fated cells. Sumoylation output is a reflection of the combined activities of the sumoylation machinery and the SUMO proteases. In this model, sumoylation output is limiting, and the NHR-25 gradient results in a gradient of unsumoylated NHR-25. 1° cells have the highest ratio of unsumoylated to sumoylated NHR-25, and the ratio decreases as NHR-25 levels drop in 2° and 3° VPCs. The dashed line indicates the constant amount of sumoylated NHR-25 produced by limiting, steady-state sumoylation. At a particular threshold, enough sumoylated NHR-25 relative to unsumoylated NHR-25 allows 3° cells to either adopt and/or maintain the correct fate.
doi:10.1371/journal.pgen.1003992.g010

particular response elements. Accordingly, sumoylation positive regulates the activity of the nuclear hormone receptors RORα and ER [41,42].

The finding that overexpression of NHR-25 strongly provoked a Muv phenotype suggests that sumoylation state of NHR-25 in VPCs is exquisitely regulated. Such regulation might be accomplished by subtle changes in availability of SUMO in different VPCs, not detected by our assays, or by the relative activities of the sumoylation machinery and the SUMO proteases. A similar competition for constant levels of SUMO regulates Epstein-Barr virus infections, where the viral BZLF protein competes with the host PML protein for limiting amounts of SUMO1 [43].

Sumoylation as a nuclear hormone receptor signal

It is intriguing to consider SMO-1 as an NHR-25 ligand parallel to hormones or metabolites bound noncovalently nuclear hormone receptors in other metazoans, and by the *C. elegans* DAF-12 receptor. Indeed, such expansion of the concept of signaling ligands could "de-orphan" many or all of the 283 *C. elegans* nuclear hormone receptors for which no traditional ligands have been identified. Detection of noncovalent ligands is very challenging; numerous mammalian NHRs remain "orphans" despite intensive efforts to find candidate ligands and evidence that the ancestral NHR was liganded [44]. In principle, SUMO can be conjugated to its target sequence motif anywhere on the surface of any protein, whereas classic NHR ligands bind only stereotyped pockets within cognate NHR LBDs. Viewed in this way, SUMO may directly regulate many NHRs (and other factors as well), whereas classical NHR ligands act more selectively on only one or a few NHRs. The multifactorial regulation of NHRs would provide ample opportunity for gene-, cell- or temporal-specificity to be established in cooperation with the SUMO ligand.

Modes of SUMO regulation in *C. elegans*

There are three ways in which SUMO can potentially interact with target proteins: i) non-covalent binding, where a protein binds either free SUMO or SUMO conjugated onto another protein; ii) sumoylation, where SUMO associates covalently with a target protein through an isopeptide linkage; and iii) poly-sumoylation, where chains of SUMO are built up from an initially mono-sumoylated substrate. In *C. elegans*, SMO-1 can bind proteins non-covalently [45] or can be covalently linked to substrates (Figure 4). Polysumoylation occurs through SUMO modification of acceptor lysines within SUMO proteins [46]. In our assays, we saw no robust polyCeSMO-1 chains compared to the hSUMO2 control, even after prolonged reaction times (Figure S6). Consistent with this result, sumoylation motifs were predicted within hSUMO1, 2 and 3, and yeast SMT3 but not in CeSMO-1. PolySUMO chains in yeast and vertebrates can be recognized by SUMO targeted ubiquitin ligases (STUbL*s*) that polyubquitinate the polySUMO chain and direct it for degradation by the 26S proteasome [46]. Judging from BLAST analysis, there are no evident homologs of the known STUbLs hsRNF4 or yeast SLX5–8 in *C. elegans*. As both *S. cerevisiae* SUMO (SMT3) and vertebrate SUMO2 and SUMO3 form polySUMO chains, it appears that *C. elegans* has lost the ability to form polySUMO chains.

Functional homology with SF-1/LRH-1

The mammalian homologs of NHR-25 (SF-1 and LRH-1) are sumoylated on two sites within the hinge region of the protein, between the DBD and LBD [21,27,47]. These SUMO acceptor sites occur at corresponding positions in NHR-25, with the site near the DBD being duplicated (Figure 6C). Additionally, our DBD sumoylation experiments suggest the presence of a fourth sumoylation site in NHR-25, conserved with *D. melanogaster* Ftz-F1 and mammalian LRH-1 (Figure 6C) [7,31]. Thus, NHR-25 appears to have sumoylation sites that are conserved in both SF-1 and LRH-1 as well as at least one site that is only conserved in LRH-1. Similarly, NHR-25 seems to combine regulation of processes that in mammals are either regulated by SF-1 only or LRH-1 only. Additionally, human SUMO1 can be conjugated onto NHR-25 and *C. elegans* SMO-1 can be conjugated onto SF-1 (Figure 4, S4). Therefore, despite the 600–1200 million years of divergence since the common ancestor of humans and nematodes, regulation of NR5A family by sumoylation appears to be incredibly ancient. There are also, however, notable differences. For instance, while LRH-1 and SF-1 strongly interact with UBC9, providing a mechanism for robust, E3 ligase-independent sumoylation [20], this did not appear to be the case for NHR-25. As indicated above, we also did not find evidence for polysumoylation of NHR-25.

Having established SUMO as an NHR-25 signal that regulates cell fate, it will be exciting to further explore how sumoylation affects the NHR-25 gene regulatory network. It will be essential in future work to identify direct NHR-25 target genes by ChIP-seq, to determine how sumoylation impacts NHR-25 response element occupancy, and to mutate sumoylation sites and response elements with genome editing technologies, such as CRISPR/Cas9 [48]. The compact *C. elegans* genome facilitates unambiguous assignment of putative response elements to regulated genes, a daunting challenge in vertebrate systems. Further, the extensive gene expression and phenotypic data accessible to the *C. elegans* community will allow identification of candidate NHR-25 target genes directly responsible for regulating animal development and physiology. Understanding how NHR-25 sumoylation regulates specific genes, and how this information is integrated into

developmental circuits will advance our understanding of combinatorial regulation in metazoan gene regulatory networks.

Materials and Methods

Molecular biology

cDNAs and promoters/binding sites were Gateway cloned (Invitrogen) into pDONR221 and pDONR-P4P1r, respectively. Mutations were introduced into the *nhr-25* cDNA using site-directed mutagenesis with oligonucleotides carrying the mutation of interest and Phusion polymerase (NEB). cDNAs and promoters were then moved by Gateway cloning into destination vectors. NHR-25 (amino acids 161–541) and NHR-25 (amino acids 1–173) were moved into the bacterial expression vector pETG-41A, which contains an N-terminal 6×His-MBP tag. CeUBC-9 and CeSMO-1 cDNAs were moved into the bacterial expression vector pETG-10A, which contains an N-terminal 6×His tag. The CeUBC-9 construct also carried an N-terminal tobacco etch virus (TEV) cleavage site for removal of the 6×His tag, similar to the hUBC9 bacterial expression construct. For Y1H experiments, 2×SF-1 binding sites were Gateway cloned into pMW2 and pMW3 [49]. For Y2H experiments, cDNAs were moved into pAD-dest and pDB-dest [18], which contain the Gal4 activation domain and DNA binding domain, respectively. For Y3H, *smo-1* was moved into pAG416-GPD-ccdB-HA [50], which results in constitutive expression. For luciferase experiments, cDNAs were moved into pDEST-CMV-Myc. For our *C. elegans* expression experiments, cDNA constructs were Gateway cloned into pKA921 along with either the *egl-17*, *wrt-2*, or *grl-21* promoter. The *egl-17* promoter was PCR cloned from N2 genomic DNA. The *wrt-2* and *grl-21* promoters (pKA279 and pKA416, respectively) were previously cloned [12]. pKA921 contains a polycistronic mCherry cassette to allow monitoring of construct expression. For our 3×Venus reporters, three-fragment Gateway cloning into pCFJ150 [51] was performed. The *8×NR5RE-pes-10Δ* promoter fragments were cloned into pDONR-P4P1r. *C. elegans* codon optimized *3×Venus* was cloned from *Prnr::CYB-1DesBox::3×Venus* [52] and an NLS was added on the 5′ end of the gene and *NLS-3×Venus* was Gateway cloned into pDONR221. The *unc-54* 3′-UTR in pDONR-P2rP3 was a gift from the Lehner lab. Primer sequences are provided in Table S2. Plasmids generated for this study are listed in Table S3.

Y2H screening and matrix assays and Y1H analyses

Yeast transformations and Y2H assays were carried out as described by Deplancke *et al.* [53]. For the Y2H screen, *S. cerevisiae* strain MaV103 carrying a pDB-*nhr-25* construct was transformed with 100 ng of the AD-Orfeome cDNA library, in which 58% of the known *C. elegans* open reading frames are fused to the Gal4 activation domain [18]. Six transformations were performed per screen and 149,800 interactions were screened, representing 12.5-fold coverage of the library. Positive interactions were selected for by growth on SC dropout plates lacking leucine, tryptophan, and histidine; these plates were supplemented with 20 mM of the histidine analog 3-aminotriazole. Interactions were confirmed by β-galactosidase staining. We identified 42 candidate interactors, but only *smo-1* was recovered multiple times (seven independent isolations). Moreover, upon cloning and retesting the candidate interactor cDNAs, only *smo-1* was confirmed as an interactor. The screen identified no other components of the SUMO machinery or known SUMO binding proteins. Generation of Y1H bait strains and Y1H analyses were performed as described [53]. pDB constructs carrying NHR-2, NHR-10, NHR-31, NHR-91, NHR-105, FAX-1, and ODR-1 cDNAs were a gift from Marian Walhout.

Protein purification

Recombinant hE1, hUBC9, hSUMO1, hSUMO2, hSENP1, and murine SF-1 LBD were purified as described [27,54–56]. 6×His-CeSMO-1 and 6×His-TEV-CeUBC-9 were expressed in BL21(λDE3) *E. coli* and purified using a similar scheme as used to purify their human counterparts [55,56]. 6×His-MBP-NHR-25 (amino acids 161–541) was freshly transformed into BL21(λDE3) *E. coli*. A 1 L culture was grown to an OD600 of ~0.8, induced with 0.2 mM isopropylthio-β-galactoside (IPTG), and shaken at 16°C for four hours. Bacteria were lysed using a microfluidizer in 20 mM Tris-HCl pH 8.0, 350 mM NaCl, 20 mM imidazole containing EDTA-free Protease Inhibitor Cocktail III (EMD Millipore). 6×His-MBP-NHR-25 was then purified using nickel affinity chromatography (5 ml His Trap FF column, GE Healthcare). Peak fractions were pooled, dialyzed into 20 mM HEPES (pH 7.5), 1 mM EDTA, and 2 mM CHAPS {3-[(3-cholamidopropyl)-dimethylammonio]-1-propanesulfonate}, and purified by anion-exchange chromatography using a MonoQ column (GE Healthcare) and eluted with a 1 M ammonium acetate gradient. Peak fractions were pooled, concentrated and 6×His-MBP-NHR-25 was purified by size-exclusion chromatography using an S200 column (GE Healthcare). Peak fractions containing 6×His-MBP-NHR-25 were pooled, concentrated, dialyzed into 20 mM Tris pH 7.5, 50 mM NaCl, 10% glycerol, flash frozen in liquid nitrogen, and stored at −80°C. Later purifications used only nickel affinity chromatography. Using this preparation in sumoylation assays produced results similar to those obtained using the preparations purified over the three aforementioned columns. 6×His-MBP-NHR-25 (amino acids 1–173) was expressed and purified using a single nickel affinity chromatography step, as described above for the 6×His-MBP-NHR-25 (amino acids 161–541) fragment.

In vitro sumoylation assays

Reactions were performed as described by Campbell *et al.* [27]. Briefly, 50 µl sumoylation reactions were set up with 0.1 µM E1, 10 µM UBC9, and 30 µM SUMO in a buffer containing 50 mM Tris-HCl (pH 8.0), 100 mM NaCl, 10 mM MgCl2, 10 mM ATP, and 2 mM DTT. Substrates were added at 1 µM and when required, 2.5 µg of hSENP1 SUMO protease was added. When *in vitro* transcribed proteins were used as substrates, 50 µl reactions were generated using a TnT T7 Quick Coupled Transcription/Translation System (Promega). 16 µl of this reaction was then used as a substrate in a 25 µl sumoylation reaction using the same molarities as described above. When SUMO protease was required, 1.25 µg of hSENP1 was added. Reactions were incubated at 37°C for the desired time, and stopped by boiling in protein sample buffer (10% Glycerol, 60 mM Tris/HCl pH 6.8, 2% SDS, 0.01% bromophenol blue, 1.25% beta-mercaptoethanol). Proteins were resolved by SDS-PAGE on either 4–12% Bis-Tris gradient gels (Invitrogen) or 3–8% Tris acetate gels (Invitrogen) followed by either Coomassie staining or immunoblotting. For immunoblotting, anti-NHR-25, anti-guinea pig-HRP (Santa Cruz), and anti-guinea pig-IR800 (Li-Cor) antibodies were used. Blots were developed using a LAS500 imager (GE Healthcare) or an Odyssey laser scanner (Li-Cor).

Electrophoretic mobility shift assay (EMSAs)

Reactions were performed as described by Campbell *et al.* [27] with the following alterations. We added 400 µg/ml of bovine serum albumin to the EMSA buffer (50 mM Tris (pH 8.0), 150 mM NaCl, 10 mM $MgCl_2$, 10 mM DTT, 10 mM ATP, and a 1 µM concentration of double-stranded oligonucleotide). Sequences of oligonucleotides are provided in Table S2. Oligonucleotides were annealed and then centrifuged in an

Amicon Ultra 0.5 ml centrifugal filter (MWCO 50). Sumoylation reactions were set up on ice and added directly to the annealed oligonucleotides (20 µl final volume). Standard reactions used 500 nM of unmodified NHR-25 substrate, titration experiments added NHR-25 in 100 nM increments from 200–700 nM. At this point SENP1 (0.5 µl) was added when appropriate. We incubated these reactions at room temperature for 30 minutes to allow both sumoylation and DNA binding to occur. Half of the EMSA reaction (10 µl) was removed and added to 2 µl of 4× protein sample buffer and denatured by boiling for five minutes. Sumoylation products in the input were analyzed by immunoblotting using anti-MBP (NEB) and anti-mouse-IR800 (LiCor) antibodies. Blots were imaged using an Odyssey laser scanner. The remaining EMSA reaction was resolved on a 4–20% TBE polyacrylamide gel (Invitrogen) at 200 volts and stained with 1× SYBR Gold (Molecular Probes) in 0.5× TBE. Gels were then imaged using a Typhoon laser scanner (GE Healthcare).

C. elegans culture and strains

C. elegans was cultured at 20°C according to standard protocols and the wild type strain is the N2 Bristol strain [57]. The following mutant and transgenic strains were used in this study: PS3972 *unc-119(ed4) syIs90 [egl-17::YFP+unc-119(+)]*, OP33 *unc119 (ed3); wgIs33 [nhr-25::TY1::EGFP::3×FLAG(92C12)+unc-119(+)]*, VC186 *smo-1(ok359)/szT1[lon-2(e678)]; +/szT1*, MH1955 *nhr-25(ku217)*. The following transgenic strains were generated for this study: HL102 *jmEx102[Pegl-17::Myc::NHR-25_mCherry+rol-6(su1006)]*, HL107, HL108, HL110 are independent lines carrying *jmEx107[Pegl-17::Myc::NHR-25(3KR)_mCherry+rol-6(su1006)]*, HL117 *jmEx118 [Pegl-17::Myc::SMO-1_mCherry+rol-6(su1006)]*, HL111 and HL112 are independent lines carrying *jmEx111[Pgrl-21::Myc::NHR-25_ mCherry+rol-6(su1006)]*, HL121 *jmEx121[Pgrl-21::Myc::SMO-1_ mCherry+rol-6(su1006)]*, HL113 and HL114 are independent lines carrying *jmEx113[Pwrt-2::Myc::NHR-25_mCherry+rol-6(su1006)]*, HL115 and HL116 are independent lines carrying *jmEx115[Pwrt-2::Myc::SMO-1_mCherry+rol-6(su1006)]*, HL153 *jmEx153[8×NR5RE (WT):pes-10Δ:NLS-3×Venus:unc-54 3′-UTR+Pmyo-2::tdTomato]*, HL155 *jmEx155[8×NR5RE (MUT):pes-10Δ:NLS-3×Venus::unc-54 3′-UTR+ Pmyo-2::tdTomato]*, HL170 *nhr-25(ku217); jmEx153*.

Constructs and microinjection

The following Gateway-based constructs were generated in pKA921: pJW522*[Pegl-17(1914 bp)::Myc::NHR-25_polycistronic_mCherry]*, pJW774 *[Pegl-17(1914 bp)::Myc:: NHR-25(3KR)_ polycistronic_mCherry]*, pJW773 *[Pegl-17(1914 bp)::Myc::SMO-1_ polycistronic_mCherry]*, pJW526 *[Pgrl-21(746 bp)::Myc::NHR-25_ polycistronic_mCherry]*, pJW775 *[Pgrl-21(746 bp)::Myc::SMO-1_polycistronic_mCherry]*, pJW524*[Pwrt-2(1380 bp)::Myc::NHR-25_polycistronic_mCherry]*, pJW776*[Pwrt-2(1380 bp)::Myc::SMO-1_polycistronic_ mCherry]*. The following Gateway-based constructs were generated in pCFJ150 [51]: pJW1109 *[8×NR5RE(WT):pes-10Δ:NLS-3×Venus:unc-54 3′-UTR]* and pJW1110 *[8×NR5RE(MUT):pes-10Δ: NLS-3×Venus::unc-54 3′-UTR]*. Plasmids were prepared using a PureYield Plasmid Midiprep System (Promega) followed by ethanol precipitation, or a Qiagen Plasmid Midi kit (Qiagen). Transgenic strains were generated by injecting 50 ng/µl of each plasmid into the *C. elegans* gonad [58] with the co-injection marker pRF4 [59]. For *8×NR5RE* reporter strain generation, N2 animals were injected with 30 ng/µl of the reporter plasmid and 5 ng/µl of co-injection marker *Pmyo-2::tdTomato* [60].

RNA interference

Feeding RNAi was performed as described, with the indicated alterations to the protocol [61]. dsRNA was initially induced for four hours in liquid culture using 0.4 mM IPTG, before bacteria were concentrated and seeded on plates also containing 0.4 mM IPTG. Bacteria carrying pPD129.36 without an insert were used for control RNAi. For *nhr-25* RNAi, synchronized L2 larvae (19–20 hours after hatching) were fed on bacteria expressing *nhr-25* dsRNA to bypass the anchor cell (AC) defect. *smo-1* RNAi was performed on late L4 or young adults. For *in vivo* reporter assays, sodium hypochlorite-treated eggs were placed on RNAi plates seeded with dsRNA induced bacteria.

Scoring VPC induction, lineaging and microscopy

To score vulva induction, nematodes were anesthetized in 10 mM levamisole, mounted onto 5% agar pads (Noble agar, Difco) and the number of daughter cells for each VPC were counted under differential interference contrast (DIC) optics. For lineaging analyses, the division pattern was followed under DIC from the two to eight cell stages [62]. Animals were mounted onto 5% agar pad with bacteria in S-basal medium without anesthesia. Olympus Fluoview FV1000 and Zeiss Axioplan microscopes were used for observation and imaging.

NHR-25 antibody

A peptide-based anti-NHR-25 antibody was raised in guinea pig (Peptide Specialty Laboratories, GmbH, Germany). Animals were immunized against four short peptides in the hinge and LBD regions: PEHQVSSSTTDQNNQINYFDQTKC (24 a.a. 141–163); SLHDYPTYTSNTTNC (15 a.a. 250–263); TSSTTTGRMTEASSC (15 a.a. 283–296) RYLWNLHSNXPTNWEC (16 a.a. 507–521).

Cell culture and luciferase assay

Human embryonic kidney (HEK) cell line 293T was maintained in Dulbecco's modified Eagle's medium (DMEM, Gibco), supplemented with 10% fetal bovine serum. Transfections were performed with polyethyleneimine (25 kDa, Sigma). The transcriptional activity of NHR-25 was tested with a luciferase vector carrying a CMV basic promoter driven by two copies of the Ftz-F1 binding consensus sequences TGAAGGTCA and TCAAGGTCA (total of four binding sites, 2×TGA-TCA::Luc) [8,63]. Cells were seeded onto 24-well plates and the next day were transfected for three hours with a polyethylenimine mixture containing 50 ng of pTK-Renilla plasmid (Promega) as an internal control, 300 ng of the luciferase reporter plasmid, and 150 ng of the appropriate expression vector. The total amount of DNA was kept constant (1 µg) by adding empty expression vector where necessary. Forty hours post-transfection, the cells were harvested and processed using the Dual Luciferase Reporter Assay System (Promega). Eight independent biological replicates from three independent experiments were assayed, and data were presented as average values with standard deviations after normalization against the Renilla luciferase activities. For immunocytochemistry, transfected cells were fixed with 4% formaldehyde (Sigma) for 10 min. After washing with PBS, cells were permeabilized with PBS containing 0.2% TritonX-100 in (PBST), washed with TBST buffer (25 mM Tris-HCl, pH 7.5, 136 mM NaCl, 2.7 mM KCl and 0.1% TritonX-100), incubated in blocking solution (2.5% skim milk and 2.5% BSA in TBST). Anti-Myc 9E10 antibody (Sigma; 1:2000 dilution) was added and incubated for overnight at 4°C. Following washing, goat-anti-mouse-TRITC conjugated 2° antibody (Jackson ImmunoResearch; 1:2000 dilution) was added and incubated at room temperature for two hours. Cells were counterstained with DAPI (1 µg/ml) to visualize the nucleus.

Supporting Information

Figure S1 SMO-1 interaction is specific to NHR-25. (A) Yeast two-hybrid analysis of the indicated proteins fused to the Gal4 activation domain (AD) or DNA binding domain (DB). Empty vector (No insert) controls are shown. β-galactosidase (LacZ) and HIS3 (3AT; 3-aminotriazole) reporters were assayed, and yeast viability was confirmed by growth on a plate lacking leucine and tryptophan (-Leu-Trp). Both NHR-25β and NHR-31 displayed self-activation activity, precluding analysis of their interactions with any of the AD fusions. (B) Due to the size of the matrix, the strains were plated on two plates. To rule out variation between plates, a negative control (i; AD and DB empty vectors) and two positive controls (RFS-1 interaction with RAD-51 (ii) and R01H10.5 (iii), respectively) are provided for each plate.
(TIF)

Figure S2 *smo-1(lf)* and *smo-1(lf); nhr-25(RNAi)* cause defects in 2° cell fate. (A) *Pegl-17::YFP* expression in vulval cells at the 4-cell stage (1° cell fate marker) in the animals of the indicated genotypes. Ectopically high expression of *Pegl-17::YFP* was observed in 2° fated cells in *smo-1(ok359)* and *smo-1(ok359); nhr-25(RNAi)* animals. (B) The *egl-17::YFP* vulva marker is expressed in *smo-1 (lf)*-induced multivulva. Wild type expression of *egl-17::YFP* seen in vulD (a) and vulC (b) in late vulva morphogenesis. In *smo-1 (ok359)* and *smo-1 (ok359); nhr-25 (RNAi)* backgrounds (c and d), Muv is induced and the 1°/2° vulva marker *egl-17::GFP* is ectopically expressed. * indicates ectopic vulvae. (C) *egl-17* has been reported to be expressed in all Pn.p cells [34]. NHR-25, NHR-25(3KR) and SMO-1 were driven by an *egl-17* promoter for *in vivo* overexpression (Figure 8) from a vector carrying a polycistronic mCherry marker. We observed mCherry expression in Pn.p cells, indicating that this promoter is active in these cells. A representative image of mCherry expression in P3.p and P6.p cells from an *[egl-17::NHR-25(3KR)_polycistronic_mCherry]* transgenic animal is provided.
(TIF)

Figure S3 SMO-1 expression is required for NHR-25 to interact with UBC-9. (A) Indicated proteins were fused to the Gal4 activation domain (AD) or DNA binding domain (DB). Empty vector (No insert) controls are shown. (A) Yeast two-hybrid data confirmed that the SMO-1 V31K β-sheet mutation still binds to UBC-9, which indicated that the mutation did not disrupt the protein. The SMO-1 di-glycine deletion (ΔGG) prevented the interaction with UBC-9. (B) Yeast three-hybrid analysis. The indicated AD and DB fusions were expressed along with the pAG416 low copy yeast expression vector carrying either no insert or SMO-1. β-galactosidase staining is provided in A and B.
(TIF)

Figure S4 Confirmation of activity of sumoylation enzymes. *In vitro* sumoylation reactions were resolved by SDS-PAGE and visualized by Coomassie staining (A,B) or anti-NHR-25 immunoblotting (C). (A and B) used a recombinant SF-1 partial hinge-LBD fragment as a substrate and (C) used a recombinant 6×His-MBP-NHR-25 (amino acids 161–541) fragment. All reactions used recombinant hE1. In (A), hE2 (UBC9) and hSUMO1 were used. (B and C) used CeUBC-9 and CeSMO-1. Recombinant hSENP1 SUMO protease was included in each experiment to demonstrate that bands reflected sumoylated species. A size standard in kilodaltons (kDa) is provided.
(TIF)

Figure S5 The NHR-25 hinge domain is sumoylated *in vitro* on three lysines. *In vitro* sumoylation reactions were resolved by SDS-PAGE and visualized by anti-NHR-25 immunoblotting (A) or Coomassie staining (B). Both reactions used hE1, hE2, hSUMO1, and a recombinant NHR-25 substrate (6×His-MBP-NHR-25 (amino acids 161–541)). In (A) recombinant hSENP1 SUMO protease was included. In (B), the substrates were wild type NHR-25 (WT) and NHR-25 2KR (K170R K236R) and NHR-25 3KR (K165 K170R K236R) mutants where SUMO acceptor lysines were mutated to arginine. A size standard in kilodaltons (kDa) is provided.
(TIF)

Figure S6 Sumo1 and SMO-1 do not readily form poly-SUMO chains. (A) Anti-NHR-25 immunoblots on sumoylation reactions incubated for the indicated number of hours. E1 enzyme was incubated with the indicated E2 and SUMO combinations. Methyl-hSUMO1 is a modified protein that blocks SUMO chain formation. The asterisk (*) indicates a non-specific band in the NHR-25 substrate control lane (no sumoylation enzymes added). NHR-25 isoforms predicted to contain one, two, and three SUMO proteins covalently attached are indicated (1-Su, 2-Su, 3-Su, respectively). (B–E) Short course sumoylation time courses using hE1, hE2, and hSUMO1 (B,D) or hE1, CeUBC-9, and CeSMO-1 (C,E). The substrate was recombinant 6×His-MBP-NHR-25 (amino acids 161–541). Reaction time in minutes, and a size standard in kilodaltons (kDa) are provided. The final lane is a substrate only control. Coomassie stained polyacrylamide gels (B, C) and anti-NHR-25 immunoblots (D,E) are shown.
(TIF)

Figure S7 Sumoylation affects NHR-25 binding to canonical SF-1 sites. (A) Sequence of binding sites used in the Y1H and EMSA experiments. The mutation in the MIS binding site (MIS MUT) is underlined. The canonical binding site of the NHR-25 ortholog, SF-1, is 5′-YCAAGGYCR-3′ (Y = T/C, R = G/A) [63]. (B) Y1H analysis. Two tandem copies of the indicated binding sites upstream of a LacZ reporter were integrated into the YM4271 yeast strain. Indicated proteins were fused to the Gal4 activation domain (AD). (C) EMSA data. Annealed oligonucleotides carrying the MIS WT, MIS MUT, and CYP11A1 binding sites were incubated with: sumoylation enzymes (hUbc9+CeSMO-1) with or without hE1 enzyme, and NHR-25 DBD substrate. Recombinant hSENP1 SUMO protease was included to demonstrate that bands reflected sumoylated species. (D) EMSA analysis of NHR-25 binding to annealed oligonucleotides carrying both MIS and CYP11A1 binding sites (2×NR5RE). Increasing amounts of sumoylated NHR-25 DBD were added to 1 μM of annealed oligos (200–700 nM NHR-25 in 100 nM increments). Both wild-type (WT) and mutated (MUT) binding sites were analyzed. (E) EMSAs were performed on the 2×NR5RE in which the NHR-25 DBD was sumoylated at 37°C for the indicated time. (C–E) The corresponding proteins in the EMSA were detected by anti-MBP immunoblotting (input). The positions of unsumoylated and sumoylated NHR-25 DBD are indicated.
(TIF)

Table S1 Overexpression of NHR-25 in hyp7 or seam cells does not cause Muv induction. Table providing scoring of overall multivulva (Muv) induction in the indicated strains/genotypes, as well as induction in individual VPCs. Number of animals (n) scored for each strain genotype is provided. Use of brackets denotes transgenic genotypes.
(DOCX)

Table S2 Sequences of oligonucleotides and gBlocks used in this study. All sequences are displayed in a 5′ to 3′ orientation. (A) Primers used to clone the indicated cDNAs and promoters. Sequences of the attB recombination sites and Myc and FLAG

epitopes are indicated as described in the table. (B) Sequences of the primers used to generate the indicated mutations by site-directed mutagenesis. (C) gBlocks used in this study. NR5 binding sites and minimal promoters are indicated as described in the table. (D) Sequences of oligonucleotides from SF-1 target gene promoters used in EMSA assays are shown. m, mouse; h, human; MIS, Mullerian Inhibiting Substance; ; CYP11A1, Cytochrome P450, Family 11, Subfamily A, Polypeptide 1; 2×NR5RE, nuclear receptor NR5 family Response Element. The NR5RE oligos carry an mMIS and hCYP11A1 binding site. SF-1 binding site is highlighted in bold.
(DOCX)

Table S3 Plasmids generated for this study. The vector backbones used for Gateway cloning are provided, as is a description of each vector. pDONR221 (Invitrogen) and pDONR-P4P1r (Invitrogen) are entry vectors for cDNA and promoter cloning, respectively. pAD and pDB are Y2H vectors for generating N-terminal fusions of the Gal4 activation domain (AD) and DNA binding domain (DB), respectively, to proteins of interest [18]. pMW2 and pMW3 are reporter vectors for Y1H assays [49]. pMW2 is used to clone DNA fragments upstream of a HIS3 reporter gene, pMW3 is used to clone DNA fragments upstream of a LacZ reporter. pETG10A is used to generate N-terminal 6×His fusions for bacterial expression. pETG41A is used to generate N-terminal 6×His-MBP fusions for bacterial expression. pDEST-CMV-Myc is used to generate N-terminal Myc fusions under the control of a CMV promoter for mammalian cell expression. pKA921 is used for two-fragment Gateway cloning to create promoter-cDNA combinations. A polycistronic mCherry cassette with an *unc-54* 3′-UTR marks the tissues where the array is expressed. pCFJ150 is used to generate *C. elegans* expression vectors through three-fragment Gateway cloning [51]. pAG415 GAL-ccbB is used for constitutive expression of cDNAs in yeast [50]. pET-DUET1 (Novagen) is used for simultaneous expression of two cDNAs in bacteria.
(DOCX)

Acknowledgments

We thank Holly Ingraham and Erik Lontok for reagents and assistance with the *in vitro* sumoylation assays; Dominik Farka for his help generating transgenic *C. elegans*; Chris Lima for his generous gift of the hE1, hE2, and hSENP1 expression vectors; the Protein Expression and Purification Core Facility of the EMBL Heidelberg for their gift of pETG-10A and pETG-41A; Sander van den Heuvel for his gift of *Pmr::CYB-1DesBox::3×Venus*; Ben Lehner for his gift of the *unc-54* 3′-UTR entry clone; Marian Walhout for her gift of pDB-NHR vectors; Matthew Knuesel and Miles Pufall for helpful discussions and technical advice; Axel Bethke, Holly Ingraham, Marek Jindra, Matthew Knuesel, Gabriela Monsalve, Sarah Petnic, Lindsey Pack, Ben Schiller, and members of the Yamamoto lab for advice and comments on the manuscript. We appreciate the help of Soledad De Guzman for preparing plates and media. Some strains were provided by the CGC, which is funded by NIH Office of Research Infrastructure Programs (P40 OD010440).

Author Contributions

Conceived and designed the experiments: JDW NB MA. Performed the experiments: JDW NB TB MA. Analyzed the data: JDW NB KA MA KRY. Contributed reagents/materials/analysis tools: JDW NB MA. Wrote the paper: JDW KA MA KRY.

References

1. Taubert S, Ward JD, Yamamoto KR (2011) Nuclear hormone receptors in nematodes: Evolution and function. Molecular and Cellular Endocrinology 334: 49–55. doi:10.1016/j.mce.2010.04.021.
2. Robinson-Rechavi M, Maina CV, Gissendanner CR, Laudet V, Sluder A (2005) Explosive Lineage-Specific Expansion of the Orphan Nuclear Receptor HNF4 in Nematodes. J Mol Evol 60: 577–586. doi:10.1007/s00239-004-0175-8.
3. Gissendanner CR, Sluder AE (2000) *nhr-25*, the *Caenorhabditis elegans* ortholog of *ftz-f1*, is required for epidermal and somatic gonad development. Dev Biol 221: 259–272. doi:10.1006/dbio.2000.9679.
4. Asahina M, Ishihara T, Jindra M, Kohara Y, Katsura I, et al. (2000) The conserved nuclear receptor Ftz-F1 is required for embryogenesis, moulting and reproduction in *Caenorhabditis elegans*. Genes Cells 5: 711–723.
5. Frand AR, Russel S, Ruvkun G (2005) Functional Genomic Analysis of *C. elegans* Molting. PLoS Biol 3: e312. doi:10.1371/journal.pbio.0030312.
6. Hada K, Asahina M, Hasegawa H, Kanaho Y, Slack FJ, et al. (2010) The nuclear receptor gene *nhr-25* plays multiple roles in the *Caenorhabditis elegans* heterochronic gene network to control the larva-to-adult transition. Dev Biol 344: 1100–1109. doi:10.1016/j.ydbio.2010.05.508.
7. Chen Z, Eastburn DJ, Han M (2004) The *Caenorhabditis elegans* nuclear receptor gene *nhr-25* regulates epidermal cell development. Mol Cell Biol 24: 7345–7358. doi:10.1128/MCB.24.17.7345-7358.2004.
8. Asahina M, Valenta T, Silhánková M, Korinek V, Jindra M (2006) Crosstalk between a nuclear receptor and beta-catenin signaling decides cell fates in the *C. elegans* somatic gonad. Dev Cell 11: 203–211. doi:10.1016/j.devcel.2006.06.003.
9. Schimmer BP, White PC (2010) Minireview: Steroidogenic Factor 1: Its Roles in Differentiation, Development, and Disease. Molecular Endocrinology 24: 1322–1337. doi:10.1210/me.2009-0519.
10. Hammer GD, Krylova I, Zhang Y, Darimont BD, Simpson K, et al. (1999) Phosphorylation of the nuclear receptor SF-1 modulates cofactor recruitment: integration of hormone signaling in reproduction and stress. Mol Cell 3: 521–526.
11. Fayard E, Auwerx J, Schoonjans K (2004) LRH-1: an orphan nuclear receptor involved in development, metabolism and steroidogenesis. Trends in Cell Biology 14: 250–260. doi:10.1016/j.tcb.2004.03.008.
12. Mullaney BC, Blind RD, Lemieux GA, Perez CL, Elle IC, et al. (2010) Regulation of *C. elegans* fat uptake and storage by acyl-CoA synthase-3 is dependent on NR5A family nuclear hormone receptor *nhr-25*. Cell Metab 12: 398–410. doi:10.1016/j.cmet.2010.08.013.
13. van der Veen AG, Ploegh HL (2012) Ubiquitin-Like Proteins. Annu Rev Biochem 81: 323–357. doi:10.1146/annurev-biochem-093010-153308.
14. Gareau JR, Lima CD (2010) The SUMO pathway: emerging mechanisms that shape specificity, conjugation and recognition. Nature 11: 861–871. doi:10.1038/nrm3011.
15. Cheng J, Kang X, Zhang S, Yeh ETH (2007) SUMO-Specific Protease 1 Is Essential for Stabilization of HIF1α during Hypoxia. Cell 131: 584–595. doi:10.1016/j.cell.2007.08.045.
16. Taylor DL, Ho JCY, Oliver A, Watts FZ (2002) Cell-cycle-dependent localisation of Ulp1, a *Schizosaccharomyces pombe* Pmt3 (SUMO)-specific protease. J Cell Sci 115: 1113–1122.
17. Holmstrom S, Van Antwerp ME, Iñiguez-Lluhí JA (2003) Direct and distinguishable inhibitory roles for SUMO isoforms in the control of transcriptional synergy. Proc Natl Acad Sci USA 100: 15758–15763. doi:10.1073/pnas.2136933100.
18. Reboul J, Vaglio P, Rual J-F, Lamesch P, Martinez M, et al. (2003) *C. elegans* ORFeome version 1.1: experimental verification of the genome annotation and resource for proteome-scale protein expression. Nat Genet 34: 35–41. doi:10.1038/ng1140.
19. Broday L, Kolotuev I, Didier C, Bhoumik A, Gupta BP, et al. (2004) The small ubiquitin-like modifier (SUMO) is required for gonadal and uterine-vulval morphogenesis in *Caenorhabditis elegans*. Genes Dev 18: 2380–2391. doi:10.1101/gad.1227104.
20. Lee MB, Lebedeva LA, Suzawa M, Wadekar SA, Desclozeaux M, et al. (2005) The DEAD-box protein DP103 (Ddx20 or Gemin-3) represses orphan nuclear receptor activity via SUMO modification. Mol Cell Biol 25: 1879–1890. doi:10.1128/MCB.25.5.1879-1890.2005.
21. Chalkiadaki A, Talianidis I (2005) SUMO-dependent compartmentalization in promyelocytic leukemia protein nuclear bodies prevents the access of LRH-1 to chromatin. Mol Cell Biol 25: 5095–5105. doi:10.1128/MCB.25.12.5095-5105.2005.
22. Poulin G, Dong Y, Fraser AG, Hopper NA, Ahringer J (2005) Chromatin regulation and sumoylation in the inhibition of Ras-induced vulval development in *Caenorhabditis elegans*. EMBO J 24: 2613–2623. doi:10.1038/sj.emboj.7600726.
23. Kroetz MB, Hochstrasser M (2009) Identification of SUMO-interacting proteins by yeast two-hybrid analysis. Methods Mol Biol 497: 107–120. doi:10.1007/978-1-59745-566-4_7.
24. Lin D-Y, Huang Y-S, Jeng J-C, Kuo H-Y, Chang C-C, et al. (2006) Role of SUMO-interacting motif in Daxx SUMO modification, subnuclear localization, and repression of sumoylated transcription factors. Mol Cell 24: 341–354. doi:10.1016/j.molcel.2006.10.019.
25. Takahashi H, Hatakeyama S, Saitoh H, Nakayama KI (2005) Noncovalent SUMO-1 binding activity of thymine DNA glycosylase (TDG) is required for its SUMO-1 modification and colocalization with the promyelocytic leukemia protein. J Biol Chem 280: 5611–5621. doi:10.1074/jbc.M408130200.
26. Ren J, Gao X, Jin C, Zhu M, Wang X, et al. (2009) Systematic study of protein sumoylation: Development of a site-specific predictor of SUMOsp 2.0. Proteomics 9: 3409–3412. doi:10.1002/pmic.200800646.

27. Campbell LA, Faivre EJ, Show MD, Ingraham JG, Flinders J, et al. (2008) Decreased Recognition of SUMO-Sensitive Target Genes following Modification of SF-1 (NR5A1). Mol Cell Biol 28: 7476–7486. doi:10.1128/MCB.00103-08.
28. Leight ER, Glossip D, Kornfeld K (2005) Sumoylation of LIN-1 promotes transcriptional repression and inhibition of vulval cell fates. Development 132: 1047–1056. doi:10.1242/dev.01664.
29. Zhang H, Smolen GA, Palmer R, Christoforou A, Van Den Heuvel S, et al. (2004) SUMO modification is required for *in vivo* Hox gene regulation by the *Caenorhabditis* elegans Polycomb group protein SOP-2. Nat Genet 36: 507–511. doi:10.1038/ng1336.
30. Chen W-Y, Lee W-C, Hsu N-C, Huang F, Chung B-C (2004) SUMO modification of repression domains modulates function of nuclear receptor 5A1 (steroidogenic factor-1). J Biol Chem 279: 38730–38735. doi:10.1074/jbc.M405006200.
31. Talamillo A, Herboso L, Pirone L, Pérez C, González M, et al. (2013) Scavenger Receptors Mediate the Role of SUMO and Ftz-f1 in *Drosophila* Steroidogenesis. PLoS Genet 9: e1003473. doi:10.1371/journal.pgen.1003473.s003.
32. Kim S, Brostromer E, Xing D, Jin J, Chong S, et al. (2013) Probing Allostery Through DNA. Science 339: 816–819. doi:10.1126/science.1229223.
33. Silhánková M, Jindra M, Asahina M (2005) Nuclear receptor NHR-25 is required for cell-shape dynamics during epidermal differentiation in *Caenorhabditis elegans*. J Cell Sci 118: 223–232. doi:10.1242/jcs.01609.
34. Dutt A, Canevascini S, Froehli-Hoier E, Hajnal A (2004) EGF Signal Propagation during *C. elegans* Vulval Development Mediated by ROM-1 Rhomboid. PLoS Biol 2: e334. doi:10.1371/journal.pbio.0020334.
35. Sarov M, Murray JI, Schanze K, Pozniakovski A, Niu W, et al. (2012) A Genome-Scale Resource for *in vivo* Tag-Based Protein Function Exploration in *C. elegans*. Cell 150: 855–866. doi:10.1016/j.cell.2012.08.001.
36. Kaminsky R, Denison C, Bening-Abu-Shach U, Chisholm AD, Gygi SP, et al. (2009) SUMO Regulates the Assembly and Function of a Cytoplasmic Intermediate Filament Protein in *C. elegans*. Dev Cell 17: 724–735. doi:10.1016/j.devcel.2009.10.005.
37. Cui M, Chen J, Myers TR, Hwang BJ, Sternberg PW, et al. (2006) SynMuv Genes Redundantly Inhibit *lin-3/EGF* Expression to Prevent Inappropriate Vulval Induction in *C. elegans*. Dev Cell 10: 667–672. doi:10.1016/j.devcel.2006.04.001.
38. Sternberg PW (2005) Vulval development. WormBook: the online review of *C. elegans* biology: 1–28. doi:10.1895/wormbook.1.6.1.
39. Hwang BJ, Sternberg PW (2004) A cell-specific enhancer that specifies *lin-3* expression in the *C. elegans* anchor cell for vulval development. Development 131: 143–151. doi:10.1242/dev.00924.
40. Chen S-H, Masuno K, Cooper SB, Yamamoto KR (2013) Incoherent feed-forward regulatory logic underpinning glucocorticoid receptor action. Proceedings of the National Academy of Sciences. doi:10.1073/pnas.1216108110.
41. Hwang EJ, Lee JM, Jeong J, Park JH, Yang Y, et al. (2009) SUMOylation of RORalpha potentiates transcriptional activation function. Biochemical and Biophysical Research Communications 378: 513–517. doi:10.1016/j.bbrc.2008.11.072.
42. Sentis S, Le Romancer M, Bianchin C, Rostan M-C, Corbo L (2005) Sumoylation of the estrogen receptor alpha hinge region regulates its transcriptional activity. Molecular Endocrinology 19: 2671–2684. doi:10.1210/me.2005-0042.
43. Adamson AL, Kenney S (2001) Epstein-barr virus immediate-early protein BZLF1 is SUMO-1 modified and disrupts promyelocytic leukemia bodies. J Virol 75: 2388–2399. doi:10.1128/JVI.75.5.2388-2399.2001.
44. Bridgham JT, Eick GN, Larroux C, Deshpande K, Harms MJ, et al. (2010) Protein Evolution by Molecular Tinkering: Diversification of the Nuclear Receptor Superfamily from a Ligand-Dependent Ancestor. PLoS Biol 8: e1000497. doi:10.1371/journal.pbio.1000497.g006.
45. Onitake A, Yamanaka K, Esaki M, Ogura T (2012) *Caenorhabditis elegans* fidgetin homolog FIGL-1, a nuclear-localized AAA ATPase, binds to SUMO. Journal of Structural Biology 179: 143–151. doi:10.1016/j.jsb.2012.04.022.
46. Tatham MH, Geoffroy M-C, Shen L, Plechanovova A, Hattersley N, et al. (2008) RNF4 is a poly-SUMO-specific E3 ubiquitin ligase required for arsenic-induced PML degradation. Nat Cell Biol 10: 538–546. doi:10.1038/ncb1716.
47. Yang F-M, Pan C-T, Tsai H-M, Chiu T-W, Wu M-L, et al. (2008) Liver receptor homolog-1 localization in the nuclear body is regulated by sumoylation and cAMP signaling in rat granulosa cells. FEBS Journal 276: 425–436. doi:10.1111/j.1742-4658.2008.06785.x.
48. Dickinson DJ, Ward JD, Reiner DJ, Goldstein B (2013) Engineering the *Caenorhabditis elegans* genome using Cas9-triggered homologous recombination. Nat Meth: 1–9. doi:10.1038/nmeth.2641.
49. Deplancke B, Mukhopadhyay A, Ao W, Elewa AM, Grove CA, et al. (2006) A Gene-Centered *C. elegans* Protein-DNA Interaction Network. Cell 125: 1193–1205. doi:10.1016/j.cell.2006.04.038.
50. Alberti S, Gitler AD, Lindquist S (2007) A suite of Gateway cloning vectors for high-throughput genetic analysis in *Saccharomyces cerevisiae*. Yeast 24: 913–919. doi:10.1002/yea.1502.
51. Frøkjaer-Jensen C, Davis MW, Hopkins CE, Newman BJ, Thummel JM, et al. (2008) Single-copy insertion of transgenes in *Caenorhabditis elegans*. Nat Genet 40: 1375–1383. doi:10.1038/ng.248.
52. Korzelius J, The I, Ruijtenberg S, Portegijs V, Xu H, et al. (2010) *C. elegans* MCM-4 is a general DNA replication and checkpoint component with an epidermis-specific requirement for growth and viability. Dev Biol: 1–12. doi:10.1016/j.ydbio.2010.12.009.
53. Deplancke B, Vermeirssen V, Arda HE, Martinez NJ, Walhout AJM (2006) Gateway-Compatible Yeast One-Hybrid Screens. Cold Spring Harbor Protocols 2006: pdb.prot4590–pdb.prot4590. doi:10.1101/pdb.prot4590.
54. Reverter D, Lima CD (2009) Preparation of SUMO proteases and kinetic analysis using endogenous substrates. Methods Mol Biol 497: 225–239. doi:10.1007/978-1-59745-566-4_15.
55. Yunus AA, Lima CD (2005) Purification and activity assays for Ubc9, the ubiquitin-conjugating enzyme for the small ubiquitin-like modifier SUMO. Meth Enzymol 398: 74–87. doi:10.1016/S0076-6879(05)98008-7.
56. Yunus AA, Lima CD (2009) Purification of SUMO conjugating enzymes and kinetic analysis of substrate conjugation. Methods Mol Biol 497: 167–186. doi:10.1007/978-1-59745-566-4_11.
57. Brenner S (1974) The genetics of *Caenorhabditis elegans*. Genetics 77: 71–94.
58. Mello CC, Kramer JM, Stinchcomb D, Ambros V (1991) Efficient gene transfer in *C. elegans*: extrachromosomal maintenance and integration of transforming sequences. EMBO J 10: 3959–3970.
59. Kramer JM, French RP, Park EC, Johnson JJ (1990) The *Caenorhabditis elegans rol-6* gene, which interacts with the *sqt-1* collagen gene to determine organismal morphology, encodes a collagen. Mol Cell Biol 10: 2081–2089.
60. Silhánková M, Port F, Harterink M, Basler K, Korswagen HC (2010) Wnt signalling requires MTM-6 and MTM-9 myotubularin lipid-phosphatase function in Wnt-producing cells. EMBO J 29: 4094–4105. doi:10.1038/emboj.2010.278.
61. Timmons L, Court DL, Fire A (2001) Ingestion of bacterially expressed dsRNAs can produce specific and potent genetic interference in *Caenorhabditis elegans*. Gene 263: 103–112.
62. Seetharaman A, Cumbo P, Bojanala N, Gupta BP (2010) Conserved mechanism of Wnt signaling function in the specification of vulval precursor fates in *C. elegans* and *C. briggsae*. Dev Biol 346: 128–139. doi:10.1016/j.ydbio.2010.07.003.
63. Ueda H, Hirose S (1991) Defining the sequence recognized with BmFTZ-F1, a sequence specific DNA binding factor in the silkworm, *Bombyx mori*, as revealed by direct sequencing of bound oligonucleotides and gel mobility shift competition analysis. Nucleic Acids Res 19: 3689–3693.
64. Hill RJ, Sternberg PW (1992) The gene *lin-3* encodes an inductive signal for vulval development in *C. elegans*. Nature 358: 470–476. doi:10.1038/358470a0.
65. Aroian RV, Koga M, Mendel JE, Ohshima Y, Sternberg PW (1990) The *let-23* gene necessary for *Caenorhabditis elegans* vulval induction encodes a tyrosine kinase of the EGF receptor subfamily. Nature 348: 693–699. doi:10.1038/348693a0.
66. Beitel GJ, Clark SG, Horvitz HR (1990) *Caenorhabditis elegans ras* gene *let-60* acts as a switch in the pathway of vulval induction. Nature 348: 503–509. doi:10.1038/348503a0.
67. Han M, Sternberg PW (1990) *let-60*, a gene that specifies cell fates during *C. elegans* vulval induction, encodes a *ras* protein. Cell 63: 921–931.
68. Chen N, Greenwald I (2004) The lateral signal for LIN-12/Notch in *C. elegans* vulval development comprises redundant secreted and transmembrane DSL proteins. Dev Cell 6: 183–192.
69. Thompson KE, Bashor CJ, Lim WA, Keating AE (2012) SYNZIP Protein Interaction Toolbox: *in Vitro* and *in Vivo* Specifications of Heterospecific Coiled-Coil Interaction Domains. ACS Synth Biol 1: 118–129. doi:10.1021/sb200015u.

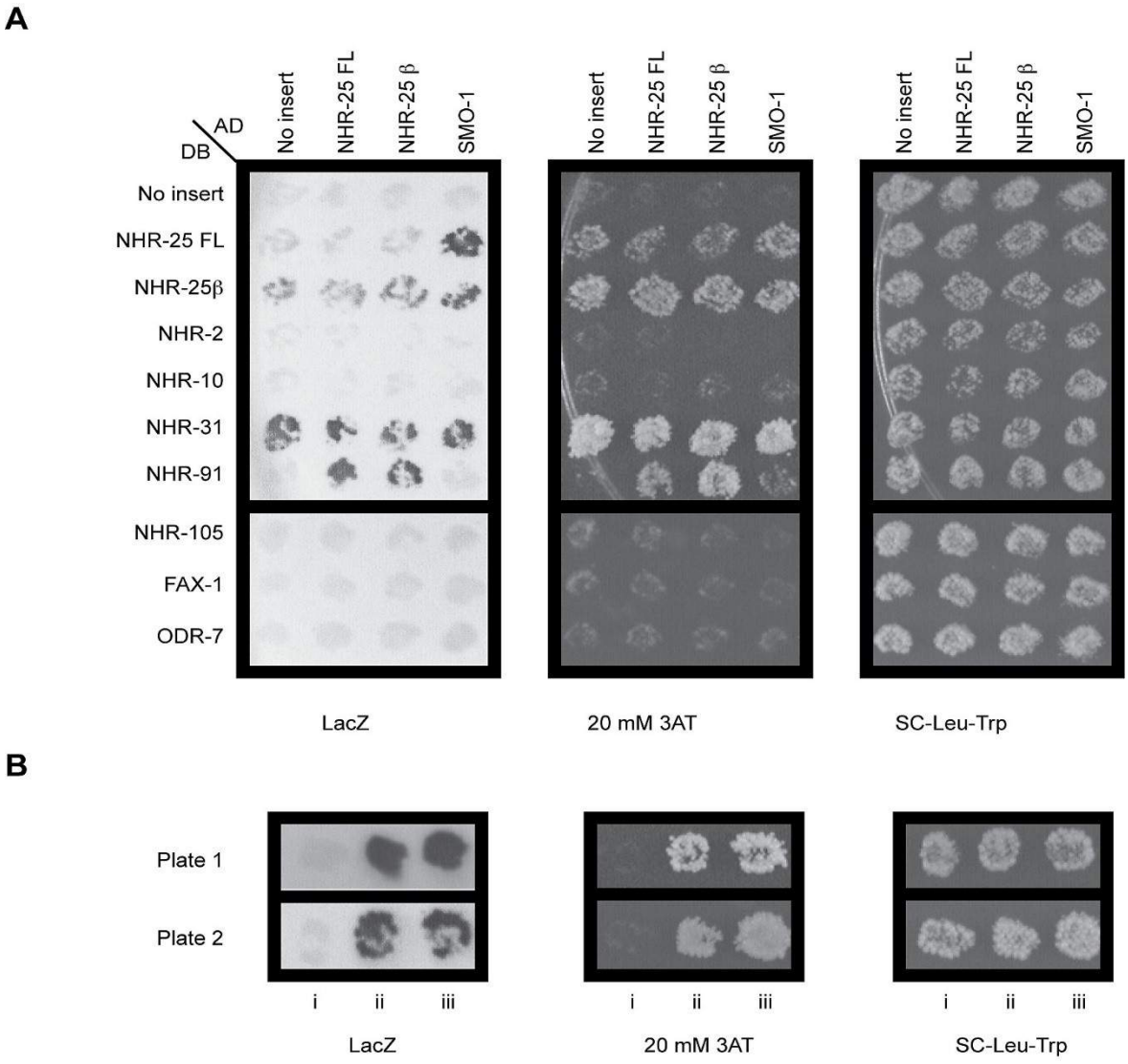
A
AD
DB
No insert
NHR-25 FL
NHR-25 β
SMO-1
No insert
NHR-25 FL
NHR-25β
NHR-2
NHR-10
NHR-31
NHR-91
NHR-105
FAX-1
ODR-7
LacZ
20 mM 3AT
SC-Leu-Trp
B
Plate 1
Plate 2
i
ii
iii
LacZ
20 mM 3AT
SC-Leu-Trp

Figure S1

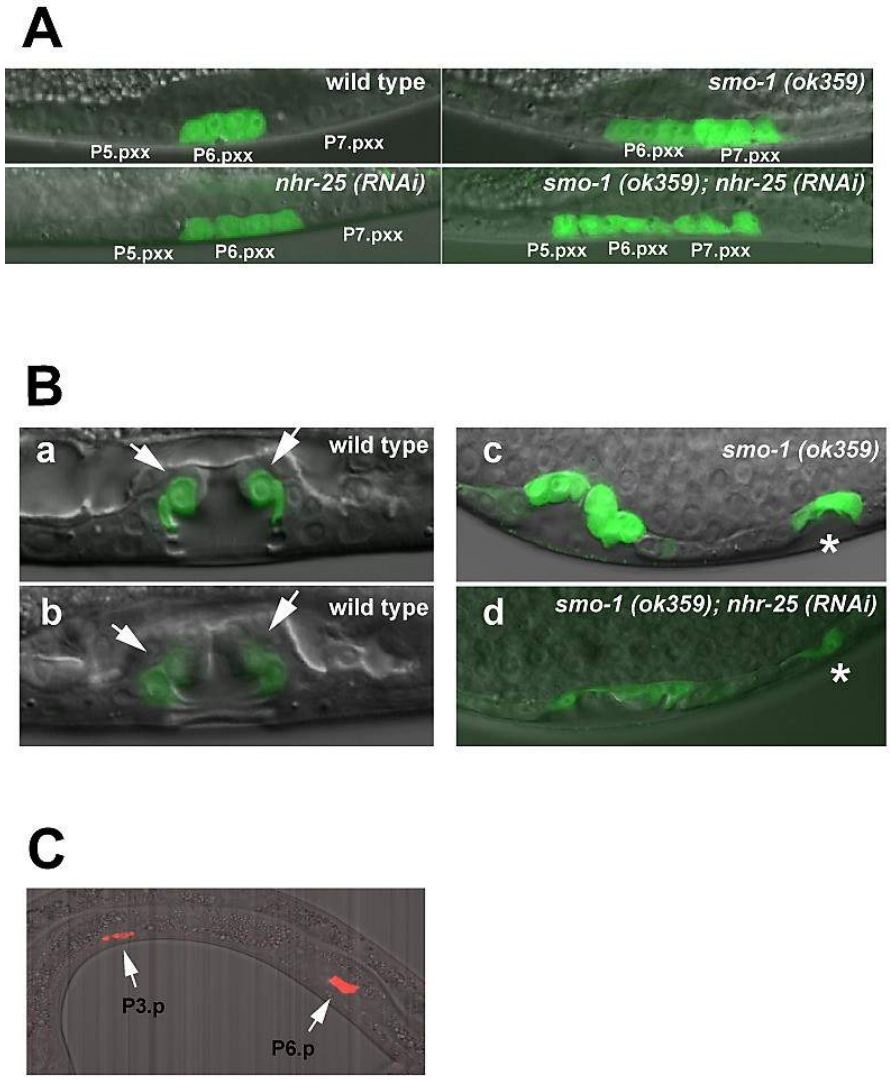
A
wild type
P5.pxx
P6.pxx
P7.pxx
smo-1 (ok359)
P6.pxx
P7.pxx
nhr-25 (RNAi)
P5.pxx
P6.pxx
P7.pxx
smo-1 (ok359); nhr-25 (RNAi)
P5.pxx
P6.pxx
P7.pxx
B
a
wild type
b
wild type
c
smo-1 (ok359)
*
d
smo-1 (ok359); nhr-25 (RNAi)
*
C
P3.p
P6.p

Figure S2

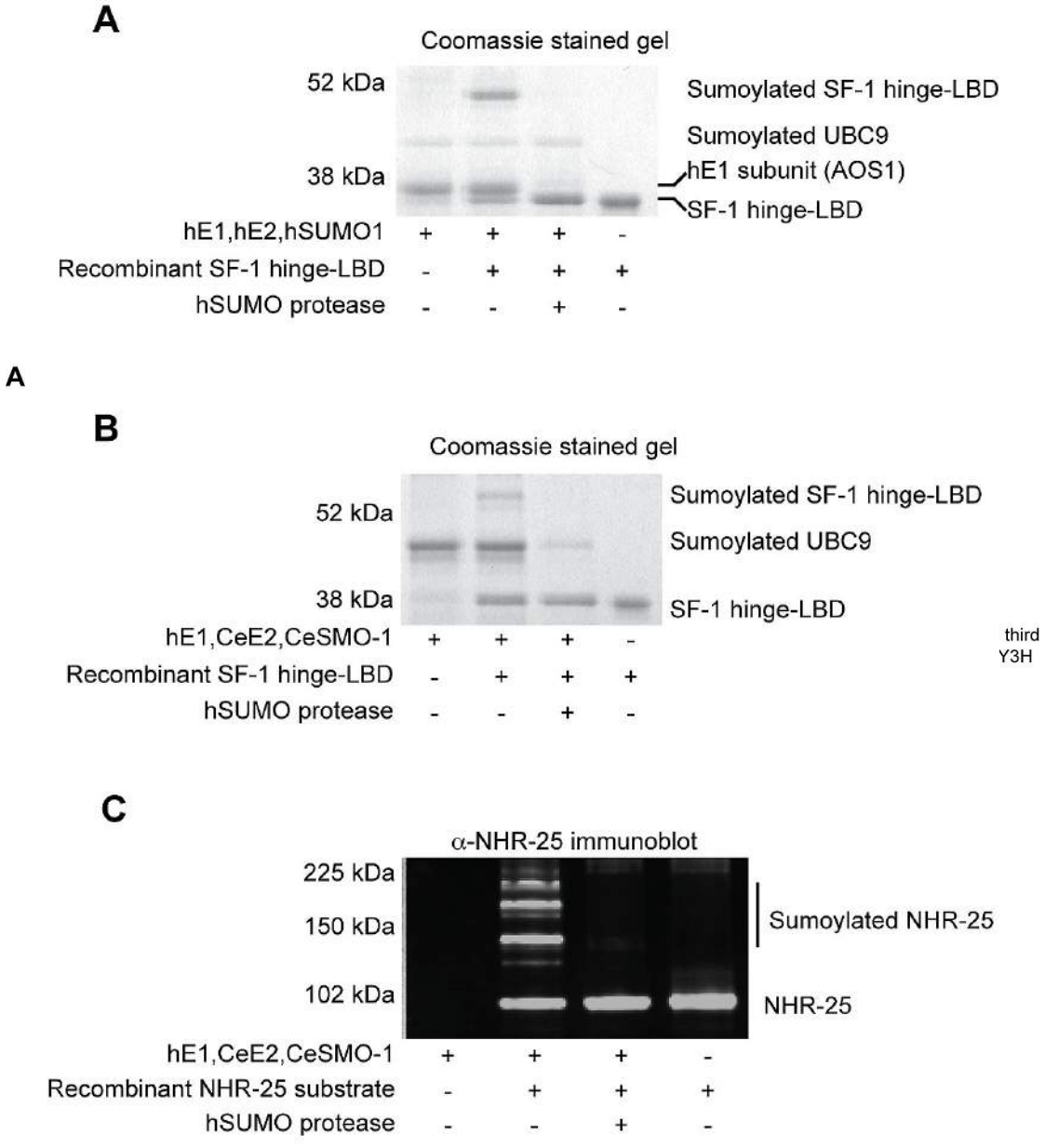
A
Coomassie stained gel
52 kDa
38 kDa
Sumoylated SF-1 hinge-LBD
Sumoylated UBC9
hE1 subunit (AOS1)
SF-1 hinge-LBD
hE1,hE2,hSUMO1 + + + -
Recombinant SF-1 hinge-LBD - + + +
hSUMO protease - - + -
A
B
Coomassie stained gel
52 kDa
38 kDa
Sumoylated SF-1 hinge-LBD
Sumoylated UBC9
SF-1 hinge-LBD
hE1,CeE2,CeSMO-1 + + + -
Recombinant SF-1 hinge-LBD - + + +
hSUMO protease - - + -
third
Y3H
C
α-NHR-25 immunoblot
225 kDa
150 kDa
102 kDa
Sumoylated NHR-25
NHR-25
hE1,CeE2,CeSMO-1 + + + -
Recombinant NHR-25 substrate - + + +
hSUMO protease - - + -

Figure S4

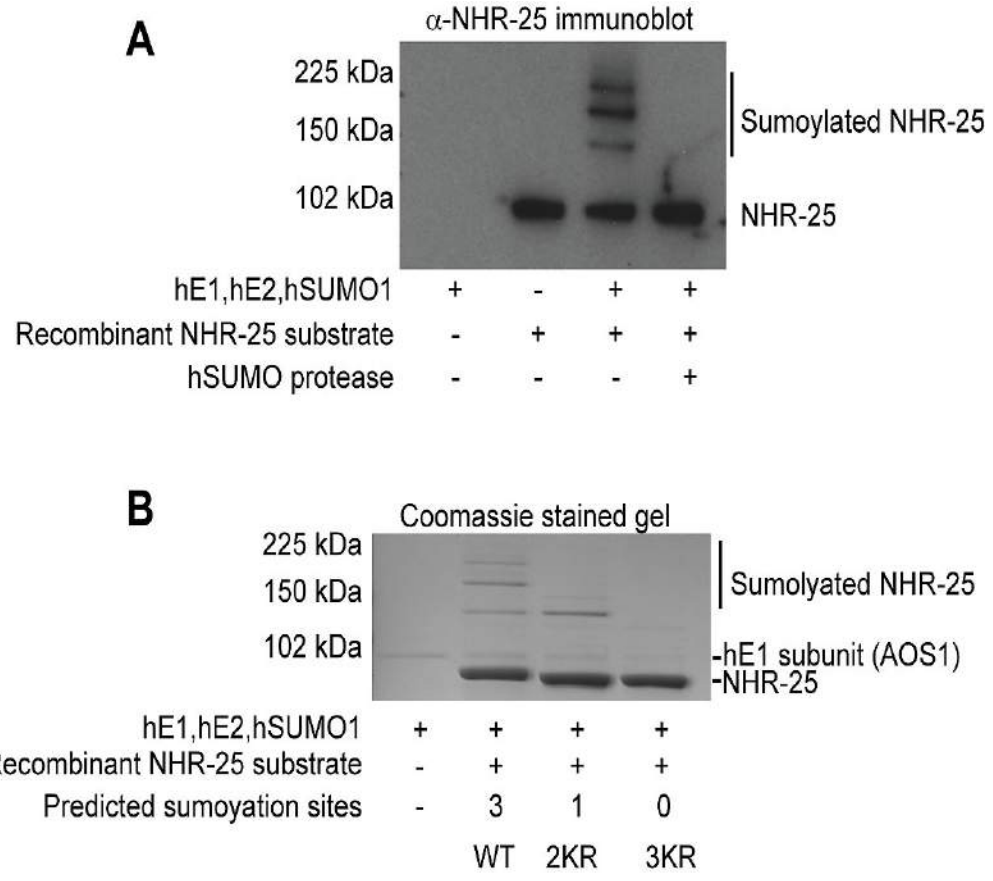
A
α-NHR-25 immunoblot
225 kDa
150 kDa
102 kDa
Sumoylated NHR-25
NHR-25
hE1,hE2,hSUMO1 + - + +
Recombinant NHR-25 substrate - + + +
hSUMO protease - - - +
B
Coomassie stained gel
225 kDa
150 kDa
102 kDa
Sumolyated NHR-25
-hE1 subunit (AOS1)
-NHR-25
hE1,hE2,hSUMO1 + + + +
Recombinant NHR-25 substrate - + + +
Predicted sumoyation sites - 3 1 0
WT 2KR 3KR

Figure S5

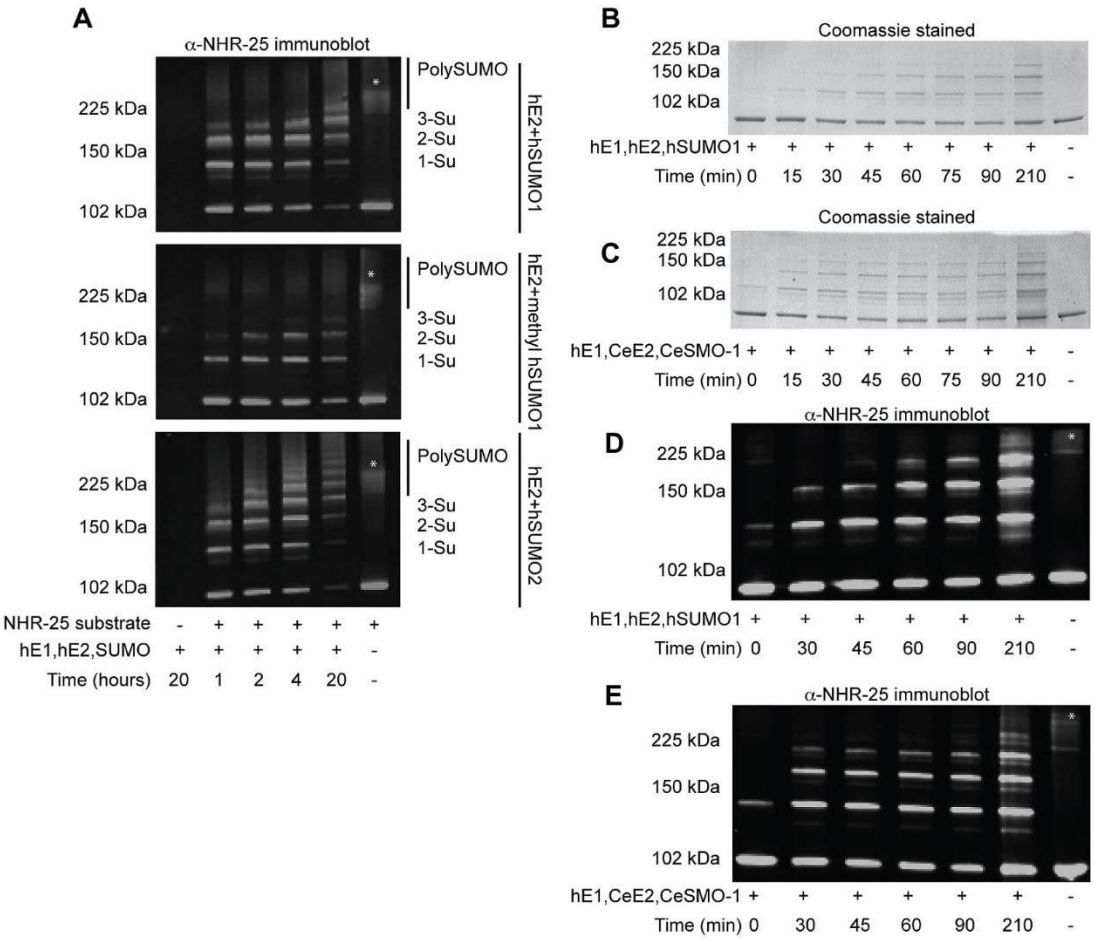
A
α-NHR-25 immunoblot
225 kDa
150 kDa
102 kDa
PolySUMO
3-Su
2-Su
1-Su
hE2+hSUMO1
hE2+methyl hSUMO1
hE2+hSUMO2
NHR-25 substrate - + + + + +
hE1,hE2,SUMO + + + + + -
Time (hours) 20 1 2 4 20 -
B
Coomassie stained
hE1,hE2,hSUMO1 + + + + + + + + -
Time (min) 0 15 30 45 60 75 90 210 -
C
Coomassie stained
hE1,CeE2,CeSMO-1 + + + + + + + + -
Time (min) 0 15 30 45 60 75 90 210 -
D
α-NHR-25 immunoblot
hE1,hE2,hSUMO1 + + + + + + -
Time (min) 0 30 45 60 90 210 -
E
α-NHR-25 immunoblot
hE1,CeE2,CeSMO-1 + + + + + + -
Time (min) 0 30 45 60 90 210 -

Figure S6

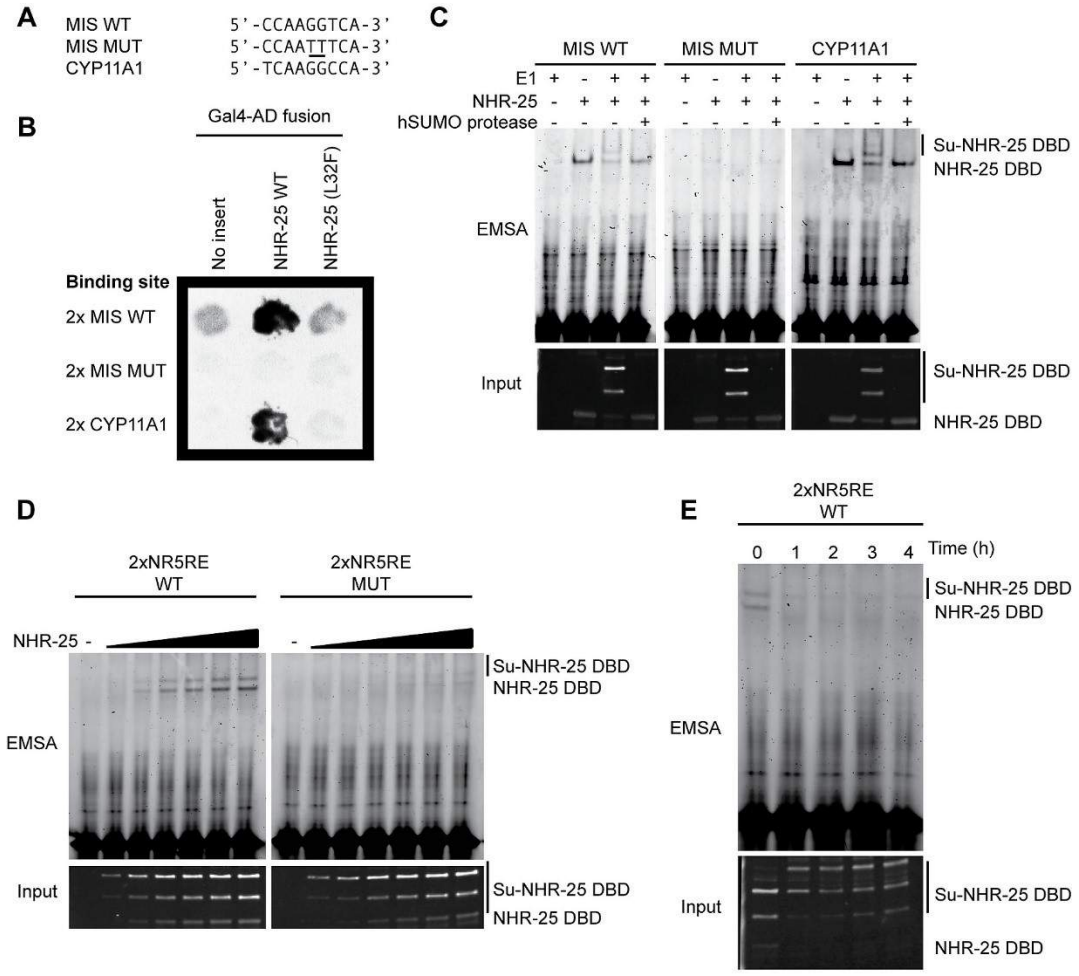
A
MIS WT 5'-CCAAGGTCA-3'
MIS MUT 5'-CCAATTTCA-3'
CYP11A1 5'-TCAAGGCCA-3'
B
Gal4-AD fusion
No insert
NHR-25 WT
NHR-25 (L32F)
Binding site
2x MIS WT
2x MIS MUT
2x CYP11A1
C
MIS WT
MIS MUT
CYP11A1
E1
NHR-25
hSUMO protease
EMSA
Input
Su-NHR-25 DBD
NHR-25 DBD
D
2xNR5RE WT
2xNR5RE MUT
NHR-25
EMSA
Input
Su-NHR-25 DBD
NHR-25 DBD
E
2xNR5RE WT
0 1 2 3 4 Time (h)
EMSA
Input
Su-NHR-25 DBD
NHR-25 DBD

Figure S7

Table S1: Overexpression of NHR-25 in hyp 7 or seam cells does not cause Muv induction

Genotype/Strain	Muv (%)	Pn.p induction (%)						n
		P3.p	P4.p	P5.p	P6.p	P7.p	P8.p	
wild type	0	0	0	100	100	100	0	60
nhr-25(RNAi)	0	0	0	98	100	100	0	79
smo-1(RNAi)	12.5	0	0	100	100	100	12.5	16
[Pnhr-25::NHR-25::GFP]								
OP33	0	0	0	100	100	100	0	45
OP33; *smo-1(RNAi)*	30	0	10	100	100	100	20	10
[Pegl-17::NHR-25]								
HL102	8.5	0	0	100	100	100	8.5	23
[Pegl-17::NHR-25(3KR)]								
HL107	18	4.5	4.5	82	100	86	9	22
HL108	18.5	0	7.4	78	96	85	11	27
HL110	22	5.5	5	89	100	89	11	18
[Pegl-17::SMO-1]								
HL117	0	0	0	100	100	100	0	99
[Pgrl-21::NHR-25]								
HL111	0	0	0	100	100	100	0	20
HL112	0	0	0	100	100	100	0	26
[Pgrl-21::SMO-1]								
HL121	0	0	0	100	100	100	0	44
[Pwrt-2::NHR-25]								
HL113	0	0	0	100	100	100	0	20
HL114	0	0	0	100	100	100	0	32
[Pwrt-2::SMO-1]								
HL115	0	0	0	100	100	100	0	20
HL116	0	0	0	100	100	100	0	46

Table S2. Sequences of oligonucleotides and gBlocks used in this study.

A) Primers for generating Gateway entry clones (attB sites are capitalized)

Primers for cloning full-length *nhr-25* cDNA (no start codon for N-terminal fusions; stop codon)
GGGGACAAGTTTGTACAAAAAAGCAGGCTGGttgactgacgtcgagaggatg
GGGGACCACTTTGTACAAGAAAGCTGGGTCCTAttatgatgccatgtacggcac

Primer for Gateway cloning FLAG-tagged cDNAs
GGGGACAAGTTTGTACAAAAAAGCAGGCTGGgattacaaggatgacgatgacaag

Primers for generating FLAG-*nhr-25* cDNA (amino acids 161-541; FLAG tag is underlined)
gattacaaggatgacgacgataagcaaactaaaatcaaaactgaa
GGGGACCACTTTGTACAAGAAAGCTGGGTCCTAcgatcggttgacagtagtgc

Primer for introducing FLAG tag and *K165R* mutation in *nhr-25* cDNA (amino acids 161-541; FLAG tag is underlined)
gattacaaggatgacgacgataagcaaactaaaatcagaactgaa

Primers for cloning *nhr-25* cDNA (amino acids 1-173; no start codon for N-terminal fusions)
GGGGACAAGTTTGTACAAAAAAGCAGGCTGGttgactgacgtcgagaggatg
GGGGACCACTTTGTACAAGAAAGCTGGGTCCTAatactcagttttgatatattcagt

Primers for cloning full-length *nhr-91* cDNA (no start codon for N-terminal fusions; no stop codon for C-terminal fusions)
GGGGACAAGTTTGTACAAAAAAGCAGGCTtggacgttgcggactcgacat
GGGGACCACTTTGTACAAGAAAGCTGGGtactcgtcgaacactagac

Primers for cloning full-length *smo-1* cDNA (no start codon for N-terminal fusions; stop codon)
GGGGACAAGTTTGTACAAAAAAGCAGGCttggccgatgatgcagctcaa
GGGGACCACTTTGTACAAGAAAGCTGGGctagaatccgcccagctgctctt

Primers for cloning *smo-1ΔF* (ends in GG) cDNA (no start codon for N-terminal fusions)
GGGGACAAGTTTGTACAAAAAAGCAGGCttggccgatgatgcagctcaa
GGGGACCACTTTGTACAAGAAAGCTGGGTCCTActatccgcccagctgctcttg

Primers for cloning *smo-1ΔGG* cDNA (sumoylation-defective; no start codon for N-terminal fusions)
GGGGACAAGTTTGTACAAAAAAGCAGGCttggccgatgatgcagctcaa
GGGGACCACTTTGTACAAGAAAGCTGGGctacagctgctcttggtagacc

Primer for fusing Myc tag onto *nhr-25* cDNA 5' end (Myc tag is underlined)
gcatcaatgcagaaagctgatctcagaggaggacctgatgactgacgtcgagaggatg

Table S3. Plasmids generated for this study.

Plasmid	Parent plasmid	Notes
pJW93	pDONR221	FLAG-NHR-25 cDNA (with stop codon) entry clone
pJW109	pDONR221	SMO-1 cDNA entry clone
pJW121	pAD-dest	SMO-1 AD fusion for Y2H
pJW135	pAD-dest	NHR-25 full lenth (stopless)-AD fusion for Y2H
pJW136	pDB-dest	NHR-25 full lenth (stopless)-DB fusion for Y2H
pJW165	pDONR221	NHR-91 cDNA entry clone
pJW238	pDONR221	NHR-25 L32F cDNA entry clone
pJW302	pDONR221	SMO-1 V31K cDNA entry clone
pJW305	pDONR221	NHR-25 K165R cDNA entry clone
pJW306	pDONR221	NHR-25 K170R cDNA entry clone
pJW309	pDONR221	SMO-1ΔGG cDNA entry clone
pJW310	pAD-dest	SMO-1ΔGG in pAD vector for Y2H
pJW311	pAD-dest	SMO-1 V31K in pAD vector for Y2H
pJW314	pDONR221	NHR-25 K165R K170R cDNA entry clone
pJW315	pDONR221	SMO-1ΔF cDNA (ends in GG) entry clone
pJW319	pDB-dest	NHR-25 K165R in pDB vector for Y2H
pJW320	pDB-dest	NHR-25 K170R in pDB vector for Y2H
pJW400	pDONR-P4P1r	egl-17 promoter entry clone
pJW414	pDB-dest	NHR-25 3KR in pDB vector for Y2H
pJW421	pDONR221	Myc-NHR-25 cDNA entry clone
pJW426	pDB-dest	NHR-25 K236R in pDB vector for Y2H
pJW427	pDONR221	NHR-25 K236R, K165R cDNA entry clone
pJW428	pDB-dest	NHR-25 K236R, K170R in pDB vector for Y2H
pJW432	pDEST-CMV-Myc	NHR-25 N-terminal Myc fusion vector for CMV driven mammalian expression
pJW501	pDB-dest	NHR-25 K236R, K165R in pDB vector for Y2H
pJW522	pKA921	P_egl-17:Myc-NHR-25 in polycistronic mCherry vector
pJW524	pKA921	P_wrt-2:Myc-NHR-25 in polycistronic mCherry vector
pJW526	pKA921	P_grl-21:Myc-NHR-25 in polycistronic mCherry vector
pJW630	pDONR221	NHR-25 3KR cDNA entry clone
pJW646	pDONR221	Myc-NHR-25 3KR cDNA entry vector
pJW647	pETG-10A	6xHIS-SMO-1 bacterial expression vector
pJW651	pDONR201	UBC-9 cDNA entry clone
pJW655	pAD-dest	UBC-9 in pAD vector for Y2H
pJW656	pDB-dest	UBC-9 in pDB vector for Y2H
pJW714	pDONR221	FLAG-NHR-25 (amino acids 161-541) cDNA entry clone
pJW722	pETG-41A	6xHIS-MBP-FLAG-NHR-25 (amino acids 161-541) bacterial expression vector
pJW741	pDONR221	TEV-UBC-9 cDNA entry clone
pJW742	pDONR221	TEV-SMO-1ΔF cDNA entry clone

Chapter 4: Unpublished results

4.1 *nhr-25(L2-RNAi)* results in normal vulva cell competences and cell fates.

Vulva precursor cells (VPCs) are induced by EGF signal sent from AC and NHR-25 is required for the proper AC formation in early L1 stage (Asahina et al., 2006). No AC or partly-functional AC formed in *nhr-25* mutants or *nhr-25* RNAi treatment leads to no- or under-induction of VPCs and consequently producing *Vul* animals. At later stages, VPC cell divisions and subset of VPC division patterns are affected when NHR-25 function is attenuated (Figure 4.1, Table 4.1-4.3). This requirement of NHR-25 is autonomous to VPCs (Chen et. al., 2004, Ward et al., 2013). However these observations only partially explain the gross morphological defects seen in *nhr-25* (*lf*) situation.

To further explore the NHR-25 requirement in vulva morphogenesis, I analyzed vulval development in greater details in *nhr-25 L2-RNAi* situation. Late onset of RNAi resulted in normal VPC competences and initial cell fate specifications as observed by the normal expression pattern for primary (1°) and secondary (2°) cell markers; *egl-17::yfp* and *lip-1::gfp* respectively (Figure 4.2, Table 4.1,4.2). But subset of vulva cells showed defects such as changes in cell division axes and cell proliferation defects. For example, VulE and C which divide in transverse (T) fashion exhibited altered division axis (L) or no division (N) and vulF no division (N) (Table 4.3). In addition, abnormal cell migrations and morphogenesis defects were seen.

4.2 NHR-25 activity is necessary for vulva cell migration.

The entire process of vulva morphogenesis occurs over the period of 20 hours starting from late L3 stage. The cell migrations and morphogenesis events of the vulva can be visualized by the expression pattern of adherens junction marker, *AJM-1::gfp*. In *nhr-25 L2-RNAi* worms, the initial short range of migration often did not occur properly

and dorsal invagination was abnormal (Figure 4.3). The terminal phenotypes could be grouped into three classes (Class I, II, III; Figure 4.4, Table 4.4). Class I was distinguished by the failure of dorsal migration of the 1° cells and their strong adherence to the ventral cuticle (Figure 4.4B). Class II phenotype exhibited defective migration of 2° cells and they failed to reach the midline and no dorsal movement (Figure 4.4C). Class 3 represented the most frequent defects (50%, Table 4.4) with the failure of migration of both 1° and 2° vulval lineages and cells remained attached to the ventral cuticle (Figure 4.4D). The penetrance for each phenotype was dependent on the strength of RNAi treatment as when *nhr-25* dsRNA-producing bacteria was mixed with control bacteria in 1:1 ratio (half dose of *nhr-25* dsRNA was ingested by worms), Class II phenotype was more frequently seen while Class III phenotype was predominant in the worms that ingested full dose of *nhr-25* dsRNA (Table 4.4). Abnormal cell contact and fusion were also observed within vulval cells or with surrounding epidermal cell, hyp7 in L4 animals (Figure B'-D'). *Nhr-25(ku217)* animals also show failure of vulva cell to reach the midline (Figure E-H).These observations indicate that NHR-25 is required for both early and later vulva morphogenesis and the migration and invagination of vulval cells are severely affected in loss-of-function of *nhr-25*.

4.3 NHR-25 is expressed in graded manner during vulva cell migration.

Consistent with the role of NHR-25 in morphogenesis during vulval development, NHR-25 was expressed in all vulval cells (Figure 4.5). The low-copy integrated transgene that contains over 20 kb upstream of *nhr-25* gene, full *nhr-25* gene fused with GFP and preserve authentic 3'-utr most likely reflects the endogenous expression pattern of NHR-25. Pn.p (1-cell stage before VPC induction) shows uniform expression in all VPCs (P3.p to P8.p). At early Pn.px (2-cell) stage, NHR-25 expression is prominent in the AC and induced P5.px, P6.px and P7.px, and decreased in tertiary fated cells (P3.p, P4.p and P8.p). Later in the 2-cell stage, expression in the AC was ceased but increased in cells in 1° lineage (P6.px) and kept its graded expression at Pn.pxx (4-cell) stage;

highest in proximal vulval cells and less but significantly high in distal vulval cells (Figure 4.5E,F). During the vulval cell migration towards the midline and in late vulva morphogenesis, all 22 cells expressed NHR-25 in high level but then it dramatically decreased and it was undetectable at the Christmas tree stage where the migration of vulval cells was completed. After the vulval cell fusion occurred to form toroidal seven rings in late L4, the NHR-25 expression in vulval cell nuclei reappeared, then diminished in the fully formed adult vulva (Figure 4.5J,K).

4.4 *nhr-25(lf)* causes abnormal expression of terminal markers, *egl-17* and *egl-26.*

Abnormal vulva cell contacts and fusions in L4 animals were seen in mutants that show altered terminal differentiation properties within vulva cell types. Severe vulva terminal defects were seen in 90% of *nhr-25 L2-RNAi* treated animals. To see any possible changes in the terminal properties of vulva cell types in *nhr-25(lf)*, I analyzed expression pattern of vulva terminal markers, *egl-17::gfp* (marker for vulC and vulD) and *egl-26::gfp* (marker for vulB1 and vulE) (Figure 4.6). In normal animals, *egl-17* is expressed in 4 VulC and 2 VulD cells. But in mutant situation, less than 2 cells for VulD in 4.5% of animals and less than 4 cells for vulC in 45.4% of animals were seen (n=22). Similarly, *egl-26::GFP* expression that were expected to be in vulB1 cells were missing in 76% of *nhr-25 L2-RNAi* treated animals (n=25). These details suggest that *nhr-25(lf)* results in altered terminal differentiations in VulC and B cell types.

4.5 *lin-3* is ectopically upregulated in the primary vulva cells in *nhr-25 (lf).*

Dysfunction of NHR-25 leads to defects in proper differentiation of vulval cells. Strong expression of NHR-25 in the vulval cell nuclei also indicates its cell autonomous function and regulation of gene transcription. EGF/LIN-3 ligand is expressed primarily

in the AC and later in vulF (P6.pxxx stage) at late vulva morphogenesis to specify the ventral uterine (uv1) cell fate (Chang et al., 1999). Previously, it was suspected that NHR-25 might regulate expression of the EGF gene *lin-3* in the vulva-inducing anchor cell but no effect of NHR-25 on expression of a *lin-3::gfp* in the AC was found (Hwang and Sternberg 2004).

Intriguingly, we observed that ectopic expression of *lin-3::gfp* exclusively in 1° vulval cell lineage at earlier (P6.pxx) vulva morphogenesis (Figure 4.7). The expression was especially frequent and high in VulE. In the wild type animals, the expression of *lin-3::gfp* was never observed in this cell type but over 40% of *nhr-25 L2-RNAi* treated worms showed the expression in vulE. Similar expression pattern was observed also in *nhr-25 L1-RNAi* treated animals and *nhr-25* (*ku217*) mutants (Figure 4.8).

AC/LIN-3 signal acts non-autonomously during vulva inductions. But VPC specific *lin-3* expression was suggested to act as a relay signal during induction process (Dutt et al., 2004). During this process, LIN-3 acts through its splice variant LIN-3L within VPCs. Thus, it could be inferred that one or more isoforms of LIN-3 are affected by NHR-25 in the primary lineages causing the ectopic expression. To verify this hypothesis and to test up-regulation of LIN-3 isoforms (S, L and XL) by NHR-25 at endogenous levels, we carried out quantitative RT-PCR analysis with isoform-specific primers on cDNAs obtained from *Vector (RNAi)* and *nhr-25(RNAi)* treatments (Figure 4.9). Our data suggest no up-regulation in the levels of LIN-3 isoforms in *nhr-25(RNAi)* treatments.

Alternately, I applied smFISH technique to detect de-repression of *lin-3* in the VPCs in *nhr-25(ku217);syIs107* animals. On average, three *lin-3* molecules were detected in the ectopic P6.pxx cells (n=4) and 21 in AC (n=10) (Figure 4.10). But the experiments were carried in the *ku217* allele that carries *lin-3::gfp* transgene. This situation could mask the endogenous levels of *lin-3* in *ku217* animals as the transgene produces extra copies of

lin-3. So, smFISH experiments need to be repeated in N2, *ku217* alone and *nhr-25(RNAi)* conditions to corroborate the ectopic GFP observations. Conclusively, our *syIs107* expression in *nhr-25(lf)* suggests possible autonomous regulation of LIN-3 by NHR-25 within P6.pxx cells.

4.6 LIN-39 expression is altered in *nhr-25 (lf)*.

The homeobox protein LIN-39 (homolog of fly *sex comb reduced* and mammalian Hox5) plays crucial role in vulva differentiation (Clark et al., 1993; Maloof and Kenyon, 1998; Shemer and Podbilewicz, 2002). Since EGF/Ras and Wnt signalings positively regulate *lin-39* and *lin-39* has been shown to interact with *nhr-25* (Chen et al., 2004), we sought to see if LIN-39 expression was regulated by NHR-25. We followed the expression using the transgenic strain carrying recombineering-based genomic fragment tagged with GFP (modENCODE strain OP18). This strain essentially showed the wild type expression similar to previously reported expression pattern during vulva development (Wagmaister et al., 2006; Penigault et al., 2011). In *nhr-25(ku217)* mutants, LIN-39 expression in Pn.p and Pn.px cells was bit higher compared to wild type pattern (Figure 4.11 A', B'). Later at P6.pxx cells, vulE and vulF express LIN-39 at the same level (vulE = vulF) in wild type while vulE expression was higher than vulF (vulE > vulF) in *nhr-25(ku217)* (Figure 4.11 C'). At the time of invagination in wild type animals, high LIN-39 expression was seen in vulA; the only vulva cell remained attached to the ventral cuticle, and decreased in dorsally migrating vulB, vulC, vulE and vulF (Figure 4.11D). However ectopically high expression was observed in vulA, vulC and vulE in *nhr-25 L2-RNAi* treated animals (Figure 4.11D'). In some animals that had Class 2 and Class 3 migration defects in *nhr-25 L2-RNAi*, robust ectopic expression was seen in vulC and VulE (Figure 4.11F,G). Thus, it should be noted that ectopic LIN-39 in defective vulva cells in *nhr-25(lf)* correlates with their non-detachment character from ventral cuticle.

4.7 NHR-25 enhances cell migration defects caused by mutations in Semaphorin pathway.

One of the major signaling pathways involved in cell migration both in vertebrates and invertebrates is the semaphorin signaling. *Smp-1* encodes a homolog of transmembrane Semaphorin 1a and *plx-1* encodes the putative SMP-1 receptor Plexin-A4 (Dalpe et al., 2005, Liu et al., 2005). The abnormal cell migrations and cell contacts seen in *nhr-25 (lf)* were reminiscent of *smp-1 (ev715)* and *plx-1(nc37)* mutations. In addition, *smp-1 (ev715)* and *plx-1(nc37)* are presumably null yet the vulval migration defect is not fully penetrant suggesting that there could be other pathway(s) regulating the process. For these reasons, I further tested the genetic interaction between *nhr-25* and semaphorin pathway genes. Loss of *smp-1* or *plx-1* caused vulva cells to fail to undergo stereotypic cell shape change and to migrate towards midline of the vulva. Typically vulA did not reach to the midline resulted in the extended cell shape. In combination of *smp-1(ev715)* and *nhr-25 L2-RNAi*, the defect in migration was drastically enhanced (Figure 4.12). 100 % of double loss of function animals showed abnormal vulva migration and it was phenotypically much severe; no invagination occurred and all vulval cells produced were aligned along the ventral cuticle. This phenotype is designated as Class 4 vulva migration defect.

4.8 SMP-1 expression is altered in *nhr-25(lf)*.

The wild type expression of SMP-1 started at Pn.pxx (4-cell) stage in both 1° and 2° lineages (Figure 4.13A). At late 4-cell stage it temporarily lost its expression in 1°, but soon it was restricted in 1° daughters, VulE and VulF (Figure 4.13 B-C). These cells serve as a dorsal vulva ring organizer and invaginate dorsally to form lumen (Dalpe et. al., 2005). Later SMP-1 expression in vulD, vulC, vulB1/B2 and vulA were observed as they migrate towards midline of the vulva as previously reported (Dalpe et al., 2005, Figure 4.10G,H). In *nhr-25 L2-RNAi*, the expression in vulE and vulF was never detected (n=15) (Figure 4.13B, D). but in later stage 81 % RNAi treated worms (n=26)

showed weak expression at vulC/vulD position (Figure 4.10F, I, J). These GFP positive cells tend to migrate dorsally. Thus these observations argues that NHR-25 and semaphorin pathways are required in epidermal cell migrations and their cooperation ensures the proper vulva morphogenesis.

4.9 EGF/Ras/MAPK pathways regulate NHR-25 expression in vulva.

Graded expression of NHR-25::GFP was seen during vulva inductions. EGF/LIN-3 signal acts as a morphogen and LIN-3 gradient regulates vulva inductions. So, the gradients of NHR-25 and inductive signals overlap during vulva formation.

To see any possible regulation of NHR-25 activity in vulva by EGF/Ras/MAPK pathways, I analyzed NHR-25::GFP expression changes both in *lf* and *gf* mutants of EGF/Ras/MAPK pathway (Figure 4.14). *Lin-15AB (n309), let-60(n1046)* and *lin-1(e1026)* represent *gf* situation for inductive pathway. In these mutants, ectopic vulva inductions was seen from P(3,4,8).p cells along with normal P(5-7).p inductions, and thus producing *Muv* animals. Interestingly, NHR-25::GFP expression was seen in both normal and ectopically induced vulva cells in all the three genetic backgrounds from Pn.p to Pn.pxxx stages (%GFP expression=100, n=30 for each double mutant). *Lin-3(RNAi)* and *lin-3(e1417)* results in decreased levels of inductive signaling and produces *Vul* animals. Reduced NHR-25::GFP expression was seen in both *lin-3(RNAi)* and *lin-3(e1417)* backgrounds. These observations suggest that EGF/Ras/MAPK pathway regulates vulva specific expression of NHR-25.

4.10 Abnormal actin organization was seen in *nhr-25 (lf)* during vulva morphogenesis.

LET-502 controls dorsal movement of vulva cells through actin regulation (Farooqui et al., 2012). To see possible changes in actin network during vuvla cell migrations in *nhr-25(RNAi)* animals, I analyzed *lifeAct::gfp* expression pattern. LifeAct

expression appeared on the lumen facing side during toroid formation in normal animals (Figure 4.15A). But in *nhr-25(RNAi)* animals, abnormally high levels of actin myofibrils were seen. Specifically this expression pattern coincides with abnormal migratory behavior of vulva cells seen in *nhr-25(lf)* situation (%90, n=10, Figure 4.15 B,C).

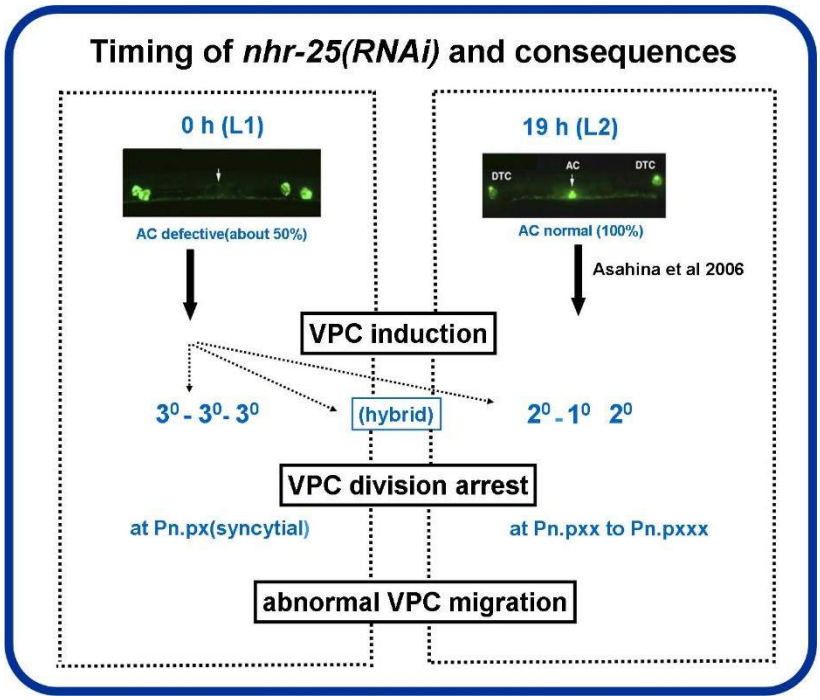

Figure 4.1 Timing of *nhr-25(RNAi)* and its consequences on vulva development

Synchronized larvae were fed with two modules of temporal *nhr-25(RNAi)*; *nhr-25(L1-RNAi)* and *nhr-25(L2-RNAi)*. *nhr-25(L1-RNAi)* results in defective AC formation and thus effecting vulva cell competence and proliferations properties. *nhr-25(L2-RNAi)* results in normal AC and vulva cell fates. But defective vulva cell proliferations and cell migrations were seen.

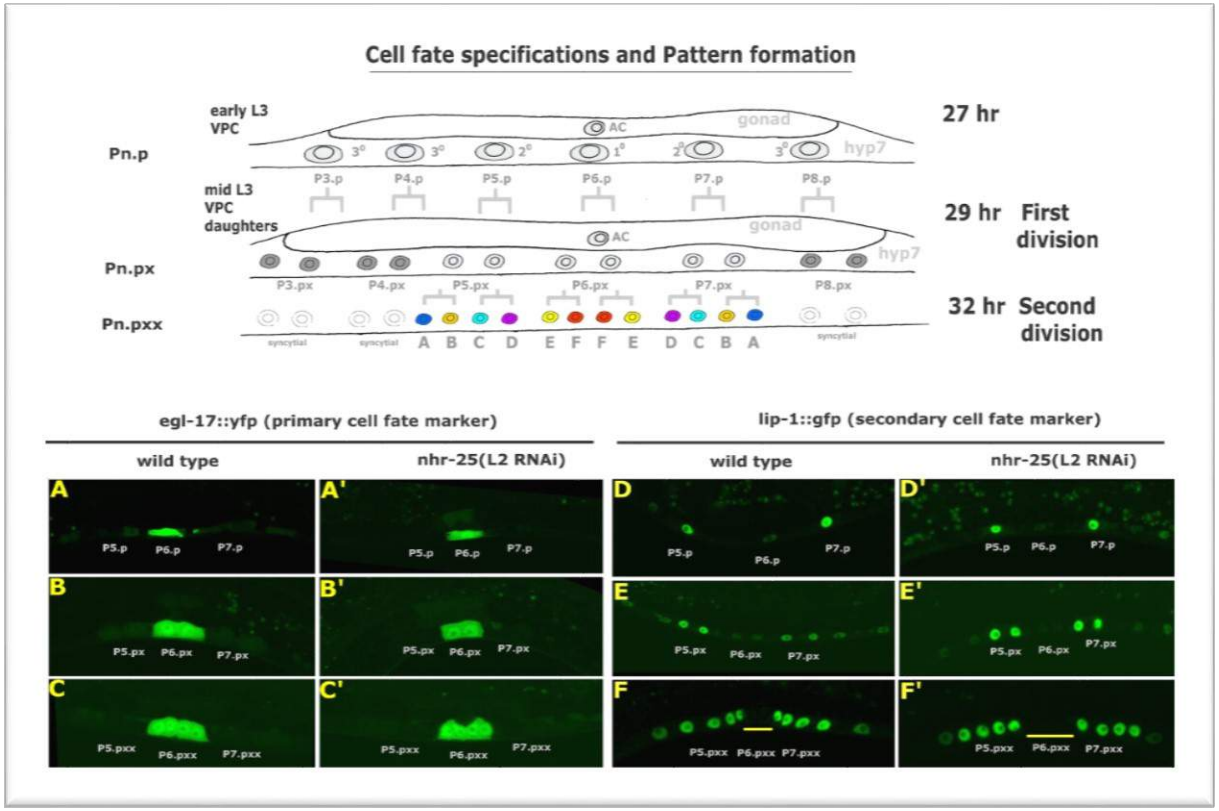

Figure 4.2 Expression pattern of early *egl-17::yfp* and *lip-1::gfp* during inductions in *nhr-25(L2-RNAi)*

Cartoon depicts temporal events that specify vulva cell fates and pattern formation from Pn.p to Pn.pxx stages. Ras signaling upregulates *egl-17::yfp* within P6.p lineages (A,B and C). LIN-12/Notch signaling maintains *lip-1::gfp* within P5/7.p lineages (D,E and F). Both marker expressions appear normal in *nhr-25 (L2-RNAi)* treated animals suggesting no alterations in cell fates.

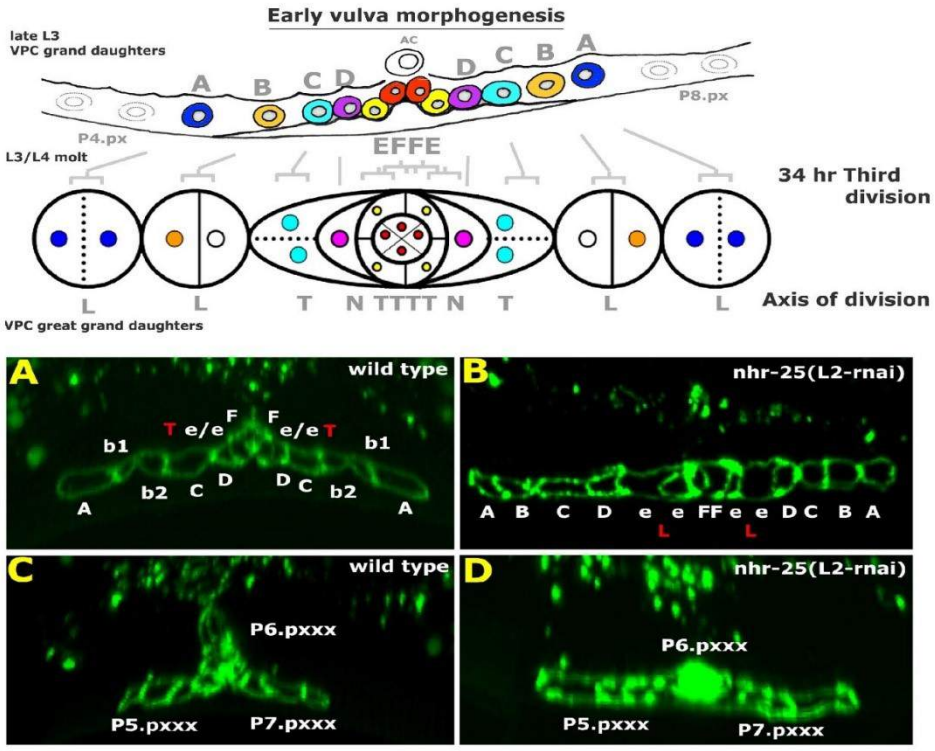

Figure 4.3 *nhr-25(L2-RNAi)* results in vulval cell lineage and migration defects

Cartoon depicts early vulva morphogenesis events. AJM-1::GFP expression localized at the apical surfaces of vulva cells and their daughters was utilized to analyze early vulva morphogenesis events in control (A, C) and *nhr-25(L2-RNAi)* treated animals (B,D). In *nhr-25(L2-RNAi)* situation, P6.pxx cells failed to move dorsally as such no lumen space was formed (B). In addition, the VulE daughters divided in abnormal axis, from normal T to defective L fashion (shown in red). At later stages, P5/7.pxxx were able to retain their normal migratory behavior towards the vulva midline (D).

Figure 4.4 *nhr-25(L2-RNAi)* results in vulval cell lineage and migration defects

Vulval cell type adherence and anatomy of vulva toroids in L4 stage animals were analyzed in control (A/A') and *nhr-25(L2-RNAi)* treated animals (B/B' to D/D'). Cartoon depicts the stereotypic positions of vulva cells and anatomy of vulva toroids VulA to F. Nomarski observations were followed in (A-D) and 3D confocal reconstructions of AJM-1::GFP in (A'-D'). Wild-type vulva is made up of a stack of seven concentric vulva rings formed temporally by the fusion of homologous vulva cell types except Vul B1 and B2 along the dorso-ventral axis (Fig A'). The Vul F toroid is the most dorsal ring within the stack. Distinctly, the Vul A cells (dark blue circles) show characteristic strong adherence property to the ventral cuticle (A). *nhr-25(L2-RNAi)* treatment results in three different classes of phenotypes that show defective adherence properties and also abnormal migrations. In addition ectopic cell contacts and fusions were seen within the toroids (B'-D'). Class1 (B') mutants show adherence defects for primary cells and class 2 (C') for secondary and class 3 (D') for all vulva cells. Arrow heads indicate the position of vulva midline. * indicate abnormal toroidal fusions. AC-Anchor Cell and U-uterus. Scale bar 10um.

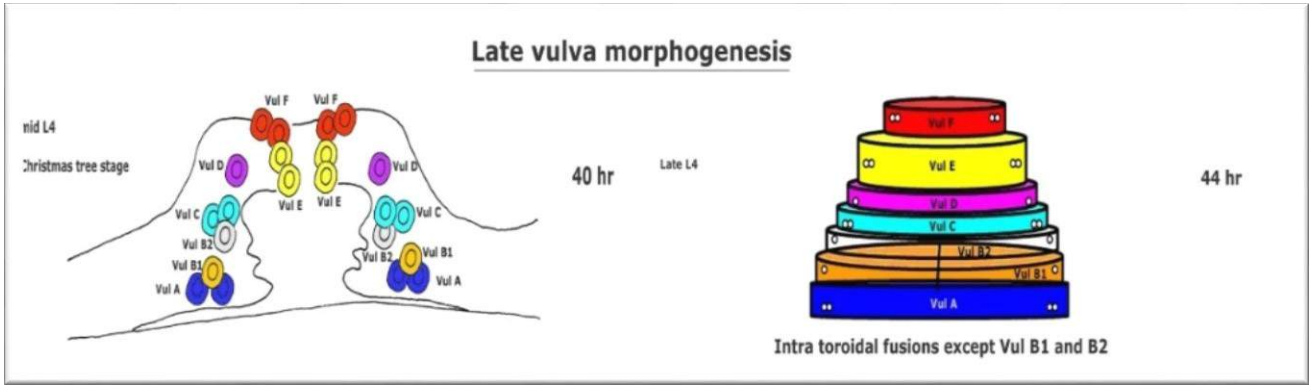
Late vulva morphogenesis
nid L4
Christmas tree stage
Vul F
Vul D
Vul C
Vul B2
Vul B1
Vul A
Vul E
40 hr
Late L4
44 hr
Intra toroidal fusions except Vul B1 and B2

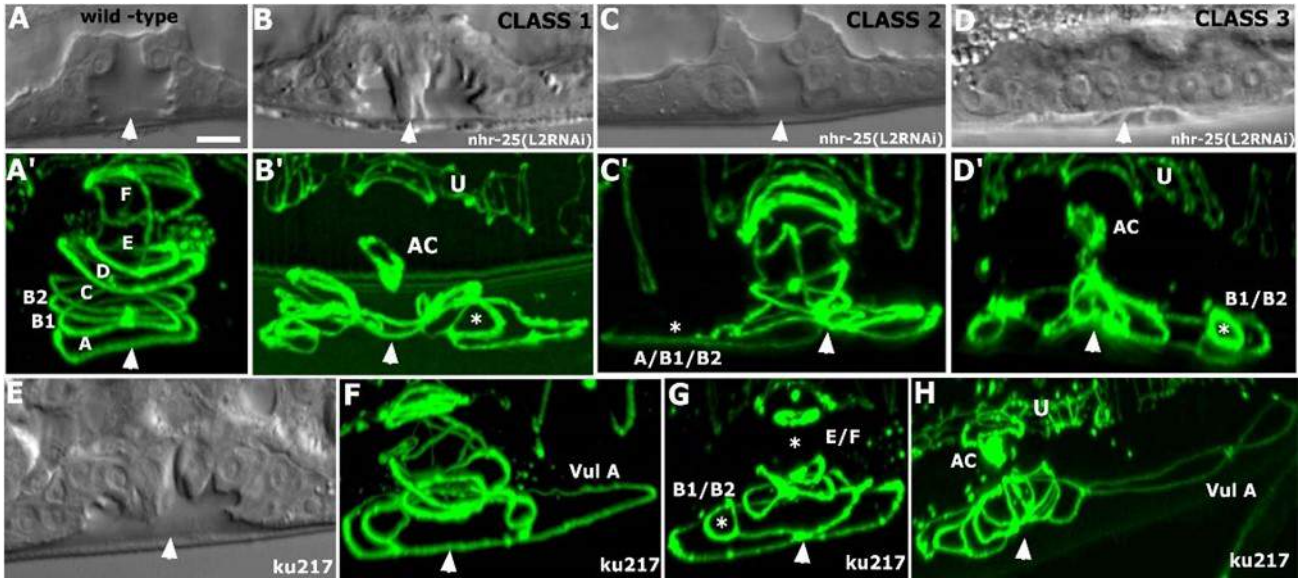
A
wild -type
B
CLASS 1
nhr-25(L2RNAi)
C
CLASS 2
nhr-25(L2RNAi)
D
CLASS 3
nhr-25(L2RNAi)
A'
F
E
D
C
B2
B1
A
B'
U
AC
C'
A/B1/B2
D'
U
AC
B1/B2
E
ku217
F
Vul A
ku217
G
E/F
B1/B2
ku217
H
U
AC
Vul A
ku217

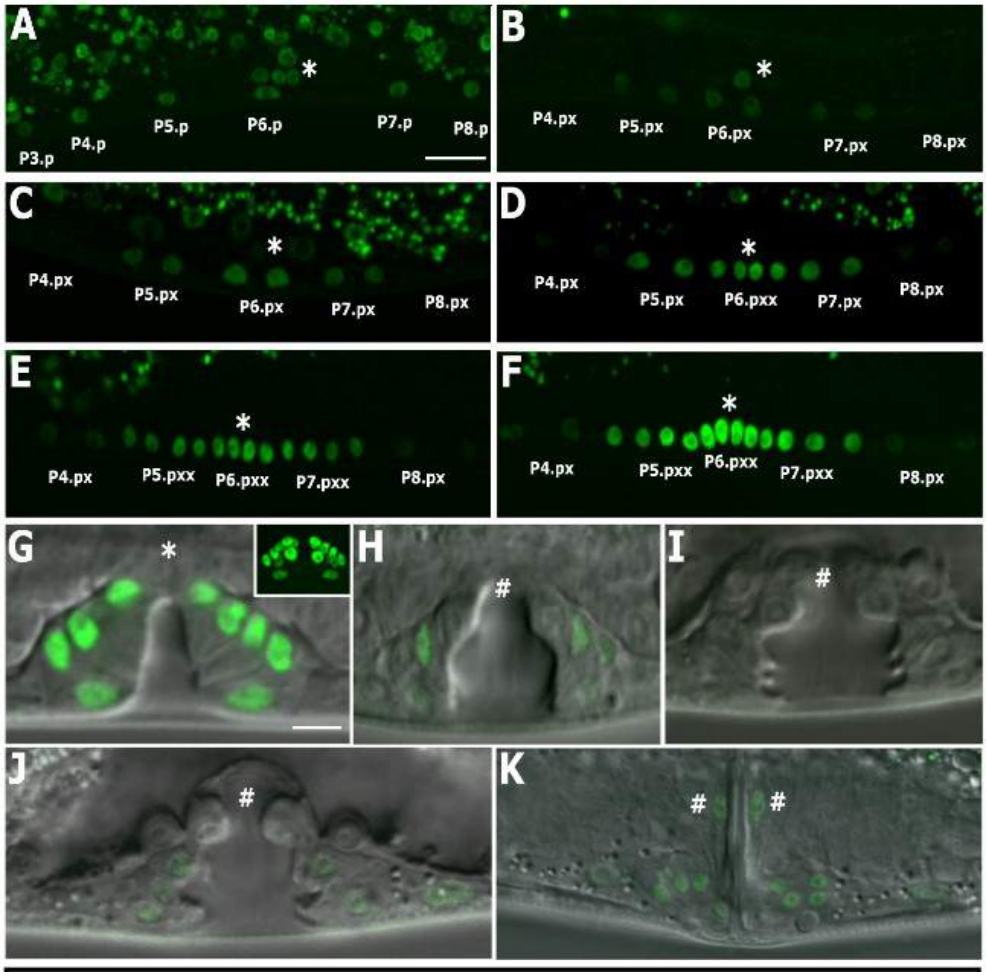

Figure 4.5 Temporal expression profile of NHR-25::GFP during vulva formation

OP33 expression was observed from Pn.p to Pn.pxxx stages. Graded expression was seen during inductions (D and E) and early vulva ell migrations (F). At bell stage (G) expression is seen in all 22 cells. At Christmas tree stage (I) expression is lost and later appears (J and K). * represents position of AC.

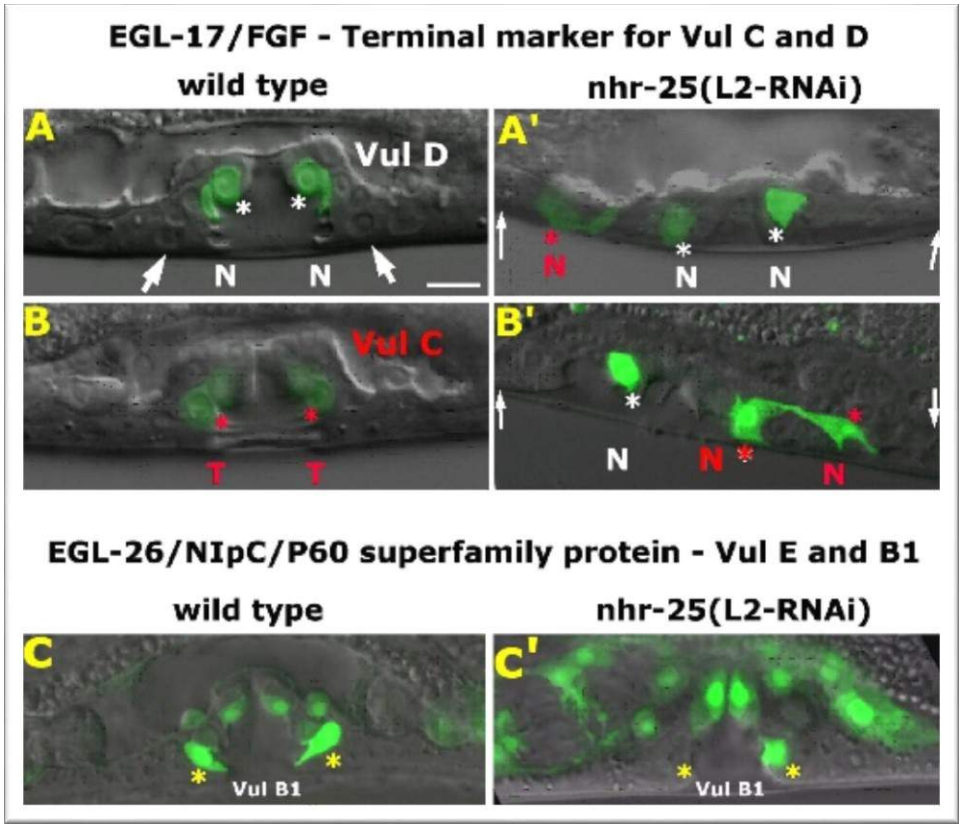

Figure 4.6 Altered L4 expression patterns of *egl-17::yfp* and *egl-26::gfp* in *nhr-25(L2-RNAi)* animals. Expression pattern of *egl-17::yfp* and *egl-26::gfp* in control treatments (Fig. A-C) and in *nhr-25(L2-RNAi)* (Fig. A'-C'). In *nhr-25(lf)* situation, Vul C specific expression of *egl-26::gfp* and Vul B specific expression of *egl-26::gfp* was altered, suggesting defects in Vul C and B terminal differentiation properties. Scale 10um.

Figure 4.7 Pattern of *lin-3::gfp* expression in *nhr-25(lf)* situation

Cartoons represent pattern of *lin-3* expression in wild type and *nhr-25(lf)* animals. In wild type, AC and VulF lineages express *lin-3* at different larval stages. The yellow arrows represent signaling from AC and brown and red arrows, cross talk between outer VulE (blue circles) and inner VulF (red circles) cells. In *nhr-25(L2-RNAi)* and *nhr-25(ku217)* animals, ectopic *lin-3* expression was observed in VulE cells. All circles with green backgrounds are positive for *lin-3* expression.

syIs107 (lin-3::gfp) reporter expression within vulva cells was observed in control (A-D), *nhr-25(L2-RNAi)* (E-H) and *nhr-25(ku217)* (I-L). White asterisks represent VulF positions, yellow VulE and red VulD. The arrow head represent the position of AC. In addition to AC, de-repression of *lin-3* was seen in VulE daughters in *nhr-25(L2-RNAi)* (E) and *nhr-25(ku217)* (I) animals. At Christmas tree (CT) stage, in normal animals, *lin-3* expression was seen VulF derived lineages (2+2=4cells) and AC expression was lost due to its fusion with uterine seam cell. The earlier ectopic *lin-3* expression seen in VulE was not observed in L4 animals *nhr-25(lf)* animals. Anterior is left and scale is 5 um.

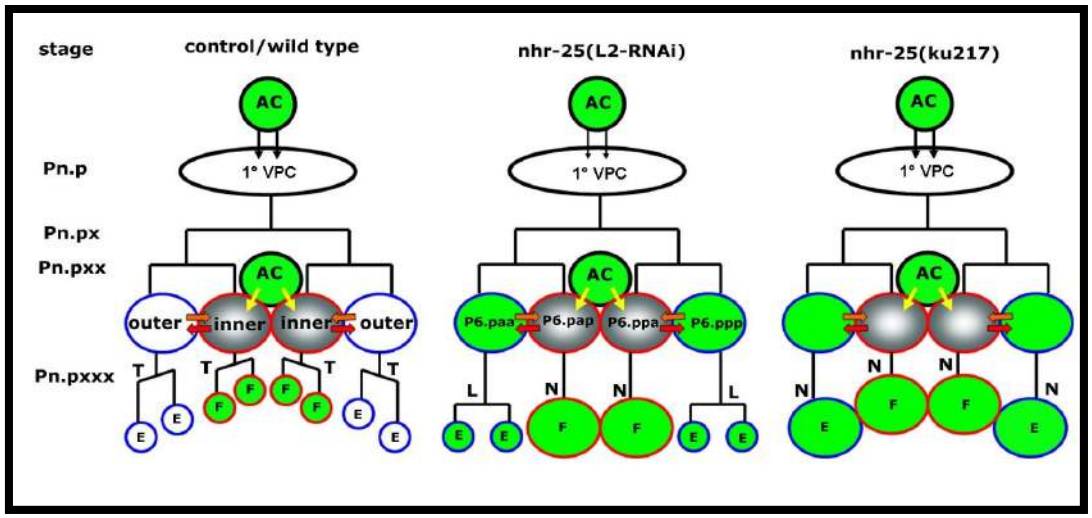
stage
control/wild type
nhr-25(L2-RNAi)
nhr-25(ku217)
Pn.p
Pn.px
Pn.pxx
Pn.pxxx
AC
1° VPC
outer
inner
inner
outer
P6.paa
P6.pap
P6.ppa
P6.ppp
T
F
E
L
N

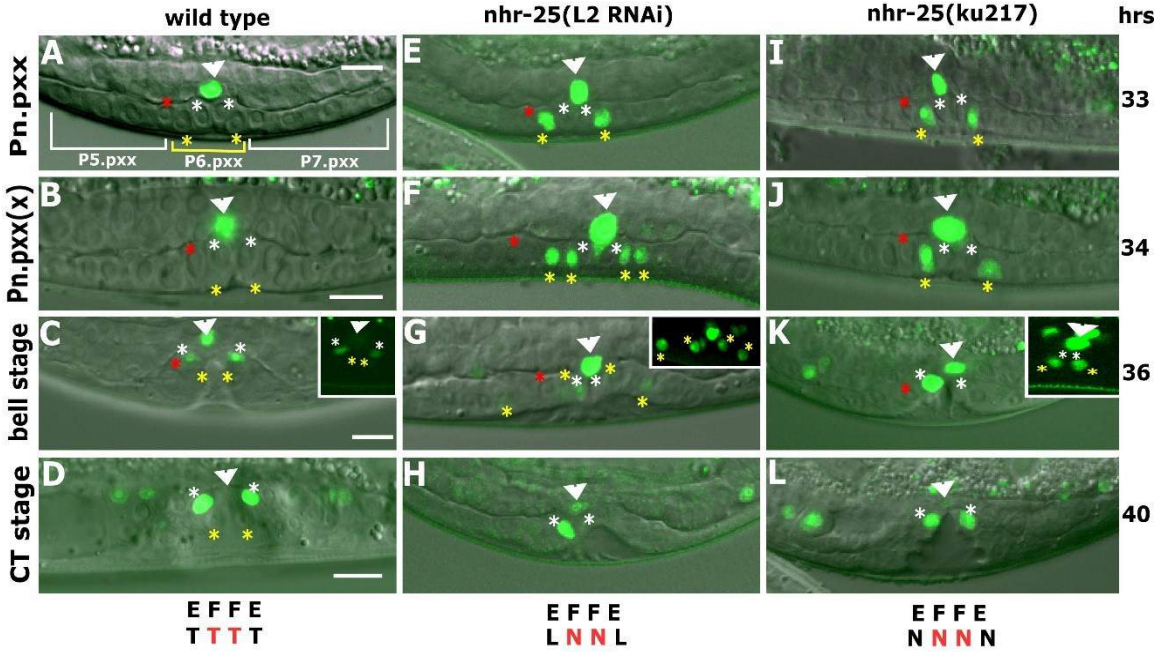
wild type
nhr-25(L2 RNAi)
nhr-25(ku217)
hrs
Pn.pxx
Pn.pxx(x)
bell stage
CT stage
A
B
C
D
E
F
G
H
I
J
K
L
P5.pxx
P6.pxx
P7.pxx
33
34
36
40
E F F E
T T T T
E F F E
L N N L
E F F E
N N N N

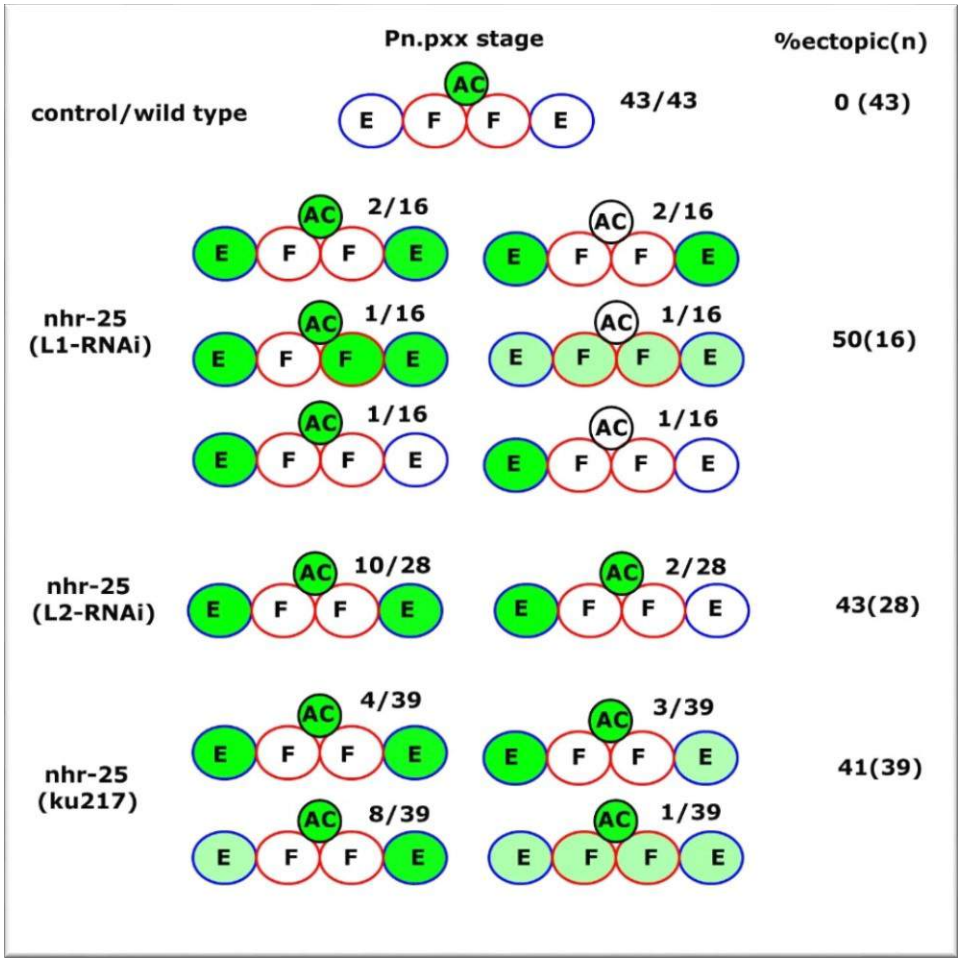

Figure 4.8 Summary of *lin-3::gfp* expression pattern in *nhr-25(lf)*

All animals observed at Pn.pxx stage. Blue circles represent VulE cells and red VulF. All light and green shaded cells are positive for *lin-3::gfp* expression. In wild type situation *lin-3::gfp* was seen only in the AC. In *nhr-25(L1-RNAi)* animals AC specific *lin-3* expression was lost in few but ectopic *lin-3* expression in P6.pxx cells was observed. In *nhr-25(L2-RNAi)* and *nhr-25(ku217)*, AC specific *lin-3* expression was observed along with ectopic expression in P6.pxx cells. % ectopic (n), *lin-3* ectopic in vulva cells, n = number of animals observed.

Figure 4.9 Quantification of endogenous *lin-3* mRNA levels in wild type and *nhr-25(RNAi)* animals.

(A) The architecture of *lin-3* genomic region with intron-exon boundaries was adopted from Dutt et.al., 2004 and re-drawn using fancygene (*Rambaldi D. and Ciccarelli F.D.* 2009). The EGF repeat that occupies exon 5 and part of exon 6a. The trans-membrane domain in the exon 7. (B) Alternative splicing within the *lin-3* locus spanning the EGF repeat and trans-membrane domains, resulted in three splice variants or minigenes, LIN-3S, LIN-3L and LIN-3XL. The small black arrows in both A and B represent the position of primer sets (C) RT-PCR analysis showing the mRNA levels of all *lin-3* isoforms. Worm lysates were obtained from 14 to 38 hrs post hatching periods. Agarose gel showing the corresponding PCR fragements: (a) Obtained from primer sets common to all three isoforms and (b) specific to individual isoforms.(D) Quantitative RT-PCR experiments were performed using RNA harvested at 32-34 hrs stage from control and *nhr-25(RNAi)* treated animals. The mean and standard deviations for individual *lin-3* isoforms from control *vector(RNAi)* -V and two independent *nhr-25(RNAi)* treatments, N1 and N2. Relative *lin-3* mRNA levels were normalized to the levels of mRNA encoding the ribosomal protein subunit *rpl-26* using the $_{dd}Ct$ method.

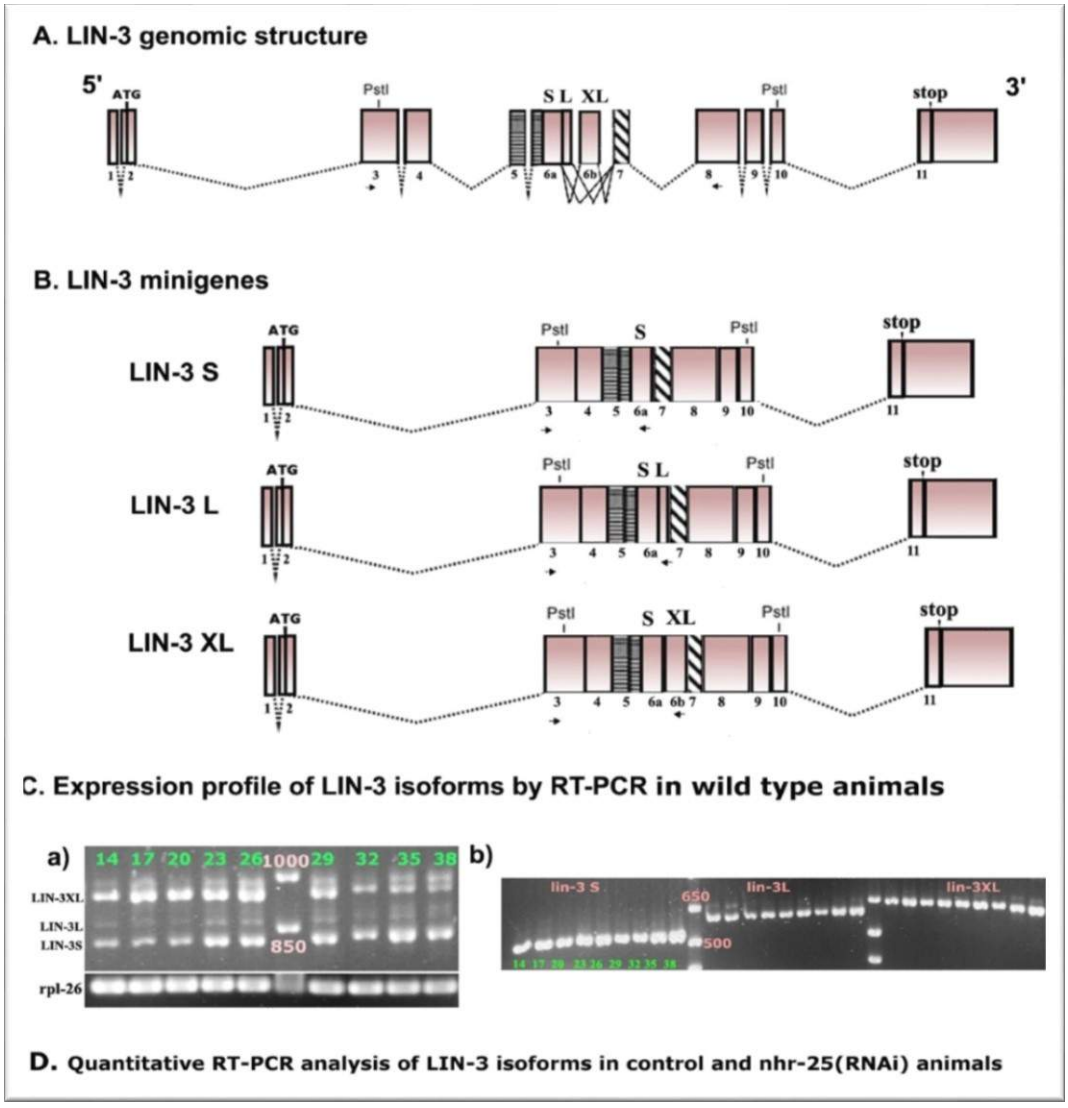
A. LIN-3 genomic structure
5'
ATG
PstI
S L XL
PstI
stop
3'
B. LIN-3 minigenes
LIN-3 S
LIN-3 L
LIN-3 XL
C. Expression profile of LIN-3 isoforms by RT-PCR in wild type animals
a)
b)
LIN-3XL
LIN-3L
LIN-3S
rpl-26
850
650
500
D. Quantitative RT-PCR analysis of LIN-3 isoforms in control and nhr-25(RNAi) animals

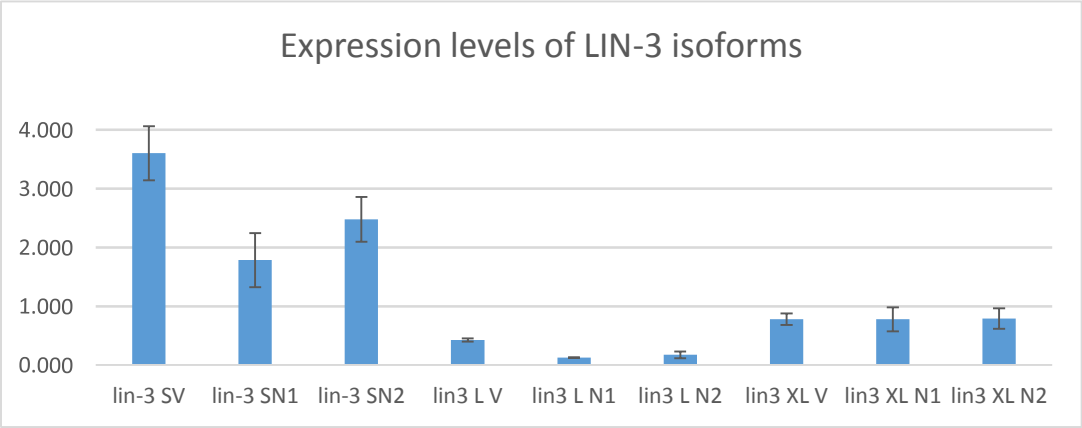
Expression levels of LIN-3 isoforms
4.000
3.000
2.000
1.000
0.000
lin-3 SV
lin-3 SN1
lin-3 SN2
lin3 L V
lin3 L N1
lin3 L N2
lin3 XL V
lin3 XL N1
lin3 XL N2

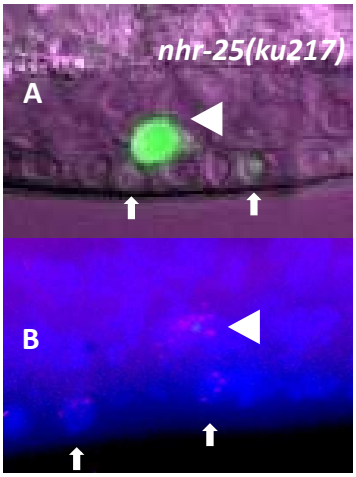

Figure 4.10 smFISH detection of *lin-3* molecules in *nhr-25(ku217);syIs107* animals. All animals were observed at Pn.pxx stage. In control animals, *lin-3* is expressed in AC only, positive GFP signal in (A) and Cy5 detection through smFISH in (C). In *nhr-25(ku217)* animals, ectopic *lin-3* is detected in vulva cells (B and D). Arrow head depicts AC and arrows ectopic vuvla cells.

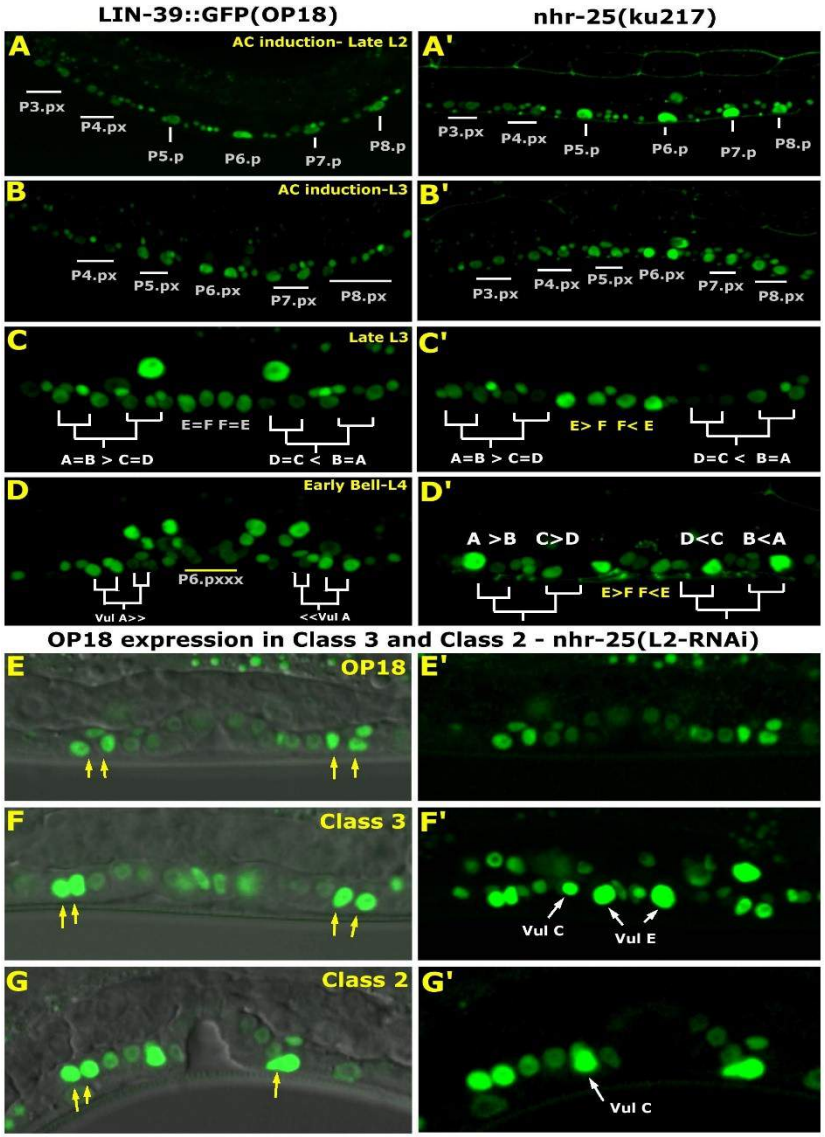

Figure 4.11 Changes in LIN-39::GFP expression in *nhr-25(L2-RNAi)* situation.

LIN-39::GFP(OP18) expression was analyzed in *nhr-25(L2-RNAi)* situation. (A) In normal animals, VulA cell type show characteristic adherence to ventral cuticle and positive LIN-39::GFP expression. (B,C) In class 3 and 2 animals in *nhr-25(L2-RNAi)*, the vulva cells that exhibited strong adherence to the ventral cuticle showed abnormal LIN-39::GFP expressions.

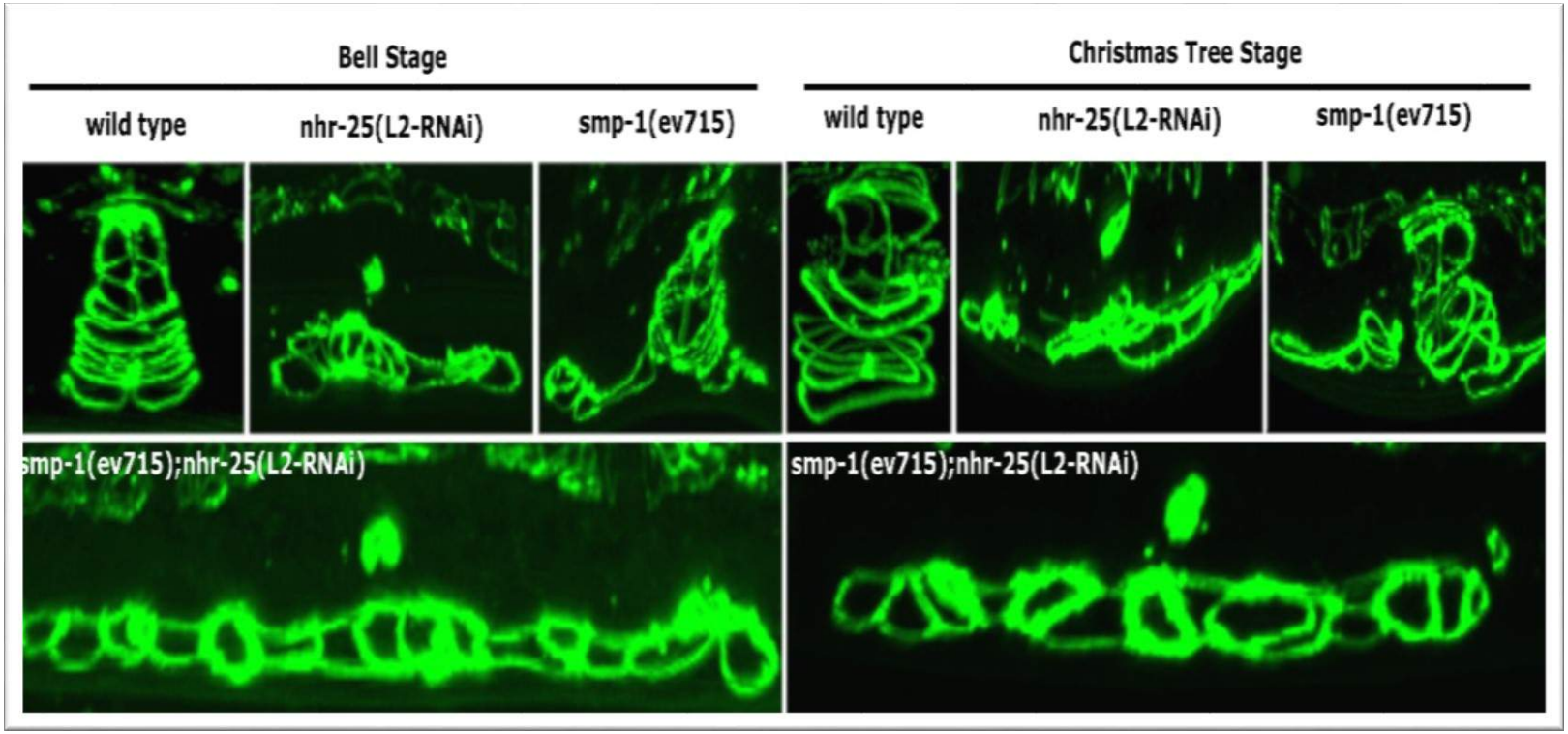

Figure 4.12 Vulva cell migratory defects in *smp-1(ev715);nhr-25(L2-RNAi)* animals.

AJM-1::GFP expression pattern was analyzed to observe vulva migratory behaviors. In *smp-1(ev715)* mutants, the most distal Vul A and B cells failed to migrate towards the midline. In *smp-1(ev715);nhr-25(L2-RNAi)* animals all vulva cells showed severe migratory behaviors. *plx-1(nc37)* and *plx-1(nc37); nhr-25(L2-RNAi)* exhibited identical phenotypes.

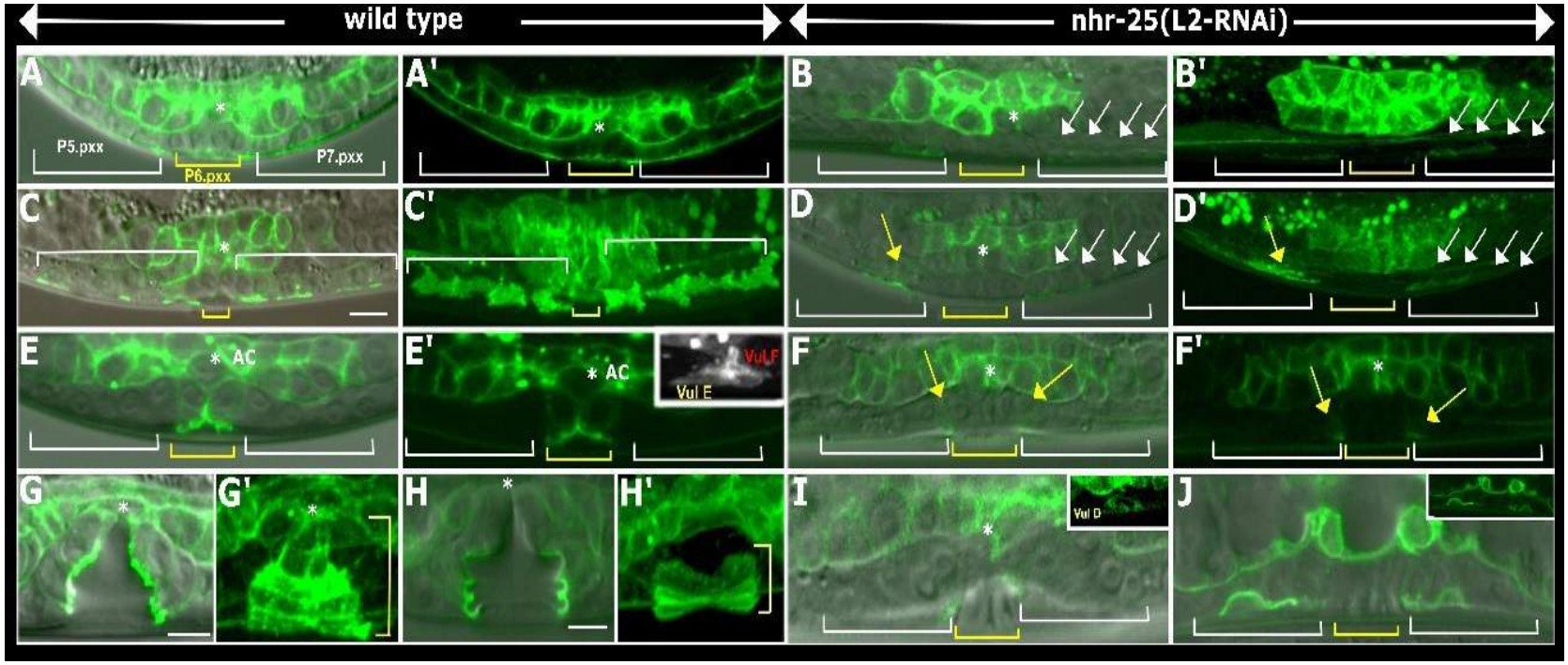

Figure 4.13 Altered SMP-1::GFP expression pattern in *nhr-25(L2-RNAi)* animals.

Expression pattern of SMP-1::GFP reporter, *evEx170* was analyzed in control (A/A' to B/B') and *nhr-25(L2-RNAi)* treated animals (C/C' to D/D'). Yellow horizontal brackets represent P6.p derived cells (1^0) and white P5/7.p lineages (2^0). The * depicts position of AC. Yellow arrows represent VulD position. (A,A') SMP-1::GFP expression seen in 2^0 lineages during cell shape changes. (B,B') VulF/E serves as dorsal ring organizer and shows high SMP-1::GFP expression. In *nhr-25(L2-RNAi)* treatment weak expression was seen within 2^0 derived cells during short range migrations (white arrows in C/C') and also absent in VulE/F at the time of dorsal ring organization (D/D').

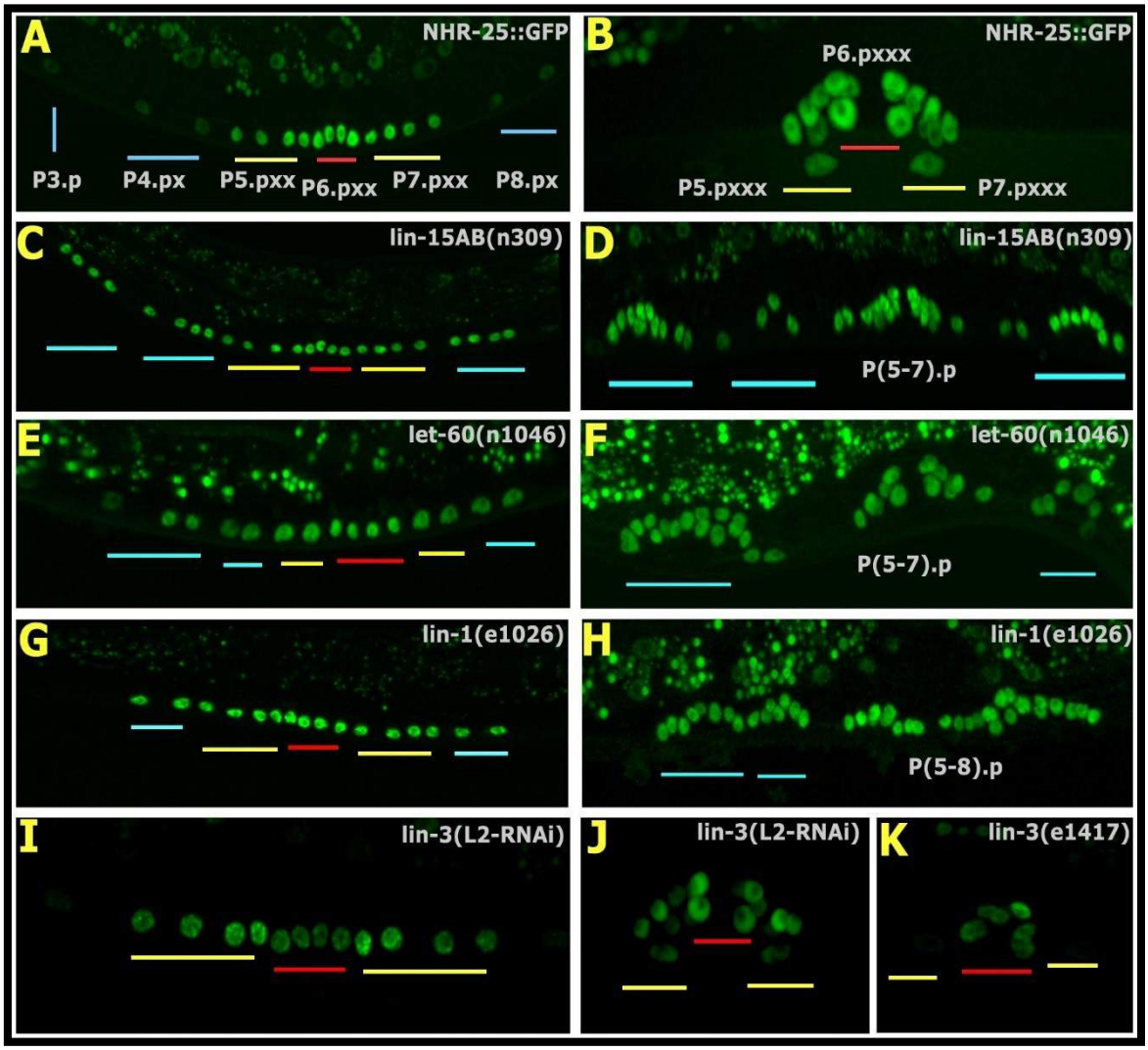

Figure 4.14 NHR-25::GFP(OP33) expression changes in EGF/Ras/MAPK pathway mutants. NHR-25::GFP(OP33) expression in control (A,B), EGF/Ras/MAPK *gf* (C-H), and EGF (*lf*) (I–K). Animals observed at Pn.pxx stages in the left panels and at Pn.pxxx stage in right panels. Red bars represent P6.p lineages, yellow – P5/7.p lineages and blue P3/4/8.p lineages. In EGF(*gf*) OP33 expression was upregulated in all induced vulva cells and the opposite in EGF(*lf*).

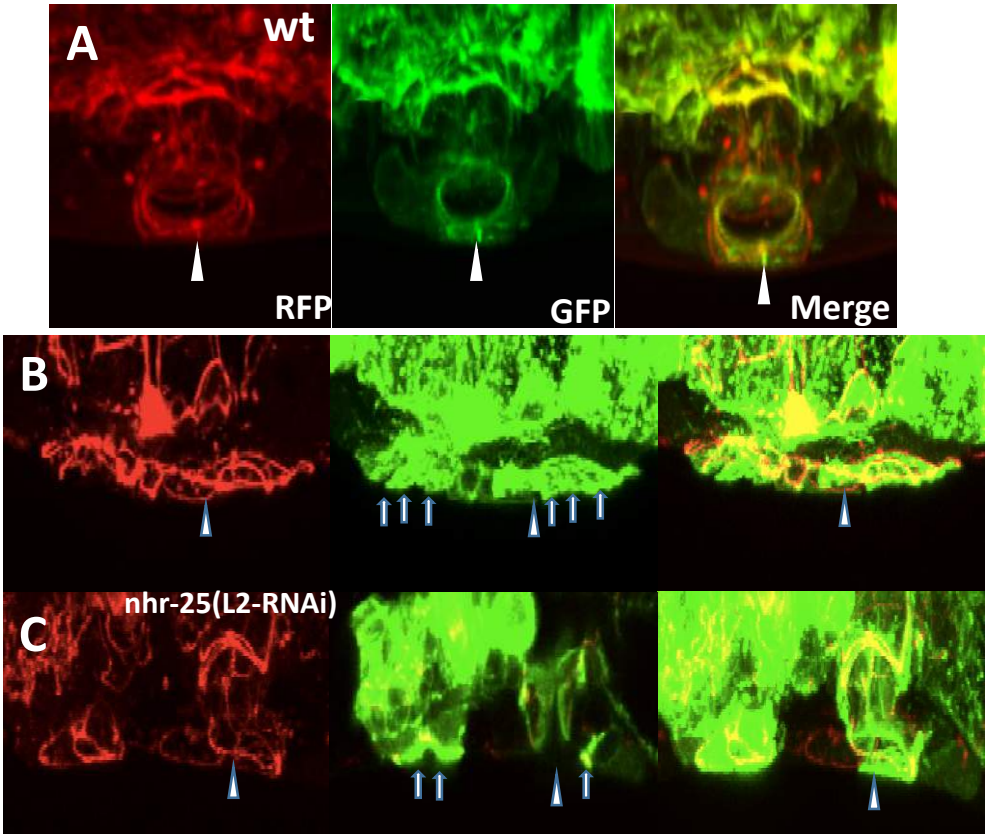

Figure 4.15 LifeAct::GFP expression changes in *nhr-25(L2-RNAi)* situation

Vulva toroid morphologies were observed through DLG-1::RFP and actin changes through lifeAct::GFP expression in wild type (A) and *nhr-25(L2-RNAi)* animals (B and C). Actin is expressed at the lumen facing side during ring formation in wild type (A). But expressed abnormally and in high manner in the defective vulva cells in *nhr-25(L2-RNAi)* animals (B and C). Arrow head depicts position of midline and arrows abnormal actin expression. Figures not drawn to scale.

Table 4.1 Generation of ACs and Pn.p inductions in *nhr-25(RNAi)* treated animals.

Genotype	% *lin-3::gfp* expression in AC		n	% Pn.p induction						Average vulva induction[a]	N
	WT	weak/absent		P3.p	P4.p	P5.p	P6.p	P7.p	P8.p		
Vector(RNAi)	96	4	52	0	0	100	100	100	0	3	64
nhr-25(L1-RNAi)	21.4	78.6	84	0	0	77.5	80	77.5	2.5	2.3	40
nhr-25(L2-RNAi)	100	0	64	0	0	100	100	100	0	3	48

Expression pattern of wild type *lin-3::gfp* in AC was used as a marker to analyze AC differentiation defects in *nhr-25(RNAi)* animals. AJM-1::GFP expression pattern in P(3-8).p cells was used to analyze the competence and induction properties of VPCs. a, average vulva induction is calculated by, number of VPCs induced/ total number of animals observed.

Table 4.2 Pn.p competence properties in temporal *nhr-25(RNAi)* treated animals.

Genotype	Onset of RNAi	% Pn.p induction						Average vulva induction[a]		N
		P3.p	P4.p	P5.p	P6.p	P7.p	P8.p	P(5-7).p	P(3-8).p	
empty vector	0	0	0	100	100	100	0	3.0	3.0	64
nhr-25(RNAi)		0	0	77.5	80	77.5	2.5	2.3	2.3	40
empty vector	4	0	0	100	100	100	0	3.0	3.0	64
nhr-25(RNAi)		0	0	82.6	82.6	78	0	2.5	2.5	23
empty vector	10	0	0	100	100	100	0	3.0	3.0	64
nhr-25(RNAi)		0	0	100	100	97.6	0	2.9	2.9	41
empty vector	20	0	0	100	100	100	0	3.0	3.0	64
nhr-25(RNAi)		0	0	100	100	100	0	3.0	3.0	48

AJM-1::GFP expression pattern in P(3-8).pxx cells was used to analyze the competence and induction properties of the VPCs. a, average vulva induction is calculated by, number of VPCs induced/ total number of animals observed.

Table 4.3 VPC lineage analysis in wild type and *nhr-25 (lf)* animals

Genotype	Feeding RNAi	VPC lineages			n'	n"
		P5.pxx	P6.pxx	P7.pxx		
N2	-	LLTN	TTTT	NTLL	22	12
nhr-25(ku217)	-	LLNN	NNNN	NNLL	16	3
		LLNN	TNNT	NNLL	18	2
		LLNN	TNNN	NNLL	17	1
		NLNN	NNNN	NNLL	15	1
N2	***Vector(RNAi)***	LLTN	TTTT	NTLL	22	8
	nhr-25(L1-RNAi)	SS	SS	SS	6	4
		NNNN	NNNN	SS	10	1
		SS	NNNN	NNNN	10	1
		NNNN	NNNN	NNNN	12	1
		LLNN	NNNN	NNLN	16	1
		NLNN	LNNL	NNLL	17	1
	nhr-25(L2-RNAi)	LLTN	TTTT	NTLL	22	2
		LLNN	LNNL	NNLL	16	1
		LLNN	LNNL	NNLL	16	1
		LLNN	LNNL	NLLL	17	1
		LLLN	ONNL	NNLL	19	1
		LLLN	ONNL	NNLL	19	1
		LLON	LNNN	NNLL	18	1

All lineage analysis was carried out in N2 background at 20^0 C. L, longitudinal plane of division axis; T, transverse; O-oblique; N- no division; S, cell adopted syncytial fate and fused with hypodermis. n', total number of vulva cells that constitute mature vulva at Pn.pxxx stage. n", number of animals observed.

Table 4.4 L4 stage *lin-3::gfp* expression pattern in *nhr-25(lf)* situation

	%lin-3::gfp in primary vulva lineages					
	wild type/control			nhr-25(L2-RNAi)		nhr-25(ku217)		
	%E	%F	(n)	%E	%F	(n)	%E	%F	(n)
Pn.pxx	0	0	(118)	43	0	(28)	41	2.5	(39)
bell	3.3	66.7	(30)	88	72	(25)	73	69	(26)
CT	0	100	(80)	8	54	(37)	14	66.7	(21)

Quantitative changes in *lin-3* expression at L4 stage in VulE and F lineages in wild type and *nhr-25(lf)* animals. n represents the number of animals observed.

Table 4.5 Summary of vulva cell migration defects in various genetic backgrounds

Rows	Genetic background	% vulva migration defects		n
		defective	wild type	
1	***jcIs1(ajm-1::gfp);vector(RNAi)***	2	98	248
2	***jcIs1;nhr-25(RNAi)***	92	8	222
3	***jcIs1;nhr-25(V+N)***	62	38	74
4	***smp-1(ev715);jcIs1;vector(RNAi)***	51	49	136
5	***smp-1(ev715);jcIs1;nhr-25(RNAi)***	100	0	235
6	***smp-1(ev715);jcIs1;nhr-25(V+N)***	100	0	100
7	***plx-1-1(nc37);jcIs1;vector(RNAi)***	47.5	53.5	166
8	***plx-1-1(nc37);jcIs1;nhr-25(RNAi)***	100	0	76
9	***plx-1-1(nc37);jcIs1;nhr-25(V+N)***	100	0	111

JcIs1 (AJM-1::GFP) animals were observed for their vulva migratory behaviors at L4 stage. Rows 2,5 and 8 represent *nhr-25(L2-RNAi)* treatments and 3,6 and 9 (V+N) treatments. n – number of animals observed for the corresponding phenotypes.

Table 4.6 Primer list for *lin-3* qRT-PCR studies.

Primers	Detected *lin-3* minigenes	Genomic amplicons (bp)	cDNA amplicons (bp)
F3-R5	S,L and XL	1166, 1230, and 1487	508, 572, 664
F3-RS	S common (most abundant)	1166	520
F3-RL	L	1230	584
F3-RXL	XL	1487	678

TGTGACCCTGAAAACTGT	lin3-fw1
GCATCCTTCTACTCTTTATGCC	lin3-fw2
CCCTTCGTGGTTTCGTCAA	lin3-fw3
GGCATAAAGAGTAGAAGGATGC	lin3-bw1
AGGAGGAAATGGTAGCGGG	lin3-bw2
TACAGTTGAGTTTCTGGG	lin3-bw3
TTGGAGTGAATCCAGAGG	lin3-bw4
CGGCAGATATAATGTACGTTTGAGCACG	lin-3-RS
GCGCAACTCCTGGTTCAAGGA	lin-3-RL
CAGTGGGCTTTATGAGAGAATTGTGC	lin-3-RXL

4.2 Remarks

NHR-25 regulates generation of AC through asymmetric cell divisions in the gonad and thus effecting vulva formation indirectly. NHR-25 expression was also seen in vulva cells. Our *nhr-25* (*ku217)* and *nhr-25(L2-RNAi)* resulted in defective vulva cell migrations and morphogenesis, suggesting autonomous roles for NHR-25 during post-AC induction events in vulva.

Unusual ectopic *lin-3::gfp* presence within primary lineages (P6.pxx) was seen in *nhr-25(lf)* animals after AC inductions. At similar stage, in normal animals, *lin-3* was detected only in AC with no expression in vulval cells. Global de-repression of *lin-3* was seen in hyp7 and other tissues (except vulva cells) in synmuv mutants. Our qPCR and preliminary smFISH studies in *nhr-25(lf)* did not detect global *lin-3* de-repression. These observations suggest that *lin-3* is regulated by NHR-25 in cell type specific manner in vulva. In the same way, it was reasoned that NHR-25 regulates AC specific *lin-3* expression through binding ACEL. But *lin-3::gfp* expression levels were not changed in post-embryonic *nhr-25(RNAi)*, suggesting no interactions. Thus, it is possible that NHR-25 represses *lin-3* within vulva cells through binding unidentified *lin-3* enhancer elements either directly or indirectly. Indeed the presence of *lin-3* within VPCs was suggested through isoform specific over expression studies that results in *Muv* (Dutt et al., 2004).

Within P6.pxx cells, ectopic expression in *nhr-25(lf)* was predominantly seen in the outer presumptive VulE cells, suggesting possible alterations in the EFFE pattern. Production of ectopic ligand in inappropriate cells may confuse neighboring vulval cells including vulF, which can cause defective initial short range migrations of vulF towards AC. Therefore it is plausible that ectopic expression is at least partly responsible for the Class 1 phenotypes in *nhr-25(RNAi)* situation.

Balanced activities of Wnt and Ras signaling regulates attachment of AC to inner VulF cells (Wang and Sternberg 2000). In our observations, no defects were seen in this phenotype in *nhr-25(lf)* animals as ACs always attracted towards the inner presumptive VulF cells. The ectopic

lin-3 can produce more *ras* and thus misbalancing *wnt* and *ras* signals within EFFE cells. Further cell ablations of the inner vulF cells leaving the outer VulE cells in *nhr-25(lf)* animals and the behavior of AC invasion towards vulva cells will provide additional evidence for any pattern alterations. Alternately, it is possible that the ectopic expression appears within EFFE at a later stage after AC attachment and both events are tightly controlled through temporally.

In control animals, *lin-3* was detected in VulF lineages at L4 stage. So, we expected that in *nhr-25(lf)* situation, *lin-3* should be seen in both VulE and VulF as it de-represses *lin-3* in VulE lineages at earlier stage. But to our surprise this scenario was not seen. Instead wild type VulF specific *lin-3* was decreased and abnormal VulE was seen in only few animals. Accordingly, VulE specific *egl-26* expression was less severely effected in *nhr-25(lf)*. These observations suggest that *nhr-25* regulates *lin-3* not only in cell type specific manner but also in stage specific manner during vulva formation. In addition to *lin-3* expression, *nhr-25* also regulates VulB specific *egl-26* and VulC/D specific *egl-17* expressions. Thus it is plausible that *nhr-25* regulates distinct gene regulatory networks within vulva cell types similar to *nhr-67* and *nhr-113* (Fernandes et al., 2007). Accordingly, abnormal fusions and cell contacts were also seen within vulva cell types suggesting altered terminal differentiation properties. Alternatively, *nhr-25* may be causing ectopic *eff-1* expression within these lineages, similar to *nhr-67* that may result in abnormal fusion within themselves.

Loss of *nhr-25* activity causes migratory defects in vulva cells, sometimes only in primary and sometimes in secondary cells and in other cases all vulva cells. Loss of *smp-1/plx-1* pathway causes defects only in secondary VulA and B cell types with ~50% penetrance. At the vulva midline, high NHR-25 expression was seen during initial cell migrations that overlaps with sequential SMP-1 expressions. Our genetic interactions suggest that *nhr-25(lf)* causes defective SMP-1 expression during cell migration. If so, *nhr-25* works epistatic to *smp-1* pathway and vulva migration defects in *smp-1(lf);nhr-25(lf)* situation should be similar to *smp-1(lf)*. Intriguingly, we observed 100% migration defects in *smp-1(lf);nhr-25(lf)* with increased severity when compared to either single *lf* situation. Thus it should be reasoned that *nhr-25* also interacts with pathways that work in parallel to *smp-1/plx-1* system (Dalpe et al., 2005).

Wnt/ planar cell polarity (PCP) pathways in vertebrates are known to regulate contact dependent inhibition process and orientation of mitotic axis during cell divisions (Vladar et al., 2009). Further studies suggested that Wnt/GTPases – RAC/RHO/ROCK homologs are crucial for regulating cytoskelteal rearrangements and spindle orientation during morphogenesis (Lapébi et al, 2011; Vladar et al., 2009). Mutants in the RAC/RHO components in *C. elegans*; *mig-2, ced-10* and *unc-73* results in abnormal vulva morphogenesis through changes in the cell division axis. Similar observations were seen in *nhr-25(RNAi)* where certain vulva cell types changes their axis of division from normal transverse division (T) to defective longitudinal (L). We also observed abnormal *lifeAct::gfp* expression within vuvla cells with migratory defects, suggesting *nhr-25* also regulates actin network during migration. LET-502/ROCK regulates network of actin myofibrils during dorsal migration within vulva (Farooqui et al., 2012). Thus it appears that *nhr-25* regulates vulva cell migrations through multple regulatory steps such as, maintainng proper SMP-1 expressions during migrations and also regulating components of cytoskeletal rearragnments. Therefore it would be interesting to see how *nhr-25* interacts with known Wnt/PCP and Wnt/GTPases pathway components during vulva formation in *C. elegans*.

Hox/LIN-39 is regulated by Wnt and EGF/LIN-3 signaling during inductions. Later, LIN-39 targets VAB-23 to regulate proper vulva morphogenesis.*Vab-23(lf)* animals show abnormal cell contacts, fusions and morphogenesis (Pellegrino et al., 2011). Surprisingly, we noticed abnormal expression of Hox/LIN-39 within vulva cells in *nhr-25(lf)* during late vulva morphogenesis that associates with non-detachment of defective vulva cells from ventral cuticle. In normal animals, VulA shows this behavior and in defective animals it was seen in VulC and E cell types. Thus both *loss* and *gain* of LIN-39 activity within vulva cells associates with abnormal vulva structure. Thus a fine balance of Hox/LIN-39 activity is necessary for proper vulva morphogenesis.

WNT signaling regulates TCF/POP-1 distribution in secondary vulva lineages to establish mirror image symmetry within vulva (JL Green et al., 2008). Polarity reversal defects were never seen in *nhr-25(lf)*. If it had occurred then expression domain of VulD specific *egl-17::gfp* should be seen in the position of VulA within P7.p lineages (wild type ABC**D**-**D**CBA to defective ABC**D**-ABC**D**). Such scenario was never seen in *nhr-25(lf)* animals. Asymmetric

distribution of β-catenins, SYS-1, LIT-1, WRM-1 play key roles in this process. NHR-25 interacts with SYS-1 and WRM-1 during asymmetric cell divisions in the gonad and male tail. Hence it is possible that NHR-25 may interact with Wnt/ β-catenins through unknown mechanism to control aspects of vulva morphogenesis.

It was quite obvious that NHR-25 acts temporally with distinct regulatory inputs during vulva development. At the time of vulva inductions, it is targeted by EGF/LIN-3 signaling in all vulva cells and at later stages targets EGF/LIN-3 in P6.pxx lineages. VAB-23 is also targeted by LIN-3 signaling during inductions.VAB-23 acts downstream of LIN-39 and NHR-25 appears to act upstream of it during morphogenesis. Interestingly, expression pattern of signaling pathways involved in vulva cell fate generations were altered later during fate execution process in *nhr-25(lf)* situation, suggesting complex interactions similar to VAB-23 roles.

NHR-25 is sumoyalted and sumoylaton of target proteins regulates their transcriptional activity (thus DNA binding) and protein-protein interactions and their subcellular localizations. During hepatocyte growth factor signaling, sumoylated Rac1 regulates lamellipodia formation, cell migration and invasion processes through controlling the levels of Rac1-GTP (Castillo-Lluva et al., 2010). In chapter 3, we showed that a fine balance of sumoylated to unsumoylated NHR-25 regulates proper vulva cell fates. Additionally NHR-25 also de-represses another Hox gene MAB-5 during seam cell development (Silhankova et al., 2005). Thus SUMO-NHR-25 interactions may repress activity of key genes and/or maintain proper cytoskeletal rearrangements during vulva morphogenesis.

Finally, the cause for the observed migration defects in *nhr-25(lf)* appears complex. Expression pattern of important vulva genes, *lin-3, lin-39*, and *smp-1*were altered in cell type specific manner. This possibly alters the normal behavior of vulva cells such as cell migration. Our data suggest that NHR-25 cooperates with various signaling cascades during morphogenesis and has the pivotal role in proper cell differentiation and function of the nematode reproductive structure, the vulva.

Chapter 5: Final conclusions

1) *Nhr-25 regulates multiple processes at multiple times during vulva formation.*

Pleiotropic phenotypes were observed during vulva formation in *nhr-25(lf)* situation. During early vulva morphogenesis, *nhr-25(lf)* causes abnormal orientation of vulva cell divisions, proliferations and migratory patterns. At later stages, ectopic cell contacts, abnormal fusions and terminal differentiations were seen within vulva cell types. Thus *nhr-25* activity is indispensable for normal vulva development.

2) *Gradient of NHR-25 expression was seen within vulva.*

High NHR-25::GFP expression was seen in 1^0 cells, intermediate in 2^0 and low in 3^0 cells during induction process. Strong expression was also seen at the vulva midline during the initiation of cell migrations. Thus suggesting vulva autonomous roles for NHR-25 during cellular inductions and migrations.

3) *A balance of sumoylated to un-sumoylated NHR-25 regulates vulva cell fates.*

Our biochemical studies identified that sumoylation of NHR-25 is required for its regulation during development. Combined activities of gradient NHR-25 expression and steady state SUMO kinetics within vulva cells generates gradient of unsumoylated NHR-25 and constant sumoylated NHR-25. Within the 3^0 cells, the ratio of sumoylated to un-sumoylated NHR-25 reaches a specific threshold to regulate cell fate specific gene expression. Accordingly, loss of *smo-1* simulates NHR-25 over-expression pertinent to 3^0 vulva cell fate specifications.

4) *NHR-25 modulates cell type specific transcription within vulva.*

During vulva formation, altered expression pattern for several genes, *lin-3, lin-39, smp-1, egl-17,* and *egl-26* was seen when NHR-25 function was attenuated. The specific down- or up-regulation of gene transcription was not seen globally. Rather it occurred in a cell type specific manner and at a particular time during development.

5) ***Inductive signaling regulates nhr-25 transcription during vulva development.***

Graded NHR-25 expression within vulva cells overlaps with activities of inductive EGF/LIN-3 signaling. *Gf* situation in inductive signaling upregulates NHR-25 expression in all the induced vulva cells and *lf* does the opposite.

Thus both transcriptional and post-translational mechanisms control NHR-25 expression and activity during *C. elegans* vulva development to confer its temporal cell type and tissue specific functions.

Chapter 6: References

Antebi, A., & Antebi, A. (2006). Nuclear hormone receptors in C. elegans. *WormBook : The Online Review of C. Elegans Biology*, 1–13. http://doi.org/10.1895/wormbook.1.64.1

Aroian, R. V, Koga, M., Mendel, J. E., Ohshima, Y., & Sternberg, P. W. The let-23 gene necessary for Caenorhabditis elegans vulval induction encodes a tyrosine kinase of the EGF receptor subfamily. *Nature*, *348*(6303), 693–9. http://doi.org/10.1038/348693a0

Aroian, R. V, & Sternberg, P. W. (1991). Multiple functions of let-23, a Caenorhabditis elegans receptor tyrosine kinase gene required for vulval induction. *Genetics*, *128*(2), 251–67.

Asahina, M., Ishihara, T., Jindra, M., Kohara, Y., Katsura, I., & Hirose, S. (2000). The conserved nuclear receptor Ftz-F1 is required for embryogenesis, moulting and reproduction in Caenorhabditis elegans. *Genes to Cells*, *5*(9), 711–723. http://doi.org/10.1046/j.1365-2443.2000.00361.x

Asahina, M., Valenta, T., Silhankova, M., Korinek, V., & Jindra, M. (2006). Crosstalk between a Nuclear Receptor and β-Catenin Signaling Decides Cell Fates in the C. elegans Somatic Gonad. *Developmental Cell*, *11*(2), 203–211. http://doi.org/10.1016/j.devcel.2006.06.003

Beitel, G. J., Tuck, S., Greenwald, I., & Horvitz, H. R. (1995). The Caenorhabditis elegans gene lin-1 encodes an ETS-domain protein and defines a branch of the vulval induction pathway. *Genes and Development*, *9*(24), 3149–3162. http://doi.org/10.1101/gad.9.24.3149

Berset, T., Hoier, E. F., Battu, G., Canevascini, S., & Hajnal, A. (2001). Notch inhibition of RAS signaling through MAP kinase phosphatase LIP-1 during C. elegans vulval development. *Science (New York, N.Y.)*, *291*(5506), 1055–1058. http://doi.org/10.1126/science.1055642

Broday, L., Kolotuev, I., Didier, C., Bhoumik, A., Gupta, B. P., Sternberg, P. W., … Ronai, Z. (2004). The small ubiquitin-like modifier (SUMO) is required for gonadal and uterine-vulval morphogenesis in Caenorhabditis elegans. *Genes and Development*, *18*(19), 2380–2391. http://doi.org/10.1101/gad.1227104

Burdine, R. D., Branda, C. S., & Stern, M. J. (1998). EGL-17(FGF) expression coordinates the attraction of the migrating sex myoblasts with vulval induction in C. elegans. *Development (Cambridge, England)*, *125*(6), 1083–1093.

Castillo-Lluva, S., Tatham, M. H., Jones, R. C., Jaffray, E. G., Edmondson, R. D., Hay, R. T., & Malliri, A. (2010). SUMOylation of the GTPase Rac1 is required for optimal cell migration. *Nature Cell Biology*, *12*(11), 1078–85. http://doi.org/10.1038/ncb2112

Chang, C., Newman, A. P., & Sternberg, P. W. (1999). Reciprocal EGF signaling back to the uterus from the induced C. elegans vulva coordinates morphogenesis of epithelia. *Current Biology*, *9*(5), 237–246. http://doi.org/10.1016/S0960-9822(99)80112-2

Chen, W. Y., Lee, W. C., Hsu, N. C., Huang, F., & Chung, B. C. (2004). SUMO modification of repression domains modulates function of nuclear receptor 5A1 (steroidogenic factor-1). *Journal of Biological Chemistry*, *279*(37), 38730–38735. http://doi.org/10.1074/jbc.M405006200

Chen, Z., Eastburn, D. J., & Han, M. (2004). The Caenorhabditis elegans nuclear receptor gene nhr-25 regulates epidermal cell development. *Mol.Cell Biol*, *24*(0270-7306 (Print)), 7345–7358.

Chen, Z., & Han, M. (2001). C. elegans Rb, NuRD, and Ras regulate lin-39-mediated cell fusion during vulval fate specification. *Current Biology*, *11*(23), 1874–1879. http://doi.org/10.1016/S0960-9822(01)00596-6

Clark, S. G., Chisholm, A. D., & Horvitz, H. R. (1993). Control of cell fates in the central body region of C. elegans by the homeobox gene lin-39. *Cell*, *74*(1), 43–55. http://doi.org/10.1016/0092-8674(93)90293-Y

Cui, M., Chen, J., Myers, T. R., Hwang, B. J., Sternberg, P. W., Greenwald, I., & Han, M. (2006). SynMuv Genes Redundantly Inhibit lin-3/EGF Expression to Prevent Inappropriate Vulval Induction in C. elegans. *Developmental Cell*, *10*(5), 667–672. http://doi.org/10.1016/j.devcel.2006.04.001

Cui, M., Fay, D. S., & Han, M. (2004). Lin-35/Rb cooperates with the SWI/SNF complex to control Caenorhabditis elegans larval development. *Genetics*, *167*(3), 1177–1185. http://doi.org/10.1534/genetics.103.024554

Cui, M., & Han, M. (2003). Cis regulatory requirements for vulval cell-specific expression of the Caenorhabditis elegans fibroblast growth factor gene egl-17. *Developmental Biology*, *257*(1), 104–116. http://doi.org/10.1016/S0012-1606(03)00033-2

Cui, M., & Han, M. (2007). Roles of chromatin factors in C. elegans development. *WormBook : The Online Review of C. Elegans Biology*, 1–16. http://doi.org/10.1895/wormbook.1.139.1

Dalpé, G., Brown, L., & Culotti, J. G. (2005). Vulva morphogenesis involves attraction of plexin 1-expressing primordial vulva cells to semaphorin 1a sequentially expressed at the vulva midline. *Development (Cambridge, England)*, *132*(6), 1387–1400. http://doi.org/10.1242/dev.01694

Dalpe, G., Dalpe, G., Culotti, J., & Culotti, J. (2005). Semaphorin-1s and Plexin-1 guided neuron and cell migrations during male tail and vulva morphogenesis. *International Worm Meeting*.

Davison, E. M., Saffer, A. M., Huang, L. S., DeModena, J., Sternberg, P. W., & Horvitz, H. R. (2011). The LIN-15A and LIN-56 transcriptional regulators interact to negatively regulate EGF/Ras signaling in Caenorhabditis elegans vulval cell-fate determination. *Genetics*, *187*(3), 803–815. http://doi.org/10.1534/genetics.110.124487

Deshpande, R., Inoue, T., Priess, J. R., & Hill, R. J. (2005). Lin-17/Frizzled and lin-18 regulate POP-1/TCF-1 localization and cell type specification during C. elegans vulval development. *Developmental Biology*, *278*(1), 118–129. http://doi.org/10.1016/j.ydbio.2004.10.020

Dolezel, D., Zdechovanova, L., Sauman, I., & Hodkova, M. (2008). Endocrine-dependent expression of circadian clock genes in insects. *Cellular and Molecular Life Sciences : CMLS*, *65*(6), 964–9. http://doi.org/10.1007/s00018-008-7506-7

Dutt, A., Canevascini, S., Froehli-Hoier, E., & Hajnal, A. (2004). EGF signal propagation during C. elegans vulval development mediated by ROM-1 Rhomboid. *PLoS Biology*, *2*(11). http://doi.org/10.1371/journal.pbio.0020334

Eisenmann, D. M. (2005). Wnt signaling (June 25, 2005). *In: The C. Elegans Resarch Community (eds.) Wormbook, doi/10.1895/wormbook.1.7.1, Http://www.wormbook.org.* http://doi.org/10.1895/wormbook.1.7.1

Eisenmann, D. M., & Kim, S. K. (2000). Protruding vulva mutants identify novel loci and wnt signalling factors that function during Caenorhabditis elegans vulva development. *Genetics*, *156*(3), 1097–1116.

Eisenmann, D. M., Maloof, J. N., Simske, J. S., Kenyon, C., & Kim, S. K. (1998). The beta-catenin homolog BAR-1 and LET-60 Ras coordinately regulate the Hox gene lin-39 during Caenorhabditis elegans vulval development. *Development (Cambridge, England)*, *125*(18), 3667–3680.

Erkut, C. (2014). C. elegans life cycle and developmental stages. http://doi.org/doi:10.6084/m9.figshare.1096220

Estes, K. A., & Hanna-Rose, W. (2009). The anchor cell initiates dorsal lumen formation during C. elegans vulval tubulogenesis. *Developmental Biology*, *328*(2), 297–304. http://doi.org/10.1016/j.ydbio.2009.01.034

Estes, K. A., Kalamegham, R., & Hanna-Rose, W. (2007). Membrane localization of the NlpC/P60 family protein EGL-26 correlates with regulation of vulval cell morphogenesis in Caenorhabditis elegans. *Developmental Biology*, *308*(1), 196–205. http://doi.org/10.1016/j.ydbio.2007.05.020

Farooqui, S., Pellegrino, M. W., Rimann, I., Morf, M. K., Müller, L., Fröhli, E., & Hajnal, A. (2012). Coordinated lumen contraction and expansion during vulval tube morphogenesis in Caenorhabditis elegans. *Developmental Cell*, *23*(3), 494–506. http://doi.org/10.1016/j.devcel.2012.06.019

Fay, D. S., & Yochem, J. (2007). The SynMuv genes of Caenorhabditis elegans in vulval development and beyond. *Developmental Biology*. http://doi.org/10.1016/j.ydbio.2007.03.016

Fayard, E., Auwerx, J., & Schoonjans, K. (2004). LRH-1: An orphan nuclear receptor involved in development, metabolism and steroidogenesis. *Trends in Cell Biology*. http://doi.org/10.1016/j.tcb.2004.03.008

Fernandes, J. S., & Sternberg, P. W. (2007). The tailless ortholog nhr-67 regulates patterning of gene expression and morphogenesis in the C. elegans vulva. *PLoS Genetics*, *3*(4), 0603–0616. http://doi.org/10.1371/journal.pgen.0030069

Fraser, A. G., Kamath, R. S., Zipperlen, P., Martinez-Campos, M., Sohrmann, M., & Ahringer, J. (2000). Functional genomic analysis of C. elegans chromosome I by systematic RNA interference. *Nature*, *408*(6810), 325–330. http://doi.org/10.1038/35042517

Fujii, T., Nakao, F., Shibata, Y., Shioi, G., Kodama, E., Fujisawa, H., & Takagi, S. (2002). Caenorhabditis elegans PlexinA, PLX-1, interacts with transmembrane semaphorins and regulates epidermal morphogenesis. *Development (Cambridge, England)*, *129*(9), 2053–63.

Gissendanner, C. R., Crossgrove, K., Kraus, K. a., Maina, C. V., & Sluder, A. E. (2004). Expression and function of conserved nuclear receptor genes in Caenorhabditis elegans. *Dev Biol*, *266*(2), 399–416. http://doi.org/S001216060300650X [pii]

Gissendanner, C. R., & Sluder, A. E. (2000). nhr-25, the Caenorhabditis elegans ortholog of ftz-f1, is required for epidermal and somatic gonad development. *Developmental Biology*, *221*(1), 259–272. http://doi.org/10.1006/dbio.2000.9679

Gleason, J. E., Korswagen, H. C., & Eisenmann, D. M. (2002). Activation of Wnt signaling bypasses the requirement for RTK/Ras signaling during C. elegans vulval induction. *Genes and Development*, *16*(10), 1281–1290. http://doi.org/10.1101/gad.981602

Gleason, J. E., Szyleyko, E. A., & Eisenmann, D. M. (2006). Multiple redundant Wnt signaling components function in two processes during C. elegans vulval development. *Developmental Biology*, *298*(2), 442–457. http://doi.org/10.1016/j.ydbio.2006.06.050

Green, J. L., Inoue, T., & Sternberg, P. W. (2008). Opposing Wnt Pathways Orient Cell Polarity during Organogenesis. *Cell*, *134*(4), 646–656. http://doi.org/10.1016/j.cell.2008.06.026

Greenwald, I. (2005). LIN-12/Notch signaling in C. elegans. *WormBook : The Online Review of C. Elegans Biology*, 1–16. http://doi.org/10.1895/wormbook.1.10.1

Greenwald, I. S., Sternberg, P. W., & Horvitz, H. R. (1983). The lin-12 locus specifies cell fates in Caenorhabditis elegans. *Cell*, *34*(2), 435–444. http://doi.org/10.1016/0092-8674(83)90377-X

Hada, K., Asahina, M., Hasegawa, H., Kanaho, Y., Slack, F. J., & Niwa, R. (2010). The nuclear receptor gene nhr-25 plays multiple roles in the Caenorhabditis elegans heterochronic gene network to control the larva-to-adult transition. *Developmental Biology*, *344*(2), 1100–1109. http://doi.org/10.1016/j.ydbio.2010.05.508

Hajduskova, M., Jindra, M., Herman, M. A., & Asahina, M. (2009). The nuclear receptor NHR-25 cooperates with the Wnt/beta-catenin asymmetry pathway to control differentiation of the T seam cell in C. elegans. *Journal of Cell Science*, *122*(Pt 17), 3051–3060. http://doi.org/10.1242/jcs.052373

Han, M., Aroian, R. V, & Sternberg, P. W. (1990). The let-60 locus controls the switch between vulval and nonvulval cell fates in Caenorhabditis elegans. *Genetics*, *126*(4), 899–913.

Hanna-Rose, W., & Han, M. (2002). The Caenorhabditis elegans EGL-26 protein mediates vulval cell morphogenesis. *Developmental Biology*, *241*(2), 247–258. http://doi.org/10.1006/dbio.2001.0514

Hill, R. J., & Sternberg, P. W. (1992). The gene lin-3 encodes an inductive signal for vulval development in C. elegans. *Nature*, *358*(6386), 470–476. http://doi.org/10.1038/358470a0

Horvitz, H. R., & Sulston, J. E. (1980). Isolation and genetic characterization of cell-lineage mutants of the nematode Caenorhabditis elegans. *Genetics*, *96*(2), 435–454. http://doi.org/10.1016/0166-2236(85)90104-3

Hwang, B. J., & Sternberg, P. W. (2004). A cell-specific enhancer that specifies lin-3 expression in the C. elegans anchor cell for vulval development. *Development (Cambridge, England)*, *131*(1), 143–151. http://doi.org/10.1242/dev.00924

Inoue, T., Oz, H. S., Wiland, D., Gharib, S., Deshpande, R., Hill, R. J., … Sternberg, P. W. (2004). C. elegans LIN-18 is a Ryk ortholog and functions in parallel to LIN-17/Frizzled in Wnt signaling. *Cell*, *118*(6), 795–806. http://doi.org/10.1016/j.cell.2004.09.001

Inoue, T., Sherwood, D. R., Aspöck, G., Butler, J. A., Gupta, B. P., Kirouac, M., … Sternberg, P. W. (2002). Gene expression markers for Caenorhabditis elegans vulval cells. *Gene Expression Patterns*, *2*(3-4), 235–241. http://doi.org/10.1016/S1567-133X(02)00055-8

Jiang, Y., Shi, H., & Liu, J. (2009). Two Hox cofactors, the Meis/Hth homolog UNC-62 and the Pbx/Exd homolog CEH-20, function together during C. elegans postembryonic mesodermal development. *Developmental Biology*, *334*(2), 535–546. http://doi.org/10.1016/j.ydbio.2009.07.034

Jorgensen, E. M., & Mango, S. E. (2002). The art and design of genetic screens: caenorhabditis elegans. *Nature Reviews. Genetics*, *3*(5), 356–369. http://doi.org/10.1038/nrg794

Kamath, R. S., Fraser, A. G., Dong, Y., Poulin, G., Durbin, R., Gotta, M., … Ahringer, J. (2003). Systematic functional analysis of the Caenorhabditis elegans genome using RNAi. *Nature*, *421*(6920), 231–237. http://doi.org/10.1038/nature01278

Kishore, R. S., & Sundaram, M. V. (2002). ced-10 Rac and mig-2 function redundantly and act with unc-73 trio to control the orientation of vulval cell divisions and migrations in Caenorhabditis elegans. *Developmental Biology*, *241*(2), 339–48. http://doi.org/10.1006/dbio.2001.0513

Kruger, R. P., Aurandt, J., & Guan, K.-L. (2005). Semaphorins command cells to move. *Nature Reviews. Molecular Cell Biology*, *6*(10), 789–800. http://doi.org/10.1038/nrm1740

Lapébie, P., Borchiellini, C., & Houliston, E. (2011). Dissecting the PCP pathway: one or more pathways?: Does a separate Wnt-Fz-Rho pathway drive morphogenesis? *BioEssays : News and Reviews in Molecular, Cellular and Developmental Biology*, *33*(10), 759–68. http://doi.org/10.1002/bies.201100023

Laudet, V. (1997). Evolution of the nuclear receptor superfamily: Early diversification from an ancestral orphan receptor. *Journal of Molecular Endocrinology*. http://doi.org/10.1677/jme.0.0190207

Leight, E. R., Glossip, D., & Kornfeld, K. (2005). Sumoylation of LIN-1 promotes transcriptional repression and inhibition of vulval cell fates. *Development (Cambridge, England)*, *132*(5), 1047–1056. http://doi.org/10.1242/dev.01664

Leung, K., Horck, F. van, & Lin, A. (2006). Asymmetrical β-actin mRNA translation in growth cones mediates attractive turning to netrin-1. *Nature.*

Liu, J., Tzou, P., Hill, R. J., & Sternberg, P. W. (1999). Structural requirements for the tissue-specific and tissue-general functions of the Caenorhabditis elegans epidermal growth factor LIN-3. *Genetics*, *153*(3), 1257–1269.

Liu, Z., Fujii, T., Nukazuka, A., Kurokawa, R., Suzuki, M., Fujisawa, H., & Takagi, S. (2005). C. elegans PlexinA PLX-1 mediates a cell contact-dependent stop signal in vulval precursor cells. *Developmental Biology*, *282*(1), 138–51. http://doi.org/10.1016/j.ydbio.2005.03.002

Maloof, J. N., & Kenyon, C. (1998). The Hox gene lin-39 is required during C. elegans vulval induction to select the outcome of Ras signaling. *Development (Cambridge, England)*, *125*(2), 181–190.

Martin, S., Nishimune, A., Mellor, J. R., & Henley, J. M. (2007). SUMOylation regulates kainate-receptor-mediated synaptic transmission. *Nature*, *447*(7142), 321–325. http://doi.org/10.1038/nature05736

Mohler, W. A., Simske, J. S., Williams-Masson, E. M., Hardin, J. D., & White, J. G. (1998). Dynamics and ultrastructure of developmental cell fusions in the Caenorhabditis elegans

hypodermis. *Current Biology : CB*, *8*(19), 1087–1090. http://doi.org/10.1016/S0960-9822(98)70447-6

Myers, T. R., & Greenwald, I. (2005). lin-35 Rb acts in the major hypodermis to oppose Ras-mediated vulval induction in C. elegans. *Developmental Cell*, *8*(1), 117–123. http://doi.org/10.1016/j.devcel.2004.11.015

Myers, T. R., & Greenwald, I. (2007). Wnt signal from multiple tissues and lin-3/EGF signal from the gonad maintain vulval precursor cell competence in Caenorhabditis elegans. *Proceedings of the National Academy of Sciences of the United States of America*, *104*(51), 20368–20373. http://doi.org/10.1073/pnas.0709989104

Nukazuka, A., Fujisawa, H., Inada, T., Oda, Y., & Takagi, S. (2008). Semaphorin controls epidermal morphogenesis by stimulating mRNA translation via eIF2alpha in Caenorhabditis elegans. *Genes & Development*, *22*(8), 1025–36. http://doi.org/10.1101/gad.1644008

Parker, K. L., Rice, D. A., Lala, D. S., Ikeda, Y., Luo, X., Wong, M., … Schimmer, B. P. (2002). Steroidogenic factor 1: an essential mediator of endocrine development. *Recent Progress in Hormone Research*, *57*, 19–36. http://doi.org/10.1210/rp.57.1.19

Pellegrino, M. W., Farooqui, S., Frohli, E., Rehrauer, H., Kaeser-Pebernard, S., Muller, F., … Hajnal, A. (2011). LIN-39 and the EGFR/RAS/MAPK pathway regulate C. elegans vulval morphogenesis via the VAB-23 zinc finger protein. *Development*. http://doi.org/10.1242/dev.071951

Pettitt, J., Wood, W. B., & Plasterk, R. H. (1996). cdh-3, a gene encoding a member of the cadherin superfamily, functions in epithelial cell morphogenesis in Caenorhabditis elegans. *Development (Cambridge, England)*, *122*(12), 4149–4157.

Piper, M., Anderson, R., Dwivedy, A., & Weinl, C. (2006). Signaling mechanisms underlying Slit2-induced collapse of Xenopus retinal growth cones. *Neuron*. Retrieved from http://www.sciencedirect.com/science/article/pii/S0896627305010548

Poulin, G., Dong, Y., Fraser, A. G., Hopper, N. A., & Ahringer, J. (2005). Chromatin regulation and sumoylation in the inhibition of Ras-induced vulval development in Caenorhabditis elegans. *The EMBO Journal*, *24*(14), 2613–23. http://doi.org/10.1038/sj.emboj.7600726

Raj, A., van den Bogaard, P., Rifkin, S. A., van Oudenaarden, A., & Tyagi, S. (2008). Imaging individual mRNA molecules using multiple singly labeled probes. *Nature Methods*, *5*(10), 877–879. http://doi.org/10.1038/nmeth.1253

Ririe, T. O., Fernandes, J. S., & Sternberg, P. W. (2008). The Caenorhabditis elegans vulva: a post-embryonic gene regulatory network controlling organogenesis. *Proceedings of the National Academy of Sciences of the United States of America*, *105*(51), 20095–20099. http://doi.org/10.1073/pnas.0806377105

Saffer, A. M., Kim, D. H., van Oudenaarden, A., & Horvitz, H. R. (2011). The caenorhabditis elegans synthetic multivulva genes prevent ras pathway activation by tightly repressing global ectopic expression of lin-3 EGF. *PLoS Genetics*, *7*(12). http://doi.org/10.1371/journal.pgen.1002418

Schindler, A. J., & Sherwood, D. R. (2013). Morphogenesis of the C. elegans vulva. *Wiley Interdiscip Rev Dev Biol*, *2*(1), 75–95. http://doi.org/10.1002/wdev.87

Schindler, A. J., & Sherwood, D. R. (2013). Morphogenesis of the Caenorhabditis elegans vulva. *Wiley Interdisciplinary Reviews: Developmental Biology*. http://doi.org/10.1002/wdev.87

Seetharaman, A., Cumbo, P., Bojanala, N., & Gupta, B. P. (2010). Conserved mechanism of Wnt signaling function in the specification of vulval precursor fates in C. elegans and C. briggsae. *Developmental Biology*, *346*(1), 128–39. http://doi.org/10.1016/j.ydbio.2010.07.003

Sharma-Kishore, R., White, J. G., Southgate, E., & Podbilewicz, B. (1999). Formation of the vulva in Caenorhabditis elegans: a paradigm for organogenesis. *Development (Cambridge, England)*, *126*(4), 691–699.

Shemer, G., Kishore, R., & Podbilewicz, B. (2000). Ring formation drives invagination of the vulva in Caenorhabditis elegans: Ras, cell fusion, and cell migration determine structural fates. *Developmental Biology*, *221*(1), 233–248. http://doi.org/10.1006/dbio.2000.9657

Shemer, G., & Podbilewicz, B. (2002). LIN-39/Hox triggers cell division and represses EFF-1/fusogen-dependent vulval cell fusion. *Genes and Development*, *16*(24), 3136–3141. http://doi.org/10.1101/gad.251202

Silhánková, M., Jindra, M., & Asahina, M. (2005). Nuclear receptor NHR-25 is required for cell-shape dynamics during epidermal differentiation in Caenorhabditis elegans. *Journal of Cell Science*, *118*(Pt 1), 223–232. http://doi.org/10.1242/jcs.01609

Sternberg, P. W. (2005). Vulval development. *WormBook : The Online Review of C. Elegans Biology*, 1–28. http://doi.org/10.1895/wormbook.1.6.1

Sulston and Horvitz. (1977). Post-embryonic cell lineages of the nematode, C. elegans. *Developmental Biology*, *56*, 110–156.

Sulston, J. E., & Horvitz, H. R. (1981). Abnormal cell lineages in mutants of the nematode Caenorhabditis elegans. *Developmental Biology*, *82*(1), 41–55. http://doi.org/10.1016/0012-1606(81)90427-9

Sulston, J. E., & White, J. G. (1980). Regulation and cell autonomy during postembryonic development of Caenorhabditis elegans. *Developmental Biology*, *78*(2), 577–97.

Sundaram, M. V. (2005). The love-hate relationship between Ras and Notch. *Genes & Development*, *19*(16), 1825–39. http://doi.org/10.1101/gad.1330605

Tapon, N., & Hall, A. (1997). Rho, Rac and Cdc42 GTPases regulate the organization of the actin cytoskeleton. *Current Opinion in Cell Biology*. http://doi.org/10.1016/S0955-0674(97)80156-1

Timmons, L., Court, D. L., & Fire, A. (2001). Ingestion of bacterially expressed dsRNAs can produce specific and potent genetic interference in Caenorhabditis elegans. *Gene*, *263*(1-2), 103–112. http://doi.org/10.1016/S0378-1119(00)00579-5

Ueda, H., Sonoda, S., Lesley Brown, J., Scott, M. P., & Wu, C. (1990). A sequence-specific DNA-binding protein that activates fushi tarazu segmentation gene expression. *Genes and Development*, *4*(4), 624–635. http://doi.org/10.1101/gad.4.4.624

Wagmaister, J. A., Gleason, J. E., & Eisenmann, D. M. (2006). Transcriptional upregulation of the C. elegans Hox gene lin-39 during vulval cell fate specification. *Mechanisms of Development*, *123*(2), 135–150. http://doi.org/10.1016/j.mod.2005.11.003

Wang, M., & Sternberg, P. W. (2000). Patterning of the C. elegans 1 degrees vulval lineage by RAS and Wnt pathways. *Development (Cambridge, England)*, *127*(23), 5047–58.

Wu, K. Y., Hengst, U., Cox, L. J., Macosko, E. Z., Jeromin, A., Urquhart, E. R., & Jaffrey, S. R. (2005). Local translation of RhoA regulates growth cone collapse. *Nature*, *436*(7053), 1020–4. http://doi.org/10.1038/nature03885

Vladar, E. K., Antic, D., & Axelrod, J. D. (2009). Planar cell polarity signaling: the developing cell's compass. *Cold Spring Harbor Perspectives in Biology*, *1*(3), a002964. http://doi.org/10.1101/cshperspect.a002964

Yoo, A. S., & Greenwald, I. (2005). LIN-12/Notch activation leads to microRNA-mediated down-regulation of Vav in C. elegans. *Science (New York, N.Y.)*, *310*(5752), 1330–1333. http://doi.org/10.1126/science.1119481

Yu, Y., Li, W., Su, K., Yussa, M., Han, W., Perrimon, N., & Pick, L. (1997). The nuclear hormone receptor Ftz-F1 is a cofactor for the Drosophila homeodomain protein Ftz. *Nature*, *385*(6616), 552–555. http://doi.org/10.1038/385552a0

Supplemental articles

During the course of my Ph.D studies, I also contributed significantly to the following research article through collaboration with Dr. Bhagwati Gupta, McMaster University, Canada.

1) Devika Sharanya, Bavithra Thillainathan, Sujatha Marri, **Nagagireesh Bojanala**, Stephane Flibotte, Donald G. Moerman, Robert H. Waterston, and Bhagwati P Gupta. *Genetic* Control of *Vulval Development* in Caenorhabditis *briggsae*. G3(Bethesda) 2012. (Co-author).

2) **S**eetharaman A., Cumbo P., **Bojanala N.,** Gupta B.P. (2010). *Conserved mechanism of Wnt signaling function in the specification of vulval precursor fates in C. elegans* and *C. briggsae*. *Developmental Biology* **346**: 128–139. (Second author).

Genetic Control of Vulval Development in *Caenorhabditis briggsae*

Devika Sharanya,* Bavithra Thillainathan,* Sujatha Marri,* Nagagireesh Bojanala,*,[1] Jon Taylor,[†] Stephane Flibotte,[†] Donald G. Moerman,[†,‡] Robert H. Waterston,[§] and Bhagwati P. Gupta*,[2]

*Department of Biology, McMaster University, Hamilton, Ontario L8S 4K1, Canada, [†]Michael Smith Laboratories and [‡]Department of Zoology, University of British Columbia, Vancouver, British Columbia V6T 1Z4, Canada, and [§]Department of Genome Sciences, University of Washington, Seattle, Washington 98195-5065

ABSTRACT The nematode *Caenorhabditis briggsae* is an excellent model organism for the comparative analysis of gene function and developmental mechanisms. To study the evolutionary conservation and divergence of genetic pathways mediating vulva formation, we screened for mutations in *C. briggsae* that cause the egg-laying defective (Egl) phenotype. Here, we report the characterization of 13 genes, including three that are orthologs of *Caenorhabditis elegans unc-84* (SUN domain), *lin-39* (*Dfd/Scr*-related homeobox), and *lin-11* (LIM homeobox). Based on the morphology and cell fate changes, the mutants were placed into four different categories. Class 1 animals have normal-looking vulva and vulva-uterine connections, indicating defects in other components of the egg-laying system. Class 2 animals frequently lack some or all of the vulval precursor cells (VPCs) due to defects in the migration of P-cell nuclei into the ventral hypodermal region. Class 3 animals show inappropriate fusion of VPCs to the hypodermal syncytium, leading to a reduced number of vulval progeny. Finally, class 4 animals exhibit abnormal vulval invagination and morphology. Interestingly, we did not find mutations that affect VPC induction and fates. Our work is the first study involving the characterization of genes in *C. briggsae* vulva formation, and it offers a basis for future investigations of these genes in *C. elegans*.

KEYWORDS
C. briggsae
C. elegans
vulva
development
cell proliferation
differentiation
morphogenesis
egg-laying
defective

Invertebrate model organisms such as the nematode *Caenorhabditis elegans* are excellent model organisms for investigating the genetic basis of development. Studies in *C. elegans* have provided insights into the cellular and molecular basis of organ formation and have revealed similarities and differences in the formation of homologous structures in metazoans.

Nematodes are an attractive system for studying the evolution of developmental mechanisms because they offer many useful features, including rapid development, transparency, and large brood size. Comparative studies in nematodes have revealed similarities and differences in the vulva, the egg-laying organ. For example, the vulval precursor cell (VPC) equivalence group in *Oschieus tipulae* and *Pristionchus pacificus* is smaller than that of *C. elegans* (Sommer 2005; Sternberg 2005). Furthermore, in *Pristionchus*, the mechanism of restricting vulval precursor competence is different. Although cell fusion limits precursor competence in *C. elegans*, programmed cell death controls this process in *P. pacificus* (Sommer 2005). In addition to these two species, vulval morphology has been examined in a large number of other nematodes, and differences have been found in the number of vulval progeny and the placement of the vulva (Felix *et al.* 2000; Felix and Sternberg 1997; Sommer *et al.* 1994; Sommer and Sternberg 1996). More recently, Kiontke *et al.* (Kiontke *et al.* 2007) examined 51 rhabditid species and identified variations in different steps of vulva development. In the *Caenorhabditis* genus, *Caenorhabditis briggsae* is an excellent model for comparative and evolutionary studies (Gupta *et al.* 2007). Sequence analyses of *C. elegans* and *C. briggsae* have suggested a divergence of approximately 30 million years (Cutter 2008). Morphologically, *C. briggsae* is almost identical to *C. elegans*; however, sequence comparison has revealed that almost one-third of all predicted genes in its genome are highly divergent (Gupta

Copyright © 2012 Sharanya *et al.*
doi: 10.1534/g3.112.004598
Manuscript received May 31, 2012; accepted for publication October 19, 2012
This is an open-access article distributed under the terms of the Creative Commons Attribution Unported License (http://creativecommons.org/licenses/by/3.0/), which permits unrestricted use, distribution, and reproduction in any medium, provided the original work is properly cited.
Supporting information is available online at http://www.g3journal.org/lookup/suppl/doi:10.1534/g3.112.004598/-/DC1.
[1]Present address: Biology Center, ASCR, Institute of Parasitology, Budweis, Czech Republic, 37005.
[2]Corresponding author: Department of Biology, McMaster University, Hamilton, ON L8S 4K1, Canada. E-mail: guptab@mcmaster.ca

and Sternberg 2003; Stein *et al.* 2003). Both organisms offer powerful tools for dissecting gene function, including rapid development, invariant cell lineages, fully sequenced genomes, and amenability to both genetic and molecular manipulation (Antoshechkin and Sternberg 2007; Gupta *et al.* 2007; Hillier *et al.* 2007; Stein *et al.* 2003; Zhao *et al.* 2010). The hermaphroditic mode of reproduction of these species is another advantage because it allows for the maintenance of mutations that affect mating and egg laying. Organisms with divergent genomes but overall morphological similarity may offer intriguing examples of how networks of genes can be regulated differently while yielding the same ultimate structure.

Comparative studies of *C. elegans* and *C. briggsae* have revealed that alterations in developmental mechanisms do not always affect morphology. For example, the expression pattern of *lin-39*, an important Hox family member (*Dfd/Scr*-related) that regulates VPC competence, differs between the two species, yet VPC induction and cell fates are conserved (Penigault and Felix 2011a). The role of the Wnt pathway effector *pop-1* (TCF/LEF family) in *C. briggsae* endomesoderm specification represents yet another case of altered gene function with no obvious change in embryonic cell divisions or tissue morphology (Lin *et al.* 2009). In another case, knockdown of the *lin-12/Notch* receptor family member *glp-1* causes a multivulva (Muv) phenotype in *C. briggsae* but not in *C. elegans* (Rudel and Kimble 2001). Thus, *glp-1* appears to have acquired a new function in negative regulation of VPC fate specification in *C. briggsae*. Such alterations in gene function without apparent changes in homologous characters were described originally as developmental system drift (DSD) (True and Haag 2001).

The egg-laying system of *C. briggsae* is well suited for comparative analysis of gene function in organ formation, and it is helpful in elucidating DSD. Morphologically, the system is identical to *C. elegans* and follows a similar sequence of developmental events. Several of the vulval characters, such as cell number, position in the midbody region, and cell fusions are shared between these two species. However, some differences also have been noted. For example, the division frequency of the P3.p vulval precursor is higher in *C. elegans* than in *C. briggsae* (Delattre and Felix 2001). Other differences that have been found include the role of anchor cell (AC) in the vulval induction process, uterine seam (utse) cell morphology, brood size, sheath-contraction rate, and reproductive efficiency (Delattre and Felix 2001; Felix 2007; Gupta and Sternberg 2003; Miller *et al.* 2004). Subtle variations in VPC responses to inductive and lateral signaling cascades also have been reported (Felix 2007; Hoyos *et al.* 2011). Thus, there are some distinct differences in the mechanisms of vulva formation and egg-laying between *C. elegans* and *C. briggsae*.

In *C. elegans*, the egg-laying system is composed of five different cell types, namely, the vulva, somatic gonad (uterus), vulva and uterine muscles, and neurons (Li and Chalfie 1990). The vulva is connected to the uterus via a multinucleated utse cell (Newman and Sternberg 1996) and serves as a passageway for egg laying. Defects in any of the egg-laying components can cause eggs to accumulate in the uterus, resulting in an Egg-laying defective (Egl) phenotype. The *C. elegans* vulva is formed by the descendants of three of six equipotent VPCs. The VPCs are the posterior daughters of P cells. At hatching, the L1 larva contains six bilaterally symmetrical pairs of P cells in the ventrolateral region. By the mid-L1 stage, P cells migrate into the ventral cord region and become arranged in a single row (numbered P1 to P12) (Sulston 1976 and Sulston and White 1980). This process involves an orchestrated series of events initiated by the directed migration of P-cell nuclei. As a nucleus migrates, it drags the rest of the cell body along with it. Several genes have been identified that affect P-cell nuclear migration, including UNC-83 (KASH domain) and UNC-84 [SUN domain (Starr 2011)]. These two proteins are localized to the outer and inner nuclear membranes, respectively (McGee *et al.* 2006), and they bridge the nuclear envelope and facilitate nuclear migration by transferring forces from the cytoskeleton to the nuclear lamina.

Soon after arriving at the ventral cord region, all 12 P cells divide once along the anteroposterior axis. Of the posterior daughters, five (P1.p, P2.p, P(9-11).p) fuse with the hyp7 syncytium during the L1 stage. P12.p produces two daughters: P12.pp, which undergoes programmed cell death, and P12.pa, which adopts a unique epidermal fate, hyp10. The remaining 6 Pn.p cells (n = 3 to 8, VPCs) remain unfused in L1 due to the action of the Hox gene *lin-39*. These VPCs respond to later developmental cues. P3.p loses competence in the L2 stage in roughly half of animals and fuses with hyp7 (termed 'F' fate).

Although all six VPCs are equally capable of giving rise to vulval tissue, only P5.p, P6.p, and P7.p do so in wild-type animals. This is due to the action of three evolutionarily conserved signal transduction pathways mediated by LET-60/Ras-MPK-1/MAPK (inductive signaling), LIN-12/Notch (lateral signaling), and Wnt-BAR-1/β-catenin (Eisenmann 2005; Greenwald 2005; Sternberg 2005). In the L3 stage, the gonadal AC secretes the ligand LIN-3/EGF that binds to LET-23/EGFR on VPCs, leading to the activation of LET-60/Ras signaling in P6.p and to a lesser extent in P5.p and P7.p. Induced P6.p serves as a source of lateral signal that activates the LIN-12/Notch receptor in P5.p and P7.p. The inductive and lateral signaling together specify 1° (P6.p) and 2° (P5.p and P7.p) cell fates. In addition, Wnt signaling also participates in this process (Gleason *et al.* 2006; Seetharaman *et al.* 2010). The remaining uninduced VPCs fuse with hyp7 after one cell division (termed 3° fate).

Forward genetics is an elegant method by which to study vulva formation in *C. briggsae* and to compare its developmental mechanisms with *C. elegans*. We have isolated mutations in *C. briggsae* AF16 by using the Egl phenotype as an assay. In this study, we describe 19 mutants, 17 of which fall into four phenotypic categories and represent 13 different genes. Class 1 mutants exhibit the Egl phenotype with normal vulval cells and morphology. Class 2 mutants lack some or all of the Pn.p cells in the ventral hypodermal region, suggesting that these genes play important roles in maintaining the correct number of P cells in the ventral hypodermal region. Class 3 mutants have a normal number of VPCs, but some precursor cells fail to be induced. Class 4 mutants affect the differentiation of vulval progeny and lead to abnormal vulval morphology in L4 larvae and a protruding vulva (Pvl) phenotype in adults. We also provide evidence that three of the genes recovered in our screen, *Cbr-lin(sy5506)* (class 2), *Cbr-lin(bh20)* (class 3), and *Cbr-lin(sy5336)* (class 4), are orthologs of *C. elegans unc-84*, *lin-39*, and *lin-11*, respectively.

The mutants and phenotypic classes described here serve as the nucleus of our effort to investigate the genes involved in vulva formation in *C. briggsae*. In addition, they provide a tool for identifying interacting genes through enhancer and suppressor screens. These findings will facilitate the comparison of cellular and molecular processes between *C. briggsae* and *C. elegans* in studying conservation and divergence in developmental mechanisms.

MATERIALS AND METHODS

Strains and culture conditions

Wild-type *C. briggsae* AF16 was used as a reference strain in all experiments. Strains were maintained at 20° using culture methods described for *C. elegans* (Brenner 1974; Wood 1988). To obtain synchronized

animals, gravid hermaphrodites were bleached. The bleach solution was prepared using sodium hypochlorite (commercial bleach) and 4 N sodium hydroxide (NaOH) at a ratio of 3:2. For 2 volumes of worms washed with M9 buffer, 1 volume of the bleach solution was added. The solution was vortexed and left to stand for 3 min at room temperature. After three consecutive washes with M9 solution, a pellet with 1 mL of remaining M9 buffer was transferred to an Eppendorf tube and placed in a shaker. Twenty-four hours later, the F1 worms were plated onto a new NG plate.

The strains used in this study are listed below (linkage groups of mapping markers are also mentioned; see www.briggsae.org for details). The *egl(bh6)* strain [allelic to *egl(bh2)*] was lost during the course of this study. The 'Cbr' prefix denotes the *C. briggae* orthologs of known *C. elegans* genes.

Mapping mutants: *dpy(sy5148) II*, *dpy(sy5022) III*, *sma(sy5330) I*, *unc(s1270) IV*, *unc(sa997) V*, *unc(sy5077) X*.

Egl and Vul mutants: *egl(bh2)*, *egl(bh6)*, *egl(bh21)*, *egl(sy5395)*, *lin(bh7)*, *lin(bh13)*, *lin(bh14)*, *lin(bh20)*, *lin(bh23)*, *lin(bh25)*, *lin(bh26)*, *lin(sy5197)*, *lin(sy5212)*, *lin(sy5336)*, *lin(sy5368)*, *lin(sy5425)*, *lin(sy5426)*, *unc(sy5505)*, *unc(sy5506)*.

Transgenic strains: *bhEx31[pRH51(hs::lin-3) + myo-2::GFP]*, *bhEx78 [pGF50(lin-11) + myo-2::GFP]*, *bhEx117[mec-7::GFP + myo-2::GFP]*, *bhEx123[C07H6 + myo-2::GFP]*, *bhEx124[C07H6 + myo-2::GFP]*, *bhEx132[F44F12 + myo-2::GFP]*, *bhEx134[F44F12 + myo-2::GFP]*, *bhEx139[pSL38(unc-84) + myo-2::GFP]*, *bhEx141 [pSL38(unc-84) + myo-2::GFP]*, *bhEx142[pSL38(unc-84) + myo-2::GFP]*, *bhEx148[pGF50(lin-11) + myo-2::GFP]*, *bhEx152[pSL38 (unc-84) + myo-2::GFP]*; *mfIs5[Cbr-egl-17::GFP + myo-2::GFP]*, *mfIs8[Cbr-zmp-1::GFP + myo-2::GFP]*.

mfIs5 and *mfIs8* animals carry a *gfp* reporter driven by the vulva-specific enhancers of *Cbr-egl-17* (748 bp) and *Cbr-zmp-1* (755 bp), respectively (Kirouac and Sternberg 2003). *bhEx117* is a transgenic HK104 line that was used in polymorphism-based mapping experiments (see below).

Mutagenesis

AF16 animals were mutagenized by soaking in 25 mM ethyl methane sulfonate (EMS) and screening for Egl and Pvl mutants in the F2 generation. To prevent worms from burrowing into the agar, we used 9-cm NG-Agarose plates (1 L of media containing 3 g of sodium chloride, 2.5 g of bacteriological peptone, and 17 g of agarose; the other components were the same as nematode growth medium). Mutagenized worms were individually transferred onto plates, and the F2 progeny were screened for Egl worms. Such animals formed the characteristic "bag of worms" phenotype as a result of the progeny hatching inside the uterus and devouring the mother (Horvitz and Sulston 1980).

From four independent F2 screens (in the range of 100,000-125,000 haploid genome sets in total), we recovered 39 independent Egl clones that bred true. An additional 34 Egl clones could not be propagated because they were either sterile or gave rise to dead progeny. Apart from animals with the Egl phenotype, we also recovered dumpy and uncoordinated mutants. One of these, twitcher, was isolated from at least three independent plates (B. P. Gupta, unpublished results). In *C. elegans* and *C. briggsae*, the twitcher phenotype is associated with *unc-22*, a gene with more than 20 kb of open reading frame that is readily mutated in EMS screens (Benian *et al.* 1993). All three twitcher mutations are recessive and have been found to be allelic (data not shown), which suggests that our screens were capable of recovering viable recessive mutations with a visible phenotype.

This study focuses on a collection of 19 mutations that reside in 13 genes (see *Results*). Compared with the original *C. elegans* Egl screen (Trent *et al.* 1983), the number of Egl mutants in our case is considerably lower. It is unclear whether this is due to differences in the population of screened worms, as Trent *et al.* did not provide an estimate of the number of worms that were screened. Based on the mapping and complementation experiments, 70% of *C. briggsae* genes (9 of 13) are represented by single mutations (see *Results*). Although this result is indicative of the screen being unsaturated, the proportion of genes defined by a single allele in our case is very similar to that of Trent *et al.* (Trent *et al.* 1983). Furthermore, it is worth pointing out that additional alleles of the existing *C. briggsae* genes may be present among the remaining 20 mutations that have yet to be characterized. This analysis is the focus of our current study.

Similar to *C. elegans* (Ferguson and Horvitz 1985; Trent *et al.* 1983), not all *C. briggsae* mutants described here affect vulva formation, indicating that defects in other egg-laying components (such as neurons and muscles) can also lead to the Egl phenotype. Each mutant was backcrossed at least three times before we performed genetic experiments. All alleles were recessive and caused no obvious maternal effect phenotype.

Microscopy, cell ablations, and VPC fates

Worms were mounted on agar pads as described previously (Wood 1988) and examined under Nomarski optics using Zeiss Axioimager D1 and Nikon Eclipse 80i microscopes. Sodium azide (1 M) was used as an anesthetic. To examine vulval lineages, L3 and L4 stage animals were mounted without any anesthetic, and coverslip edges were sealed with Vaseline to prevent dehydration. For GFP reporter-expressing strains, epifluorescence was visualized with a Zeiss Axioplan microscope equipped with the GFP filter HQ485LP (Chroma Technology), a power source (Optiquip 1500) and a 200 W OSRAM Mercury bulb. Cell ablation experiments were performed as described (Avery and Horvitz 1987).

VPC fates were examined in L3 and L4 stage animals under a Nomarski microscope. If a VPC fused with hyp7 as a single cell without dividing, it was assigned an 'F' (Fused) fate. If the VPC divided once and its daughters (Pn.px, where x denotes both anterior and posterior cells) fused with hyp7, it was assigned a 3° (tertiary) fate. If the VPC was induced to give rise to more than 4 vulval progeny (Pn.pxxx cells), it was considered fully induced and assigned an 'I' (induced) fate [includes 1° and 2° fates as described previously (Sternberg and Horvitz 1986)]. Vulval induction score was calculated as described previously (Gupta *et al.* 2006). In *sy5353* and *sy5353*; *bh20* mutants some of the Pn.p appeared small and morphologically similar to P12.pa (Seetharaman *et al.* 2010). These were termed as "small" cells.

To determine inter-VPC distances in *lin-39* mutants, animals were bleach synchronized. Distances among the 5 VPC pairs (P3.p-P4.p, P4.p-P5.p, P5.p-P6.p, P6.p-P7.p, P7.p-P8.p) were measured in mid-to-late L2 stage animals using Nikon NIS Elements software.

Pharmacological assays

Serotonin and fluoxetine were used to analyze the pharmacological response of some of the Egl mutants. Serotonin (35 mM) and fluoxetine (1 mg/mL) solutions were freshly prepared in M9 buffer. The assay was performed in 96-well microtiter dishes using 50 μL of drug in individual wells. As a control, the same volume of M9 buffer was placed in adjacent wells. L4 animals were picked a day before the assay and allowed to grow for 18-24 hr before placing them individually into drug and M9 containing wells. After incubating worms for 1 hr at

Table 1 Results of complementation experiments

m1/+	*m2/m2*	Animals Showing Phenotype	Phenotype Scored
bh2/+	*bh6*	39% (n = 28)	Egl
bh7/+	*bh14*	0% (n = 60)	Vul
bh7/+	*bh20*	0% (n = 23)	Vul
bh14/+	*bh20*	0% (n = 31)	Vul
sy5197 /+	*bh13*	62% (n = 8)	Sma, vulval invagination abnormal
bh13/+	*bh25*	0% (n = 30)	Egl, Sma, vulval invagination abnormal
sy5336/+	*sy5368*	58% (n = 12)	Egl, vulval invagination abnormal

room temperature, the number of eggs laid by each worm was counted. Assays were repeated at least three times.

Heat shock protocol

L1 animals of the *bhEx31* strain were transferred to standard NG agar plates containing *Escherichia coli* OP50 bacteria and grown for a desired period of time. Plates were sealed with Parafilm M (American National Can) and heat shocked in a water bath. We tested various heat shock conditions by fixing the temperature at 37° and varying the duration of the exposure. Two different types of pulses, *i.e.* a single long pulse (between 0:30 hr and 1:30 hr) and multiple short pulses (either consisting of four 30-min pulses each separated by 1-hr rest period or two 1-hr pulses separated by 1h, *i.e.*, 1-hr-r rest period), were tested. Animals were heat shocked at different time points after transferring L1 worms on bacteria-containing plates. After the initial trials, we chose 37° for 1 hr for all subsequent experiments. After heat shock treatment, animals were shifted back to 20°. Vulval induction and morphology were examined at stage L4.

Egl penetrance assay

L4 animals were placed individually into six-well nematode growth medium–agar plates and observed over a 3-day period. Egl phenotype was classified as Egl (no laid eggs, "bag of worms" appearance), semi-egl (few eggs initially but eventually formed "bag of worms"), and Non-Egl (no defect, phenotypically wild type).

Complementation tests

Complementation tests between two vulval mutants (*m1* and *m2*) were performed by crossing *m1*/+ heterozygote males (obtained by crossing *m1/m1* hermaphrodites to *myo-2::gfp* carrying *mfIs5* or *mfIs8* males) to *m2/m2* hermaphrodites. The presence of the *gfp* transgene allowed us to identify cross progeny. In the F2 generation, vulval phenotype in L4 worms was scored under Nomarski optics. Complementation tests were carried out for mutations belonging to the same phenotypic categories. Table 1 lists all combinations that were tested and the results.

Phenotypic marker-based genetic mapping

We tested the linkage of *lin-11(sy5336)* with several phenotypic markers that were assigned to various chromosomes. The website www.briggsae.org shows a larger list of mapping experiments involving these markers. The *sy5336* mutation was linked to *sma(sy5330)* (Table 2). Together these two genes define a single linkage group that was assigned chromosome 1 based on *sy5336* molecular identity and synteny of the *lin-11* genomic region (http://www.wormbase.org). The *unc(sy5506)* mutation was linked to chromosome X based on the Unc phenotype of F1 males derived from a cross of *sy5506* hermaphrodites to AF16 males.

Insertion-deletion (indel) and snip-SNP-based genetic mapping

All mutations except *lin(bh14)* and *Cbr-lin-11* alleles were mapped to chromosomes by bulk segregant analysis (BSA) using Indels and snip-SNPs (Table 3, Supporting Information, Figure S1). The cross scheme was as follows. Hermaphrodites of a given mutant strain were crossed with either normal or GFP fluorescing *(bhEx117)* HK104 males. F1 cross progeny were picked and cloned. In the next generation (F2), phenotypically mutant and wild-type animals (20 each) were picked separately and processed to obtain genomic DNA. Genomic DNA was prepared by placing worms into 5 to 10 μL of lysis buffer (containing Proteinase K). The solution was incubated at 60° for 1 hr followed by heat inactivation of Proteinase K at 95°. This crude genomic DNA prep was frozen at –20° and used as a template in polymerase chain reaction experiments. The detailed indel mapping protocol and primers have been published previously (Koboldt *et al.* 2010). We reported earlier the single recombinant analysis of *lin(sy5506)* using the indel bhP26. The distance between the two loci was determined to be 10% (Koboldt *et al.* 2010).

SNP chip–based genetic mapping

In addition to the aforementioned polymorphism-based BSA mapping, we used a microarray chip mapping approach to localize the mutations on chromosomes (Table 3). For this, a 12x oligo microarray chip containing approximately 4500 SNPs was designed using methods similar to those for *C. elegans* (Flibotte *et al.* 2009). An earlier version of the *C. briggsae* chip contained almost 9700 SNPs and was successfully used to map mutations (Zhao *et al.* 2010). *C. briggsae* Egl animals were mated with HK104 males, and F1 heterozygotes were cloned. In the F2 generation, 100 mutant worms were picked and allowed to grow on 10 6-cm Petri plates close to starvation. The worms were washed off with M9 buffer. Genomic DNA was extracted using the QIAGEN Blood and Tissue DNeasy kit (cat. no. 69504). DNA hybridization, measurement of fluorescence intensity and ratio analysis were performed as described previously (Flibotte *et al.* 2009; Maydan *et al.* 2007). Based on the mapping signal intensity and the arc of the signal (Figure S2), the approximate chromosomal locations of mutations were determined (Zhao *et al.* 2010). In some cases, such as *sy5505*, arc pattern was not obvious, rendering the analysis less reliable. Overall, the SNP-chip data agreed with seven of the indel and snip-SNP BSA mapping results (Table 3). Independent verification of these results by phenotypic-marker-based classical mapping has not been performed.

Table 2 Linkage mapping of *Cbr-lin-11* using phenotypic markers

Marker	LG	Data
sma(sy5330)	*I*	2/39 Sma were Egl
dpy(sy5148)	*II*	19/29 Egl segregated Dpy
dpy(5022)	*III*	11/18 Egl segregated Dpy
unc(s1270)	*IV*	16/24 Egl segregated Unc
unc(sa997)	*V*	24/32 Unc segregated Egl
unc(sy5077)	*X*	15/32 Unc segregated Egl

Table 3 Linkage mapping of mutations by BSA and SNP-chip techniques

Gene	Allele	Chromosomal Location	
		BSA-Based	SNP Chip-Based
egl(sy5395)	*sy5395*	1: left arm (bhP19)	–
lin(bh7)	*bh7*	1 (cb-m142, cb650)	1: 4.5 Mb
lin(bh13)	*bh13*	1: left arm (bhP42)	1: 4 Mb
lin(bh25)	*bh25*	1[a] (cb650)	–
egl(bh2)	*bh2*	1: center (bhP42)	1: 7.5 Mb
Cbr-lin-11	*sy5336*	–	1: 7.9 Mb[b]
Cbr-lin-39	*bh20*	3: right arm[c] (bhP40)	–
unc(sy5505)	*sy5505*	5: center/right arm (bhP5, cb-m103)	5: 8.5 Mb
lin(sy5425)	*sy5425*	5: center (bhP5)	–
Cbr-unc-84	*sy5506*	X: right arm[c] (bhP26)	–
egl(bh21)	*bh21*	X (bhP25)	X: 11.5 Mb
lin(bh14)	*bh14*	I (bhP1)	–
lin(bh26)	*bh26*	X: right arm (bhP26)	X: 12.5 Mb

Tightly linked indel and snip-SNP markers are shown in brackets. Dashes (–) indicate a lack of map information.
[a] Likely to be located on the left arm.
[b] Previous study (Zhao *et al.* 2010).
[c] Previous study (Koboldt *et al.* 2010).

Molecular biology and transgenics

Transgenic worms were generated by injecting DNA into the syncytial gonad of adult hermaphrodites using *myo-2*::*GFP* (pPD118.33) as a transformation marker (S. Q. Xu, B. Kelly, B. Harfe, M. Montgomery, J. Ahnn, S. Getz, and A. Fire, personal communication). The microinjection technique was described previously (Mello *et al.* 1991).

The pSL38 plasmid, which contained a *C. elegans unc-84* rescuing fragment (McGee *et al.* 2006), was injected at 4 ng/μL in *unc(sy5505)* and *unc(sy5506)* animals. Stable lines (*sy5505*: *bhEx141* and *bhEx142*, *sy5506*: *bhEx139* and *bhEx152*) were analyzed for the rescue of Unc, P cell migration, and Egl phenotypes.

The hs::*lin-3* transgenic animals, *bhEx31*, carry the pRH51 plasmid [50 ng/μL (Katz *et al.* 1995)]. pRH51 contains the EGF domain of *lin-3* along with a synthetic signal peptide. The expression of *lin-3* is under the control of the *hsp16-41* promoter (pPD49.83).

For the rescue of *Cbr-lin-39* mutants, *C. elegans* cosmids C07H6 and F44F12, containing the entire *lin-39* genomic region, were injected into *bh20* animals. Two stable lines were obtained for each cosmid (*bhEx123* and *bhEx124* with C07H6 at 20 ng/μL; *bhEx132* and *bhEx134* with F44F12 at 0.7 ng/μL). VPC induction and Egl phenotypes were analyzed in transgenic animals. A greater proportion of F44F12 stable lines showed rescue of the Egl phenotype compared to C07H6. Therefore, we focused on *bhEx132* and *bhEx134* transgenic animals for all subsequent analyses.

Cbr-lin-11 cDNA was amplified using the ProtoScript first strand kit (NEB, #E6500S). The primers cb-lin-11-up-1 and cb-lin-11-down-2 (Table S1) were used. Whole RNA was prepared from the mixed stage animals using a previously described TRIZOL method (Burdine and Stern 1996). The *C. elegans lin-11*-rescuing plasmid pGF50 (Freyd 1991) was injected at 20 ng/μL. pGF50 contains a 19-kb subclone of cosmid ZK273 that was previously shown to rescue *C. elegans lin-11* mutants (Freyd 1991). Two stable lines (*bhEx78* and *bhEx148*) were generated for pGF50 (20 ng/μL), both of which rescued Egl and vulval invagination defects in *sy5336* animals.

Sequencing

All primer sequences are listed in Table S1. The exons of *Cbr-unc-84* were amplified using primer pairs GL793/GL795, GL800/GL801, GL806/812, and GL809/810. To sequence the intermediate regions, primers GL802, GL807, and GL808 were used. A 403-bp deletion between exons 6 and 7 (genomic location +5006 and +5408) was identified that introduces an in-frame stop codon downstream of the deleted region.

Cbr-lin-39 exons were amplified from *bh20* and *bh23* alleles using primer pairs GL380/GL381, GL382/GL383, GL384/GL385, GL389/GL390, and GL391/GL392. The *bh23* mutation contains a 364-bp deletion overlapping with the 5′ region of the *Cbr-lin-39* coding sequence. The deletion is located between -158 (upstream of the ATG start site) and +207 (in exon 1). The *bh20* allele carries a point mutation in exon 3 (G9427 to A) that corresponds to the homeodomain region.

The *Cbr-lin-11* ORF was amplified in two fragments using primer pairs cb-lin-11-up-1/cb-lin-11-down-7 and cb-lin-11-up-5/cb-lin-11-down-1. Sequencing primers were cb-lin-11-up-1, cb-lin-11-up-4, cb-lin-11-up-6, cb-lin-11-up-7, cb-lin-11-up-8, cb-lin-11-up-9, cb-lin-11-down-1, cb-lin-11-down-5, cb-lin-11-down-7, and cb-lin-11-down-8. Both *lin-11* alleles, *sy5336* and *sy5368*, affect splicing. *sy5336* causes a G to A transition (G4403 to A) in the splicing acceptor site of intron 7 and is likely to disrupt intron 7 splicing. The *sy5368* mutation affects the splicing donor site of intron 6 (G3340 to A) and is predicted to introduce a premature in-frame stop codon 52 nucleotides downstream.

Statistical analysis

Statistical analyses were performed using InStat 2.0 (GraphPad) Software. Two-tailed *P* values were calculated in unpaired *t*-tests, and values less than 0.05 were considered statistically significant.

RESULTS

Overview of the genetic screen

We screened for egg-laying defective (Egl) mutants after EMS mutagenesis of AF16 animals (see *Materials and Methods* for details). Of 39 Egl mutants identified, we report the characterization of 19 mutants. Seventeen of these fell into 13 complementation groups and were placed into four distinct phenotypic categories (Table 4). Of the remaining 2, *lin(sy5212)* and *lin(sy5426)*, *sy5212* is a fully penetrant Vul mutant and could not be outcrossed. In rare circumstances, VPC induction in *sy5212* animals was observed only for P6.p. All other VPCs fused to hyp7 during the L2 and L3 stages. The other mutant, *sy5426*, has variable vulva defects (a combination of missing VPCs, uninduced VPCs, and abnormal morphogenesis) and could not be

Table 4 Overview of *C. briggsae* egg-laying defective mutants

Class	Features	Gene	Alleles	Mutation	Egl Penetrance (%)			
					Non-Egl	Semi-Egl	Egl	n
1	Wild-type vulva	*egl(bh2)*[a]	2	*bh2*	0	69	31	103
		egl(bh21)	1	*bh21*	0	41	59	120
		egl(sy5395)	1	*sy5395*	6	32	62	244
2	Fewer Pn.p cells	*unc(sy5505)*	1	*sy5505*	22	17	61	127
		Cbr-unc-84	1	*sy5506*	56	21	23	100
3	Reduced VPC induction	*lin(bh7)*	1	*bh7*	81	12	7	137
		lin(bh14)	1	*bh14*	39	32	29	133
		Cbr-lin-39	2	*bh20*	0	4	96	140
				bh23	0	0	100	41
4	Abnormal vulval invagination	*Cbr-lin-11*	2	*sy5336*	0	0	100	100
				sy5368	0	0	100	100
		lin(bh13)[#]	2	*bh13*	1	1	98	102
		lin(bh26)	1	*bh26*	0	0	100	100
		lin(bh25)	1	*bh25*	1	23	76	105
		lin(sy5425)	1	*sy5425*	36	25	39	104
–	Unclassified	*lin(sy5212)*	–	*sy5212*	0	0	100	49
		lin(sy5426)	–	*sy5426*	0	0	100	29

Egl, animals did not lay eggs at all; n: number of animals scored; Non-Egl, animals continued to lay eggs throughout their reproductive life; Semi-Egl, animals laid eggs initially but became Egl afterward.
[a] The phenotype of the other allele of this locus was not characterized in detail.

uniquely classified. We used indel-based BSA, snip-SNP, and SNP-chip mapping approaches (Koboldt *et al.* 2010; Zhao *et al.* 2010) to localize the mutations to chromosomes (Table 3).

Class 1 mutants consist of three loci, each of which shows morphologically wild-type vulval development and a vulva-uterine connection (utse). The Egl phenotype of these animals is likely to result from defects in neuronal and/or muscle components of the egg-laying system. Class 2 is composed of two mutants, both of which are uncoordinated and frequently lack VPCs. In some cases, these animals lack a functional vulva and develop an Egl phenotype. Class 3 mutants are represented by three loci, each of which shows reduced VPC induction. The strongest allele in this class, *bh23*, causes a fully penetrant Egl defect. The largest phenotypic category, class 4, is composed of five loci. Mutations belonging to this class do not affect VPC induction but cause abnormal vulval invagination and morphology. The adults frequently have Pvl and Egl phenotypes.

Class 1 mutants have defects in egg-laying components other than the vulva and utse

The examination of vulval phenotype in class 1 mutants revealed that VPCs and their progeny were unaffected. Vulval cells invaginated correctly and gave rise to a morphology characteristic of the wild-type animals. Furthermore, the utse was normal and was located on the top of the vulval apex (data not shown). To examine defects in other components of the egg-laying system, we treated animals with drugs that affect neuronal and muscle activities. In *C. elegans*, hermaphrodite-specific neurons (HSNs) control egg-laying behavior (Croll 1975; Horvitz *et al.* 1982; Weinshenker *et al.* 1995). In response to external cues, such as food, HSNs release serotonin (*i.e.*, 5-hydroxytryptamine or 5-HT) into the neuromuscular synapse, which then acts on the postsynaptic receptors in the vulval muscle to stimulate the release of eggs. Authors investigating the role of HSNs have used serotonin and fluoxetine [a serotonin reuptake inhibitor that increases the amount of neurotransmitter available to post-synaptic receptors (Baldessarini 1996; Dempsey *et al.* 2005)] to characterize the neuronal basis of the Egl phenotype. Serotonin and fluoxetine drug assays can distinguish between pre- and postsynaptic defects (*i.e.*, between HSN and vulva muscle). Mutants resistant to fluoxetine that lay eggs in the presence of exogenous serotonin are likely to have abnormal HSNs, whereas resistance to both drugs suggests a postsynaptic signaling defect. We found that *egl(sy5395)* animals, when exposed to serotonin, had a modest but consistent increase in the number of eggs laid compared with the control, but *egl(bh21)* and *egl(bh2)* were unaffected (Figure 1). Fluoxetine exposure had no obvious effect on any of the strains. These results suggest that the Egl phenotype in *sy5395* animals may be caused by abnormal differentiation of HSNs. In the case of *bh21* and *bh2* mutants, the cellular basis of the Egl phenotype remains to be identified.

Class 2 mutants have defects in nuclear migration and include *Cbr-unc-84*

The class 2 mutants *unc(sy5505)* and *unc(sy5506)* have fewer and more variable numbers of P cells in the ventral hypodermal region. Animals homozygous for either of these mutations move in a slow and uncoordinated manner. Microscopic observations revealed fewer than 12 P-cell nuclei in the ventral hypodermal region (Figure 2A). This phenotype was temperature sensitive, such that the loss of P cells was greater at higher temperatures (Figure 2A and data not shown). Nearly two-thirds of the animals had an Egl phenotype due to the absence of some or all of the P(5-7).p VPCs (Tables 4 and 5, Figure 3A). We also observed a hyp7 nuclear migration defect in the *sy5506* strain. Unlike wild-type animals where no hyp7 nuclei are observed in the dorsal hypodermis, *sy5506* worms had many hyp7 nuclei in this region (Figure 2, B and C).

In *C. elegans*, similar phenotypes are caused by mutations in two genes, *unc-83* (KASH domain) and *unc-84* (SUN domain), which affect nuclear migration during development (Malone *et al.* 1999; Starr *et al.* 2001; Sulston and Horvitz 1981). One of these, *unc-84*, is located on the right arm of chromosome X. We found that *sy5506* also maps to the right arm of chromosome X close to the bhP27 polymorphism (see *Materials and Methods*), a region that contains *Cbr-unc-84*/*CBG07416* and is syntenic to *unc-84*.

To further confirm that *unc(sy5506)* defines the *Cbr-unc-84* gene, we generated transgenic *sy5506* animals carrying an *unc-84* rescuing

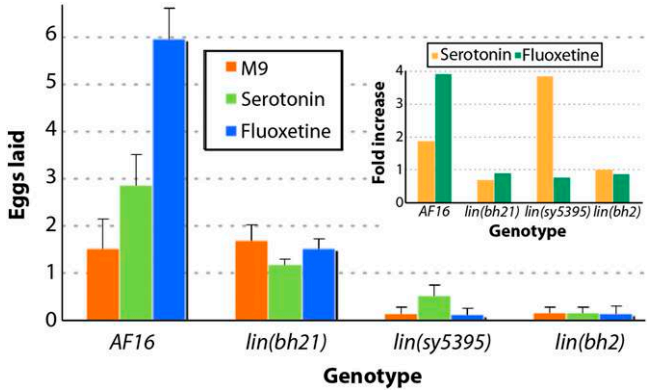

Figure 1 Egg-laying responses of class 1 mutants. The graph shows the average number of eggs laid by animals in M9 buffer (control) and serotonin and fluoxetine drug–containing solutions. The fold increase in egg laying in drug solution (over M9 buffer control) is plotted in the inset graph.

plasmid called pSL38 (McGee *et al.* 2006). The transgenic animals showed rescue of the hyp7 and P-cell nuclear migration defects (51% *bhEx139* animals with normal hyp7 nuclear migration, n = 35, and 90% P nuclei present in ventral cord, n = 91, at 20°, compared with 100% abnormal hyp7 nuclear migration and 42% P-cell nuclei, n = 23, in *sy5506*). The Egl and VPC induction defects in mutants also were rescued (69% of *bhEx139* animals laying eggs, n = 94, compared with 56% in *sy5506*, n = 100; see Table 5 for VPC induction).

Finally, we sequenced the *Cbr-unc-84* genomic region in *unc (sy5506)* animals and identified a 403-bp deletion covering parts of exons 6 and 7 (Figure 2D, also see *Materials and Methods*). These results demonstrate that *sy5506* is an allele of *Cbr-unc-84*. In *C. elegans*, UNC-84 protein contains a SUN domain, a transmembrane domain and an intervening linker region (Malone *et al.* 1999; McGee *et al.* 2006). Based on the sequence alignment, the *sy5506* mutation is located in the linker region of Cbr-UNC-84. In *C. elegans*, this region interacts with UNC-83 to facilitate localization of other cytoskeletal components that are crucial for nuclear positioning in hyp7 and P cells.

The phenotype of *sy5505* animals differs from *Cbr-unc-84(sy5506)* in two respects. First, they are more sensitive to increased temperature as evidenced by their inability to grow at 29° (Figure 2A). Second, no hyp7 migration defect was observed in *sy5505* animals (data not shown). We also generated transgenic *sy5505* strains carrying the *unc-84* plasmid pSL38 (*bhEx141* and *bhEx142*) but did not observe rescue of the mutant phenotype (Table 5 and data not shown). These results together with linkage data (Table 3) suggest that *sy5505* is not allelic to *Cbr-unc-84* and is likely a different gene. The phenotype of *sy5505* is similar to mutations in *unc-83* in *C. elegans*; however, the possibility that *sy5505* is an allele of *Cbr-unc-83* has not been tested.

Class 3 mutants exhibit reduced VPC induction

Four mutations define class 3 genes, all of which cause a reduction in the number of vulval progeny (see VPC induction score in Table 5) and abnormal invagination (Figure 3). In these animals, some or all P (3-8).p fail to divide and fuse with surrounding hypodermis ('F' fate; Table 5). The phenotype is weakest in *lin(bh7)* (only one VPC uninduced; Figure 3B) but fully penetrant in *lin(bh23)* (all VPCs uninduced; Figure 3E). The other two alleles, *lin(bh14)* and *lin(bh20)*, are intermediate (Figure 3, C and D), with *bh20* being somewhat more severe as determined by fewer cases of P6.p induction (15%; see Table 5) and rudimentary vulval invagination. This observation agrees well with the vulval induction score, cell lineage, and Egl penetrance of the animals (Tables 4, 5, and 6). The *bh20* and *bh23* mutations also cause abnormal folding of gonad arms and subtle uncoordinated phenotypes (data not shown).

Next, we examined the VPC induction defect in some detail. As the defect in *bh7*, *bh14*, and *bh20* animals is predominantly limited to 2° precursors (P5.p and P7.p), we wanted to determine whether these two VPCs lack the potential to respond to an external signal and are

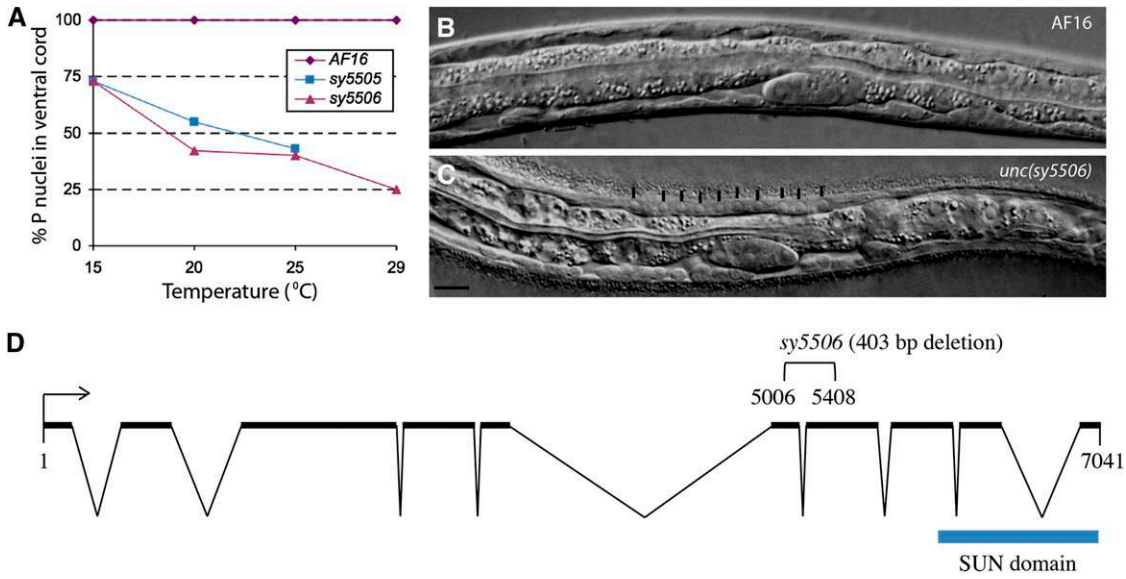

Figure 2 Nuclear migration defects in class 2 mutants and molecular analysis of *Cbr-unc-84*. (A) P-cell nuclei in the ventral cord region of mutants vary with temperature. At greater temperatures, fewer nuclei are visible. *sy5505* animals are very sick at 29° and could not be examined. Each data point consists of 25 or more animals. (B, C) Wild-type AF16 and *sy5506* L1 stage animals, respectively. The hyp7 nuclei in the *sy5506* animals fail to migrate and are located in the dorsal region (marked with vertical lines). Scale bar is 10 μm. (D) Open reading frame of *Cbr-unc-84*. *sy5506* causes a 403-bp deletion.

Table 5 Vulval induction pattern in Class 2 and 3 mutants

Class	Genotype	VPC Induction Score	% VPC Fate Pattern (F/3°/I)						n
			P3.p	P4.p	P5.p	P6.p	P7.p	P8.p	
	AF16	3	61/39/0	0/100/0	0/0/100	0/0/100	0/0/100	0/100/0	101
2	*unc(sy5505)*	1.7 ± 1.3	39/4/0	0/35/0	0/0/50	0/0/75	0/0/48	2/37/0	52
	sy5505; bhEx141	1.2 ± 1.2	25/2/00	8/8/00	0/0/31	0/0/62	0/0/31	4/13/0	52
	sy5505; bhEx142	1.4 ± 1.1	24/4/0	2/18/0	0/0/38	0/0/62	0/0/38	4/11/0	45
	Cbr-unc-84(sy5506)	1.9 ± 1.2	31/14/0	10/18/0	0/0/53	0/0/82	0/0/51	14/25/0	51
	sy5506; bhEx139	2.9 ± 0.4[a]	54/30/0	0/86/0	0/0/96	0/0/100	0/0/94	0/93/0	91
	sy5506; bhEx152	2.9 ± 0.4[a]	57/31/0	2/90/0	0/0/94	0/0/100	0/0/96	0/94/0	51
3	*lin(bh7)*	2.3 ± 1	77/23/0	54/46/0	28/4/68	5/0/95	32/2/66	43/57/0	56
	lin(bh14)	2.3 ± 1	91/9/0	71/29/0	35/0/65	1/0/99	33/0/67	65/35/0	78
	Cbr-lin-39(bh20)	0.2 ± 0.4	100/0/0	100/0/0	100/0/0	85/0/15	100/0/0	100/0/0	155
	bh20; bhEx134	1 ± 0.9[a]	100/0/0	97/3/0	93/0/7	40/0/60	71/0/29	99/1/0	88
	bh20; bhEx132	0.5 ± 0.5[a]	100/0/0	100/0/0	99/0/1	54/0/46	100/0/0	100/0/0	81
	Cbr-lin-39(bh23)	0	96/4/0	96/4/0	88/12/0	96/4/0	96/4/0	100/0/0	50

VPC fates are classified into three categories: F, fused with hyp7 without division, 3°, fused with hyp7 after one cell division, I, induced (either 1°, 2°, or a hybrid fate that could not be uniquely classified). See *Materials and Methods* for details. For *sy5505* and *sy5506* animals missing VPCs were excluded from the analysis. VPC, vulval precursor cells.

[a] VPC induction is significantly higher compared to the parental strain, $P < 0.0001$.

unable to adopt an induced fate. In *C. elegans*, AC is necessary for VPC induction because it secretes LIN-3/EGF ligand that activates the LET-23/EGFR-LET-60/RAS-MPK-1/MAPK pathway in VPCs (Hill and Sternberg 1992; Kimble 1981). To this end, we ablated the central VPC, *i.e.*, P6.p, during the L2 stage and examined the fates of the remaining VPCs. We predicted that P5.p and P7.p would receive greater levels of AC signal, perhaps triggering VPC induction. In wild-type animals, P6.p ablation causes full induction of P5.p and P7.p, whereas P4.p and P8.p adopt vulval fates in some cases (Table 7). In our experiment, *bh7* animals exhibited an induction pattern similar to AF16. Thus, P5.p and P7.p were induced in all cases (Table 7 compared with intact *bh7* animals in Table 5). The frequencies of induced VPCs were much lower in *bh14* animals (Table 7). In total, five of nine animals had some vulval tissue as a result of P5.p and P7.p induction (P5.p adopted 1° fate in three cases and P7.p in the remaining two). Only one of these animals had induction of both P5.p and P7.p (P5.p 1° and P7.p 2°). The remaining VPCs adopted an 'F' fate. Similar manipulations in *bh20* animals also caused P5.p and P7.p to be induced, albeit rarely (Table 7). Of the 19 cases, 4 had few vulval progeny. In two of these, P5.p appeared to adopt a 1°–like fate (no P7.p induction), whereas the other two had a hybrid 1°/2° lineage. This result is in contrast to intact *bh20* animals in which P5.p and P7.p are never induced (Table 5). Taken together, these results suggest that in the absence of the central P6.p, the neighboring VPCs in these three mutants can be induced by the AC-mediated signal, and they can give rise to vulval tissue.

Overexpression of *lin-3* suppresses the VPC induction defect in a subset of class 3 mutants

In *C. elegans*, LIN-3 signaling plays a role in maintaining the competence of VPCs by preventing their fusion with hyp7 (Myers and Greenwald 2007). This allows unfused VPCs to initiate Ras-MAPK

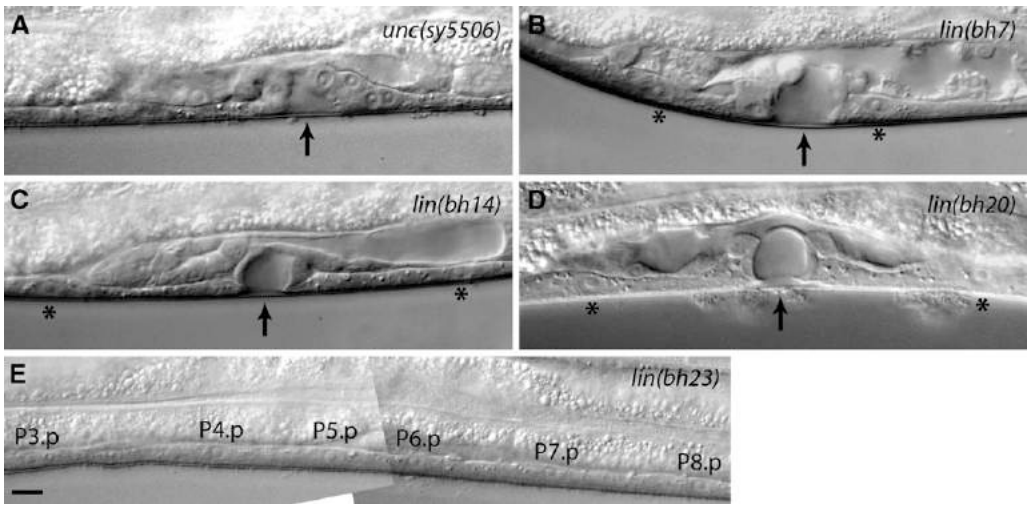

Figure 3 Vulva phenotypes of class 2 and 3 mutants. Arrows point to the center of invagination. Animals were examined at the mid-L4 stage. (A) Fewer VPCs are present in *sy5506* animals due to a defect in P-cell nuclear migration. In this case P6.p and P7.p are induced to form the vulva. P5.p and P8.p are missing. (B) One or more VPCs in *bh7* animals remain uninduced. In this example, P5.p and P6.p are induced. P4.p and P7.p have adopted an F fate (asterisks). (C, D) *bh14* and *bh20* animals showing a similar vulval morphology defect. In both cases invagination is formed by P6.p progeny, whereas P5.p and P7.p have adopted an F fate (asterisks). (E) A *bh23* animal showing no vulval induction. All VPCs have adopted an F fate. Scale bar is 10 μm.

Table 6 Vulval cell lineage analysis of class 3 and 4 mutants

Genotype	VPCs						n
	P3.p	P4.p	P5.p	P6.p	P7.p	P8.p	
AF16	S/SS	SS	LLTN	TTTT	NTLL	SS	>50
lin(bh7)	SS	SS	LLTN	TTTT	NTLL	SS	4
	S	SS	LLTN	TTTT	NTLL	SS	1
	S	S	S	TTTT	NTLL	SS	1
	S	SS	LLTN	TTTT	NTLL	OOLL	1
	S	S	SS	TTTT	NTLL	SS	1
	S	SS	LLTN	TOOT	S	SS	1
	S	S	S	TTTT	S	S	1
lin(bh14)	S	S	S	TTTT	OTLL	S	1
	S	S	LLTN	TTTT	NTLL	S	2
	S	S	LLTN	TTTT	NTLL	SS	1
	S	S	S	TTTT	S	S	2
	S	SS	NTOL	TTTT	S	S	1
	S	S	S	OOTT	S	S	1
	S	S	S	TTTT	S	S	1
	S	S	LLTN	TTTT	S	S	2
lin(bh20)	S	S	S	S	S	S	13
	S	S	S	TTTT	S	S	3
	S	S	S	OOOO	S	S	1
	S	S	S	TTTD	S	S	1
	S	S	S	OTTT	S	S	1
lin(bh23)	S	S	S	S	S	S	12
lin(sy5336)	SS	SS	LLLL	LTTT	LLLL	SS	2
	SS	SS	LLLL	ODTO	LLLL	SS	1
	S	SS	LLLL	OOOO	LLLL	SS	1
	SS	SS	LLLL	OOTO	LLLL	SS	1
	S	SS	LLLL	OTOT	LLLL	SS	1

Cells attached to the cuticle are underlined. D, division plane not observed; L, longitudinal; O, oblique; N, no cell division; n, number of animals scored; S, cell fused with syncytium; T, transverse plane of cell division.

signaling to promote vulval induction. A similar mechanism could operate in *C. briggsae* as well, which would be consistent with the results of our aforementioned cell ablation experiments in which P5.p and P7.p often were induced in the absence of P6.p, possibly by responding to a greater level of gonad-derived signal. To test this directly, we monitored the effect of increased doses of LIN-3/EGF on VPC induction in *bh7*, *bh14*, and *bh20* animals. A *C. elegans lin-3* transgene under the control of a heat shock promoter was introduced in *C. briggsae*. This transgene was previously used in *C. elegans* and causes a Muv phenotype (Katz *et al.* 1995). Heat shocks given during early stages (0-18 hr post-L1) and late stages (30 hr post-L1 and beyond) had no effect on vulval development (Figure 4A and data not shown). However, 20-28 hr post-L1, animals (VPC one-cell stage, Pn.p) developed a Muv phenotype when subjected to heat shock (Figure 4A). The Muv penetrance was highest at the 24 hr post-L1 time point (58%, see Figure 4A, AC visible in all cases at the time of heat shock), which corresponds to the late-L2/early-L3 stage and precedes the division of dorsal uterine precursors. All VPCs were induced, although P3.p appeared to be somewhat refractory in this assay (Figure 4C).

Next, we examined the effect of *lin-3* overexpression in *bh7*, *bh14* and *bh20* animals. Heat shocks at the 24 hr post-L1 time point induced a Muv phenotype in *bh7* animals similar to the control (Figure 4B). The *bh14* animals showed a similar but reduced response (Figure 4B). In contrast, no Muv phenotype was observed in *bh20* animals (Figure 4B). Examination of cell fates revealed that greater doses of LIN-3 induced VPCs in all 3 genetic backgrounds, including *bh20* in which P6.p was threefold more likely to be induced compared to the control (Figure 4C). These results show that increased VPC induction in class 3 mutants is most likely caused by the activation of a pathway homologous to LIN-3/EGF signaling in *C. elegans*.

Class 3 mutations *bh20* and *bh23* are alleles of *Cbr-lin-39*

The cell fusion defect in class 3 mutants was similar to that of *C. elegans* with mutant Hox gene *lin-39* alleles that cause P(3-8).p cells to

Table 7 Effect of cell ablations on VPC fates in class 3 mutants

Genotype	VPC Fate (Induced/Uninduced)						n
	P3.p	P4.p	P5.p	P6.p	P7.p	P8.p	
mfIs5(egl-17::gfp)	0/100	30/70	100/0	x	100/0	70/30	10
lin(bh7)	0/100	67/33	100/0	x	100/0	17/83	6
lin(bh14)	0/100	0/100	33/67	x	22/78	0/100	9
	0/100	0/100	x	x	100/0	0/100	1
lin(bh20)	0/100	0/100	15/85	x	5/95	0/100	19

'x' denotes VPCs that were ablated during the early-L2 stage. See Table 5 for a description of VPC fates. Uninduced refers to F and 3° fates. n, number of animals scored; VPC, vulval precursor cells.

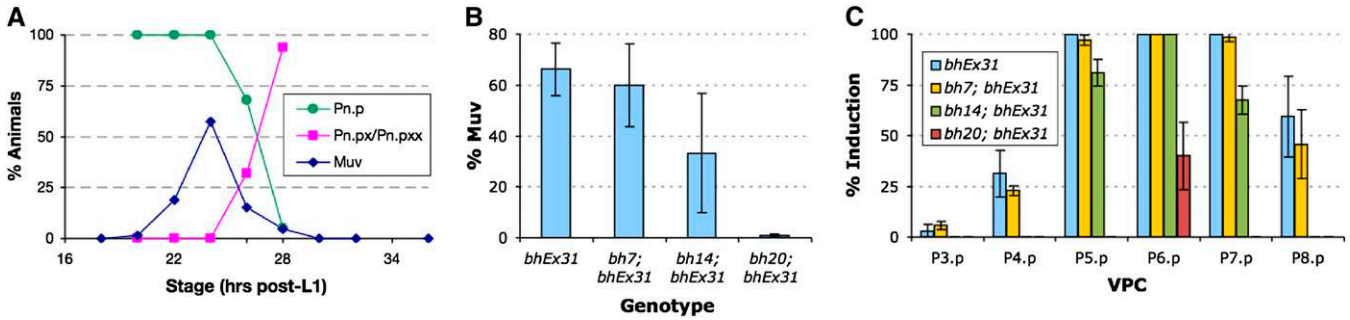

Figure 4 Effect of *lin-3* overexpression on VPC induction in class 3 mutants. The *bhEx31* transgenic strain carries a *hs::lin-3* plasmid from *C. elegans* (see *Materials and Methods* for details). (A) The graph shows the proportion of Pn.p (1-cell stage), Pn.px (2-cell stage), and Pn.pxx (4-cell stage) *bhEx31* animals at different time points of development (green and pink lines). The heat shock-induced Muv phenotype of *bhEx31* is also plotted (blue line). Almost 60% of animals, when subjected to heat shock at 24 hr after L1, develop a Muv phenotype. The Muv penetrance decreases rapidly after the VPCs start to divide such that by 30 hr, when all VPCs have divided, heat shock has no effect on VPC induction (no Muv phenotype develops). Pn.p and progeny stages were determined from a total of 16 to 20 animals for each time point. For Muv penetrance analysis, each time point contained (starting from the L1+18 hr stage) 25, 63, 328, 118, 300, 214, 86, 25, and 81 animals, respectively. (B) The graph shows the Muv phenotype in mutants after the heat shock at 24 hr. The Muv frequency in *bh7* animals is similar to the control *(bhEx31)*, slightly reduced in *bh14*, and not present in *bh20* animals. The number of animals examined in each case was 154 (control), 50 (*bh7*), 159 (*bh14*), and 112 (*bh20*). (C) The pattern of VPC induction in animals plotted in graph B. Although all VPCs can be induced in the control and *bh7* to varying extents, only the central 3, P(5-7).p, do so in *bh14*, and only one (P6.p) is induced in *bh20* animals. For each genotype, we examined 32 (control), 70 (*bh7*), 37 (*bh14*), and 95 (*bh20*) animals.

fuse to surrounding hypodermis (Clark *et al.* 1993). Therefore, we wanted to determine whether any of these are alleles of *Cbr-lin-39*. Using Indel mapping, we had earlier placed *lin(bh20)* on the right arm of chromosome 3 (Koboldt *et al.* 2010). This region includes *C. elegans lin-39* ortholog (http://www.wormbase.org). Therefore, we took a candidate gene approach and sequenced the exonic regions of *Cbr-lin-39* in *bh20* animals. A single point mutation (G9427 to A) was found that is predicted to replace a conserved arginine (R) with glutamine (Q) at position 169 in the homeodomain region (Figure 5A). Considering that *lin(bh23)* animals show a similar but more severe VPC induction defect, we suspected that this could be another allele of *Cbr-lin-39*. Sequencing of the *Cbr-lin-39* region in this strain identified a 364 bp deletion affecting the promoter and translational start site (Figure 5A).

We also carried out a transgene rescue experiment for *lin(bh20)* animals using a *C. elegans lin-39*-rescuing genomic DNA clone. Examination of transgenic animals revealed a rescue of the VPC competence defect in both cases (Table 5). The Egl defect also was rescued in these lines (animals laying eggs: *bhEx132* 83%, n = 29 and *bhEx134* 24%, n = 124; compared with 4% in *bh20* alone, n = 140).

Pn.p cells lack competence and are irregularly placed in *Cbr-lin-39* mutants

In *C. elegans*, *lin-39* acts at multiple times during vulval development. In the L1 and L2 stages, it prevents Pn.p cells from fusing to hyp7 (Clark *et al.* 1993). Later on in stage L3, it is up-regulated by Ras signaling to promote vulval induction (Maloof and Kenyon 1998). To determine whether *Cbr-lin-39* mutants cause cell fusion defects in *C. briggsae*, we used a junction-associated marker *dlg-1::GFP* (Seetharaman *et al.* 2010). In wild-type AF16, P(3-8).p remain unfused in the late-L1 and L2 stages and become competent to form the vulval tissue (Figure 5B). In the majority of *bh20* animals, the corresponding cells were fused by early-to-mid-L2 stage (60.7%, n = 28). In the remaining cases, one or two Pn.p cells were protected (P5.p and P6.p 21.4% and P6.p alone 17.8%, n = 28; Figure 5C). The proportion of animals with unfused cells was much lower at later stages and was limited to P6.p (mid-L3 stage: P6.p 30.8%, n = 13; L4 stage: P6.p 12.5%, n = 24).

As it has been previously reported that the spacing of Pn.p cells in the ventral hypodermis is less regular in *C. elegans lin-39* mutants (Clark *et al.* 1993), we measured VPC spacing in *Cbr-lin-39* animals. Our results agreed with the findings in *C. elegans* and revealed that both *Cbr-lin-39* alleles cause greater variability in VPC placement (Figure 5, D and E). Although all inter-VPC distances were affected, the phenotype was most pronounced in the P6.p-P7.p pair. Interestingly, the P5.p-P6.p pair in *C. briggsae* showed the reverse of *C. elegans*.

bh20 is epistatic to *Cbr-pry-1(sy5353)*

We recently demonstrated a conserved role for *pry-1*−mediated Wnt signaling in 2° VPC fate specification (Seetharaman *et al.* 2010). In *Cbr-pry-1*, animals P5.p and P6.p are always induced, but P7.p often is not (Figure 5F). The inability of P7.p to contribute to vulval tissue is likely due to a change in cell fate as judged by its small nucleus and P12.pa-like appearance. *Cbr-pry-1* mutants also exhibit ectopic induction of P3.p and P4.p and to some extent P8.p, resulting in the formation of multiple ventral protrusions (pseudovulvae). Thus, both a lack of induction (P7.p) and excessive induction phenotypes are observed in *Cbr-pry-1* animals.

Given that *lin-39* acts genetically downstream of *pry-1* in *C. elegans* (Gleason *et al.* 2002), we examined the genetic interaction of *Cbr-lin-39* with *Cbr-pry-1*. As expected, *Cbr-lin-39*(*bh20*) suppressed the increased induction phenotype of *Cbr-pry-1(sy5353)*. Ectopic vulval induction was inhibited due to VPCs frequently adopting F fates (n = 42; P6.p was induced in 24% cases; Figure 5G). However, the small nucleus phenotype of P7.p, P8.p, and P11.p was not suppressed by *bh20* (Figure 5G and data not shown). Therefore, one of the following may be true: either the residual activity of *Cbr-lin-39* in *bh20* animals is greater than the threshold needed for VPC size specification or *Cbr-lin-39* mediates only a subset of *Cbr-pry-1* function.

Class 4 mutations affect vulval invagination and morphology

This class consists of seven mutants, all of which have defective vulval morphology (Table 8). Microscopic observations revealed that the

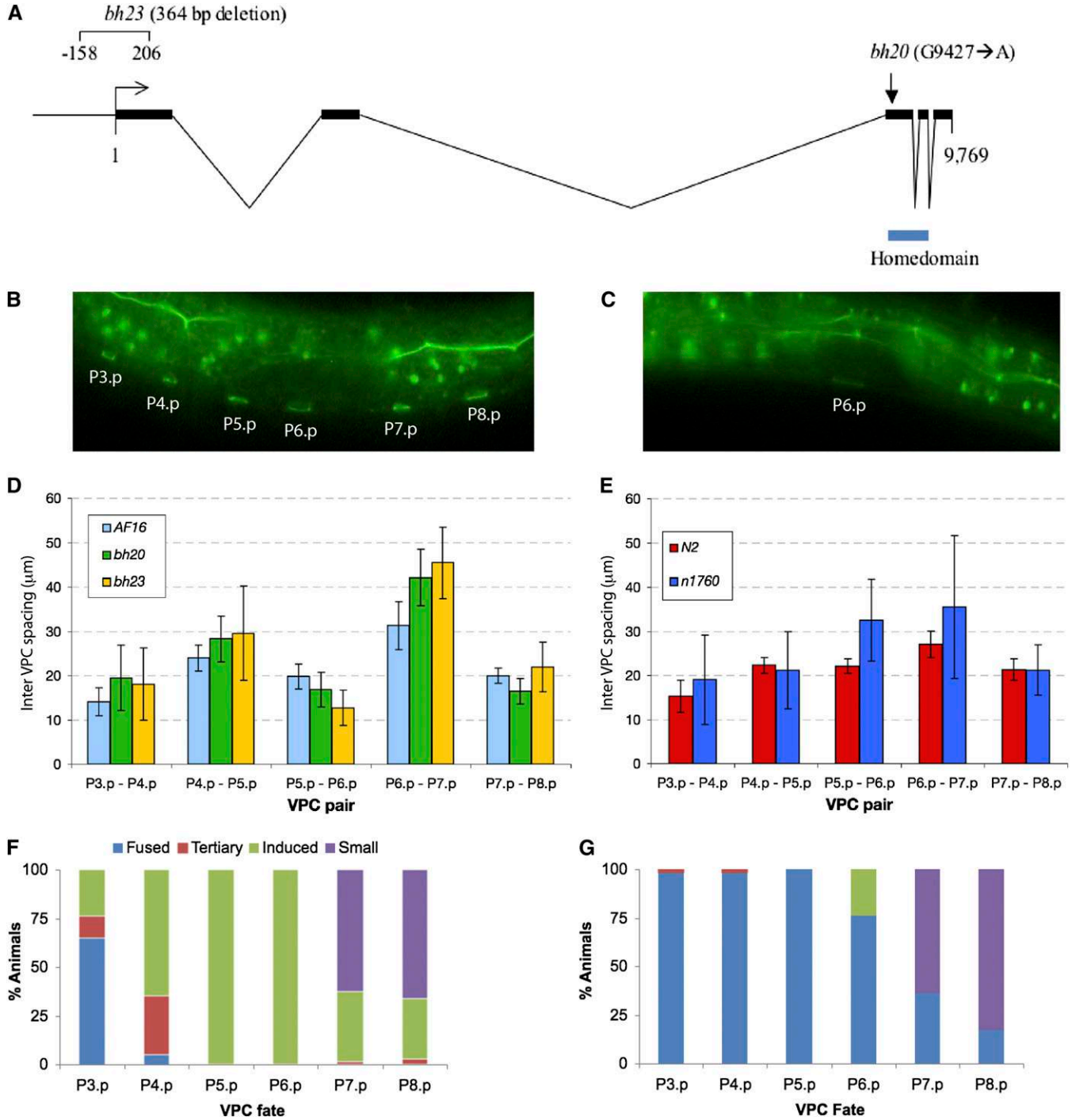

Figure 5 Genomic organization and mutant phenotypes of *lin-39*. (A) *C. briggsae lin-39* open reading frame. Exons are represented by thick lines. The positions of the homeodomain and two mutations are shown. (B, C) Unfused VPCs revealed by *dlg-1*::*GFP* expression. (B) Wild-type AF16 and (C) *bh20* L2 stage animals. In this *bh20* animal only P6.p ring is visible. (D, E) Inter-VPC spacing in *lin-39* alleles in *C. elegans* and *C. briggsae*. VPCs are irregularly spaced in mutants, which is reflected in greater SDs. (F, G) Excessive induction of VPC phenotype in *sy5353* animals is suppressed by *bh20*. (F) *sy5353* and (G) *bh20*; *sy5353* double mutant. VPC fates are shown as Fused, 3°, induced (1° and 2°) and small (P12.pa-like).

animals have the correct number of VPCs and their progeny but the cells fail to invaginate correctly (Figure 6). In addition to the Egl phenotype, the adults exhibit a Pvl phenotype (Table 8). Complementation and mapping experiments revealed a total of five loci, three of which are located on chromosome 1 with the others on chromosome 5 and the X chromosome (Table 3). Two of the chromosome 1 genes have additional alleles (*bh13* and *sy5197* on the left arm, *sy5336* and *sy5368* close to the center).

The *sy5336* and *sy5368* mutations cause a fully penetrant Egl phenotype. A distinctive feature of these animals, with regards to egg laying, is rudimentary vulval invagination and defects in the connection of the vulva to the uterus (Figure 6B). The analysis of VPC

Table 8 Vulval morphology defects in class 4 mutants

Gene	Allele	Abnormal Vulval Morphology	Pvl
lin(bh13)	*bh13*	71% (69)	29% (110)
	sy5197	51% (39)	ND
lin(bh25)	*bh25*	47% (36)	7.4% (148)
lin(bh26)	*bh26*	86% (51)	51.8% (110)
lin(sy5425)	*sy5425*	83% (35)	17.9% (95)
lin(sy5336)	*sy5336*	100% (100)	83.9% (152)
	sy5368	100% (100)	51.2% (162)

Number of animals scored are shown inside parentheses. ND, not done; Pvl, protruding vulva.

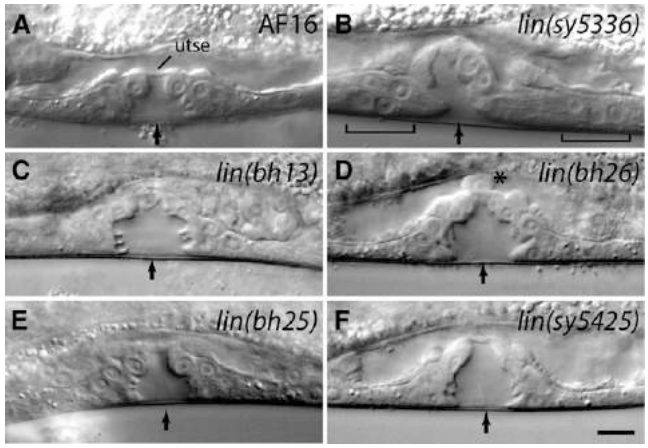

Figure 6 Vulval morphology defects in class 4 mutants. Animals were examined at mid-L4 stage. Arrows mark the center of invagination. (A) Wild type. The utse is visible as a thin line above the vulva. (B) The 2° lineage vulval cells fail to invaginate (shown by brackets). The utse cannot be clearly identified. (C, D) The vulval opening is blocked due to a failure in the migration of the 1° lineage cells. (E, F) Vulval invagination is abnormal. In addition, the utse in a *bh25* animal (E) is thicker compared with the wild type. Scale bar is 10 μm.

lineages revealed errors in cell divisions and adherence properties of some of the 2° lineage cells (Table 6). Other phenotypes included low brood size (*sy5336*: 21 ± 5, n = 11; *sy5368*: 10 ± 2, n = 12) and defective mating. The hermaphrodites are unable to mate at all, whereas males can mate, although very poorly (data not shown).

The *bh13* and *sy5197* animals are small and mildly sluggish. Some also have abnormally folded gonad arms. These phenotypes accompany Egl and vulval invagination defects in both outcrossed strains (Tables 4 and 8, Figure 6C), suggesting they are linked to a single gene. We looked at the vulval morphology in L4 stage animals and found that the 1° lineage cell nuclei are abnormally placed. In addition, the utse cannot be clearly observed in these animals (Figure 6C). A combination of the vulva and utse defects appears to cause a physical block in the egg-laying passage.

The vulval morphology defect in *bh26* animals shares some similarity with that of *bh13* animals (Figure 6D compared with Figure 6C). Specifically, the nuclei of the 1° lineage cells fail to migrate correctly, thereby blocking the connection between the vulva and the uterus. We also observed defects in the migration of the AC and a lack of utse (Figure 6D). Other defects included abnormal gonad arms and sterility.

The remaining two class 4 mutants, *lin(bh25)* and *lin(sy5425)*, have weaker Egl and Pvl phenotypes compared with others in this category (Table 8). In both cases, vulval cells invaginate and form finger-like structures, but the overall morphology is abnormal (Figure 6, E and F). The penetrance of the vulval defect is greater in *sy5425* compared with *bh25*, although an opposite trend was observed for the Egl phenotype. We also noted that the utse is somewhat thicker in *bh25* animals (Figure 6E), although its contribution to the Egl phenotype is unclear. Interestingly, some *sy5425* animals showed ectopic P4.p and P8.p induction. This phenotype is present in the outcrossed strain, so it is either caused by the same mutation or another very closely linked mutation. More work is needed to distinguish between these two possibilities. We also observed significant embryonic and early larval lethality in the *sy5425* strain (18%, n = 284).

Cbr-lin-11 mutations disrupt vulva and utse morphogenesis

The vulva and utse defects of *lin(sy5336)* and *lin(sy5368)* animals strongly resemble those of *C. elegans lin-11* mutants (Ferguson *et al.* 1987; Newman *et al.* 1999). In addition, the thermotaxis defect of the animals is also similar [(Hobert *et al.* 1998) Figure 7B], which is reflected in their lack of preference to the cultivation temperature. Therefore, we carried out transgene rescue experiments to examine whether these two lines carry mutant alleles of *Cbr-lin-11*. Stable lines carrying a 19-kb genomic clone of *C. elegans lin-11* (*bhEx78* and *bhEx148*, on the *sy5336* genetic background) showed rescue of the vulva, utse, and Egl defects (*bhEx78*: 47% wild-type vulva and utse, n = 32, non-Egl 8%, n = 25; *bhEx148*: 71% wild-type vulva and utse, n = 31, non-Egl 12.5%, n = 48; compared with *Cbr-lin-11* mutants in Table 8). We also sequenced the *Cbr-lin-11* locus in both alleles and identified molecular changes that are predicted to disrupt splicing in the homeobox region (Figure 7A, also see *Materials and Methods*).

The aforementioned rescue experiments demonstrate that *C. elegans lin-11* can substitute for *Cbr-lin-11* function in *C. briggsae* and suggest that *lin-11* function is evolutionarily conserved. This is also supported by the analysis of the cDNA and protein sequences. The *lin-11* cDNA (*C. elegans*: 1218 bp, 10 exons; *C. briggsae*: 1239 bp, 10 exons) (see Figure S3 for *C. briggsae* sequence) is 80% conserved, and the corresponding proteins are 87% identical (94% similar).

To examine the vulval defect in *Cbr-lin-11* animals, we used the two GFP-based markers *Cbr-egl-17 (mfIs5)* and *Cbr-zmp-1 (mfIs8)*. In *C. elegans*, *egl-17* and *zmp-1* have been used extensively in cell fate specification studies (Cui and Han 2003; Gupta *et al.* 2003; Inoue *et al.* 2002). The dissection of the regulatory regions of these genes has revealed evolutionarily conserved sequences (Kirouac and Sternberg 2003). In the wild-type *C. briggsae*, the earliest expression of *Cbr-egl-17::gfp* is observed in mid/late-L4 stage animals in the presumptive vulC and vulD (Seetharaman *et al.* 2010). In the case of *Cbr-zmp-1::gfp*, GFP fluorescence is primarily observed in the presumptive vulE (Seetharaman *et al.* 2010). We found that the expression of both markers was absent in *Cbr-lin-11(sy5336)* animals (Table 9). This result supports our previous findings and a crucial role of *lin-11* in vulval cell differentiation (Gupta *et al.* 2003).

Despite the high conservation in *lin-11* sequence and function, we did observe an interesting difference in the AC placement between the two species. Unlike *C. elegans lin-11* animals, in which ACs fail to migrate and are located on the vulval apex in most animals (*n389*: 81.1%, n = 53; Figure 7C), no such phenotype was observed in *C. briggsae* (*sy5336*: 0%, n = 47 and *sy5368*: 0%, n = 52; Figure 7D).

DISCUSSION

We report the isolation and characterization of mutations in 13 genes in *C. briggsae* that are involved in the development and function of the

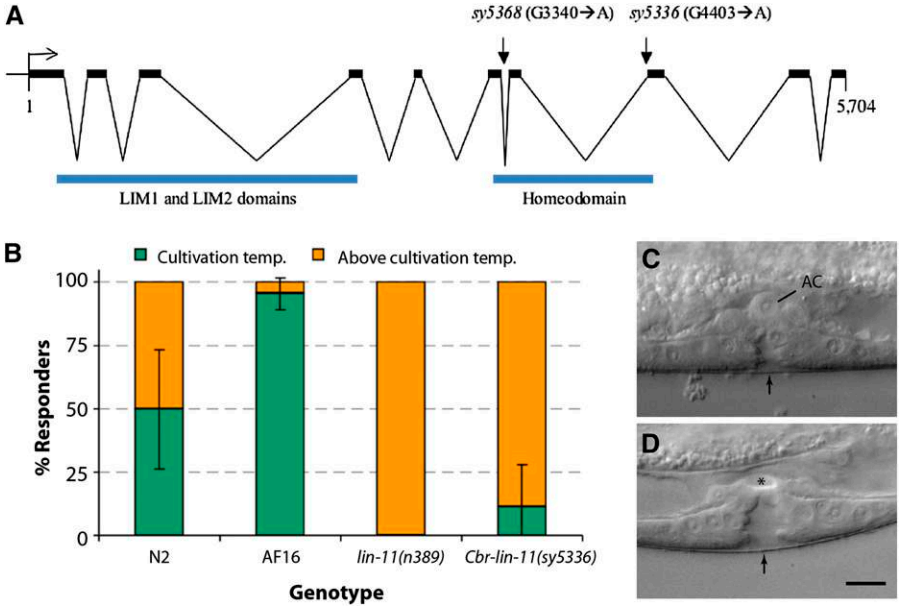

Figure 7 Genomic organization of *Cbr-lin-11* and mutant phenotypes. (A) *Cbr-lin-11* open reading frame showing LIM and homeodomain regions as well as mutations. Both alleles affect the homeodomain region. (B) Graph shows the thermotaxis response of the wild-type and *lin-11* animals. Wild-type animals prefer to live near the temperature at which they were initially grown, whereas *lin-11* animals do not demonstrate such behavior. Instead, they are thermophilic. (C) *lin-11(n389)*. The AC is located at the vulval apex. (D) *Cbr-lin-11(sy5336)*. No AC can be observed at the corresponding location (asterisk). Scale bar in C and D is 10 μm.

egg-laying system. To date, this is the largest set of genes identified by a forward genetics approach in this species. Ten of these genes are involved in various steps of vulval development (Figure 8). Transgene rescue and molecular analyses have revealed that three genes are orthologs of *unc-84*, *lin-39*, and *lin-11*. Together, these mutant strains serve as valuable tools for comparative and evolutionary studies. Another genetic screen in *C. briggsae* was previously carried out to identify dauer pathway genes (Inoue *et al.* 2007). The screen identified several mutations, including alleles of *Cbr-daf-2* (insulin receptor), *Cbr-daf-3* (Smad), and *Cbr-daf-4* (TGF-β family receptor). Genetic studies revealed that although the functions of *C. elegans* orthologs are conserved in *C. briggsae*, the two species exhibit differences in their temperature sensitivities. Thus, comparative genetics approaches are useful for revealing the similarities and differences in biological processes between *C. elegans* and *C. briggsae*.

Egl phenotype-based genetic screens were first carried out in *C. elegans* and led to the identification of many genes involved in vulval development (Ferguson and Horvitz 1985; Trent *et al.* 1983). Characterization of their function revealed a genetic pathway for the formation of the vulva (Ferguson *et al.* 1987). During the past decade and a half, this knowledge has been extended to other distant species, such as *P. pacificus* and *O. tipulae*, resulting in a better understanding of the evolutionary changes in the mechanism of vulva formation. Screens in *O. tipulae* have identified several mutations affecting vulva formation. Although the majority of these cause defects in VPC division and competence (Dichtel *et al.* 2001; Louvet-Vallee *et al.* 2003), others affecting vulva centering and hyper- and hypo-induced phenotypes also have been identified (Dichtel *et al.* 2001). Similar mutant classes have been found in *P. pacificus* screens as well (Eizinger *et al.* 1999; Sommer 2005). Compared with *C. elegans*, the phenotypic spectrum in these two species is quite different. For example, mutations affecting Pn.p fate (*e.g.*, 1° converted to 2° or 3°) were recovered quite frequently in *C. elegans* but not in *O. tipulae* or *P. pacificus*. Interestingly, our screens in *C. briggsae* also revealed differences from *C. elegans*. We did not find Pn.p fate mutants, and one-half of the mutants examined show defects in cell invagination and morphogenesis (Table 8, Figure 8). It is not clear whether this phenotypic distribution is typical in *C. briggsae* or whether it results from the lack of saturation in the screen or another reason. It is worth pointing out that in our experience, Egl animals in *C. briggsae* are more difficult to identify in a standard F2 screen in the presence of predominantly non-Egl worms. This may be at least partly caused by the tendency of *C. briggsae* to retain fewer eggs in the uterus compared to *C. elegans* (B. P. Gupta, unpublished results; T. Inoue and M. A. Felix, personal communications). The difficulty in isolating Egls could have limited the recovery of vulva-specific mutants and the phenotypic classes in our screens. Future genetic screens using different approaches will help to address this issue. Furthermore, combining a vulva-specific GFP reporter with an Egl phenotype may be a useful approach, as it will minimize the recovery of non-vulval mutations.

Phenotypic classes recovered in our screen

We have isolated four phenotypic classes of worms, all of which affect egg laying. Mutations in one of these (class 1) have normal vulva and utse morphologies. To investigate the role of sex muscles and HSNs, we used serotonin and fluoxetine drugs to induce egg laying. *sy5395* mutants showed a mild but obvious increase in egg laying in response to serotonin, suggesting that the muscle function is intact. However, *bh2* and *bh21* did not respond to any of the drugs, suggesting that muscle function may be impaired.

The class 2 mutations *sy5505* and *sy5506* affect nuclear migration in a temperature-dependent manner. Both alleles cause animals to develop Egl and Unc phenotypes due to the failure of P nuclei to migrate into the ventral cord region. The phenotype of *unc(sy5506)* animals can be rescued by a *C. elegans unc-84* transgene, suggesting that *sy5506* is an allele of *Cbr-unc-84*. This conclusion is also supported by our mapping and allele sequencing data. The remaining two classes of mutations alter the number of vulval progeny and vulval invagination. *Cbr-lin-39* is required for the maintenance of VPC competence and appears to act

Table 9 Expression of vulval cell fate markers in *Cbr-lin-11* mutants

Genotype	GFP Fluorescence in Vulval Progeny	n
mfIs5 (egl-17::gfp)	vulC: 79%, vulC and vulD: 21%	113
sy5336; mfIs5	None	104
mfIs8 (zmp-1::gfp)	vulA: 2%, vulE: 91%, vulA and vulE: 7%	128
sy5336; mfIs8	None	61

GFP, green fluorescent protein; n, number of animals scored.

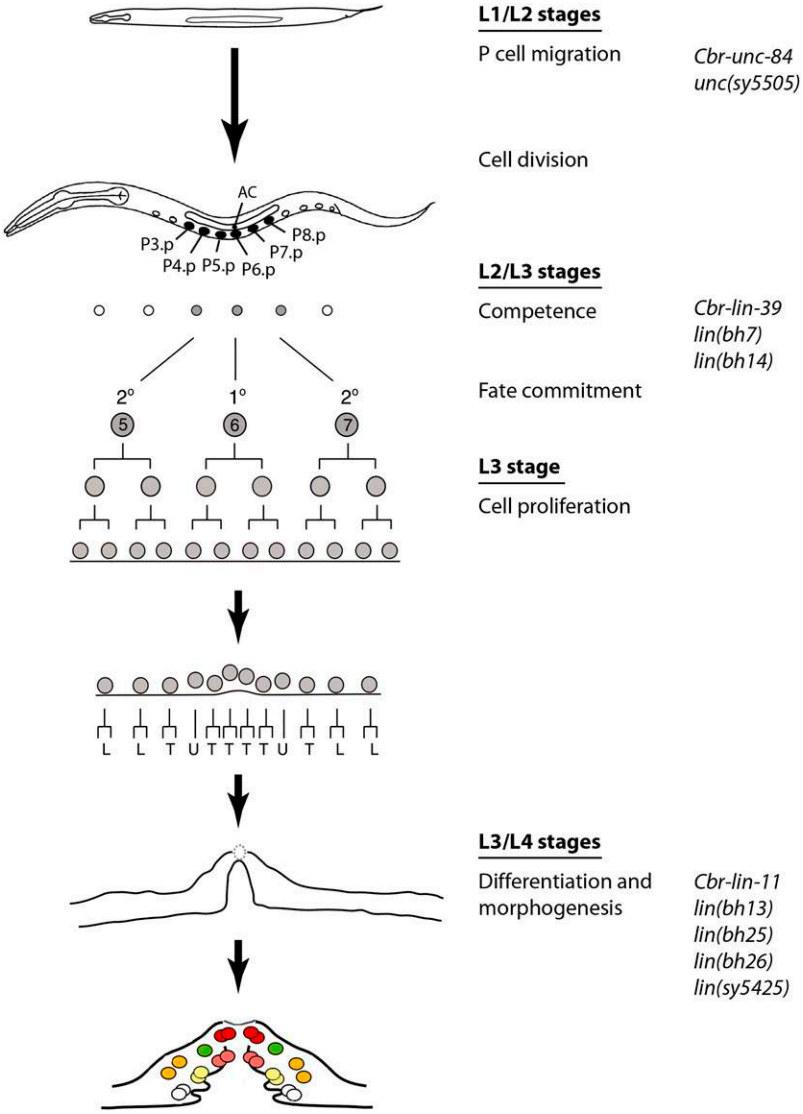

Figure 8 Vulval development in *C. briggsae* and the proposed roles of genes described in this study. P-cell migration into the ventral hypodermal region is mediated by the class 2 genes. Subsequently, P cells divide, and six of their posterior daughters (Pn.p, n = 3−8), termed VPCs, become capable of giving rise to the vulval tissue. Their competence appears to be regulated by the class 3 genes. VPC progeny differentiate and undergo morphogenetic changes during the L3 and L4 stages. The class 4 genes are required in these processes.

downstream of *Cbr-pry-1*/*axin*-mediated Wnt signaling. *Cbr-lin-11* controls vulval cell differentiation and tissue morphogenesis. Both genes belong to conserved families of transcription factors (the *Dfd/Scr*-related Hox family and the *LIM-Hox* family, respectively).

Nuclear migration in *C. briggsae* is mediated by a conserved SUN domain protein

Nuclear migration plays important roles in diverse cellular processes, including cell division, cell polarity and cell migration. In *C. elegans*, well-studied nuclear migration events are observed with the hyp7 syncytium (dorsal side of the hypodermis) and a set of hypodermal blast cells (P cells) that form the vulva. Genetic analysis of these events has revealed that UNC-83 (KASH domain) and UNC-84 (SUN domain) proteins form a bridge-like structure to connect the nucleus to microtubules, motor proteins, and other cytoskeletal components. The movement of Kinesin and Dynein motors in a coordinated manner causes the nucleus to move in a specific direction. The vulval defects in *C. briggsae sy5505* and *sy5506* animals are typical of *unc-83* and *unc-84* mutants. Both alleles exhibit a temperature-sensitive phenotype and display Egl and Unc phenotypes. The phenotypes of *sy5506* animals can be efficiently rescued by a *C. elegans unc-84* genomic clone, which demonstrates that *unc-84* plays a conserved role in nuclear migration in both species.

Genes affecting cell fusion in *C. briggsae*

We isolated two alleles of *Cbr-lin-39*, both of which prevent VPC induction. In *C. elegans*, P(3-8).p escape fusion in the L1 and L2 stages and remain competent to respond to induction during the L3 stage (Sternberg 2005). This process is regulated by *lin-39* (Clark *et al.* 1993). The expression of *lin-39* at the L2 stage appears to be partly controlled by BAR-1/β-catenin−mediated Wnt signaling because in *bar-1* mutants, *lin-39* expression in VPCs is reduced, resulting in fusion of some VPCs to the hyp7 syncytium (Eisenmann *et al.* 1998). Our experiments on *Cbr-lin-39* suggest that the function of *lin-39* in VPC competence is conserved in *C. briggsae*. This finding is supported by the analysis of mutant phenotype, rescue experiments, cell fusion studies using the *dlg-1*::*GFP* marker, and genetic interaction with *Cbr-pry-1* (Axin family). Our previous results involving RNA interference−mediated knockdown of *Cbr-lin-39* (Seetharaman *et al.* 2010) also support these findings.

lin-39 orthologs also have been identified in *O. tipulae* and *P. pacificus*. *Oti-lin-39* appears to control VPC competence by

preventing fusion of Pn.p cells in the late-L1/early-L2 stages (Louvet-Vallee *et al.* 2003). However, the function of *Ppa-lin-39* appears to have diverged. In *Ppa-lin-39* mutants, VPCs undergo programmed cell death instead of fusing with the hypodermis (Eizinger and Sommer 1997). Taken together, these findings suggest that although *lin-39* function is conserved in *Caenorhabditis* and *Oscheius* species, it has acquired new roles in *Pristionchus*. In the future, analysis of the role of *lin-39* in additional nematode species will allow for a more detailed comparison of its roles in vulval development.

In addition to *Cbr-lin-39*, we have uncovered two other loci, *lin (bh7)* and *lin(bh14)*, that control VPC competence. The phenotype of both mutants is weaker than that of *bh20* animals, perhaps due to weak hypomorphic alleles. Alternatively, these genes may have some redundant function. More alleles are required to distinguish between these two possibilities. The induction of P5.p and P7.p in *bh7* and *bh14* animals is frequently affected. To test the induction potential of these two VPCs, we carried out two complementary experiments. We examined their pattern of division after ablation of P6.p. Furthermore, the effect of *lin-3* overexpression was investigated. We found that in the absence of P6.p, the P5.p and P7.p cells were induced to various extents, suggesting that these VPCs can respond to inductive signal. This conclusion is strongly supported by the *lin-3* dosage experiments. High doses of *lin-3* during the L2 stage caused ectopic VPC induction, resulting in a Muv phenotype. We can therefore conclude that class 3 genes interact with a LIN-3-like inductive signal to regulate VPC competence in *C. briggsae*.

lin-11 is a key regulator of vulval morphogenesis

lin-11 is a founding member of the LIM homeobox family of genes. Mutations in *lin-11* were originally isolated in genetic screens for worms that failed to lay eggs (Ferguson and Horvitz 1985). Subsequently, phenotypic analyses showed a wide-range of defects affecting vulval morphology (Freyd *et al.* 1990; Gupta *et al.* 2003), utse formation (Newman *et al.* 1999), and neuronal differentiation (Hobert *et al.* 1998; Sarafi-Reinach *et al.* 2001). *C. briggsae lin-11* mutants exhibit defects in the egg-laying system similar to those observed in *C. elegans lin-11* animals. Thus, vulval cells fail to invaginate, and a functional connection between the vulva and the uterus is not established. These phenotypes can be rescued by a *C. elegans lin-11* genomic fragment, suggesting that *lin-11* regulatory and coding sequences are evolutionarily conserved. This supports our previous conclusions on the conservation of *lin-11* regulation by Wnt and LIN-12/Notch signaling pathways in the vulva and π cell differentiation (Marri and Gupta 2009).

Outside the reproductive system, *lin-11* also is involved in the differentiation of several olfactory and chemosensory neurons (Sarafi-Reinach *et al.* 2001). We have not yet characterized the neuronal role of *Cbr-lin-11* in detail, but we have found that *Cbr-lin-11* mutants have a thermotaxis defect similar to that reported in *C. elegans lin-11* animals. Thus, similar to the egg-laying system, the role of *lin-11* in thermosensory behavior is also conserved. The recovery of *Cbr-lin-11* alleles provides a unique opportunity to investigate the mechanism of cell differentiation in *C. briggsae* and *C. elegans*.

DSD in *C. briggsae* vulva formation

Kiontke *et al.* 2007 had earlier reported variations in several steps of vulva formation in Rhabditid species. These included changes in Pn.p cell competence, cell division pattern, and vulva position. The phenotypic analysis of *C. briggsae* vulva mutants and molecular cloning of the 3 loci in which the mutations are located has revealed DSD in homologous processes. We observed interesting differences in at least three cases. First, the P5.p-P6.p inter-VPC distance in *lin-39* mutants tends to be lower in *C. briggsae* than in *C. elegans*. Second, *lin-39* does not interact with *pry-1* to enhance the small nuclear size phenotype of posterior Pn.p cells in *C. briggsae* as it does in *C. elegans* (Penigault and Felix 2011b). Finally, *Cbr-lin-11* animals do not show AC migration defects, which is one of the hallmarks of *lin-11* mutants in *C. elegans*. These results reveal the differences in developmental mechanisms that exist despite conservation of vulval morphology in these two species.

C. briggsae as a model for the study of vulval development

C. briggsae is increasingly being used in comparative developmental and evolutionary studies. In recent years, a number of publications have described processes such as sex determination (Guo *et al.* 2009; Hill *et al.* 2006; Kelleher *et al.* 2008), dauer formation (Inoue *et al.* 2007), pheromone receptor signaling (McGrath *et al.* 2011), embryogenesis (Lin *et al.* 2009; Zhao *et al.* 2008), and vulva formation in *C. briggsae* (Felix 2007; Hoyos *et al.* 2011; Marri and Gupta 2009; Penigault and Felix 2011a; Seetharaman *et al.* 2010). The findings have revealed similarities and differences in developmental processes.

The analysis of the vulval precursor fates in *C. briggsae* has revealed the role of conserved signaling pathway genes such as Ras, Notch, and Wnt. However, a detailed examination of gene function and pathways could not be carried out due to the lack of mutations affecting specific steps in the vulval development process. The mutations described in this study represent the first systematic effort in *C. briggsae* to investigate the genetic basis of vulva formation. Future work is needed to reveal the mechanism of gene function and to further compare *C. briggsae* to *C. elegans*. The results will ultimately help clarify how distinct processes form almost identical vulval structures in these two species.

ACKNOWLEDGMENTS

We thank Takao Inoue and Shahla Gharib for isolating *lin-11* alleles, Veena Deekonda, Nayasta Ademmana, and Carly Ching for assistance in experiments, and Takao Inoue for critical comments. Two of the transgenic strains *mfIs5* and *mfIs8* were kindly provided by Marie-Anne Felix (Institut Jacques Monod). The genetic screens were carried out in the laboratory of Paul Sternberg. This work was supported by the Natural Sciences and Engineering Research Council Discovery grant to B.P.G. Work in the laboratory of D.G.M. was supported by Genome Canada, Genome British Columbia and the Canadian Institutes for Health Research.

LITERATURE CITED

Antoshechkin, I., and P. W. Sternberg, 2007 The versatile worm: genetic and genomic resources for *Caenorhabditis elegans* research. Nat. Rev. Genet. 8: 518–532.

Avery, L., and H. R. Horvitz, 1987 A cell that dies during wild-type *C. elegans* development can function as a neuron in a *ced-3* mutant. Cell 51: 1071–1078.

Baldessarini, R. J., 1996 Drugs and the treatment of psychiatric disorders: antimanic and antidepressant agents, pp. 249–263 in *Goodman and Gilman's Pharmacological Basis of Therapeutics*, Ed. 12, edited by L. L. Brunton, B. A. Chabner, and B. C. Knollmann. McGraw-Hill, New York.

Benian, G. M., S. W. L'Hernault, and M. E. Morris, 1993 Additional sequence complexity in the muscle gene, unc-22, and its encoded protein, twitchin, of *Caenorhabditis elegans*. Genetics 134: 1097–1104.

Brenner, S., 1974 The genetics of *Caenorhabditis elegans*. Genetics 77: 71–94.

Burdine, R. D., and M. J. Stern, 1996 Easy RNA isolation from *C. elegans*: a TRIZOL based method. Worm Breed. Gaz. 14: 10.

Clark, S. G., A. D. Chisholm, and H. R. Horvitz, 1993 Control of cell fates in the central body region of *C. elegans* by the homeobox gene lin-39. Cell 74: 43–55.

Croll, N. A., 1975 Indolealkylamines in the coordination of nematode behavioral activities. Can. J. Zool. 53: 894–903.
Cui, M., and M. Han, 2003 Cis regulatory requirements for vulval cell-specific expression of the *Caenorhabditis elegans* fibroblast growth factor gene egl-17. Dev. Biol. 257: 104–116.
Cutter, A. D., 2008 Divergence times in *Caenorhabditis* and *Drosophila* inferred from direct estimates of the neutral mutation rate. Mol. Biol. Evol. 25: 778–786.
Delattre, M., and M. A. Felix, 2001 Polymorphism and evolution of vulval precursor cell lineages within two nematode genera, *Caenorhabditis* and *Oscheius*. Curr. Biol. 11: 631–643.
Dempsey, C. M., S. M. Mackenzie, A. Gargus, G. Blanco, and J. Y. Sze, 2005 Serotonin (5HT), fluoxetine, imipramine and dopamine target distinct 5HT receptor signaling to modulate *Caenorhabditis elegans* egg-laying behavior. Genetics 169: 1425–1436.
Dichtel, M. L., S. Louvet-Vallee, M. E. Viney, M. A. Felix, and P. W. Sternberg, 2001 Control of vulval cell division number in the nematode Oscheius/Dolichorhabditis sp. CEW1. Genetics 157: 183–197.
Eisenmann, D. M., 2005 Wnt signaling (June 25, 2005). WormBook, ed. The *C. elegans* Research Community WormBook, doi/10.1895/wormbook.1.7.1, http://www.wormbook.org.
Eisenmann, D. M., J. N. Maloof, J. S. Simske, C. Kenyon, and S. K. Kim, 1998 The beta-catenin homolog BAR-1 and LET-60 Ras coordinately regulate the Hox gene *lin-39* during *Caenorhabditis elegans* vulval development. Development 125: 3667–3680.
Eizinger, A., and R. J. Sommer, 1997 The homeotic gene *lin-39* and the evolution of nematode epidermal cell fates. Science 278: 452–455.
Eizinger, A., B. Jungblut, and R. J. Sommer, 1999 Evolutionary change in the functional specificity of genes. Trends Genet. 15: 197–202.
Felix, M. A., 2007 Cryptic quantitative evolution of the vulva intercellular signaling network in *Caenorhabditis*. Curr. Biol. 17: 103–114.
Felix, M. A., and P. W. Sternberg, 1997 Two nested gonadal inductions of the vulva in nematodes. Development 124: 253–259.
Felix, M. A., P. De Ley, R. J. Sommer, L. Frisse, S. A. Nadler *et al.*, 2000 Evolution of vulva development in the Cephalobina (Nematoda). Dev. Biol. 221: 68–86.
Ferguson, E. L., and H. R. Horvitz, 1985 Identification and characterization of 22 genes that affect the vulval cell lineages of the nematode *Caenorhabditis elegans*. Genetics 110: 17–72.
Ferguson, E. L., P. W. Sternberg, and H. R. Horvitz, 1987 A genetic pathway for the specification of the vulval cell lineages of *Caenorhabditis elegans*. Nature 326: 259–267.
Flibotte, S., M. L. Edgley, J. Maydan, J. Taylor, R. Zapf *et al.*, 2009 Rapid high resolution single nucleotide polymorphism-comparative genome hybridization mapping in *Caenorhabditis elegans*. Genetics 181: 33–37.
Freyd, G., 1991 Molecular analysis of the *Caenorhabditis elegans* cell lineage gene lin-11. Ph.D. Thesis, Massachusetts Institute of Technology, Boston.
Freyd, G., S. K. Kim, and H. R. Horvitz, 1990 Novel cysteine-rich motif and homeodomain in the product of the *Caenorhabditis elegans* cell lineage gene lin-11. Nature 344: 876–879.
Gleason, J. E., H. C. Korswagen, and D. M. Eisenmann, 2002 Activation of Wnt signaling bypasses the requirement for RTK/Ras signaling during *C. elegans* vulval induction. Genes Dev. 16: 1281–1290.
Gleason, J. E., E. A. Szyleyko, and D. M. Eisenmann, 2006 Multiple redundant Wnt signaling components function in two processes during *C. elegans* vulval development. Dev. Biol. 298: 442–457.
Greenwald, I., 2005 LIN-12/Notch signaling in *C. elegans* (August 4, 2005). WormBook, ed. The *C. elegans* Research Community WormBook, doi/10.1895/wormbook.1.10.1, http://www.wormbook.org.
Guo, Y., S. Lang, and R. E. Ellis, 2009 Independent recruitment of F box genes to regulate hermaphrodite development during nematode evolution. Curr. Biol. 19: 1853–1860.
Gupta, B. P., and P. W. Sternberg, 2003 The draft genome sequence of the nematode *Caenorhabditis briggsae*, a companion to *C. elegans*. Genome Biol. 4: 238.
Gupta, B. P., M. Wang, and P. W. Sternberg, 2003 The C. elegans LIM homeobox gene lin-11 specifies multiple cell fates during vulval development. Development 130: 2589–2601.
Gupta, B. P., J. Liu, B. J. Hwang, N. Moghal, and P. W. Sternberg, 2006 sli-3 negatively regulates the LET-23/epidermal growth factor receptor-mediated vulval induction pathway in *Caenorhabditis elegans*. Genetics 174: 1315–1326.
Gupta, B. P., R. Johnsen, and N. Chen, 2007 Genomics and biology of the nematode *Caenorhabditis briggsae* (May 3, 2007). WormBook, ed. The *C. elegans* Research Community WormBook, doi/10.1895/wormbook.1.10.1, http://www.wormbook.org.
Hill, R. J., and P. W. Sternberg, 1992 The gene lin-3 encodes an inductive signal for vulval development in *C. elegans*. Nature 358: 470–476.
Hill, R. C., C. E. de Carvalho, J. Salogiannis, B. Schlager, D. Pilgrim *et al.*, 2006 Genetic flexibility in the convergent evolution of hermaphroditism in *Caenorhabditis nematodes*. Dev. Cell 10: 531–538.
Hillier, L. W., R. D. Miller, S. E. Baird, A. Chinwalla, L. A. Fulton *et al.*, 2007 Comparison of *C. elegans* and *C. briggsae* genome sequences reveals extensive conservation of chromosome organization and synteny. PLoS Biol. 5: e167.
Hobert, O., T. D'Alberti, Y. Liu, and G. Ruvkun, 1998 Control of neural development and function in a thermoregulatory network by the LIM homeobox gene lin-11. J. Neurosci. 18: 2084–2096.
Horvitz, H. R., and J. E. Sulston, 1980 Isolation and genetic characterization of cell-lineage mutants of the nematode *Caenorhabditis elegans*. Genetics 96: 435–454.
Horvitz, H. R., M. Chalfie, C. Trent, J. E. Sulston, and P. D. Evans, 1982 Serotonin and octopamine in the nematode *Caenorhabditis elegans*. Science 216: 1012–1014.
Hoyos, E., K. Kim, J. Milloz, M. Barkoulas, J. B. Penigault *et al.*, 2011 Quantitative variation in autocrine signaling and pathway crosstalk in the *Caenorhabditis* vulval network. Curr. Biol. 21: 527–538.
Inoue, T., D. R. Sherwood, G. Aspock, J. A. Butler, B. P. Gupta *et al.*, 2002 Gene expression markers for *Caenorhabditis elegans* vulval cells. Mech. Dev. 119(Suppl 1): S203–S209.
Inoue, T., M. Ailion, S. Poon, H. K. Kim, J. H. Thomas *et al.*, 2007 Genetic analysis of dauer formation in *Caenorhabditis briggsae*. Genetics 177: 809–818.
Katz, W. S., R. J. Hill, T. R. Clandinin, and P. W. Sternberg, 1995 Different levels of the *C. elegans* growth factor LIN-3 promote distinct vulval precursor fates. Cell 82: 297–307.
Kelleher, D. F., C. E. de Carvalho, A. V. Doty, M. Layton, A. T. Cheng *et al.*, 2008 Comparative genetics of sex determination: masculinizing mutations in *Caenorhabditis briggsae*. Genetics 178: 1415–1429.
Kimble, J., 1981 Alterations in cell lineage following laser ablation of cells in the somatic gonad of *Caenorhabditis elegans*. Dev. Biol. 87: 286–300.
Kiontke, K., A. Barriere, I. Kolotuev, B. Podbilewicz, R. Sommer *et al.*, 2007 Trends, stasis, and drift in the evolution of nematode vulva development. Curr. Biol. 17: 1925–1937.
Kirouac, M., and P. W. Sternberg, 2003 cis-Regulatory control of three cell fate-specific genes in vulval organogenesis of *Caenorhabditis elegans* and *C. briggsae*. Dev. Biol. 257: 85–103.
Koboldt, D. C., J. Staisch, B. Thillainathan, K. Haines, S. E. Baird *et al.*, 2010 A toolkit for rapid gene mapping in the nematode *Caenorhabditis briggsae*. BMC Genomics 11: 236.
Li, C., and M. Chalfie, 1990 Organogenesis in *C. elegans*: positioning of neurons and muscles in the egg-laying system. Neuron 4: 681–695.
Lin, K. T., G. Broitman-Maduro, W. W. Hung, S. Cervantes, and M. F. Maduro, 2009 Knockdown of SKN-1 and the Wnt effector TCF/POP-1 reveals differences in endomesoderm specification in *C. briggsae* as compared with *C. elegans*. Dev. Biol. 325: 296–306.
Louvet-Vallee, S., I. Kolotuev, B. Podbilewicz, and M. A. Felix, 2003 Control of vulval competence and centering in the nematode *Oscheius* sp. 1 CEW1. Genetics 163: 133–146.
Malone, C. J., W. D. Fixsen, H. R. Horvitz, and M. Han, 1999 UNC-84 localizes to the nuclear envelope and is required for nuclear migration and anchoring during *C. elegans* development. Development 126: 3171–3181.
Maloof, J. N., and C. Kenyon, 1998 The Hox gene lin-39 is required during *C. elegans* vulval induction to select the outcome of Ras signaling. Development 125: 181–190.

Marri, S., and B. P. Gupta, 2009 Dissection of lin-11 enhancer regions in *Caenorhabditis elegans* and other nematodes. Dev. Biol. 325: 402–411.

Maydan, J. S., S. Flibotte, M. L. Edgley, J. Lau, R. R. Selzer *et al.*, 2007 Efficient high-resolution deletion discovery in *Caenorhabditis elegans* by array comparative genomic hybridization. Genome Res. 17: 337–347.

McGee, M. D., R. Rillo, A. S. Anderson, and D. A. Starr, 2006 UNC-83 IS a KASH protein required for nuclear migration and is recruited to the outer nuclear membrane by a physical interaction with the SUN protein UNC-84. Mol. Biol. Cell 17: 1790–1801.

McGrath, P. T., Y. Xu, M. Ailion, J. L. Garrison, R. A. Butcher *et al.*, 2011 Parallel evolution of domesticated Caenorhabditis species targets pheromone receptor genes. Nature 477: 321–325.

Mello, C. C., J. M. Kramer, D. Stinchcomb, and V. Ambros, 1991 Efficient gene transfer in *C.elegans*: extrachromosomal maintenance and integration of transforming sequences. EMBO J. 10: 3959–3970.

Miller, M. A., A. D. Cutter, I. Yamamoto, S. Ward, and D. Greenstein, 2004 Clustered organization of reproductive genes in the *C. elegans* genome. Curr. Biol. 14: 1284–1290.

Myers, T. R., and I. Greenwald, 2007 Wnt signal from multiple tissues and lin-3/EGF signal from the gonad maintain vulval precursor cell competence in *Caenorhabditis elegans*. Proc. Natl. Acad. Sci. USA 104: 20368–20373.

Newman, A. P., and P. W. Sternberg, 1996 Coordinated morphogenesis of epithelia during development of the *Caenorhabditis elegans* uterine-vulval connection. Proc. Natl. Acad. Sci. USA 93: 9329–9333.

Newman, A. P., G. Z. Acton, E. Hartwieg, H. R. Horvitz, and P. W. Sternberg, 1999 The lin-11 LIM domain transcription factor is necessary for morphogenesis of *C. elegans* uterine cells. Development 126: 5319–5326.

Penigault, J. B., and M. A. Felix, 2011a Evolution of a system sensitive to stochastic noise: P3.p cell fate in Caenorhabditis. Dev. Biol. 357: 419–427.

Penigault, J. B., and M. A. Felix, 2011b High sensitivity of *C. elegans* vulval precursor cells to the dose of posterior Wnts. Dev. Biol. 357: 428–438.

Rudel, D., and J. Kimble, 2001 Conservation of glp-1 regulation and function in nematodes. Genetics 157: 639–654.

Sarafi-Reinach, T. R., T. Melkman, O. Hobert, and P. Sengupta, 2001 The lin-11 LIM homeobox gene specifies olfactory and chemosensory neuron fates in C. elegans. Development 128: 3269–3281.

Seetharaman, A., P. Cumbo, N. Bojanala, and B. P. Gupta, 2010 Conserved mechanism of Wnt signaling function in the specification of vulval precursor fates in *C. elegans* and *C. briggsae*. Dev. Biol. 346: 128–139.

Sommer, R. J., 2005 Evolution of development in nematodes related to *C. elegans* (December 14, 2005). WormBook, ed. The *C. elegans* Research Community WormBook, doi/10.1895/wormbook.1.10.1, http://www.wormbook.org.

Sommer, R. J., and P. W. Sternberg, 1996 Evolution of nematode vulval fate patterning. Dev. Biol. 173: 396–407.

Sommer, R. J., L. K. Carta, and P. W. Sternberg, 1994 The evolution of cell lineage in nematodes. Dev. Suppl. 1994: 85–95.

Starr, D. A., 2011 Watching nuclei move: insights into how kinesin-1 and dynein function together. BioArchitecture 1: 9–13.

Starr, D. A., G. J. Hermann, C. J. Malone, W. Fixsen, J. R. Priess *et al.*, 2001 *unc-83* encodes a novel component of the nuclear envelope and is essential for proper nuclear migration. Development 128: 5039–5050.

Stein, L. D., Z. Bao, D. Blasiar, T. Blumenthal, M. R. Brent *et al.*, 2003 The genome sequence of *Caenorhabditis briggsae*: a platform for comparative genomics. PLoS Biol. 1: E45.

Sternberg, P. W., 2005 Vulval development (June 25, 2005). WormBook, ed. The *C. elegans* Research Community WormBook, doi/10.1895/wormbook.1.10.1, http://www.wormbook.org.

Sternberg, P. W., and H. R. Horvitz, 1986 Pattern formation during vulval development in *C. elegans*. Cell 44: 761–772.

Sulston, J. E., 1976 Post-embryonic development in the ventral cord of Caenorhabditis elegans. Philos. Trans. R. Soc. Lond. B. Biol. Sci. 275: 287–297.

Sulston, J. E., and H. R. Horvitz, 1981 Abnormal cell lineages in mutants of the nematode *Caenorhabditis elegans*. Dev. Biol. 82: 41–55.

Sulston, J. E., and J. G. White, 1980 Regulation and cell autonomy during postembryonic development of Caenorhabditis elegans. Dev. Biol. 78: 577–597.

Trent, C., N. Tsuing, and H. R. Horvitz, 1983 Egg-laying defective mutants of the nematode *Caenorhabditis elegans*. Genetics 104: 619–647.

True, J., and E. Haag, 2001 Developmental system drift and flexibility in evolutionary trajectories. Evol. Dev. 3: 109–119.

Weinshenker, D., G. Garriga, and J. H. Thomas, 1995 Genetic and pharmacological analysis of neurotransmitters controlling egg laying in *C. elegans*. J. Neurosci. 15: 6975–6985.

Wood, W. B., 1988 *The nematode Caenorhabditis elegans*. Cold Spring Harbor Laboratory Press, New York.

Zhao, Z., T. J. Boyle, Z. Bao, J. I. Murray, B. Mericle *et al.*, 2008 Comparative analysis of embryonic cell lineage between *Caenorhabditis briggsae* and *Caenorhabditis elegans*. Dev. Biol. 314: 93–99.

Zhao, Z., S. Flibotte, J. I. Murray, D. Blick, T. J. Boyle *et al.*, 2010 New tools for investigating the comparative biology of *Caenorhabditis briggsae* and *C. elegans*. Genetics 184: 853–863.

Communicating editor: D. S. Fay

Developmental Biology 346 (2010) 128–139

Contents lists available at ScienceDirect

Developmental Biology

journal homepage: www.elsevier.com/developmentalbiology

Evolution of Developmental Control Mechanism

Conserved mechanism of Wnt signaling function in the specification of vulval precursor fates in *C. elegans* and *C. briggsae*

Ashwin Seetharaman [1,2], Philip Cumbo [1], Nagagireesh Bojanala [3], Bhagwati P. Gupta *

Department of Biology, McMaster University, Hamilton, ON, Canada L8S 4K1

ARTICLE INFO

Article history:
Received for publication 9 February 2010
Revised 17 June 2010
Accepted 1 July 2010
Available online 17 July 2010

Keywords:
Nematode
C. elegans
C. briggsae
Vulval development
Signal transduction
Wnt signaling

ABSTRACT

The *C. elegans* hermaphrodite vulva serves as a paradigm for understanding how signaling pathways control organ formation. Previous studies have shown that Wnt signaling plays important roles in vulval development. To understand the function and evolution of Wnt signaling in *Caenorhabditis* nematodes we focused on *C. briggsae*, a species that is substantially divergent from *C. elegans* in terms of the evolutionary time scale yet shares almost identical morphology. We isolated mutants in *C. briggsae* that display multiple pseudo-vulvae resulting from ectopic VPC induction. We cloned one of these loci and found that it encodes an Axin homolog, Cbr-PRY-1. Our genetic studies revealed that *Cbr-pry-1* functions upstream of the canonical Wnt pathway components *Cbr-bar-1* (*β-catenin*) and *Cbr-pop-1*(*tcf/lef*) as well as the Hox target *Cbr-lin-39* (*Dfd/Scr*). We further characterized the *pry-1* vulval phenotype in *C. briggsae* and *C. elegans* using 8 cell fate markers, cell ablation, and genetic interaction approaches. Our results show that ectopically induced VPCs in *pry-1* mutants adopt 2° fates independently of the gonad-derived inductive and LIN-12/Notch-mediated lateral signaling pathways. We also found that *Cbr-pry-1* mutants frequently show a failure of P7.p induction. A similar, albeit low penetrant, defect is also observed in *C. elegans pry-1* mutants. The genetic analysis of the P7.p induction defect revealed that it was caused by altered regulation of *lin-12* and its transcriptional target *lip-1* (MAP kinase phosphatase). Thus, our results provide evidence for LIN-12/Notch-dependent and independent roles of Wnt signaling in promoting 2° VPC fates in both nematode species.

© 2010 Elsevier Inc. All rights reserved.

Introduction

Multicellular organisms have evolved complex cell communication machinery that enables cells to recognize and respond to a diverse range of extracellular signals. This interaction is crucial for the survival of organisms and their ability to function as coherent systems. Communication between cells and their environment is mediated by receptors that interact with specific ligands to transduce the signal into the cell. This leads to the activation of a cascade of intracellular proteins, many of which are components of a relatively small set of evolutionarily conserved signaling pathways, such as Ras, Notch, and Wnt (Bray, 2006; Eisenmann, 2005; Logan and Nusse, 2004; Sundaram, 2005). Among these, the Wnt signaling pathway has been shown to control diverse developmental processes including cell proliferation, cell polarity, and cell migration (Eisenmann, 2005; Widelitz, 2005). Studies on Wnt signaling have identified several genes that encode pathway components such as Wnt (ligand), Frizzled (receptor) and β-Catenin (transcriptional regulator). Analysis of their function has revealed that in normal cells, in the absence of Wnt ligands, β-Catenin is actively degraded by the action of a protein complex that contains scaffolding proteins Axin and APC and a serine/threonine kinase GSK3β (Logan and Nusse, 2004). The interaction of Wnts with Frizzled receptors activates the pathway leading to the dissociation of this complex, allowing cytoplasmic β-Catenin to translocate to the nucleus and interact with the TCF/LEF factor to regulate gene transcription.

The nematode *C. elegans* is a leading model organism to understand the mechanism of Wnt signaling function in development. Genetic studies in *C. elegans* have shown that Wnt signaling controls multiple processes including embryonic patterning, gonadogenesis, neuronal differentiation, male hook formation, and vulval development (Eisenmann and Kim, 2000; Eisenmann et al., 1998; Gleason et al., 2002; Maloof et al., 1999; Rocheleau et al., 1997; Salser and Kenyon, 1992; Siegfried and Kimble, 2002; Sternberg and Horvitz, 1988; Thorpe et al., 1997; Yu et al., 2009). The downstream targets of the pathway include three Hox genes, *lin-39 (Deformed/Sex combs reduced (Dfd/Scr) family)*, *mab-5 (Antennapedia/Ultrabithorax/abdominal-A (Antp/Ubx/Abd-A) family)* and *egl-5 (Abdominal-B (Abd-B) family)* that are expressed in multiple tissues and control diverse cell fates (Eisenmann, 2005; Kenyon et al., 1997).

Due to its simplicity, the *C. elegans* vulva has been successfully used to study the regulation and function of Wnt signaling pathway

* Corresponding author. Fax: +1 905 522 6066.
E-mail address: guptab@mcmaster.ca (B.P. Gupta).
[1] Co-first authors.
[2] Present address: University of Toronto, Ontario, Canada.
[3] Present address: Biology Center, ASCR, Institute of Parasitology, Budweis, Czech Republic, 37005.

0012-1606/$ – see front matter © 2010 Elsevier Inc. All rights reserved.
doi:10.1016/j.ydbio.2010.07.003

components. The vulva develops from three of six ventral hypodermal cells (termed P3.p to P8.p) that escape fusion to the surrounding hypodermal syncytium, hyp7, during the L1 stage and become vulval precursor cells (VPCs). This process is mediated by *lin-39* since all Pn.p cells in *lin-39* mutants fuse to hyp7 in the L1 stage. The *lin-39* activity is also required during the L2 stage to prevent VPCs from fusing to hyp7, and maintaining their competence to respond to patterning signals. The L2-stage expression of *lin-39* is positively regulated by the BAR-1 (β-Catenin)-mediated canonical Wnt signaling pathway. In *bar-1* mutants *lin-39* activity is greatly reduced which causes VPCs to inappropriately fuse with hyp7 (Eisenmann et al., 1998). The other Wnt pathway components that regulate VPC competence include 5 Wnt ligands (LIN-44, CWN-1, CWN-2, EGL-20, and MOM-2), 3 Frizzled receptors (LIN-17, MOM-5, and MIG-1), PRY-1 (Axin), and POP-1 (TCF/LEF) (Eisenmann, 2005; Gleason et al., 2002; Gleason et al., 2006; Inoue et al., 2004). The expression analysis of Wnt pathway genes has revealed that multiple tissues could act as sources of Wnt signals (including gonad, muscles, and many cells in the tail region) (Gleason et al., 2006; Herman et al., 1995; Inoue et al., 2004; Whangbo and Kenyon, 1999). The finding that Wnt ligands form anteroposterior gradient and pattern certain cell fates (Coudreuse et al., 2006) provides support to a model that similar signals originating from non-vulval tissues may differentially affect VPC fates.

In addition to Wnt, VPCs also respond to inductive signaling initiated by the LIN-3/Epidermal Growth Factor (EGF) ligand and lateral signaling via the LIN-12/Notch receptor (Greenwald, 2005; Sternberg, 2005). The LIN-3/EGF, secreted by a gonadal anchor cell (AC), interacts with the LET-23/EGF receptor and initiates a MPK-1/MAP kinase-mediated signaling pathway in VPCs. This causes P6.p to adopt a 1° fate. The interactions between P(5-7).p, mediated by LIN-12/Notch lateral signaling, confers a 2° fate on P5.p and P7.p. The induced VPCs, P(5-7).p, divide during L3/L4 stages to generate 22 progeny that differentiate to form 7 different cell types (vulA to vulF) (Sharma-Kishore et al., 1999). The remaining uninduced VPCs (P3.p, P4.p and P8.p) adopt a 3° fate and fuse to hyp7. The presence of various regulators of the signaling pathways, genetic redundancies, as well as crosstalks between pathways, ensures that a 3°-3°-2°-1°-2°-3° spatial pattern is reproducibly generated.

The simplicity and ease of experimental manipulations of the vulva has facilitated comparative developmental analysis among nematode species. These findings have revealed similarities and differences in some of the underlying developmental mechanisms (Eizinger and Sommer, 1997; Felix, 2005, 2007; Sommer, 2005; Sommer and Sternberg, 1996; Tian et al., 2008; Zheng et al., 2005). For example, the *lin-17*/*Frizzled* receptor ortholog in *Pristionchus pacificus* represses vulval cell fates, whereas in *C. elegans lin-17* promotes VPC competence and cell fates (Eisenmann, 2005; Zheng et al., 2005). The *P. pacificus* and *Oscheius tipulae lin-39* orthologs represent another case of evolutionary conservation and divergence of gene function. While the *O. tipulae lin-39* promotes VPC competence similar to *lin-39* in *C. elegans* (Louvet-Vallee et al., 2003), the *P. pacificus lin-39* prevents VPCs from undergoing programmed cell death (Eizinger and Sommer, 1997).

Among the species that are closely related to *C. elegans*, *C. briggsae* is used extensively in comparative studies (Gupta et al., 2007). Although the two species diverged roughly 30 million years ago (Cutter, 2008), morphologically they appear very similar. This provides a unique opportunity to study gene function and signaling pathways in specifying homologous processes. We are taking a forward genetics approach to study the mechanism of vulval development in *C. briggsae*. This work focuses on *pry-1* (*Axin* family) and its interactions with Wnt and LIN-12/Notch signaling pathway components in VPC fate specification. We found that the *Cbr-pry-1* mutants display a unique pattern of vulval induction defect that is characterized by ectopically induced P3.p, P4.p, and P8.p, and an uninduced P7.p. The genetic analysis of *Cbr-pry-1* interaction with other genes revealed that *Cbr-bar-1 (β-catenin)-Cbr-pop-1 (tcf/lef)*-mediated canonical Wnt signaling plays an essential role in promoting VPC competence and cell proliferation in *C. briggsae*. The downstream targets of the pathway include the *Hox* gene *Cbr-lin-39*. To understand the mechanism of *pry-1*-mediated Wnt signaling function we used a combination of cell fate markers, laser microsurgery, and genetic interaction experiments. The findings show that ectopically induced VPCs in *pry-1* mutants, in both *C. elegans* and *C. briggsae,* acquire 2° fate independently of the gonad-derived inductive signaling and LIN-12/Notch-mediated lateral signaling pathways. However, interestingly, in the case of P7.p our data suggests that *pry-1* acts genetically upstream of *lin-12* and its transcriptional target *lip-1* to promote vulval cell fate. Taken together these findings reveal that Wnt signaling utilizes multiple mechanisms to specify the spatial pattern of VPC fates in *C. elegans* and *C. briggsae*.

Materials and Methods

Strains and general methods

The general methods for culturing and genetic manipulations have been previously described (Brenner, 1974). All experiments were carried out at 22 °C unless otherwise noted. The staging of animals was primarily based on the gonad morphology as described in Wormatlas (Hall and Altun, 2008). The gonad arms initiate turning during mid-L3 stage and by mid-L4 stage arms are in close proximity to the center of vulval invagination formed by P(5-7).p progeny.

Various mutations used in this study are listed below in the alphabetical order. Where known, the locations of mutations and transgenic strains are indicated. The '*Cbr*' prefix denotes the *C. briggsae* ortholog of a *C. elegans* gene.

C. briggsae: AF16 (wild type), *Cbr-pry-1 (sy5353) I, Cbr-pry-1 (sy5270) I, Cbr-pry-1(sy5411) I, Cbr-unc-119(st20000) III, mfIs5[Cbr-egl-17::GFP, myo-2::GFP], mfIs8[Cbr-zmp-1::GFP, myo-2::GFP], mfIs29 [lip-1::GFP, myo-2::GFP], mfEx33[dlg-1::GFP, myo-2::dsRed], mfIs42[sid-2(+), myo-2::dsRed], bhEx59[hsp::Cbr-pry-1, myo-2::GFP], bhEx83[Cbr-pry-1-5 kb::GFP, unc-119(+)], bhEx84[Cbr-pry-1-3.8 kb::GFP, unc-119 (+)].*

C. elegans: N2 (wild type), *lin-12(n137) III, lin-12(n952) III, lin-12 (n676n909) III, lip-1(zh15) IV, pop-1(hu9) I, pry-1(mu38) I, unc-119 (ed4) III, ayIs4[egl-17::GFP, dpy-20(+)] I, bhEx53[daf-6::YFP, myo-2::GFP], deIs4[dpy-20(+), ajm-1::GFP, lin-39TX::GFP (yeast DNA)], muIs32 [mec-7::GFP] II, syIs54[ceh-2::GFP, unc-119(+)] II, syIs80[lin-11::GFP, unc-119(+)] III, syIs101[dhs-31::GFP, unc-119(+)] IV, wyEx3372[syg-2::GFP], zhIs4[lip-1::GFP, unc-119(+)] III.*

The transgenic animals carrying extrachromosomal arrays were generated by standard microinjection technique (Mello et al., 1991) using *C. elegans unc-119* (Maduro and Pilgrim, 1995) and *myo-2::GFP* (pPD118.33) (S. Q. Xu, B. Kelly, B. Harfe, M. Montgomery, J. Ahnn, S. Getz and A. Fire, personal communication) as transformation markers. The concentrations of plasmids that were injected as part of this study are: *hsp::Cbr-pry-1* 25 ng/μl, *Cbr-pry-1::GFP* (each of 3.8 kb and 5 kb promoter fragment) 100 ng/μl, *daf-6::YFP* 100 ng/μl.

The synchronized L1 stage *hsp::Cbr-pry-1* animals were heat shocked at 31 °C for 24 hrs and subsequently grown at 22 °C until adulthood. Cell ablation experiments were performed as described (Avery and Horvitz, 1987). The gonad precursors (Z1 to Z4) were ablated during the L1 stage whereas VPCs were ablated during the L2 stage. Worms were recovered from slides and allowed to grow until L4 stage. Vulval phenotypes were examined using Nomarski optics.

Vulval phenotype and induction analysis

We scored VPC competence and induction during the L2-L4 stages. A VPC was considered induced if it gave rise to 4 or more progeny that had invaginated. With the exception of P7.p and P8.p in *pry-1* mutants

that appear morphologically similar to P12.pa (referred as P12.pa-like fate), an uninduced VPC can adopt either an F fate (no division and fusion to hyp7 syncytium in L2) or a 3° fate (one division followed by fusion of both daughters to hyp7 in L3). In wild-type animals (*C. elegans* and *C. briggsae*) P4.p and P8.p always adopt a 3° fate, while P3.p does in ~20°-50% of cases (F fate in the remainder). Statistical analyses were performed using InStat 2.0 (GraphPad) Software. Two-tailed P values were calculated in unpaired t tests and values less than 0.05 were considered statistically significant.

Unlike wild type animals in which P3.p, P4.p and P8.p fuse to hyp7, in *pry-1* mutants these Pn.p cells can be ectopically induced to divide (termed 'Overinduced'). Additionally, *pry-1* mutants frequently show a failure of P7.p induction (termed 'Underinduced'). Thus, the same animal can exhibit both Overinduced and Underinduced phenotypes.

Isolation and mapping of C. briggsae pry-1

The *Cbr-pry*-1 mutants were isolated in a genetic screen for animals that exhibit defects in vulval induction. Wild-type L4 stage AF16 animals were fed with 25 mM Ethyl Methanesulfonate (EMS; Sigma) for 3 hrs using standard procedures (Wood, 1988). More than 500,000 haploid genomes were screened and F2 animals showing multiple pseudo-vulvae were isolated. Putative lines that showed a reproducible phenotype were retained and backcrossed three to four times.

The complementation and linkage studies revealed that three mutants *sy5270, sy5353* and *sy5411* define a locus on LG*I* and map close to a levamisole-resistant mutant *lev(sy5440)* (*www.briggsae.org*). Subsequently, polymorphism (insertion-deletion or indel)-based mapping (using HK104 isolate) was used to determine the physical location of *sy5353*. The indels were computationally identified and validated by PCR amplification of roughly 250 bp flanking sequences and analyzed by agarose gel electrophoresis (Koboldt et al., 2010). Of the five Chromosome I indels, *bhP1* (fpc3441), *bhP7* (fpc4171), *bhP19* (fpc2695), *bhP29* (fpc4140) and *bhP42* (fpc4184), three (*bhP1, bhP7* and *bhP42)* showed strong linkage to *sy5353* (based on band intensities of PCR amplified DNA on 4% Invitrogen UltraPure Agarose 1000). The *bhP29* was weakly linked (Figs. 1A and S1, data not shown) whereas *bhP19* showed no linkage to *sy5353*. We also recovered recombinants between *sy5353, bhP1* and *bhP42* and determined that *sy5353* maps 2 mu away from *bhP1* (1 recombinant out of the total 46 chromosomes tested) whereas *bhP1* and *bhP42* are 5 mu apart (3 recombinants out of the total 60 chromosomes tested). A search for the *C. elegans* orthologs in *C. briggsae* genome (CB3 assembly) identified *Cbr-pry-1* as a candidate gene that is ~1.2 Mb away from *bhP42 (www.wormbase.org)*.

Molecular biology

All PCR and sequencing primers are listed in Supplementary Table 1. The *pry-1(mu38) ayIs4; lin-12(n676n909), pry-1(mu38); lip-1 (zh15),* and *pop-1(hu9); muIs32; lin-12(n952)* strains were confirmed by sequencing *lin-12* (primers GL477/GL478), *lip-1* (GL466/GL467/GL468), and *pop-1* (GL508/GL509) mutations, respectively (Berset et al., 2001; Greenwald and Seydoux, 1990; Korswagen et al., 2002).

The *Cbr-pry-1* locus was PCR amplified in two large fragments (excluding intron 7) using primers GL104, GL106 (3.6 kb) and GL107, GL105 (2.2 kb). No mutation was detected in any of the exons or exon-intron junctions in *sy5270* animals suggesting that the mutation may be located in a non-coding regulatory region. In the case of *sy5353* there is a G to A transition at the first base of intron 6 that is predicted to disrupt the splicing donor site. There are two in frame stop codons (TAA and TGA) within 40 bp. The *sy5411* allele carries a GC insertion in exon 5 (+1761 from translational start site, flanking sequences TCGGCGCGC and CAGCCGTAC) that is expected to alter the reading frame leading to the introduction of two premature in frame stop codons (TGA and TAA) within 125 bp. All mutations were confirmed by sequencing both strands.

To construct *Cbr-pry-1::GFP*, 3.6 kb and 5 kb 5' UTR fragments were amplified by PCR using primers GL306/GL218 and GL217/GL218, respectively. The PCR products were digested (*Sph*I and *Sal*I for 3.6 kb, *Pst*I and *Sal*I for 5 kb) and subcloned into pPD95.69 (Fire lab vector, *www.addgene.com*). The *daf-6::YFP* construct was made by subcloning a 3 kb *Pst*I, *Kpn*I digested 5' UTR fragment (amplified by PCR using primers GL176/GL177) into pPD136.61.

All RNAi constructs were made by subcloning PCR products into *Sac*I, *Kpn*I digested double-T7 RNAi vector L4440 (Fire Lab vector kit, *www.addgene.com*). The DNA fragments are as follows: 0.9 kb genomic fragment of *Cbr-sys-1* (primers GL311/GL312), 2.3 kb genomic fragment of *Cbr-pop-1* (GL184/GL185), 2.4 kb genomic fragment of *Cbr-lin-39* (GL313/GL314), and 1.5 kb genomic fragment of *Cbr-lip-1* (GL464/GL465). The heat-shock promoter (hsp16-41) driven *Cbr-pry-1* construct was made by subcloning the full-length *Cbr-pry-1* cDNA into the Fire lab pPD49.83 vector.

RNAi

Since the wild type *C. briggsae* (AF16) is resistant to environmental RNAi, we used a transgenic strain *mfIs42* that carries wild type copy of the *C. elegans sid-2* gene. *mfIs42* animals are sensitive to environmental RNAi similar to the wild-type *C. elegans* (Winston et al., 2007). RNAi was performed on plates containing 0.6% Na_2HPO_4, 0.3% KH_2PO_4, 0.1% NH_4Cl, 0.5% Casamino Acids, 2% Agar, 1 mM $CaCl_2$, 1 mM $MgSO_4$, 0.0005% cholesterol, 0.2% β-lactose, and 50 μg/ml Carbenicillin. Plates were seeded with 100 μl of overnight grown HT115 bacterial culture in LB and Carbenicillin media that produces dsRNA of the gene of interest. Three to 5 L4 stage worms were placed on RNAi plates and the phenotypes of F1 progeny were examined. For genes that caused sterility and early stage lethality, animals were subjected to RNAi treatment during L1 larval stage. All RNAi experiments were repeated 3-4 times and batches that produced consistent results were analyzed.

The *C. briggsae* genome contains two *lin-12*-like genes one of which appears to be a *Cbr-lin-12* paralog (99% sequence identity) *(www.wormbase.org)*. The *Cbr-lin-12* RNAi construct used in this study is expected to inactivate both copies. This construct was described earlier and used to study *lin-12* function in *C. briggsae* (Felix, 2007). The amplified genomic region lacks significant sequence similarity to *Cbr-glp-1*, a *Cbr-lin-12*/*Notch* family member, ruling out the possibility of an RNAi off-target effect. Furthermore, the *Cbr-lin-12 and Cbr-glp-1* RNAi phenotypes are different and can be easily distinguished (Rudel and Kimble, 2001; Rudel and Kimble, 2002) (BPG, unpublished). Hence the *Cbr-lin-12* RNAi results described below are likely to be specific to *Cbr-lin-12* and its paralog.

Results

Isolation and molecular characterization of C. briggsae pry-1

To identify genes involved in vulval development in *C. briggsae*, we carried out EMS mutagenesis screens and isolated mutants that exhibit ectopic vulval induction leading to the formation of multiple pseudo-vulvae in adults. Out of 10 such mutants that were recovered from the screen, three (*sy5270, sy5353*, and *sy5411*) failed to complement (Table 1) and defined a locus on chromosome 1. All three alleles showed high frequency of ectopically induced VPCs (Table 1). In many cases (40%; n = 25 for *sy5353*) the migration of gonad arms was also defective. The males also showed abnormal tail morphologies such as ectopic anterior rays, crumpled spicules and pseudovulvae-like structures (data not shown).

To understand the mechanism of *sy5353* function in vulval development, we determined the molecular identity of the locus. A combination of phenotypic markers, polymorphism-based mapping,

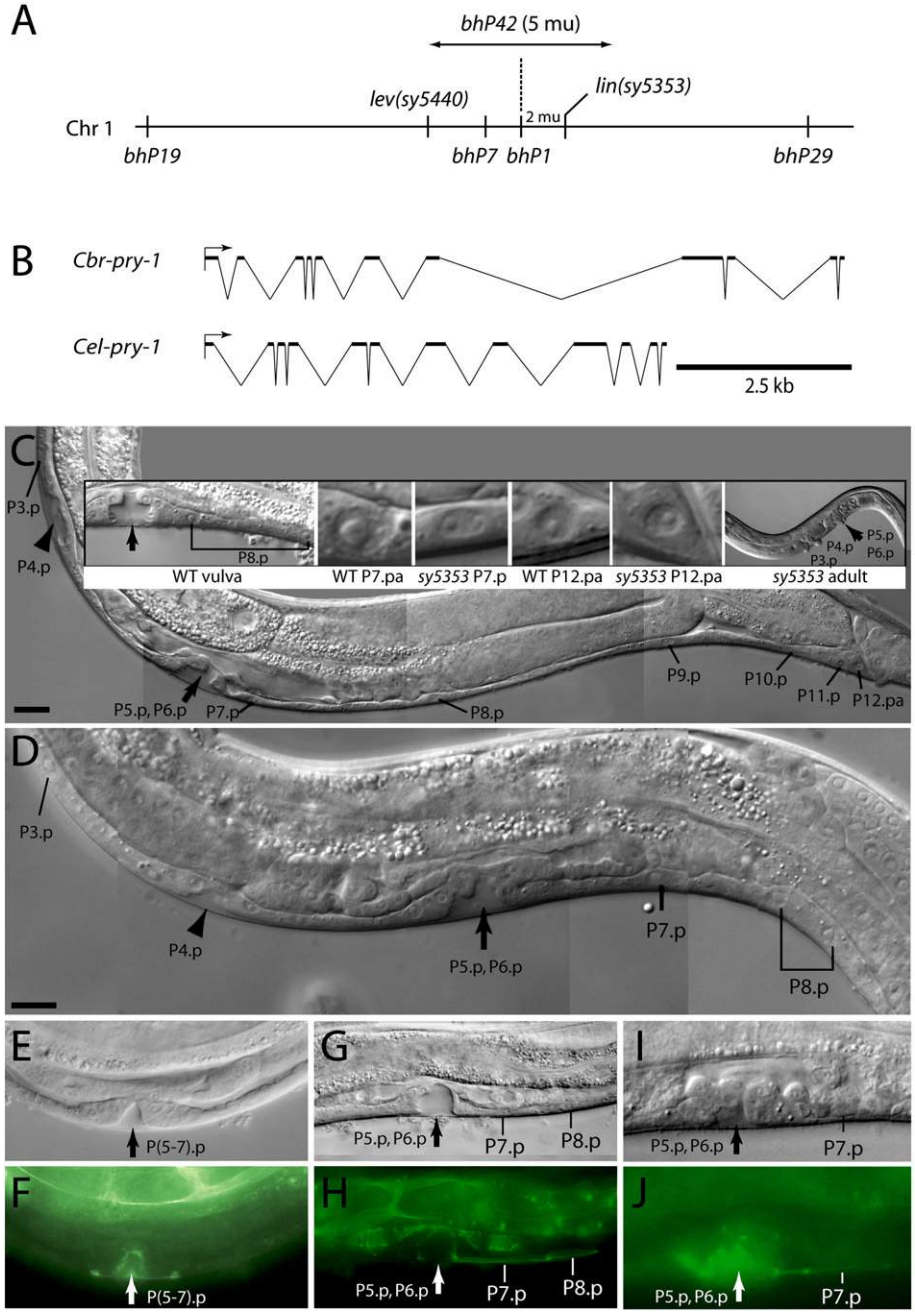

Fig. 1. (A) The locations of various markers and *lin(sy5353)* on chromosome 1. The *sy5353* mutation is tightly linked to indels *bhP7, bhP1* and *bhP42*. (B) The open reading frames (ORFs) of *pry-1* in *C. briggsae* and *C. elegans*. Major differences between the two ORFs include one less exon and two larger introns towards the 3' end in *C. briggsae* compared to *C. elegans*. (C-J) Vulval induction defect in *pry-1* mutants. Thick arrows mark the main vulva whereas arrowheads mark ectopic vulval invaginations. (C) The posterior VPCs are uninduced in a *sy5353* animal. The inset panels show a wild-type (WT) vulva and the nuclei of P7.p, P7.pa and P12.pa in WT and *sy5353* animals, and a *sy5353* adult showing anterior pseudovulvae. (D) A *pry-1(mu38)* animal showing induced P4.p and uninduced P7.p. (E-J) Analysis of the cell fusion defect using *dlg-1::GFP (mfEx33)* in *Cbr-pry-1(sy5353)* and *ajm-1::GFP (dels4)* in *pry-1(mu38)*. Unlike the wild type (E, F) where the progeny of P(5-7).p fuse to form seven concentric toroids, in the *sy5353* animal (G, H) P7.p and P8.p precursors remain unfused. (I, J) An unfused P7.p in *pry-1(mu38)* revealed by *ajm-1::GFP* expression. Anterior is to the left in all cases. The scale bars in C (same for E-J, except inset in C) and D are 10 μm.

and *C. briggsae* genome sequence assembly (Hillier et al., 2007) enabled us to take a candidate gene approach. A search for the *C. elegans* orthologs in the vicinity of linked polymorphisms *bhP1, bhP7* and *bhP42* (Fig. 1A and Supplementary Fig. 1) revealed a Wnt pathway component *pry-1* (*Axin* family) that is known to negatively regulate vulval induction (Gleason et al., 2002). The results of the following experiments indicate that *sy5353* is an allele of *C. briggsae pry-1*. First, we found that the RNAi-mediated knockdown of *Cbr-pry-1* phenocopies *sy5353* (Table 1). Second, overexpression of *Cbr-pry-1* full-length cDNA (using *hsp16-41* heat-shock promoter, *hsp::Cbr-pry-1*) rescues the mutant phenotype in more than half of the *sy5353* animals (53% wild type, n = 163, compared to 3% wild type, n = 39 in *sy5353* animals without heat shock). Finally, we sequenced *Cbr-pry-1* alleles and identified *sy5353* and *sy5411* mutations that introduce premature in-frame stop codons (see Materials and Methods and Supplementary Fig. 2), suggesting that both are likely to be *Cbr-pry-1* hypomorphs.

A comparison of the *pry-1* genomic regions between *C. elegans* and *C. briggsae* revealed the absence of one exon, as well as comparatively larger sizes for two introns in *C. briggsae* (Fig. 1B). We aligned protein sequences of Axin family members in nematodes and vertebrates to

Table 1
Vulval induction analysis in mutant and RNAi-treated animals.

Genotype	RNAi target	% Induced VPCs						% Overinduced	Average VPC induction	n
		P3.p	P4.p	P5.p	P6.p	P7.p	P8.p			
+	-	0	0	100	100	100	0	0	3.0	50
Cbr-pry-1(sy5353)	-	39	82	100	100	17	21	93	3.7 +/- 0.9	44
Cbr-pry-1(sy5411)	-	76	86	98	100	2	12	95	3.7 +/- 0.7	43
Cbr-pry-1(sy5270)	-	53	47	100	100	77	32	86	4.1 +/- 1.1	50
Cbr-pry-1(sy5270/sy5353)	-	58	68	100	100	11	32	nd	nd	47
Cbr-pry-1(sy5270/sy5411)	-	54	74	100	100	4	36	nd	nd	50
+	-	X	X	X	X	100	57	na	na	7
Cbr-pry-1(sy5353)	-	X	X	X	X	0	0	na	na	8
mfIs42	-	0	0	100	100	100	0	0	3.0	100
mfIs42	*Cbr-pry-1*	2	3	100	100	98	2	6	3.1 +/- 0.3	90
Cbr-pry-1(sy5353); mfIs42	-	58	86	100	100	38	20	98	3.8 +/- 0.9	50
mfIs42	*Cbr-sys-1*	0	0	100	100	100	0	0	3.0	27
Cbr-pry-1(sy5353); mfIs42	*Cbr-sys-1*	78	70	100	100	59	22	82 (P=0.2225)	4.2 +/- 1.2 (P=0.1628)	27
mfIs42	*Cbr-bar-1*	0	0	100	100	100	0	0	3.0	30
Cbr-pry-1(sy5353); mfIs42	*Cbr-bar-1*	26	26	100	100	86	17	49 (P<0.0001)	3.4 +/- 0.8 (P=0.0799)	35
mfIs42	*Cbr-pop-1*	0	0	5	5	5	0	0	0.2 +/- 0.7	77
Cbr-pry-1(sy5353); mfIs42	*Cbr-pop-1*	12	22	78	83	54	12	31 (P<0.0001)	2.6 +/- 1.4 (P<0.0001)	59
mfIs42	*Cbr-mab-5*	0	0	100	100	100	0	0	3.0	100
Cbr-pry-1(sy5353); mfIs42	*Cbr-mab-5*	33	67	97	100	41	36	96 (P=0.8340)	3.8 +/- 0.8 (P=0.8159)	70
mfIs42	*Cbr-lin-39*	0	0	10	55	24	0	0	0.9 +/- 0.9	29
Cbr-pry-1(sy5353); mfIs42	*Cbr-lin-39*	7	4	30	89	15	0	7 (P<0.0001)	1.4 +/- 1.1 (P<0.0001)	27
mfIs42	*Cbr-lin-12*	0	5	100	100	100	0	5	3.1 +/- 0.2	44
Cbr-pry-1(sy5353); mfIs42	*Cbr-lin-12*	66	83	100	100	83	22	95 (P=0.8176)	4.5 +/- 1.0 (P<0.0022)	41
mfIs42	*Cbr-lip-1*	0	0	100	100	100	0	0	3.0	25
Cbr-pry-1(sy5353); mfIs42	*Cbr-lip-1*	60	55	100	100	71	19	88 (P=0.3683)	3.4 +/- 0.6 (P=0.097)	58
+	-	0	0	100	100	100	0	0	3.0	30
pry-1(mu38)	-	24	6	100	100	82	10	31	3.2 +/- 0.6	89
*pop-1(hu9)**	-	0	0	100	100	100	0	0	3.0	38
pop-1(hu9) pry-1(mu38)	-	0	0	100	100	97	0	0	3.0 +/- 0.2	31
+	*lin-12*	0	0	100	100	100	0	0	3.0	50
pry-1(mu38)	*lin-12*	38	13	100	100	85	8	49 (P=0.5364)	3.4 +/- 0.7 (P=0.2209)	53
+	*lip-1*	0	0	100	100	100	0	0	3.0	100
pry-1(mu38)	*lip-1*	16	7	100	100	98	4	28 (P=0.7305)	3.1 +/- 0.3 (P=1.0000)	57
lip-1(zh15)	-	0	0	100	100	100	0	0	3.0	30
pry-1(mu38); lip-1(zh15)#	-	65	47	100	100	96	68	92 (P<0.0001)	4.0 +/- 0.5 (P<0.0001)	77
lin-12(n952)	-	27	73	84	97	81	81	92	4.4 +/- 1.1	37
lin-12(n952)	*pop-1*	5	25	100	90	100	80	70 (P=0.1691)	3.9 +/- 1.0 (P=0.08)	20
*pop-1(hu9); lin-12(n952)**	-	0	31	88	100	100	94	100	3.8 +/- 0.5 (P=0.0107)	16
+	*lin-39*	0	0	55	55	73	0	0	1.8 +/- 0.8	22
lin-12(n952)	*lin-39*	0	13	30	39	39	9	9 (P<0.0001)	1.2 +/- 1.4 (P<0.0001)	23

'+' refers to wild-type genetic background (*C. briggsae* AF16 and *C. elegans* N2). 'X' denotes Pn.p cells that were ablated during the L2 stage. *Strains carry *mec-7::GFP (muls32)*. #Strain carries *egl-17::GFP (ayIs4)*. VPC: vulva precursor cell, n: number of animals examined, nd: not done, na: not applicable.

identify domains in *Cbr*-PRY-1 that may facilitate homodimerization and interactions with *C. briggsae* homologs of APC, GSK-3β and β-Catenin (Behrens et al., 1998; Ikeda et al., 1998; Luo et al., 2005; Schwarz-Romond et al., 2007) (Supplementary Fig. 3). The *C. briggsae* PRY-1 is 70% identical to its counterpart in *C. elegans* with various domains being 70-85% conserved (Supplementary Fig. 4). This level of identity is close to APR-1 (APC homolog; 77% identical) but much lower than GSK-3 (GSK-3β homolog; 95% identical).

pry-1 mutants exhibit both Overinduced and Underinduced phenotypes

The *Cbr-pry-1* alleles were isolated based on the presence of ectopic pseudo-vulvae in adults. The analysis of vulval phenotype in mid-L4 stage animals showed a unique defect in VPC induction pattern. Specifically, P3.p, P4.p, and P8.p were ectopically induced in most animals whereas P7.p remained uninduced (Table 1) (see Materials and Methods). The P5.p and P6.p fates were unaffected. We also looked at the placement of AC in such animals and found that it was always located on the top of P6.p and its descendents (data not shown). Frequently individual animals exhibited both Overinduced and Underinduced phenotypes (Fig. 1C). A similar, albeit less penetrant, defect was also observed in *C. elegans pry-1* mutants (Fig. 1D, Table 1). In some cases only P5.p and P6.p were induced, a phenotype that has previously been reported in *C. elegans* (Gleason et al., 2002). The vulval cell lineages of mutant animals further supported these findings (Table 2). Thus, *pry-1* appears to play a similar role in both species.

A careful examination of Pn.p cells in *Cbr-pry-1* mutants revealed an additional defect in that all P(7-11).p cell nuclei were significantly smaller in size compared to wild type, appearing similar to P12.pa (Fig. 1A inset). It remains to be determined whether such a morphological change is caused by transformation to P12.pa-like cell fate. This phenotype is distinct from *C. elegans pry-1(mu38)* which do not show an obvious change in the morphology of posterior Pn.p cells (except P11.p) (see P7.p in Fig. 1D, data not shown). Considering that mutations in *C. elegans* Wnt pathway genes cause cell fate transformation due to alterations in Hox gene expression (Korswagen et al., 2002; Maloof et al., 1999), it is tempting to speculate that similar changes may underlie the Pn.p transformation phenotype in *Cbr-pry-1* mutants.

We examined posterior VPCs in *pry-1* mutants using cell junction-associated markers *ajm-1* (in *C. elegans*) and *dlg-1* (in *C. briggsae*) that identify epithelial cell boundaries. The AJM-1 (novel coiled-coil protein) and DLG-1 (*Drosophila* Disc Large family) are localized to apical junctions and are required for maintaining the integrity and polarity of junctional subdomains (Bossinger et al., 2001; Firestein and Rongo, 2001; Koppen et al., 2001). The *GFP* reporters for these genes mark VPCs and their progeny that do not fuse to the hyp7 (see Figs. 1E,F for *dlg-1::GFP* expression) (Sharma-Kishore et al., 1999) (Marie-Anne Felix, personal communication), and remain competent to respond to patterning signals. We found that uninduced P7.p and

Table 2
Cell lineage analysis of *pry-1* mutants in *C. elegans* and *C. briggsae*.

Genotype	P3.p	P4.p	P5.p	P6.p	P7.p	P8.p	n
Wild type*	S/SS	SS	LLTN	TTTT	NTLL	SS	25#
pry-1(mu38)	SON	SS	LLTN	OOTL	SOL	NLL	1
	SS	SS	LLTN	TTTT	NTLL	SS	1
	LLON	SS	LLTN	TTTT	NTLL	SS	1
	S	SS	LLTN	TOOO	NTLL	SS	1
	SS	SS	LLON	OTOL	S	NNNN	1
	S	SS	LLON	TTTT	LDOO	S	1
Cbr-pry-1(sy5353)	S	SS	LLLN	TLOO	U	U	1
	SL	SS	LLLN	ONTO	U	U	1
	NNNN	SS	LLLN	TONN	U	NNNN	1
	LNN	LNNT	LLON	TOOT	NOLL	NN	1
	TNNO	LNNO	LLLN	OOTO	U	U	1
	LNND	NNNN	LLON	TTTT	NTLL	U	1
	ONS	LNNT	LLTN	OOTT	U	SS	1
	SS	SS	LLON	TOTO	U	DNL	1
Cbr-pry-1(sy5411)	SN	LLNN	LLTN	TTTT	UU	NN	1
	NOLL	NNOT	NNNN	TOOT	UU	NN	1
	NNNN	NNNN	NTON	TOTO	UU	U	1
Cbr-pry-1(sy5270)	SOO	LOO	LLON	OOOD	NTLL	SS	1
	NNON	LNNT	LLON	OTOL	U	ONNL	1
	OTNO	LONO	LLON	TTTT	NLLN	SS	1
	SS	SS	LLLN	OTTO	NOLL	SNN	1
	S	NNNO	LLLN	OOOO	U	NONO	1
	SS	SS	LLLN	OOOO	NN	SS	1
	LNNL	SNL	LLLN	OOTO	U	NODL	1

*Wild-type *C. elegans* (N2) and *C. briggsae* (AF16) animals. #In each case lineages were observed for 25 animals. S, cell fused with syncytium; T, transverse plane of cell division; L, longitudinal; O, oblique; D, division plane not observed; N, no cell division; U, unfused cells that did not divide and appeared morphologically similar to P12.pa; n, number of animals examined. The cells attached to cuticle are underlined. In all cases, anchor cell was located on the top of the P6.p progeny.

P8.p in *pry-1* mutants are frequently unfused (Figs. 1G-J), which indicates that their lack of proliferation may be due to other defects. We also observed some cases of unfused P(9-11).p in *pry-1* mutants, which is similar to that reported earlier (Myers and Greenwald, 2007). These results suggest that in addition to maintaining competence, Wnt signaling also plays an important role in promoting cell proliferation and differentiation.

To determine whether P7.p and P8.p induction in *pry-1* mutants is inhibited by some unknown signal from neighboring VPCs we carried out VPC isolation experiments in *C. briggsae*. For this P(3-6).p cells were ablated during the early L2 stage with P7.p and P8.p being left intact. In contrast to wild-type animals where isolated P7.p and P8.p always adopted induced fates, these VPCs in *Cbr-pry-1(sy5353)* animals failed to do so (Table 1). It is unclear whether a lack in competence is due to the inability of VPCs to respond to signals that promote vulval cell proliferation or the Pn.p cells adopted a non-vulval fate.

Cbr-pry-1 is expressed in vulval precursors and their progeny

The molecular cloning of *Cbr-pry-1* facilitated the analysis of its expression pattern during development. We designed transcriptional *GFP* reporter plasmids using the 5' upstream genomic region of *Cbr-pry-1* (3.6 kb and 5 kb) and generated transgenic lines in *C. briggsae*. The *Cbr-pry-1::GFP* was expressed throughout the development, a finding similar to the *C. elegans pry-1* (Korswagen et al., 2002). The earliest expression was observed in embryos in numerous hypodermal cells. During the larval stages, the majority of the expression was seen in neurons in the ventral hypodermal region (Figs. 2A-D). Between L2 and L3 stages *Cbr-pry-1::GFP* was expressed in all six VPCs (see Figs. 2A-D for subsets of Pn.p cells). There was no obvious difference in the level of GFP fluorescence among the VPCs. The expression continued to persist in the vulval progeny of L4 stage animals (Figs. 2E-H), suggesting that *Cbr-pry-1* may also play a role in differentiation and morphogenetic processes. This is consistent with the abnormal vulval morphology in *Cbr-pry-1* mutants (Figs. 1C,G).

Cbr-pry-1 interacts with Wnt pathway components and a nuclear target in C. briggsae

Given that *Cbr-pry-1* encodes an Axin-like protein and that Axins are bona fide components of the canonical Wnt signaling pathway, we tested the interaction of *Cbr-pry-1* with *C. briggsae* orthologs of *C. elegans* Wnt pathway genes in vulval cell proliferation. The *Cbr-sys-1 (β-catenin)* knock-down (by RNAi) had no significant effect on the *Cbr-pry-1(sy5353)* vulval phenotype (Table 1), although animals exhibited severe defects in gonad morphology and were frequently sterile (data not shown). However, a similar RNAi experiment involving another *β-Catenin*, *Cbr-bar-1*, strongly suppressed the Overinduced phenotype of *Cbr-pry-1(sy5353)* (Table 1), suggesting that *Cbr-bar-1* is likely to act genetically downstream of *Cbr-pry-1*. We also found that compared to control animals P7.p in *Cbr-pry-1(sy5353); Cbr-bar-1 (RNAi)* was significantly more induced ($p = 0.0002$, Table 1).

Next, we examined the role of the *tcf/lef* family member *Cbr-pop-1* in *Cbr-pry-1*-mediated vulval development. The RNAi-mediated knock-down of *Cbr-pop-1* suppressed ectopic VPC induction in *Cbr-pry-1(sy5353)* (54% induced, 10% P12.pa-like, 36% 3°, and no F fates, $n = 59$ animals compared to 38% induced, 62% P12.pa-like and no 3°, or F fates, $n = 50$ animals in control) (Table 1). Similar to *Cbr-bar-1* RNAi, we also found an increased number of induced P7.p in *Cbr-pry-1 (sy5353) Cbr-pop-1(RNAi)* animals (Table 1). Interestingly, *Cbr-pop-1 (RNAi)* animals alone showed severe defects in vulval cell proliferation (no P12.pa-like, 55% 3° and 29% F fates, $n = 25$) (Fig. 3A, Table 1), suggesting its essential role in regulating VPC competence and induction. Although no such defect was observed in *C. elegans pop-1 (RNAi)* and *pop-1(hu9)* (a viable hypomorph) animals, both strongly suppressed the *pry-1(mu38)* phenotype (Table 1 and data not shown). These results demonstrate that *bar-1-pop-1*-mediated canonical Wnt signaling plays a conserved role in vulval development in *C. elegans* and *C. briggsae*.

Studies in *C. elegans* have identified transcriptional targets of Wnt signaling that include Hox genes *lin-39 (Dfd/Scr* family) and *mab-5* (*Antp* Hox family) (Eisenmann, 2005). *lin-39* is required at multiple times in vulval cells. During the L2 stage, *lin-39*-mediated canonical Wnt signaling prevents VPCs from fusing to the hyp7 syncytium (Eisenmann et al., 1998). Later on, during the L3 stage, *lin-39* is involved in the specification of VPC fates (Eisenmann, 2005). Unlike *lin-39*, *mab-5* appears to play a limited role in vulval development. *mab-5* is expressed in P7.p and P8.p and regulates the responsiveness of these two cells to inductive signal (Clandinin et al., 1997; Salser et al., 1993). We found that the RNAi-mediated knock-down of *Cbr-mab-5* had no effect on VPC induction in either wild type or *Cbr-pry-1(sy5353)* animals (Table 1). By contrast *Cbr-lin-39* RNAi caused abnormal vulval morphology due to cell fusion and cell fate specification defects (37% F and 33% 3° fates, respectively; $n = 46$ Pn.p cells) (Fig. 3B, Table 1). We also examined the *Cbr-pry-1 (sy5353); Cbr-lin-39(RNAi)* animals and found that of the 54% of P(3-8).p ($n = 28$) that were unfused in L2 (i.e., did not adopt an F fate), one-third fused to hyp7 in L3 (3° fate) whereas the remaining cells were induced giving rise to vulval progeny that invaginated during L4 stage. Overall, the RNAi-mediated knock-down of *Cbr-lin-39* strongly suppressed the Overinduced phenotype of *Cbr-pry-1(sy5353)* animals (Table 1). These results demonstrate that, similar to *C. elegans*, *Cbr-lin-39* acts downstream of *Cbr-pry-1* to regulate VPC competence and cell fate in *C. briggsae*.

Ectopically induced VPCs in pry-1 mutants acquire 2° fates

The ectopic induction of VPCs in *pry-1* mutants led us to examine cell fates using GFP-based markers. For this we made use of six different reporter genes in *C. elegans* (*syg-2* – immunoglobulin superfamily, *daf-6* – *patched*-related, *dhs-31* – short-chain dehydrogenase/reductase, *egl-17* – *fibroblast growth factor (fgf)* family, *lin-11* – LIM homeobox family, and *ceh-2* – *Drosophila empty spiracles (ems)*

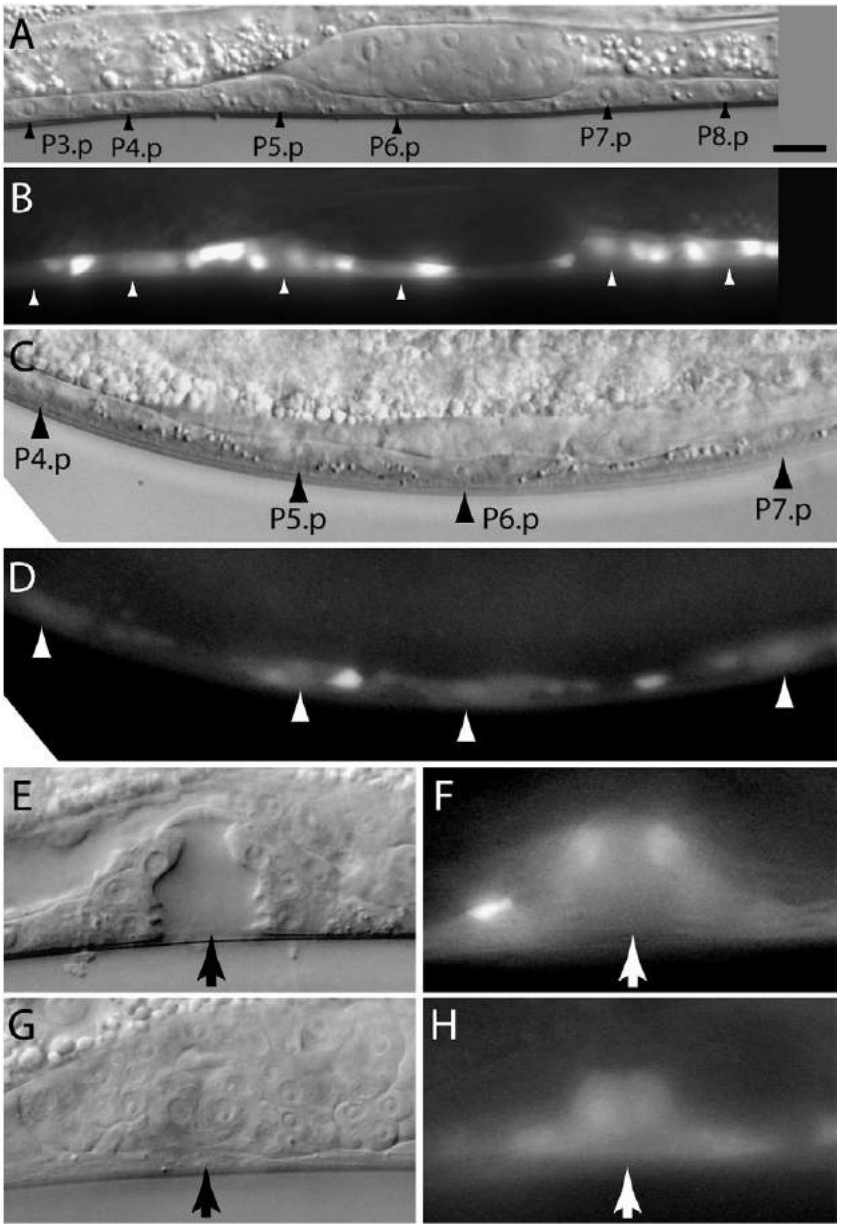

Fig. 2. *Cbr-pry-1::GFP* transcriptional reporter expression in *C. briggsae*. L2 stage *bhEx83* (A, B) and L3 stage *bhEx84* (C, D) transgenic animals showing GFP fluorescence in VPCs (arrowheads) and adjacent neuronal cells. Not all VPCs are visible in C and D. (E-H) *Cbr-pry-1::GFP* continues to be expressed in vulval progeny at later stages. GFP fluorescing cells viewed from two different focal planes in a mid-L4 stage *bhEx83* animal. The arrows mark the center of vulval invagination. Anterior is to the left in all cases. The scale bar in A is 10 μm.

homeodomain family) and two in *C. briggsae* (*Cbr-zmp-1* – zinc metalloproteinase family and *Cbr-egl-17*). These reporter genes are expressed in subsets of 1° and 2° lineage vulval cells and serve as faithful markers to assess induced VPC fates (Burdine et al., 1998; Felix, 2007; Gupta et al., 2003; Inoue et al., 2002; Perens and Shaham, 2005; Shen et al., 2004). In the case of *pry-1(mu38)* we found that four 2° lineage markers, namely *egl-17::GFP (ayIs4)*, *lin-11::GFP (syIs80)*, *ceh-2::GFP (syIs54)* (all mid/late-L4 stage) and *dhs-31::GFP (syIs101)* (old adult stage), were expressed in the progeny of all induced VPCs, P6.p excepted (Fig. 4A). Consistent with this, the expression of 1° lineage markers *egl-17::GFP (ayIs4)* (early/mid-L3 stage), *daf-6::YFP (bhEx53)* and *syg-2::GFP (wyEx3372)* (both mid/late-L4 stage) was localized to P6.p progeny (Fig. 4B). A similar phenotype was observed in *Cbr-pry-1(sy5353)* animals. Thus, *Cbr-egl-17::GFP* (*mfIs5*; a 2° lineage marker during mid-L4 stage) was expressed in the progeny of all induced VPCs, except P6.p, suggesting that these cells had

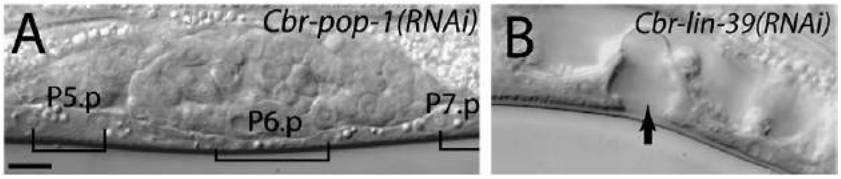

Fig. 3. Vulval induction defects in RNAi-treated animals. (A) *Cbr-pop-1(RNAi)*. P(5-7).p have adopted uninduced 3° fates. (B) Vulval invagination in a *Cbr-lin-39(RNAi)* animal formed by the progeny of P6.p. Other VPCs are uninduced. Anterior is to the left in both animals. The scale bar is 10 μm.

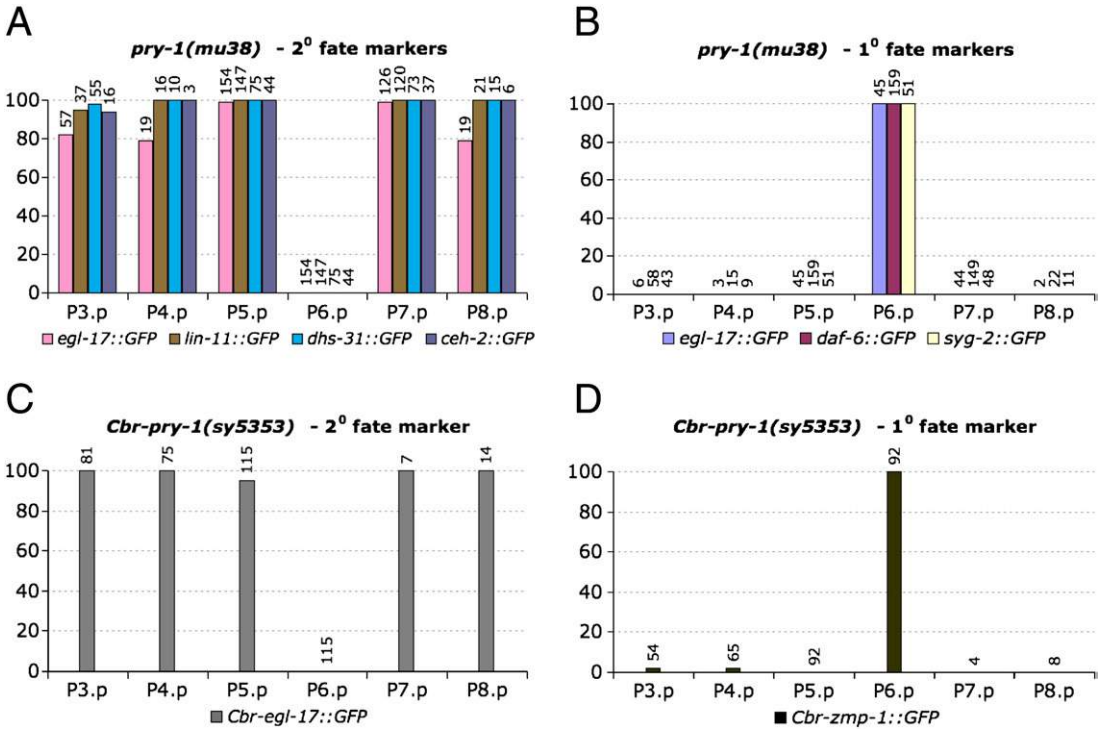

Fig. 4. Expression analysis of vulval cell fate markers in *pry-1* mutants. The y-axis represents the percentage of VPCs expressing the marker. The numbers above the bars show induced VPCs that were examined for GFP fluorescence. The 2° lineage markers are expressed in the progeny of all but P6.p whereas 1° lineage markers are expressed in P6.p progeny only. (A) 2° lineage markers in *C. elegans* – *egl-17::GFP (ayIs4)*, *lin-11::GFP (syIs80)*, *dhs-31::GFP (syIs101)*, and *ceh-2::GFP (syIs54)*. (B) 1° lineage markers in *C. elegans* – *egl-17::GFP (ayIs4)*, *daf-6::YFP (bhEx53)*, and *syg-2::GFP (wyEx3372)*. (C) 2° lineage marker *Cbr-egl-17::GFP (mfIs5)* in *C. briggsae*. (D) 1° lineage marker *Cbr-zmp-1::GFP (mfIs8)* in *C. briggsae*.

adopted 2° fates (Fig. 4C). In no case was *Cbr-egl-17::GFP* expression observed in P6.p progeny. This agrees with *Cbr-zmp-1::GFP* expression (*mfIs8*; a 1° lineage marker during late-L4 stage) that was restricted to P6.p progeny (Fig. 4D). Taken together, these results provide evidence that activated Wnt signaling confers 2° fate on VPCs in both species and that this mechanism is evolutionarily conserved.

VPCs in pry-1 mutants can adopt 2° fates in a gonad-independent manner

Previous studies have shown that the gonad plays an important role in vulval induction. The gonadal AC is a source of the LIN-3/EGF ligand that activates the LET-23/EGFR-mediated MPK-1/MAP kinase signaling pathway in VPCs leading to the specification of 1° and 2° fates (Sternberg, 2005). In addition, at least two Wnt genes (*mom-2* and *lin-44*) are expressed in several gonadal cells (Inoue et al., 2004), suggesting that the gonad may also be the source of a Wnt signal. For these reasons we assessed the contribution of the gonad to the *pry-1* phenotype by ablating gonad precursors in L1 stage. The examination of cell fates by 1° and 2° markers (*Cbr-zmp-1::GFP* and *Cbr-egl-17::GFP*, respectively) revealed that induced VPCs in gonad-ablated *Cbr-pry-1* mutants acquire a 2° fate (100%, n = 19 cells in 8 animals) (Fig. 5A,B; Table 3). In no case was a 1° fate observed in such ablated animals (n = 10 induced cells in 5 animals). Similar results were also obtained in *C. elegans pry-1(mu38)* animals using *egl-17::GFP* marker (57% 2° fate, n = 7 induced cells in 11 animals and no 1° fate, n = 5 induced cells in 6 animals) (Table 3). Thus, in both species Wnt signaling appears to be capable of conferring 2° fates independently of a gonad-derived signal.

VPCs in pry-1 mutants can adopt 2° fates in the absence of LIN-12/Notch signaling

Since the LIN-12/Notch-mediated lateral signaling pathway is required for 2° fate induction in *C. elegans* (Greenwald, 2005; Sternberg, 2005), we examined its role in *pry-1*-mediated VPC fate specification. Previous studies have shown that *Cbr-lin-12* is involved in *C. briggsae* vulval development (Felix, 2007; Rudel and Kimble, 2002). We took the RNAi approach to examine *Cbr-lin-12* interaction with *Cbr-pry-1* in vulval cells. Although the RNAi-mediated knock-down of *Cbr-lin-12* in control animals caused a subtle Overinduced phenotype due to rare ectopic induction of P4.p (5%, n = 44) (Table 1) and an abnormal vulval morphology (Fig. 5C), similar to that reported earlier (Felix, 2007) (also see Materials and Methods), it did not suppress ectopic vulval induction in *Cbr-pry-1(sy5353)* animals (Fig. 5D, Table 1).

Similar to *C. briggsae* the *lin-12* RNAi in *C. elegans* also had no effect on the *pry-1(mu38)* vulva phenotype (Table 1). We further examined the *lin-12*-independent role of *pry-1* using a null allele, *n676n909*. In *lin-12(n676n909)* animals, P5.p, P6.p, and P7.p each adopt a 1° fate (Greenwald et al., 1983), resulting in an abnormally large vulval protrusion (termed protruding vulva or Pvl) in adults. We generated *pry-1(mu38); lin-12(n676n909)* double mutant animals carrying *egl-17::GFP (ayIs4)* and found that such animals exhibit a combination of Overinduced and Pvl phenotypes (Fig. 5E) and show GFP fluorescence in ectopically induced VPCs (Fig. 5F). In these animals (n = 12) P5.p and P7.p were always induced but had no detectable level of GFP fluorescence. These results demonstrate that vulval development in *pry-1* mutants can occur in the absence of *lin-12* function and ectopically induced VPCs are capable of adopting a 2° fate.

We also examined the interaction of *pry-1* with *lip-1* (MAP kinase phosphatase), a transcriptional target of *lin-12*, that promotes 2° VPC fate by inhibiting MAP kinase activity and a 1° cell fate (Berset et al., 2001). The RNAi-mediated knock-down of *lip-1* in both *C. elegans* and *C. briggsae pry-1* mutants had no obvious effect on vulval induction except that P7.p was almost always induced (Table 1). The *lip-1* hypomorph (deletion allele *zh15*) also failed to suppress the *pry-1* Overinduced phenotype. On the contrary, we observed a significant increase in induced VPCs in *pry-1(mu38); lip-1(zh15)* double mutants compared to *pry-1(mu38)* (92% vs. 31%) (Table 1). In these animals 98% of ectopically induced VPCs (n = 140) adopted a 2° fate as judged by the expression of *egl-17::GFP (ayIs4)*.

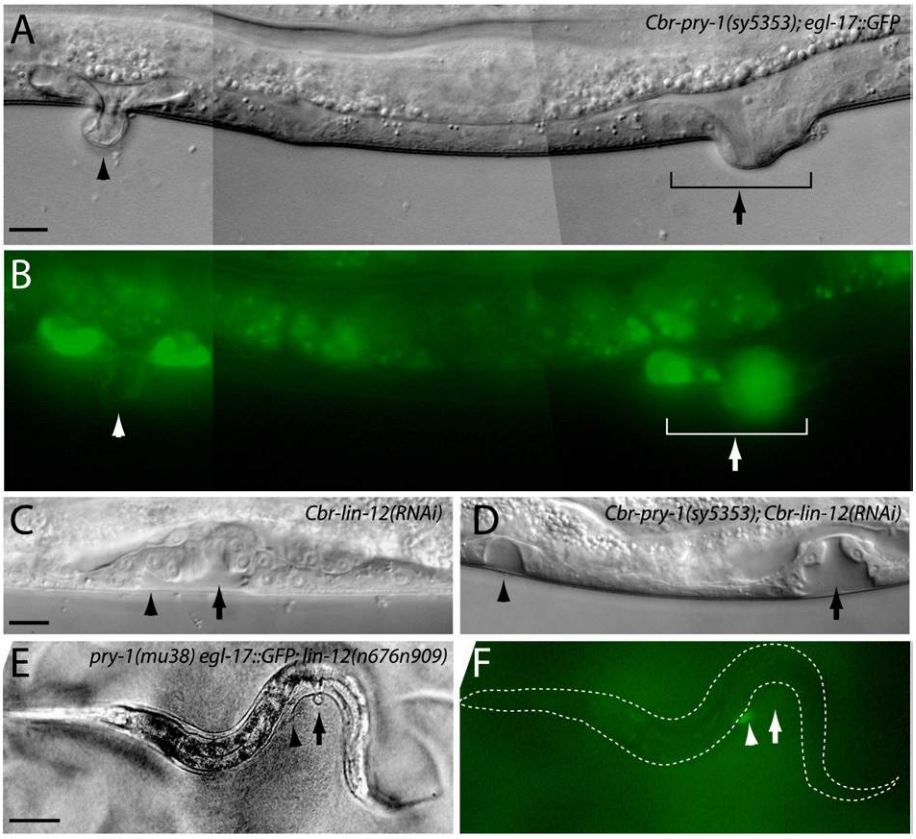

Fig. 5. Gonad-independent and *lin-12*-independent induction of VPCs in *pry-1* mutants. The ectopic vulval invagination and pseudo-vulvae are shown by arrowheads whereas main vulvae by arrows. (A, B) In this gonad-ablated *Cbr-pry-1(sy5353)* animal, *egl-17::GFP* expression can be observed in the progeny of P3.p, P5.p and P6.p. (C) A *Cbr-lin-12(RNAi)* animal showing ectopic induction of P4.p. (D) P7.p induction defect in *sy5353* is rescued by *Cbr-lin-12(RNAi)*. In this animal P4.p was also induced. (E, F) A *pry-1(mu38); lin-12(n676n909)* double mutant showing ectopic pseudovulva (due to induced P4.p) and protruding vulva phenotypes. The *egl-17::GFP* expression can be seen in the progeny of P4.p (arrowhead). Anterior is to the left in all cases. The scale bars are 10 μm (A-D) and 100 μm (E,F).

While the above results suggest that *pry-1* function does not depend upon LIN-12/Notch pathway activity in both *C. elegans* and *C. briggsae*, these data do not rule out the possibility that *lin-12* may act upstream of Wnt signaling to promote 2° fates. To address this possibility we performed experiments with a weak gain-of-function *C. elegans lin-12* allele *n952* that causes ectopic vulval induction in roughly two-thirds of animals (Table 1) (Greenwald et al., 1983). The incomplete penetrance of *lin-12(n952)* provides a sensitized genetic background to test the impact of alterations in Wnt pathway effectors *pop-1* and *lin-39* on vulval induction. We found that although *lin-39 (RNAi)* strongly suppressed *lin-12(n952)* vulval phenotype, *pop-1 (hu9)* and *pop-1(RNAi)* had no such effect (Table 1). These results suggest a simple model in which Wnt and LIN-12/Notch signaling pathways function independently via *lin-39* to specify 2° VPC fates in *C. elegans*.

Table 3
Induced VPCs in gonad-ablated *pry-1* mutants acquire 2° fates.

Genotype	Induced VPCs (Fraction of induced VPCs showing GFP fluorescence)						n
	P3.p	P4.p	P5.p	P6.p	P7.p	P8.p	
mfIs5	0	0	0	0	0	0	5
Cbr-pry-1(sy5353); mfIs5	4 (4/4)	3 (3/3)	4 (4/4)	8 (8/8)	0	0	8
ayIs4	0	0	0	0	0	0	5
ayIs4 pry-1(mu38)	0	3 (1/3)	0	1 (0/1)	2 (2/2)	1 (1/1)	11

n, number of animals examined.

Inhibition of lin-12/Notch signaling in pry-1 mutants promotes P7.p induction

Although the RNAi-mediated knock-down of *Cbr-lin-12* did not suppress ectopic vulval induction in *Cbr-pry-1(sy5353)* animals, we noted that it increased P7.p induction significantly (P = 0.0003, Table 1) and gave rise to a wild-type vulva in most animals (Fig. 5D). A similar trend was also observed in *pry-1(mu38); lin-12 (RNAi)* animals but the difference was statistically not significant (Table 1). This suggested that persistent activity of *lin-12/Notch* signaling in *pry-1* mutants might interfere with P7.p induction and cell fate specification. To examine this, we analyzed *lip-1* reporter expression that, in response to a *lin-12* signal, is upregulated in presumptive 2° VPCs in *C. elegans* (Berset et al., 2001). The expression of *lip-1::GFP* in *C. briggsae (mfIs29)* was first observed in all six VPCs during the L2 stage (50%, n = 14) (Figs. 6A,B). This pattern was dynamic, such that by the early/mid-L3 (Pn.p) stage the fluorescence could be seen in only P5.p and P7.p and was undetectable in other Pn.p cells (48%, n = 21) (Figs. 6C,D and data not shown). This indicates that while *lip-1* expression in *C. briggsae* is maintained in 2° precursors it is rapidly downregulated in 1° and other cells. An analogous pattern was observed in mid-L3 (Pn.px) stage animals although in few cases (27%, n = 11 animals) faint GFP fluorescence was also detected in P4.p and P8.p daughters. At later stages no fluorescence was seen in P(5-7).p progeny.

The analysis of *lip-1* reporter expression in *Cbr-pry-1(sy5353)* animals revealed a similar profile but the fluorescence was much higher in P7.p and P8.p cells. Thus, in L2 stage animals all six VPCs were seen fluorescing, with P7.p and P8.p being the brightest in half of the animals (n = 6) that showed GFP fluorescence (Figs. 6E,F). By the

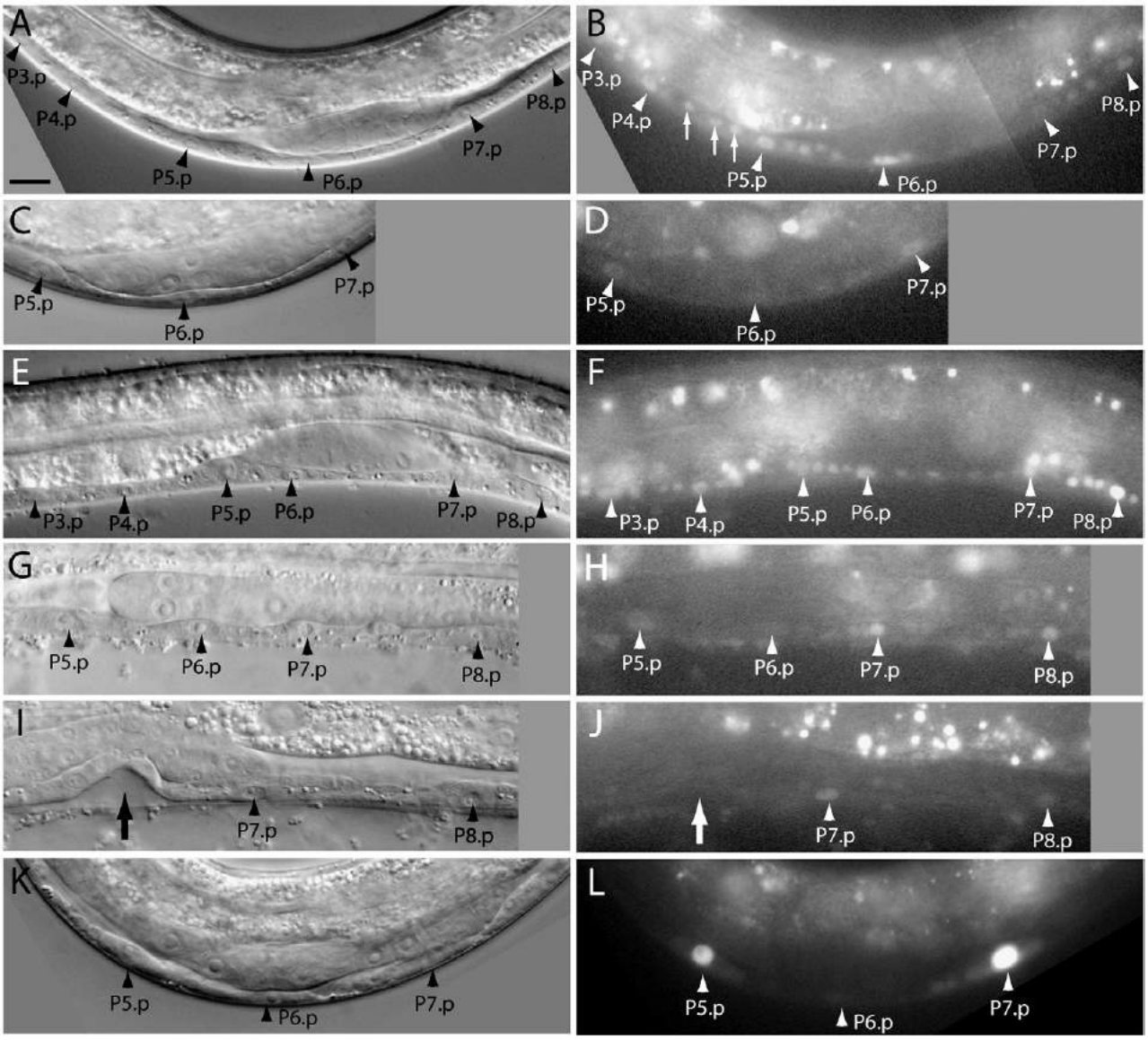

Fig. 6. *lip-1::GFP* expression patterns in wild type and *pry-1* mutants. Arrowheads point to VPCs whereas small arrows to some of the neuronal cells. The big arrows in panels I and J show vulval invagination formed by the progeny of P5.p and P6.p. (A-D) AF16; (E-J) *Cbr-pry-1(sy5353)*; (K, L) *pry-1(mu38)*. (A, B) The P(3-8).p VPCs and some of the neurons in this L2 stage animal can be seen fluorescing. (C, D) An early/mid-L3 stage animal showing GFP fluorescence in P5.p and P7.p. The fluorescence in P6.p is almost invisible. (E, F) P7.p and P8.p are fluorescing at a higher level in this L2 stage animal compared to other Pn.p cells. (G-J) The same two precursors continue to fluoresce at early/mid-L3 (G, H), and early-L4 (I, J) stages. (K, L) P7.p is fluorescing brightly compared to the P5.p. Anterior is to the left in all cases. The scale bar is 10 μm.

early/mid-L3 (Pn.p) stage, fluorescence had rapidly faded in P6.p and other anterior VPCs, however, P7.p and P8.p continued to fluoresce brightly (90%, n = 11 *GFP* expressing animals) (Figs. 6G,H). After the mid-L3 (Pn.px) stage, other than P7.p and P8.p, no VPC progeny showed detectable level of fluorescence (71%, n = 14 *GFP* expressing animals) (Figs. 6I,J). Similar to *C. briggsae* we found that *lip-1::GFP* expression in *C. elegans pry-1(mu38)* L2 stage animals was also higher in P7.p compared to anterior VPCs (37%, n = 19 *GFP* expressing animals) (Figs. 6K,L). These results show an abnormal pattern of *lip-1* expression in *pry-1* mutants and provide a molecular basis for P7.p induction defect in both species.

To further investigate genetic interaction between *lip-1* and *pry-1*, we examined P7.p phenotype in *pry-1* mutants by reducing *lip-1* activity. Consistent with our *lip-1* expression data, we found that RNAi-mediated knock-down of *Cbr-lip-1* in *Cbr-pry-1(sy5353)* animals caused a significant increase in P7.p induction (P = 0.0034) (Table 1). A similar, but weak, phenotype was also observed in *C. elegans pry-1(mu38); lip-1(RNAi)* and *pry-1(mu38); lip-1(zh15)* animals (P = 0.0163 and 0.1175, respectively) (Table 1). Furthermore, induced P7.p in *pry-1(mu38); lip-1(zh15)* animals showed *egl-17::GFP (ayIs4)* expression (100%, n = 60), suggesting that they adopted a 2° fate. Taken together, these findings provide evidence for a conserved interaction between Wnt and LIN-12/Notch signaling pathways to specify the 2° fate of P7.p in *C. elegans* and *C. briggsae*.

Discussion

Due to their apparent morphological similarity, *C. elegans* and *C. briggsae* offer unique advantages in comparative analysis of gene function and signaling networks. To study how homologous tissues are patterned in these two species, we are focusing on the vulva, a reproductive organ necessary for mating and egg laying. We carried out genetic screens in *C. briggsae* and isolated mutants that show defects in vulval development. In this study we report characterization of three of the mutants that exhibit an Overinduced phenotype and show that they are alleles of *Cbr-pry-1*. Our genetic experiments

have revealed that *Cbr-pry-1* functions in *Cbr-bar-1-Cbr-pop-1*-mediated canonical Wnt signaling pathway to regulate VPC induction and fate specification. We have also identified *Cbr-lin-39* Hox gene as a downstream target of this pathway. These findings demonstrate that, similar to *C. elegans*, canonical Wnt signaling pathway is involved in *C. briggsae* vulva formation. Both over- and under-activation of Wnt signaling causes vulval abnormalities thereby highlighting its key role in development. A recent study has shown that changes in environmental conditions have significant effects on Wnt signaling-mediated vulval induction (Braendle and Felix, 2008). This serves to further demonstrate the physiological importance of this pathway in patterning the vulva.

Wnt signaling confers 2° fate on VPCs

Previous studies have demonstrated the essential role of Wnt signaling in maintaining VPC competence (Eisenmann et al., 1998; Myers and Greenwald, 2007). During the L2 stage *bar-1*-mediated Wnt signaling promotes *lin-39* activity in P(3-8).p and allows these cells to respond to patterning signals in the L3 stage. Our work has revealed that in addition to its role in VPC competence, Wnt signaling also promotes a specific cell fate in *C. elegans* and *C. briggsae*. Previous work by Gleason and colleagues (Gleason et al., 2002) showed that activated Wnt signaling causes excessive vulval cell proliferation. However it was unclear whether vulval progeny adopted a specific fate. Subsequently, Myers and Greenwald (Myers and Greenwald, 2007) argued that ectopic vulval progeny in *pry-1* mutants could arise from spurious cell divisions due to high *lin-39* levels. To address this issue we analyzed cell fates in *pry-1* mutants using established molecular markers. We found that induced VPCs, except P6.p, in *pry-1* mutants adopted a 2° fate as judged by a panel of 8 GFP-based markers (6 in *C. elegans* and 2 in *C. briggsae*). The use of wide range of reporters used in our assay (i.e., ligands, cell surface receptors, metalloproteases, and transcription factors) serves to demonstrate that Wnt signaling orchestrates expression of many important genes needed to confer a 2° fate. In these animals the P6.p fate remained unaltered. Further experiments revealed that 2° VPC fates are specified independently of the gonad-derived inductive signal since induced VPCs in gonad-ablated animals showed 2° marker expression similar to that seen in intact animals. These results significantly extend our understanding of *pry-1*-mediated Wnt signaling function in two nematode species and suggest that Wnt signaling plays both permissive role (in maintaining competence) and instructive role (in specifying cell fate) in vulval development.

The 2° fates of induced VPCs in *pry-1* mutants prompted us to examine the relationship between Wnt and LIN-12/Notch signaling in vulval development. We found that alterations in the activities of LIN-12/Notch pathway receptor *lin-12* and its transcriptional target *lip-1* did not suppress ectopic vulval induction defect in *pry-1* mutants. Thus, activated Wnt signaling in *C. elegans* and *C. briggsae* is sufficient to promote vulval development in the absence of lateral signaling. This raises the question of evolutionary roles of Wnt and LIN-12/Notch pathways in 2° fate specification. Perhaps the two pathways evolved as redundant mechanisms to robustly specify a 2° VPC fate. The completed genome sequences of *Elegans* group species (such as *C. remanei* and *C. brenneri*) provide opportunities to address such questions.

Wnt signaling and P7.p fate specification

Our work has uncovered novel roles of the Wnt signaling pathway in *C. elegans* and *C. briggsae* vulval development that involve both positive and negative regulation of cell fates. We found that P3.p, P4.p, and P8.p in *pry-1* mutants are frequently induced to adopt a 2° fate whereas P7.p remains largely uninduced. This is likely to be caused by activated Wnt signaling since RNAi knock-downs of *Cbr-bar-1* and *Cbr-pop-1* promoted P7.p induction in *Cbr-pry-1* mutants. Since LIN-12/Notch-mediated lateral signaling specifies the 2° fate of P7.p, we examined its role in mediating *pry-1* function. Our results showed that the expression of *lip-1* in *pry-1* mutants was significantly higher in P7.p compared to P5.p and persisted in L4 stage animals. This pattern differs from wild type where *lip-1* is dynamically regulated in P(5-7).p and is not observed beyond mid-L3 stage. This suggests that a failure to downregulate *lip-1* in *Cbr-pry-1* mutants may be the basis of the P7.p induction defect. Considering that LIP-1 is a MAP kinase phosphatase, one model is that the persistence of high level of LIP-1 activity in P7.p (directly or indirectly induced by Wnt signaling) abnormally antagonizes *mpk-1* (MAP kinase, Ras pathway component) function such that the Ras pathway response in P7.p falls below the minimum threshold needed to promote an induced fate. It is equally possible that misregulation of *lip-1* interferes with the expression of *lin-12* target genes that in turn causes P7.p to remain uninduced. Consistent with these possibilities, we found that lowering *lip-1* activity (either by directly targeting *lip-1* or its upstream activator *lin-12*) in *pry-1* mutants suppressed the P7.p induction defect.

While our results provide evidence for a genetic interaction between Wnt and LIN-12/Notch signaling pathways, more work is needed to understand the mechanism of interaction and its biological role in P7.p development. In this respect, reverse genetics and genomics approaches could prove valuable in dissecting the roles of Wnt and LIN-12/Notch pathway genes and their downstream targets. These studies may uncover the function of new genes thereby revealing their mechanism of function and signaling crosstalk. Ultimately, the findings will help understand how changes in gene expression and interactions are regulated to generate tissue morphology.

Acknowledgments

We are indebted to Marie-Anne Félix (Institut Jacques Monod) for generously providing some of the transgenic strains and RNAi bacterial clones. The genetic screen was carried in the laboratory of Paul Sternberg (Caltech). We thank Shahla Gharib for isolating *sy5270*, Bavithra Thillainathan for help in mapping *sy5353*, Kang Shen (Stanford University) for providing *syg-2::GFP (wyEx3372)* strain, and Zhongying Zhao (University of Washington, Seattle) for the *C. briggsae unc-119* deletion allele *st20000*. We also thank Nathan Farrar for helpful comments on the manuscript. Some of the strains were obtained from the *Caenorhabditis* Genetics Center. This work was supported by funds from the Natural Sciences and Engineering Research Council of Canada and Canada Research Chairs Program to BPG.

Appendix A. Supplementary data

Supplementary data associated with this article can be found, in the online version, at doi:10.1016/j.ydbio.2010.07.003.

References

Avery, L., Horvitz, H.R., 1987. A cell that dies during wild-type *C. elegans* development can function as a neuron in a *ced-3* mutant. Cell 51, 1071–1078.
Behrens, J., Jerchow, B.A., Wurtele, M., Grimm, J., Asbrand, C., Wirtz, R., Kuhl, M., Wedlich, D., Birchmeier, W., 1998. Functional interaction of an axin homolog, conductin, with beta-catenin, APC, and GSK3beta. Science 280, 596–599.
Berset, T., Hoier, E.F., Battu, G., Canevascini, S., Hajnal, A., 2001. Notch inhibition of RAS signaling through MAP kinase phosphatase LIP-1 during *C. elegans* vulval development. Science 291, 1055–1058.
Bossinger, O., Klebes, A., Segbert, C., Theres, C., Knust, E., 2001. Zonula adherens formation in *Caenorhabditis elegans* requires *dlg-1*, the homologue of the *Drosophila* gene *discs large*. Dev. Biol. 230, 29–42.
Braendle, C., Felix, M.A., 2008. Plasticity and errors of a robust developmental system in different environments. Dev. Cell 15, 714–724.
Bray, S.J., 2006. Notch signalling: a simple pathway becomes complex. Nat. Rev. Mol. Cell Biol. 7, 678–689.
Brenner, S., 1974. The genetics of *Caenorhabditis elegans*. Genetics 77, 71–94.

Burdine, R.D., Branda, C.S., Stern, M.J., 1998. EGL-17(FGF) expression coordinates the attraction of the migrating sex myoblasts with vulval induction in *C. elegans*. Development 125, 1083–1093.
Clandinin, T.R., Katz, W.S., Sternberg, P.W., 1997. Caenorhabditis elegans HOM-C genes regulate the response of vulval precursor cells to inductive signal. Dev. Biol. 182, 150–161.
Coudreuse, D.Y., Roel, G., Betist, M.C., Destree, O., Korswagen, H.C., 2006. Wnt gradient formation requires retromer function in Wnt-producing cells. Science 312, 921–924.
Cutter, A.D., 2008. Divergence times in *Caenorhabditis* and *Drosophila* inferred from direct estimates of the neutral mutation rate. Mol. Biol. Evol. 25, 778–786.
Eisenmann, D. M., 2005. Wnt signaling. WormBook. ed. The *C. elegans* Research Community, WormBook. doi:10.1895/wormbook.1.7.1, http://www.wormbook.org.
Eisenmann, D.M., Kim, S.K., 2000. Protruding vulva mutants identify novel loci and Wnt signaling factors that function during Caenorhabditis elegans vulva development. Genetics 156, 1097–1116.
Eisenmann, D.M., Maloof, J.N., Simske, J.S., Kenyon, C., Kim, S.K., 1998. The beta-catenin homolog BAR-1 and LET-60 Ras coordinately regulate the Hox gene *lin-39* during *Caenorhabditis elegans* vulval development. Development 125, 3667–3680.
Eizinger, A., Sommer, R.J., 1997. The homeotic gene *lin-39* and the evolution of nematode epidermal cell fates. Science 278, 452–455.
Felix, M.A., 2005. An inversion in the wiring of an intercellular signal: evolution of Wnt signaling in the nematode vulva. Bioessays 27, 765–769.
Felix, M.A., 2007. Cryptic quantitative evolution of the vulva intercellular signaling network in *Caenorhabditis*. Curr. Biol. 17, 103–114.
Firestein, B.L., Rongo, C., 2001. DLG-1 is a MAGUK similar to SAP97 and is required for adherens junction formation. Mol. Biol. Cell 12, 3465–3475.
Gleason, J.E., Korswagen, H.C., Eisenmann, D.M., 2002. Activation of Wnt signaling bypasses the requirement for RTK/Ras signaling during *C. elegans* vulval induction. Genes Dev. 16, 1281–1290.
Gleason, J.E., Szyleyko, E.A., Eisenmann, D.M., 2006. Multiple redundant Wnt signaling components function in two processes during *C. elegans* vulval development. Dev. Biol. 298, 442–457.
Greenwald, I., 2005. LIN-12/Notch signaling in *C. elegans*. WormBook. ed. The *C. elegans* Research Community, WormBook. doi:10.1895/wormbook.1.10.1, http://www.wormbook.org.
Greenwald, I., Seydoux, G., 1990. Analysis of gain-of-function mutations of the *lin-12* gene of *Caenorhabditis elegans*. Nature 346, 197–199.
Greenwald, I.S., Sternberg, P.W., Horvitz, H.R., 1983. The *lin-12* locus specifies cell fates in *Caenorhabditis elegans*. Cell 34, 435–444.
Gupta, B. P., Johnsen, R., Chen, N., 2007. Genomics and biology of the nematode *Caenorhabditis briggsae*. WormBook. ed. The *C. elegans* Research Community, WormBook. doi:10.1895/wormbook.1.136.1, http://www.wormbook.org.
Gupta, B.P., Wang, M., Sternberg, P.W., 2003. The *C. elegans* LIM homeobox gene *lin-11* specifies multiple cell fates during vulval development. Development 130, 2589–2601.
Hall, D.H., Altun, Z.F., 2008. *C. elegans* Atlas. Cold Spring Harbor Laboratory Press, New York.
Herman, M.A., Vassilieva, L.L., Horvitz, H.R., Shaw, J.E., Herman, R.K., 1995. The *C. elegans* gene *lin-44*, which controls the polarity of certain asymmetric cell divisions, encodes a Wnt protein and acts cell nonautonomously. Cell 83, 101–110.
Hillier, L.W., Miller, R.D., Baird, S.E., Chinwalla, A., Fulton, L.A., Koboldt, D.C., Waterston, R.H., 2007. Comparison of *C. elegans* and *C. briggsae* Genome Sequences Reveals Extensive Conservation of Chromosome Organization and Synteny. PLoS Biol. 5, e167.
Ikeda, S., Kishida, S., Yamamoto, H., Murai, H., Koyama, S., Kikuchi, A., 1998. Axin, a negative regulator of the Wnt signaling pathway, forms a complex with GSK-3beta and beta-catenin and promotes GSK-3beta-dependent phosphorylation of beta-catenin. EMBO J. 17, 1371–1384.
Inoue, T., Oz, H.S., Wiland, D., Gharib, S., Deshpande, R., Hill, R.J., Katz, W.S., Sternberg, P.W., 2004. *C. elegans* LIN-18 is a Ryk ortholog and functions in parallel to LIN-17/Frizzled in Wnt signaling. Cell 118, 795–806.
Inoue, T., Sherwood, D.R., Aspock, G., Butler, J.A., Gupta, B.P., Kirouac, M., Wang, M., Lee, P.Y., Kramer, J.M., Hope, I., Burglin, T.R., Sternberg, P.W., 2002. Gene expression markers for *Caenorhabditis elegans* vulval cells. Mech. Dev. 119 (Suppl 1), S203–S209.
Kenyon, C.J., Austin, J., Costa, M., Cowing, D.W., Harris, J.M., Honigberg, L., Hunter, C.P., Maloof, J.N., Muller-Immergluck, M.M., Salser, S.J., Waring, D.A., Wang, B.B., Wrischnik, L.A., 1997. The dance of the Hox genes: patterning the anteroposterior body axis of *Caenorhabditis elegans*. Cold Spring Harb. Symp. Quant. Biol. 62, 293–305.
Koboldt, D.C., Staisch, J., Thillainathan, B., Haines, K., Baird, S.E., Chamberlin, H.M., Haag, E.S., Miller, R.D., Gupta, B.P., 2010. A toolkit for rapid gene mapping in the nematode Caenorhabditis briggsae. BMC Genomics 11, 236.
Koppen, M., Simske, J.S., Sims, P.A., Firestein, B.L., Hall, D.H., Radice, A.D., Rongo, C., Hardin, J.D., 2001. Cooperative regulation of AJM-1 controls junctional integrity in *Caenorhabditis elegans* epithelia. Nat. Cell Biol. 3, 983–991.
Korswagen, H.C., Coudreuse, D.Y., Betist, M.C., van de Water, S., Zivkovic, D., Clevers, H.C., 2002. The Axin-like protein PRY-1 is a negative regulator of a canonical Wnt pathway in *C. elegans*. Genes Dev. 16, 1291–1302.
Logan, C.Y., Nusse, R., 2004. The Wnt signaling pathway in development and disease. Annu. Rev. Cell Dev. Biol. 20, 781–810.
Louvet-Vallee, S., Kolotuev, I., Podbilewicz, B., Felix, M.A., 2003. Control of vulval competence and centering in the nematode *Oscheius* sp. 1 CEW1. Genetics 163, 133–146.
Luo, W., Zou, H., Jin, L., Lin, S., Li, Q., Ye, Z., Rui, H., Lin, S.C., 2005. Axin contains three separable domains that confer intramolecular, homodimeric, and heterodimeric interactions involved in distinct functions. J. Biol. Chem. 280, 5054–5060.
Maduro, M., Pilgrim, D., 1995. Identification and cloning of *unc-119*, a gene expressed in the *Caenorhabditis elegans* nervous system. Genetics 141, 977–988.
Maloof, J.N., Whangbo, J., Harris, J.M., Jongeward, G.D., Kenyon, C., 1999. A Wnt signaling pathway controls hox gene expression and neuroblast migration in C. elegans. Development 126, 37–49.
Mello, C.C., Kramer, J.M., Stinchcomb, D., Ambros, V., 1991. Efficient gene transfer in *C. elegans*: extrachromosomal maintenance and integration of transforming sequences. EMBO J. 10, 3959–3970.
Myers, T.R., Greenwald, I., 2007. Wnt signal from multiple tissues and *lin-3*/EGF signal from the gonad maintain vulval precursor cell competence in *Caenorhabditis elegans*. Proc. Natl Acad. Sci. USA 104, 20368–20373.
Perens, E.A., Shaham, S., 2005. *C. elegans daf-6* encodes a patched-related protein required for lumen formation. Dev. Cell 8, 893–906.
Rocheleau, C.E., Downs, W.D., Lin, R., Wittmann, C., Bei, Y., Cha, Y.H., Ali, M., Priess, J.R., Mello, C.C., 1997. Wnt signaling and an APC-related gene specify endoderm in early C. elegans embryos. Cell 90, 707–716.
Rudel, D., Kimble, J., 2001. Conservation of glp-1 regulation and function in nematodes. Genetics 157, 639–654.
Rudel, D., Kimble, J., 2002. Evolution of discrete Notch-like receptors from a distant gene duplication in *Caenorhabditis*. Evol. Dev. 4, 319–333.
Salser, S.J., Kenyon, C., 1992. Activation of a C. elegans Antennapedia homologue in migrating cells controls their direction of migration. Nature 355, 255–258.
Salser, S.J., Loer, C.M., Kenyon, C., 1993. Multiple HOM-C gene interactions specify cell fates in the nematode central nervous system. Genes Dev. 7, 1714–1724.
Schwarz-Romond, T., Fiedler, M., Shibata, N., Butler, P.J., Kikuchi, A., Higuchi, Y., Bienz, M., 2007. The DIX domain of Dishevelled confers Wnt signaling by dynamic polymerization. Nat. Struct. Mol. Biol. 14, 484–492.
Sharma-Kishore, R., White, J.G., Southgate, E., Podbilewicz, B., 1999. Formation of the vulva in *Caenorhabditis elegans*: a paradigm for organogenesis. Development 126, 691–699.
Shen, K., Fetter, R.D., Bargmann, C.I., 2004. Synaptic specificity is generated by the synaptic guidepost protein SYG-2 and its receptor, SYG-1. Cell 116, 869–881.
Siegfried, K.R., Kimble, J., 2002. POP-1 controls axis formation during early gonadogenesis in C. elegans. Development 129, 443–453.
Sommer, R. J., 2005. Evolution of development in nematodes related to *C. elegans*. WormBook. ed. The *C. elegans* Research Community, WormBook. doi:10.1895/wormbook.1.46.1, http://www.wormbook.org.
Sommer, R.J., Sternberg, P.W., 1996. Apoptosis and change of competence limit the size of the vulva equivalence group in *Pristionchus pacificus*: a genetic analysis. Curr. Biol. 6, 52–59.
Sternberg, P. W., 2005. Vulval development. WormBook. ed. The *C. elegans* Research Community, WormBook. doi:10.1895/wormbook.1.6.1, http://www.wormbook.org.
Sternberg, P.W., Horvitz, H.R., 1988. lin-17 mutations of Caenorhabditis elegans disrupt certain asymmetric cell divisions. Dev. Biol. 130, 67–73.
Sundaram, M.V., 2005. The love-hate relationship between Ras and Notch. Genes Dev. 19, 1825–1839.
Thorpe, C.J., Schlesinger, A., Carter, J.C., Bowerman, B., 1997. Wnt signaling polarizes an early C. elegans blastomere to distinguish endoderm from mesoderm. Cell 90, 695–705.
Tian, H., Schlager, B., Xiao, H., Sommer, R.J., 2008. Wnt signaling induces vulva development in the nematode *Pristionchus pacificus*. Curr. Biol. 18, 142–146.
Whangbo, J., Kenyon, C., 1999. A Wnt signaling system that specifies two patterns of cell migration in *C. elegans*. Mol. Cell 4, 851–858.
Widelitz, R., 2005. Wnt signaling through canonical and non-canonical pathways: recent progress. Growth Factors 23, 111–116.
Winston, W.M., Sutherlin, M., Wright, A.J., Feinberg, E.H., Hunter, C.P., 2007. *Caenorhabditis elegans* SID-2 is required for environmental RNA interference. Proc. Natl Acad. Sci. USA 104, 10565–10570.
Wood, W.B. (Ed.), 1988. The Nematode *Caenorhabditis elegans*. Cold Spring Harbor Laboratory Press, Cold Spring Harbor New York.
Yu, H., Seah, A., Herman, M.A., Ferguson, E.L., Horvitz, H.R., Sternberg, P.W., 2009. Wnt and EGF pathways act together to induce C. elegans male hook development. Dev. Biol. 327, 419–432.
Zheng, M., Messerschmidt, D., Jungblut, B., Sommer, R.J., 2005. Conservation and diversification of Wnt signaling function during the evolution of nematode vulva development. Nat. Genet. 37, 300–304.

Curriculum Vitae

NAGAGIREESH BOJANALA

OBJECTIVE

To ingrain and instruct an attitude that adapts suitably to the scientific knowledge and serves to fulfil scientific pursuit of an individual or a group.

EDUCATIONAL BACKGROUND

- 2008 to present: Ph.D in Molecular genetics and Developmental biology.
  Location: Biology center, ASCR, v.v.i, Ceske Budejovice, Czech Republic.

- 2005-2008**:** Master of Science in Developmental Biology.
  Location: Department of Biology, McMaster University, Hamilton, Canada.

- 2000-2002: Master of Science in Biotechnology.
  Location: Department of Biotechnology, Sri Venkateswara University, India.

- 1997-2000: Bachelor of Science (Chemistry, Botany and Zoology).
  Location: Department of Sciences, Sri Venkateswara University, India.

RESEARCH EXPERIENCE

Duration1: Jan 2013 to March 2015. (Post-Doctoral Scholar)
Title **:** Dissecting mechanistic insights through which EGL-26 controls vulva organogenesis.
Supervisor**:** Dr. Wendy Hanna-Rose
Place **:** 104D life sciences building, State College, PA, USA, 16802.

Duration 2: June 2008 to present (Doctoral Thesis).
Title **:** Modulation of C. elegans vulva organogenesis by nuclear hormone receptor NHR-25.
Supervisor**:** Dr. Masako Asahina Jindrova.
Place **:** Biology center, ASCR, v.v.i, Ceske Budejovice, Czech Republic, 37005.

Duration 3 : Jan 2005 to May 2008.
Title **:** Genetic analysis of *pry-1/axin* in *Caenorhabditis briggsae.*

Supervisor **:** Dr. Bhagwati Prasad Gupta.
Place **:** Department of Biology, McMaster University, Hamilton, Canada.

Publications:

1) Jordan D. Ward*, **Nagagireesh Bojanala***, Teresita Bernal, Kaveh Ashrafi, Masako Asahina, and Keith R. Yamamoto. *Sumoylated NHR-25/NR5A regulates cell fate during C. elegans vulval development.*Published: December 12, 2013. DOI: 10.1371/journal.pgen.1003992. * Equal Contribution.

2) Devika Sharanya, Bavithra Thillainathan, Sujatha Marri, **Nagagireesh Bojanala**, Stephane Flibotte, Donald G. Moerman, Robert H. Waterston, and Bhagwati P Gupta. *Genetic* Control of *Vulval Development* in Caenorhabditis *briggsae*. G3(Bethesda) 2012. doi: 10.1534/g3.112.004598. (Co-author).

3) **S**eetharaman A., Cumbo P., **Bojanala N.,** Gupta B.P. (2010). Conserved mechanism of Wnt signaling function in the specification of vulval precursor fates in C. elegans and C. briggsae. *Developmental Biology* 346: 128–139. (Second author).

RESEARCH/TECHNICAL SKILL SET

- Vulva cell lineage analysis using DIC optics.
- Analysis of cell fate/differentiation properties of vulva cells using fluorescent markers.
- Complementation, two- factor and three- factor mapping, and SNP mapping.
- Forward genetic screens – EMS and MOS-1 mediated mutagenesis screens.
- Reverse genetic/RNAi screens.
- Worm DNA/RNA isolations.
- Basic molecular cloning techniques and PCR/qRT-PCR techniques.
- Single molecule fluorescent in situ hybridization (smFISH).
- DIC/Fluorescent Microscopy – expertise in Olympus FV10-ASW.
- Laser Microsurgery/ablations and Microinjection techniques.
- 3D and 4D real time data analysis using IMARIS.
- Expertise in Adobe Photoshop and ImageJ.
-

RESEARCH ABSTRACTS SUBMITTED AT CONFERENCES

1) June 26-30, 2013, 19th International *C. elegans* Meeting, UCLA.

"Dissecting the mechanistic insights through which EGL-26 controls vulva organogenesis". Nagagireesh Bojanala, Avni upadhyay, Hongliu Sun, Matt Crook,

Ariana Detwiler, Nishat Seraj, Sarah Chang, Jimmy Goncalves, Ryan Fine, Nick Serra, and Wendy Hanna-Rose.

2) June 7 – 10, 2012, University of Wisconsin, Madison. *C. elegans* Development, Cell Biology, & Gene Expression Meeting.

"*C. elegans* nuclear hormone receptor, *nhr-25* regulates vulval terminal cell properties and migrations during development". Nagagireesh Bojanala , Marek Jindra and Masako Asahina.

3) June 22-26, 2011, 18 th International Worm Meeting, UCLA.

"Sumoylation of *C. elegans* nuclear receptor NHR-25 promotes proper organogenesis" Jordan D. Ward, Nagagireesh Bojanala, Teresita Bernal, Marek Jindra, Kaveh Ashrafi, Keith R. Yamamoto, Masako Asahina.

„Vulval organogenesis involves an interaction between SMO-1 and the nuclear receptor NHR-25" Jordan D. Ward, Nagagireesh Bojanala, Teresita Bernal, Marek Jindra, Kaveh Ashrafi, Keith R. Yamamoto, Masako Asahina.

4) Sept 16-20, 2011. EMBO conference series, Sitges, Spain.

Nuclear Receptors: From Molecular Mechanism to Health and Disease.
"Sumoylation of *C. elegans* nuclear receptor NHR-25 promotes proper organogenesis" Jordan D. Ward, Nagagireesh Bojanala, Teresita Bernal, Marek Jindra, Kaveh Ashrafi, Keith R. Yamamoto, Masako Asahina.

5) June 17-20, 2010. *C. elegans* EMBO conference series, Heidelberg, Germany.

"Regulation of the nuclear receptor NHR-25 by sumoylation during *C. elegans* vulva formation". Nagagireesh Bojanala, Jordan D. Ward , Teresita Bernal, Marek Jindra, Kaveh Ashrafi, Keith R. Yamamoto, Masako Asahina.

6) Aug 31st-Sept 4th, 2010, CSHL Nuclear Receptors and Disease Conference, Cold Spring Harbor Laboratories, NY, USA.

"Sumoylation of *C. elegans* nuclear receptor NHR-25 promotes proper organogenesis" Jordan D. Ward, Nagagireesh Bojanala, Teresita Bernal, Marek Jindra, Kaveh Ashrafi, Keith R. Yamamoto, Masako Asahina.

INVITED TALKS

Ph.D seminar series, Advances in biology and genetics, Institute of Molecular Genetics, Prague,CZ. Organizer: Petr Svoboda.

Presented an invited talk " *C. elegans* as a model organism for developmental genetics" at Ph.D student seminar series "Bugs and Beasts" during 2009.

Presented an invited talk " Forward Genetic Tools available for *C. elegans* research " at Ph.D student seminar series "Heavy Tools" during 2010.

Ph.D course on developmental biology, **Masaryk University, Brno, CZ. Organizer: Viteslav Bryja.**

Presented an invited talk " *C. elegans* as a model organism for developmental genetics" during 2011.

TEACHING ACTIVITIES

- Fall 2014; **Biology 430/BMB430 – Instructor**, Penn State University, USA.

  Planned and conducted weekly reading assignments, lecture series, quizzes and exams for BMB-BIOL 430. Assisted and monitored learning assistants and group leaders during the course. Interacted with students on review sessions, weekly office hours and individual meetings to assist them in exams, quizzes and problem sets. Advised students on their future career prospects.

- May 2009 to present: Involved in the teaching/lab activities to explain "C. *elegans* as a model organism for developmental genetics" for the practical course in developmental biology at University of South Bohemia.

- June 2008 to present: Provided necessary teaching and technical help to the undergraduate and master's students at Masako lab.

- January 2005 to March 2007: Worked as an undergraduate teaching assistant for 1A03 (Introductory biology) and 3MO3 (Developmental biology) courses conducted by Department of Biology, McMaster University, Canada.

ACADEMIC ACHIEVEMENTS

- 2003: Qualified for National Eligibility Test-Lectureship (NET-LS), conducted by Council of Scientific and Industrial Research, Govt. of India.

- 2002: Secured 4th position among the class during M.Sc Biotechnology program.

- 2000: Secured 1st ranks in M.Sc qualifying entrance examinations in Biotechnology, Biochemistry and Virology programs conducted by Sri Venkateswara University and Sri Krishnadevaraya University in India.

DECLARATION

I hereby declare that the above given information is correct to the best of my knowledge and belief.

Thanking you,

Date: May 16, 2015

Yours Sincerely,

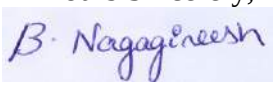

Place: Ceske Budejovice

(NAGAGIREESH BOJANALA)